LATERAL TORSIONAL BUCKLING OF WOODEN BEAMS WITH MID-SPAN LATERAL BRACING

Ye Hu

Thesis submitted to the
Faculty of Graduate and Postdoctoral Studies
in partial fulfillment of the requirements
for the degree of Master of Applied Science in Civil Engineering

Department of Civil Engineering

Faculty of Engineering

University of Ottawa

Abstract

An analytical and numerical investigation is conducted for the lateral torsional buckling analysis of wooden beam with a mid-span lateral brace subjected to symmetrically distributed loading. Two models are developed; one for the case of a rigid brace and another one for the case of a flexible brace. The analytical solutions are based on the principle of stationary potential energy and a Fourier expansion of the buckling displacement fields and bending moments. The validity of both models are verified against 3D finite element analyses in ABAQUS. Where applicable, verifications were also conducted against available solutions from previous studies. Parametric studies were conducted to investigate the effect of geometric and material parameters on the critical moments. The results indicate the presence of two separate groups of potential buckling modes, symmetric and anti-symmetric, with fundamentally different behavioural characteristics. The governing buckling mode is shown to depend on the bracing height, load height and lateral brace stiffness. The study shows that beyond a certain threshold bracing height, the critical moment is governed by the antisymmetric mode of buckling. Also, above a certain optimum bracing stiffness, no increase is observed in the critical moments. The models developed are used to construct a comprehensive database of parametric investigations which are then employed for developing simplified equations for determining the threshold heights, associated critical moments, and optimum stiffness.

Acknowledgements

I would have never been able to complete my thesis without the guidance of my supervisors Dr. Magdi Mohareb and Dr. Ghasan Doudak. I would like to express my deepest gratitude to Dr. Magdi Mohareb, for his excellent guidance, profound knowledge and patience. Those meetings we had in the last two years would be my greatest and most valuable experience in my student career.

I would also like to thank Yang Du and Juanying Yi, who as friends and brothers, were always willing to help and give me their best suggestions.

Finally, I would like to thank my parents Zhaohui Hu and Yingping Hu, my fiancée Xiaohui Shi, for their endless sacrifice and encouragement throughout the good times and difficult ones.

TABLE OF CONTENTS

LIST OF FIGURES

LIST OF TABLES

1. Introduction

1.1 Background

Lateral torsional buckling (LTB) is an important ultimate limit state in the design of timber beams. A laterally unsupported member that is bent about the strong axis can experience out-of-plane bending and twisting when the magnitude of loads reaches a limiting critical value. It is thus important to reliably and accurately determine the LTB capacity of beams. The LTB capacity is influenced by several factors: moment gradient, load height, bracing, etc. In practical situations, the applied loads may be offset from the section shear centre. For example, if the load is applied at the top face, it will induce an additional destabilizing effect. Contrarily, if a lateral brace is provided, it will increase the LTB capacity. Currently, no recommendations are provided for the combined effect of bracing height and load height effects.

1.2 Material Properties of Wood

Due to the wood fiber orientation, wood can be characterized as a circularly orthotropic material (wood handbook 2010). Thus, wood has independent mechanical properties along the Longitudinal (L), Radial (R) and Tangential (T) directions (Fig. 1.1). The longitudinal direction is parallel to the fibres, the radial direction is oriented from the tree centre outwards and the tangential direction is oriented to the longitudinal and radial directions. Three groups of elastic parameters, 12 parameters in total, are therefore needed when dealing with the bending stiffness of wood members.

For an orthotropic material, the stress-strain relationship can be expressed by Eq. (3.1)

$$\begin{Bmatrix} \varepsilon_L \\ \varepsilon_R \\ \varepsilon_T \\ \gamma_{LR} \\ \gamma_{LT} \\ \gamma_{RT} \end{Bmatrix} = \begin{bmatrix} 1/E_L & -\mu_{RL}/E_R & -\mu_{TL}/E_T & & & \\ -\mu_{LR}/E_L & 1/E_R & -\mu_{TR}/E_T & & & \\ -\mu_{LT}/E_L & -\mu_{RT}/E_R & 1/E_T & & & \\ & & & 1/G_{LR} & & \\ & & & & 1/G_{LT} & \\ & & & & & 1/G_{RT} \end{bmatrix} \begin{Bmatrix} \sigma_L \\ \sigma_R \\ \sigma_T \\ \sigma_{LR} \\ \sigma_{LT} \\ \sigma_{RT} \end{Bmatrix} \tag{3.1}$$

where

E_L = Young's modulus along the longitudinal direction;

E_R = Young's modulus along the radial direction;

E_T = Young's modulus along the tangential direction;

G_{LR} = Shear modulus in the LR plane;

G_{LT} = Shear modulus in the LT plane;

G_{RT} = Shear modulus in the RT plane;

μ_{RL} = Poisson's ratio for deformation along the longitudinal direction cause by stress along the radial direction;

μ_{LR} = Poisson's ratio for deformation along the radial direction cause by stress along the longitudinal direction;

μ_{TL} = Poisson's ratio for deformation along the longitudinal direction cause by stress along the tangential direction;

μ_{LT} = Poisson's ratio for deformation along the tangential direction cause by stress along the longitudinal direction;

μ_{TR} = Poisson's ratio for deformation along the radial direction cause by stress along the tangential direction;

μ_{RT} = Poisson's ratio for deformation along the tangential direction cause by stress along the radial direction;

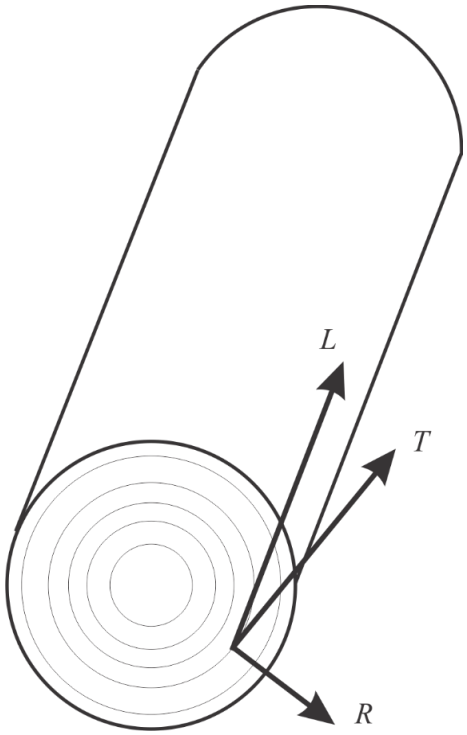

Figure 1.1 Longitudinal, Radial, and Tangential Direction

The properties along the R and T directions are similar and can typically be considered to identical, as seen in Table 1.1 (FPL 2010). This simplification allows for the reduction of the 12 independent parameters to 9, thereby simplifying the linear elastic properties as provided in Eq. (3.2).

$$\begin{Bmatrix} \varepsilon_L \\ \varepsilon_R \\ \varepsilon_T \\ \gamma_{LR} \\ \gamma_{LT} \\ \gamma_{RT} \end{Bmatrix} = \begin{bmatrix} 1/E_L & -\mu_{LR}/E_T & -\mu_{LT}/E_T & & & \\ -\mu_{RL}/E_L & 1/E_T & -\mu_{RT}/E_T & & & \\ -\mu_{TL}/E_L & -\mu_{TR}/E_T & 1/E_T & & & \\ & & & 1/G_{LT} & & \\ & & & & 1/G_{LT} & \\ & & & & & 1/G_{RT} \end{bmatrix} \begin{Bmatrix} \sigma_L \\ \sigma_R \\ \sigma_T \\ \sigma_{LR} \\ \sigma_{LT} \\ \sigma_{RT} \end{Bmatrix} \tag{3.2}$$

Table 1.1 Elastic ratio for various species at approximately 12% moisture content

Species	G_{LR}/E_L	G_{LT}/E_L	Species	G_{LR}/E_L	G_{LT}/E_L
Oak, red	0.089	0.081	Larch, western	0.063	0.069
Yellow-poplar	0.075	0.069	Loblolly	0.082	0.081
Bald cypress	0.063	0.054	Pine, Pond	0.05	0.045
Cedar, western red	0.087	0.086	Pine, Slash	0.055	0.053
Hemlock, western	0.038	0.032	Spruce, Sitka	0.064	0.061
Pine, Sugar	0.124	0.113	Spruce, Engelmann	0.124	0.12
Species	E_T/E_L	E_R/E_L	Species	E_T/E_L	E_R/E_L
Oak, red	0.082	0.154	Larch, western	0.065	0.079
Yellow-poplar	0.043	0.092	Loblolly	0.078	0.113
Bald cypress	0.039	0.084	Pine, Pond	0.041	0.071
Cedar, western red	0.055	0.081	Pine, Slash	0.045	0.074
Hemlock, western	0.031	0.058	Spruce, Sitka	0.043	0.078
Pine, Sugar	0.087	0.131	Spruce, Engelmann	0.059	0.128

Due to symmetry of properties in the R and T directions, one can equate the following parameters $\mu_{LR}/E_T = \mu_{RL}/E_L$, $\mu_{LT}/E_T = \mu_{TL}/E_L$ and $\mu_{RT}/E_T = \mu_{TR}/E_R$. Hence the nine elastic parameters reduced to six independent parameters which affects the LTB capacity investigation. In Xiao (2014), a sensitivity analysis between the critical moment and 6 elastic properties is given in Table 1.2. The table clearly indicates that only modulus of elasticity (E_L) in the longitudinal direction and transverse shear modulus G_T are found of significance in relation to the LTB capacity.

Table 1.2 Effect of Constitutive parameters on critical moments as predicted by FEA

case	$\frac{E_L}{E_{L\text{-}ref}}$	$\frac{G_{LT}}{G_{LT\text{-}ref}}$	$\frac{E_T}{E_{T\text{-}ref}}$	$\frac{\mu_{RL}}{\mu_{RL\text{-}ref}}$	$\frac{\mu_{RT}}{\mu_{RT\text{-}ref}}$	$\frac{G_{RT}}{G_{RT\text{-}ref}}$	$\frac{M_{cr}}{M_{cr\text{-}ref}}$
Reference case	1	1	1	1	1	1	1.00
1	1.5	1	1	1	1	1	1.24
2	0.5	1	1	1	1	1	0.697
3	1	1.5	1	1	1	1	1.20
4	1	0.5	1	1	1	1	0.735
5	1	1	1.5	1	1	1	1.00
6	1	1	0.5	1	1	1	1.00
7	1	1	1	1.5	1	1	1.00
8	1	1	1	0.5	1	1	1.00
9	1	1	1	1	1.5	1	1.00
10	1	1	1	1	0.5	1	1.00
11	1	1	1	1	1	1.5	1.01
12	1	1	1	1	1	0.5	0.988

In the following sections, all beam members are considered to be characterized by two constants in a manner similar to isotropic materials. To simplify the notation E_L is replaced with E and G_{LT} is replaced with G.

1.3 General Lateral Torsional Buckling Theory

1.3.1 Direct Equilibrium method

Timoshenko and Gere (1961) developed the classical closed form solution for a laterally unsupported beam member with doubly symmetric cross section subjected to uniform moment M through direct equilibrium. The governing equations are:

$$\begin{aligned} GJ\frac{d\theta}{dz} - EC_w\frac{d^3\theta}{dz^3} + \frac{du}{dz}M = 0 \\ EI_{yy}\frac{d^2u}{dz^2} - \theta M = 0 \end{aligned} \tag{3.3}$$

where u is lateral displacement, θ is the twist angle, I_{yy} is the weak moment of inertia, J is the Saint-Venant torsional constant, and C_w is a warping constant of the beam. By differentiating Eq. (3.3) with respect to z, one obtains

$$\frac{d^4\theta}{dz^4} - 2\alpha \frac{d^2\theta}{dz^2} - \beta\theta = 0 \tag{3.4}$$

where

$$\alpha = \frac{GJ}{2EC_w} \qquad \beta = \frac{M^2}{E^2 I_{yy} C_w}$$

The solution of Eq.(3.4) takes the form:

$$\theta = A_1 \sin mz + A_2 \cos mz + A_3 e^{nz} + A_4 e^{-nz} \tag{3.5}$$

where

$$m = \sqrt{-\alpha + \sqrt{\alpha^2 + \beta}} \quad n = \sqrt{\alpha + \sqrt{\alpha^2 + \beta}}$$

To determine the magnitude of constants A_1 through A_4, the four boundary conditions for simply supported member relative to twist are enforced, i.e.,

$$\theta(0) = \theta(L) = \theta''(0) = \theta''(L) = 0 \tag{3.6}$$

By enforcing the boundary conditions one obtains $A_2 = A_3 = A_4 = 0$ and the characteristic equation

$$\sin mL = 0 \tag{3.7}$$

The smallest magnitude of $m = \pi/L$, and the corresponding critical moment is

$$M_{cr} = \frac{\pi}{L}\sqrt{EI_{yy}C_w\left(1 + \frac{EC_w\pi^2}{GJL^2}\right)} \tag{3.8}$$

1.3.2 Total potential energy method

Another means of obtaining the buckling solution is to determine the moment that corresponds to the neutral stability condition. For a typical structure in equilibrium, there exists three possible equilibrium conditions, namely unstable, stable, or neutral. When an equilibrium state is unstable (Fig. 1.2a), the system equilibrium is vulnerable and cannot revert back to its equilibrium state after small outside interference (Fig. 1.2b). However, for stable equilibrium, the system is able to revert back to its original equilibrium state after

removal of any disturbance (Fig. 1.2c). The neutral stability condition lies at the border between the stable and unstable equilibria. In a structural system, this corresponds to a critical buckling load.

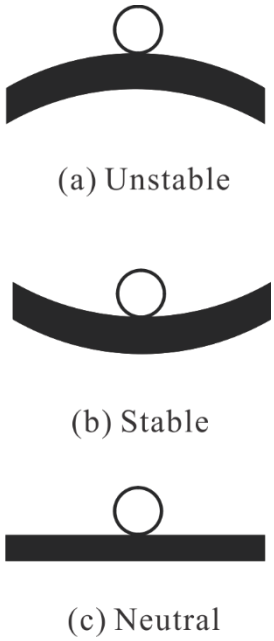

Figure 1.2 Three equilibrium conditions

The total potential energy π has two components, the internal strain energy U and load potential energy V gained, i.e.,

$$\pi = U + V \tag{3.9}$$

For a laterally unrestrained simply supported doubly symmetric cross-section beam member, the internal strain energy stored arises from lateral displacement, twist, and warping and can be expressed by (e.g., Trahair 1993)

$$U = \frac{1}{2}\int_0^L EI_{yy}u''^2 dz + \frac{1}{2}\int_0^L EC_w\theta''^2 dz + \frac{1}{2}\int_0^L GJ\theta'^2 dz \tag{3.10}$$

The load potential energy gain is given by

$$V = +\int_0^L M\theta u'' dz \tag{3.11}$$

where the bending moment $M(z) = M_{\max} m(z)$ is expressed as the product of the peak bending moment $M_{\max}$ and a function $m(z)$ which reflects the bending moment distribution along the beam.

In order to obtain an approximate buckling solution, one needs to assume displacement functions which satisfy the essential boundary conditions. For a beam simply supported relative to twist and lateral displacement, these are $u(0) = u(L) = \theta(0) = \theta(L) = 0$. Also, it is desirable, but not necessary, to meet the natural boundary conditions. For a simply supported beam, these are $u''(0) = u''(L) = \theta'''(0) = \theta''(L) = 0$. The following assumed displacement functions meet all essential and boundary conditions for the simply supported case.

$$u(z) = A\sin(\pi z/L), \quad \theta(z) = B\sin(\pi z/L) \tag{3.12}$$

From Eq. (3.12), one can approximately express the functional π as a function of $\pi \approx \pi(A,B)$ by substituting into Eq.(3.10). To recover the equilibrium state, the stationary condition $\delta\pi = 0$ needs to be satisfied, i.e.,

$$\delta\pi = \frac{\partial \pi}{\partial A}\delta A + \frac{\partial \pi}{\partial B}\delta B = 0$$

Since A, B are arbitrary constants, one has $\partial\pi/\partial A = \partial\pi/\partial B = 0$, by setting the above system in a matrix form, one has,

$$\left([K] + M_{\max}[K_G]\right)\begin{Bmatrix} A \\ B \end{Bmatrix} = \{0\} \tag{3.13}$$

where $[K]$ is elastic stiffness matrix and $[K_G]$ is geometric stiffness matrix.

For a linear system, the equilibrium state can be shown to also coincide with the neutral stability condition. The Eigen value problem $\left|[K] + M_{\max}[K_G]\right| = 0$ in Eq. (3.13) is solved to yield an approximation of the critical bending moment $M_{\max}$. For the special case where moments within the span are constant, the displacement functions assumed in Eq. (3.12) are exact and equation 1.11 yields critical moment prediction in exact agreement with Eq. (3.8)

1.4 Load Height Effect

A load applied at the top of the beam induces an additional destabilizing twisting moment $M_1 = Q\theta h/2$ (Fig. 1.3a) which reduces the LTB capacity while a load applied at the bottom of the beam is associated with a restoring moment $M_2 = Q\theta h/2$ (Fig. 1.3b) which increases the LTB capacity.

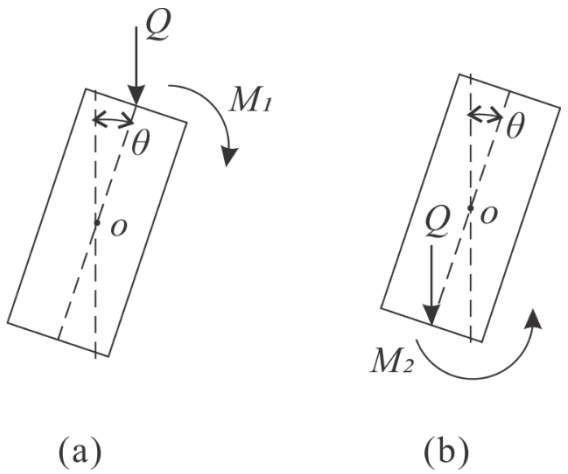

Figure 1.3 Load height effect on beam member cross section (a) Destabilizing Moment M_1 due to top face loading, (b) Restoring moment M_2 due to bottom face loading

For a beam subjected to a load Q acting at z_0 that is offset by a distance a below the shear centre, the additional load potential energy V_D gained by the load height effect is given by

$$V_D = +\frac{1}{2}Qa\left[\theta(z_0)\right]^2 \tag{3.14}$$

The additional term given by Eq. (3.14) needs to be added to that in Eq. (3.11) to account for the load height effect. For the simply supported beam considered in Section 1.3, by assuming the same approximate displacement and twisting functions given by Eq. (3.12), evoking the equilibrium conditions by setting $\delta\pi = 0$ or $\partial\pi/\partial A = \partial\pi/\partial B = 0$ and solving the resulting eigen value (Trahair 1993), one obtains the critical load Q as

$$\frac{QL}{4M_0} = 1.35\left\{\sqrt{1+\left(\frac{0.54P_y a}{M_0}\right)^2} + \frac{0.54P_y a}{M_0}\right\} \tag{3.15}$$

where

$$M_0 = \sqrt{\frac{\pi^2 EI_{yy}}{L^2}\left(GJ + \frac{\pi^2 EC_w}{L^2}\right)}\ ; \qquad P_y = \frac{\pi^2 EI_{yy}}{L^2}\ ;$$

To generalize the load height effect for other boundary conditions and loading patterns, some standards (e.g., AS4100-1998, Eurocode 3-1992, AF&PA-2003) have adopted either the effective length or the equivalent moment factor methods. These standards are reviewed in the following section.

1.4.1 Relevant Standard Provisions

Although the primary focus of the present study is to investigate the lateral torsional buckling of wooden beams, the majority of lateral torsional buckling research pertains to steel members. As such, the following sections will survey lateral torsional buckling provisions for both steel and wood members.

1.4.1.1 Canadian Steel Design Standards (CSA S16-14)

The critical elastic moment of the unbraced segment in the steel design standard (CSA 2014) is given by

$$M_{cr} = \omega_2 \frac{\pi}{L}\sqrt{EI_{yy}GJ + \left(\frac{\pi E}{L}\right)^2 I_{yy}C_w} \tag{3.16}$$

where ω_2 is a coefficient that accounts for increased moment resistance of a laterally unsupported doubly symmetric beam segment when subject to a moment gradient. Though for unbraced beam segments, no solution has been given to deal with the situation where the load is acting above shear centre, the standard states that the associated destabilizing effect shall be taken into account using a rational method (CSA, 2014), and loads applied at top flange has been addressed by effective method. For pin-ended beams, one obtains:

$$M_{cr} = \frac{\pi}{1.2L}\sqrt{EI_{yy}GJ + \left(\frac{\pi E}{1.2L}\right)^2 I_{yy}C_w} \tag{3.17}$$

For all other cases,

$$M_{cr} = \frac{\pi}{1.4L}\sqrt{EI_{yy}GJ + \left(\frac{\pi E}{1.4L}\right)^2 I_{yy}C_w} \tag{3.18}$$

1.4.1.2 Australia Standards: steel structures (AS4100-1998)

Under the Australian Standards (section 5.6), the nominal member moment capacity M_b is given by

$$M_b = \alpha_m \alpha_s M_s \tag{3.19}$$

where α_m = moment modification factor, α_s = a slenderness reduction factor, and M_s = nominal section moment capacity. The slenderness reduction factor shall be calculated as follows

$$\alpha_s = 0.6\left[\sqrt{\left[\left(\frac{M_s}{M_{cr}}\right)^2 + 3\right]} - \frac{M_s}{M_{cr}}\right] \tag{3.20}$$

the reference buckling moment M_{cr} is given by

$$M_{cr} = \frac{\pi}{L_e}\sqrt{EI_{yy}GJ + \left(\frac{\pi E}{L_e}\right)^2 I_{yy}C_w} \tag{3.21}$$

Where the effective length L_e accounts for fixity conditions relative to twist, lateral displacement and load height effect. It takes the form

$$L_e = k_r k_t k_l L \tag{3.22}$$

where k_t is a twist restraint factor, k_r is lateral rotation restraint factor and k_l is the load height factor given in Table 1.3, 1.4, and 1.5.

Table 1.3 Load height factor (k_l)

Longitudinal position of the load	Restraint arrangement*	Load height position	
		shear centre	Top flange
Within segment	FF,FP,FL,PP,PL,LL,	1.0	1.4
	FU,PU	1.0	2.0
At segment end	FF,FP,FL,PP,PL,LL,	1.0	1.0
	FU,PU	1.0	2.0

Table 1.4 Twist restraint factors (k_t)

Restraint arrangement	Factor, k_t
FF,FL,LL,FU	1.0
FP,PL,PU	$1+\frac{\left[\left(\frac{d_1}{l}\right)\left(\frac{t_f}{2t_w}\right)^3\right]}{n_w}$
PP	$1+\frac{\left[2\left(\frac{d_1}{l}\right)\left(\frac{t_f}{2t_w}\right)^3\right]}{n_w}$

Table 1.5 Lateral rotation restraint factors (k_r)

Restraint arrangement	Ends with lateral rotation restraints	Factor, k_r
FU,PU	Any	1
FF,FP,FL,PP,PL,LL	None	1
FF,FP,PP	One	0.85
FF,FP,PP	Both	0.7

where

d_1 = clear depth between flanges ignoring fillets or welds

n_w = number of webs

t_f = thickness of critical flange

t_w = thickness of web

* F = fully restrained, L = laterally restrained, P = partially restrained, U = unrestrained. Example: FP is fully restrained at the first end of the member and partially restrained at the second end.

1.4.1.3 European Committee for Standardization (Eurocode 3-1992)

For a laterally unsupported prismatic beam with a doubly symmetric cross-section bent about the major axis, the critical moment formula in the Annex F of the Eurocode 3 (CEN 1992) includes the load height effect as provided in Eq.(3.23)

$$M_{cr} = C_1 \frac{\pi^2 EI_{yy}}{(KL)^2} \left\{ \left[\left(\frac{K}{K_w} \right)^2 \frac{C_w}{I_{yy}} + \frac{(KL)^2 GJ}{\pi^2 EI_{yy}} + (C_2 a)^2 \right]^{0.5} - C_2 a \right\} \qquad (3.23)$$

where C_1, C_2 are factors depending on the loading and end restraint conditions which can be determined from Table 1.6 and Table 1.7, K and K_w are effective length factors for end rotation on plan and end warping, respectively. The effective length factor K and K_w vary from 0.5 for full fixity to 1.0 for no fixity and 0.7 when one end is fixed and the other end free, a is the load height relative to cross-section shear centre.

Table 1.6 values of factors C_1 , C_2corresponding to values of: end moment loading

loading and support condition	bending moment diagram (r)	C_1			C_2		
		Value of K					
		1	0.7	0.5	1	0.7	0.5
	1.0	1.0	1.0	1.0	-		
	0.8	1.1	1.3	1.3			
	0.5	1.3	1.5	1.5			
	0.3	1.6	1.7	1.8			
	0.0	1.9	2.1	2.2			
	-0.3	2.3	2.5	2.6			
	-0.5	2.7	3.0	3.1			
	-0.8	2.9	3.0	3.1			
	-1.0	2.8	3.1	3.1			

Table 1.7 values of factors, corresponding to values of: transverse loading

loading and support conditions	C_1		C_2	
	Value of K			
	1.00	0.50	1.00	0.50
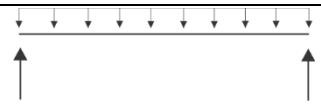	1.13	0.97	0.46	0.30
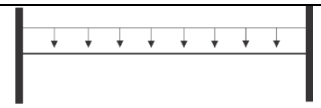	1.29	0.71	1.56	0.65
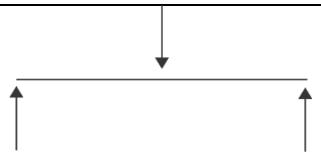	1.37	1.07	0.55	0.43
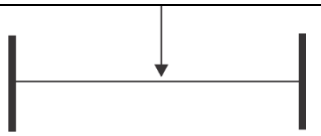	1.57	0.94	1.27	0.72
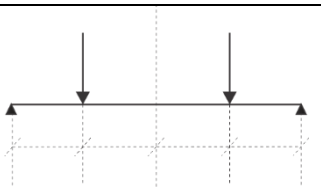	1.05	1.01	0.43	0.41

1.4.1.4 American Forest and Paper Association (AFPA-2003)

Section 2.1.3.2 of AFPA (2003) provides recommendations on incorporating the load height effect by introducing a load eccentricity factor C_e when determining the critical buckling moments. For members with rectangular cross-sections, the critical buckling moment is given by,

$$M_{cr} = \frac{1.3 C_b C_e E'_{y05} I_{yy}}{l_u} \tag{3.24}$$

where

C_b = equivalent moment factor for different loading and support condition; (Table 1.8)

l_u = unbraced length;

E'_{y05} = adjusted modulus of elasticity for bending about weak axis at the fifth percentile.

Table 1.8 C_b and k^* factor for different load conditions

Loading condition	Laterally braced at point of loading	Laterally unbraced at point of loading	
	C_b	C_b	k^*
Equal end moments	2.30	-	-
Equal opposite end moments	1.00	-	-
Uniformly distributed load	1.00	1.13	1.44
concentrated load at centre	1.67	1.35	1.72
Equal concentrated loads unless specified otherwise			
Two loads at 1/3 points	1.00	1.14	1.63
Three loads at 1/4 points	1.11	1.14	1.45
Four loads at 1/5 points	1.00	1.14	1.51
Five loads at 1/6 points	1.05	1.14	1.45
Six loads at 1/7 points	1.00	1.13	1.47
Seven loads at 1/8 points	1.03	1.13	1.44
>8 loads with equal spacing	1.00	1.13	1.46

The load eccentricity factor C_e is given by

$$C_e = \sqrt{\eta^2 + 1} - \eta \tag{3.25}$$

where

$$\eta = \frac{1.3k^* d}{l_u} \tag{3.26}$$

where d is the height of the beam cross section , k^* is a constant based on loading and support conditions (Table 1.8) ranging from 1.44 to 1.72.

1.5Beam bracing effects

1.5.1 Relevant Theoretical Developments

The LTB failure involves both lateral displacements and twisting. For this reason, beam bracing normally can be categorized into two types: lateral bracing (Fig 1.4a), torsional brace (Fig 1.4b). Conceptually, warping bracing is a theoretical possibility. However, for rectangular wood sections with generally small warping effects in estimating LTB capacity, such bracing becomes ineffective and has not gained much attention in wooden beams.

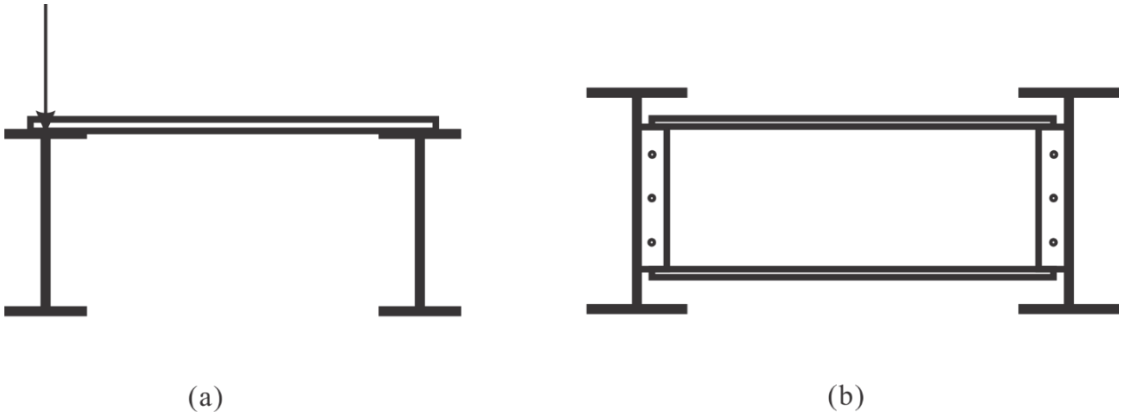

Figure 1.4 Beam bracing (a) lateral bracing (b) torsional bracing

In practical situations, not all braces are rigid enough to fully restrain the lateral displacement, and hence this type of brace is referred to as partial. Both rigid brace and partially brace are investigated in this thesis.

1.5.2 Relevant Theoretical Developments

Trahair (1993) developed a closed form solution for the LTB capacity under uniform moment with a central lateral-torsional rigid restraint. When the beam member buckles, displacement and twisting angle at the centre point vanish and the beam buckles anti-symmetrically with two half waves. Since each half span can be regarded as simply supported and has an effective length of $L/2$, the author provided the following expression.

$$M_{cr} = \frac{2\pi}{L}\sqrt{EI_{yy}GJ + \left(\frac{\pi E}{2L}\right)^2 I_{yy}C_w} \qquad (3.27)$$

A review of how the bracing effect are addressed in different standards is presented next.

1.5.3 Review of standards for bracing effect

1.5.3.1 National Design Specification for wood construction (NDS-2015)

The design standard determines the LTB capacity of wood beam member by multiplying the reference bending design value by the beam stability factor C_L as provided in Eq. (1.29)

$$C_L = \frac{1+\left(F_{be}/F_b^*\right)}{1.9} - \sqrt{\left[\frac{1+\left(F_{be}/F_b^*\right)}{1.9}\right]^2 - \frac{F_{be}/F_b^*}{0.95}} \tag{3.28}$$

where

F_b^* = Reference bending design value multiplied by all applicable adjustment factor except flat use factor, volume factor and beam stability factor;

$F_{be} = 1.20E'_{\min}/R_B^2$;

$E'_{\min}$ = Adjustment design value for modulus of elasticity for beam and column stability;

$R_B = \sqrt{l_e d/b^2}$;

The effect of lateral bracing is included in the NDS (2015) by introducing the effective length l_e as determined in accordance with Table 1.9.

Table 1.9 Effective length for bending members

Single span beam	where $l_u/h < 7$		where $l_u/h \geq 7$
Equal end moment		$l_e = 1.84 l_u$	
uniformly distributed load	$l_e = 2.06 l_u$		$l_e = 2.06 l_u + 3h$
concentrated load at centre with no intermediate lateral support	$l_e = 1.08 l_u$		$l_e = 1.37 l_u + 3h$
For Equal Concentrated loads with lateral supports			
One concentrated load at centre		$l_e = 1.11 l_u$	
Two loads at 1/3 points		$l_e = 1.68 l_u$	
Three loads at 1/4 points		$l_e = 1.54 l_u$	
Four loads 1/5 points		$l_e = 1.68 l_u$	
Five loads at 1/6 points		$l_e = 1.73 l_u$	
Six loads at 1/7 points		$l_e = 1.78 l_u$	
Seven or more equidistant		$l_e = 1.84 l_u$	

1.5.3.2 American Forest and Paper Association (AFPA-2003)

As already detailed in Section 1.4.1, Technical Report 14 of (AFPA-2003), incorporates the effect of lateral bracing on the critical moments by providing equivalent moment gradient factors C_b for beams laterally braced at the points of loading that are different from moment gradients for beams that are laterally unbraced at point of loading (Table 1.8).

1.6 Motivation for Present Study

Although the effect of lateral brace and load height effect have been included in some design codes as has been summarized in the previous sections, no recommendations are provided for the simultaneous effect of varying the brace height and load height. The current study attempts to fill this gap in knowledge by developing models and simplified equations which capture such effects.

1.7 Research Objectives

The objective of this thesis is to investigate the effect of both the load height and brace height on the LTB capacity of wood beam members. More specifically, the research goals are to:

- Develop an analytical model for simply supported wood beam member subjected to symmetrically distributed load and with mid-span brace.
- Verify the accuracy of the theoretical model by validating it against a commercial FEA software (ABAQUS) for different load conditions.
- Investigate the load height and brace height effect on LTB critical moment and buckling mode for different load types with rigid lateral brace.
- Investigate the load height and brace height effect on LTB critical moment and buckling mode for different load types with flexible lateral brace.

1.8 Outline of the Thesis

Present Chapter 1 provides the theoretical background, and research objectives. Chapter 2 presents a literature review on the lateral torsional buckling studies for beams, with emphasis on studies involving lateral bracing and load height effects.

Chapter 3 is written in a paper format and develops an analytical model for the LTB analysis of simply supported wooden beam member with rigid lateral brace acting at mid-span. Two loading types have been investigated, mid-span point load and uniformly distributed load. The study determines the critical moments and the threshold bracing. Simplified design expressions and design examples are presented as part of the study.

Chapter 4 is also written in a paper format and develops an analytical model for simply supported wooden beam with flexible lateral brace provided at midspan. The model

provides a basis to determine the threshold bracing stiffness. A simplified design expression and design examples are provided.

Chapter 5 provides the summary, conclusions that obtained from the theoretical model and FEA model in chapter 3 and chapter 4 and recommendation for future research.

References

[1] American Forest and Paper Association. (2003). Technical Report 14: Designing for lateral-torsional stability in wood members. Washington, D.C.

[2] American Wood Council (2015), National Design Specification® for Wood Construction, Leesburg, VA.

[3] European Committee for Standardization. (1992). Eurocode (EC) 3: Design of steel structures part 1.1: general rules and rules for buildings, Prestandard ENV 1993-1-1:1992. Brussels, Belgium.

[4] Canadian Standards Association. (2014). Design of steel structures. CSA standard S16-14. Mississauga, ON.

[5] Canadian Standards Association. (2014). Design of steel structures. CSA standard SO86-14. Mississauga, ON.

[6] Isopescu, D., Stanila, O., Asatanei, I. (2012). "Analysis of Wood Bending Properties on Standardized Samples and Structural Size Beams Tests." Buletinul Insititutului PolitehnicDIN Din Iasi, Publicat de Universitatea Tehnică „Gheorghe Asachi" din Iaşi

[7] Standards Australia. (1998). Steel structures. Australian standard AS 4100-1998. Homebush, Australia.

[8] Trahair, N. S. (1993). *Flexural-Torsional Buckling of Structures*, CRC Press Inc. Florida, USA.

[9] Forest Products Laboratory. (2010). Wood handbook-Wood as an engineering material. General Technical Report FPL-GTR-190. Madison, Wisconsin, USA

Notation

a = Distance of load offset from cross-section shear centre;

C_L = Beam stability factor;

C_b = Equivalent moment factor for different loading and support condition;

C_e = Load height factor for top loaded beams;

C_w = Warping constant;

d_1 = clear depth between flanges ignoring fillets or welds;

E_L = Young's modulus along the longitudinal direction;

E_R = Yong's modulus along the radial direction;

E_T = Young's modulus along the tangential direction;

$E'_{\min}$ = Adjustment design value for modulus of elasticity for beam and column stability;

E'_{y05} = Adjusted modulus of elasticity for bending about weak axis at the fifth percentile;

F_b^* = Reference bending design value multiplied by all applicable adjustment factor except flat use factor, volume factor and beam stability factor;

G_{LR} = Shear modulus in the LR plane;

G_{LT} = Shear modulus in the LT plane;

G_{RT} = Shear modulus in the RT plane;

h = Height of the wood beam cross-section;

I_{yy} = Weak moment of inertial;

J = Saint-Venant torsional constant;

K = Effective length factor for end rotation on plane;

K_w = Effective length factor for end warping;

$[K]$ = Elastic stiffness matrix;

$[K_G]$ = Geometric stiffness matrix;

k_l = Load height factor;

k_r = Lateral rotation restraint factor;

k_t = Twist restraint factor;

k^* = Constant based on loading and support condition;

L = Span of the beam;

L_e = Effective length account for fixity condition;

l_e = Effective length account for intermediate lateral support;

l_u = Unbraced length;

M_b = Nominal member moment capacity in AS design standards;

M_{cr} = Critical moment;

$M_{\max}$ = Peak bending moment along the longitudinal direction in wood beam member;

M_s = Nominal section moment capacity;

M_0 = Reference critical moment for beam;

n_w = Number of webs;

P_y = Reference critical load for column;

Q = Concentrated load;

R_B = Slenderness ratio;

t_f = Thickness of critical flange;

t_w = Thickness of web;

U = Internal strain energy;

u = Lateral displacement;

V = Load potential energy gained;

V_D = Load potential energy gained by load height effect;

z = Longitudinal coordinates;

z_0 = Arbitrary coordinates along the span;

α_m = Moment modification factor;

α_s = Slenderness reduction factor;

μ_{LR} = Poisson's ratio for deformation along the radial direction cause by stress along the longitudinal direction;

μ_{LT} = Poisson's ratio for deformation along the tangential direction cause by stress along the longitudinal direction;

μ_{RL} = Poisson's ratio for deformation along the longitudinal direction cause by stress along the radial direction;

μ_{RT} = Poisson's ratio for deformation along the tangential direction cause by stress along the radial direction;

μ_{TL} = Poisson's ratio for deformation along the longitudinal direction cause by stress along the tangential direction;

μ_{TR} = Poisson's ratio for deformation along the radial direction cause by stress along the tangential direction;

θ = Twist angle along the longitudinal direction;

π = Total potential energy;

ω_2 = Coefficient to account for increased moment resistance of a laterally unsupported doubly symmetric beam segment when subject to a moment gradient.

2. LITERATURE REVIEW

2.1 General

The present investigation aims at investigating the interactions between the effects of load height, bracing height, and bracing stiffness on the lateral torsional buckling (LTB) capacity of wood beam. Thus, Section 2.2. of the present chapter provides a review of studies investigating the load height effect. A review of studies investigating the effect of lateral on LTB is then presented in Section 2.3. Some of these studies have focused on the effect of bracing flexibility (Section 2.3.1) while others have tackled the combined effect of bracing height and flexibility on LTB capacity (Section 2.3.2). Section 2.4 provides an overview of investigations on the combined effect of load height and bracing height on LTB capacity.

2.2 Studies on load height effect

The effect of load height has been widely investigated. Earlier studies focusing on the topic include the work of Timoshenko (1936), Winter (1941), Schrader (1941) Austin et al. (1955), Pettersson (1952), who dealt with various load conditions and boundary conditions (including simply supported beams, fixed end beams and cantilevers). The topic has also been tackled in numerically in a number of lateral torsional bucking studies. These include Prescott and Carrington (1920), Pi et al. (1992), Ings and Trahair (1987), Andrade and Camotim (2005), Mohri and Potier-Ferry (2006), Andrade et al. (2007), Erkmen and Mohareb (2008), Wu and Mohareb (2010), Trahair (2013), Lamb and Eamon (2015) and Sahraei et al. (2015). The effect of load height has been the primary focus of several other studies which are discussed in more details in the following sections.

Kerensky et al. (1956) reviewed and modified previous lateral torsional buckling solutions for beams of doubly and mono-symmetric cross-sections and developed expressions for critical stresses. The work also included the effect of top flange loading. The authors proposed an increase of the effective length by a factor of 1.2 to account for the buckling stress reduction induced by top flange loading.

Nethercot and Rockey (1971) proposed a generalized lateral torsional buckling solution for beams subjected to various load distributions and end support conditions. The effect of load height effect was captured by introducing coefficients into the critical moment equation.

JingPing et al. (1988) adopted the Rayleigh-Ritz method to approximately evaluate the inelastic lateral torsional buckling capacity of simply supported beam-columns subjected to two symmetric transverse concentrated loads. The solution accounted for the effect of load height as well as residual stresses typical of wide welded flange sections. The authors concluded that the load height can affect the inelastic lateral torsional buckling capacity by as much as 26%.

Helwig et al. (1997) conducted a shell-based parametric FEA study to investigate the effects of the moment gradient and load height on the critical moment of mono-symmetric laterally unsupported beam. Based on their parametric study, the authors developed a modified moment gradient expression which captures the load height effect.

Samanta and Kumar (2006) conducted a parametric study based on the ABAQUS S8R5 shell element to investigate the effect of span to height ratio and the mono-symmetry parameter on the elastic distortional buckling capacity of simply supported beams with mono-symmetric sections. Loading cases investigated were: uniform sagging moments, distributed loads and mid-span point loads acting at top and bottom flanges. The results from this study showed that the buckling capacity of the beam significantly increases as the loads are moved towards the bottom flange.

Yura et al. (2008) developed an expression for the global elastic lateral critical buckling moment capacity for twin girders subjected to uniform moments. An FEA model based on the 8-node shell element in ANSYS was developed for the twin-beam system. Three loading conditions were investigated: uniformly distributed load, point load and uniform moments. Doubly symmetric and singly symmetric sections were investigated. The results from this study show that, for twin-beam systems, load height effects can be ignored when estimating the lateral buckling capacity of doubly symmetric sections as the difference in critical moments between top and bottom flange loading is less than 5%. However, for singly symmetric sections, load height effects could induce a difference of 15% when the smaller flange is under compression.

White and Kim (2008) conducted a reliability analysis to assess the validity of AASHTO (2004) and AISC (2005) lateral torsional buckling provisions against moment gradients as obtained from a large experimental database. The procedures were found conservative for

mid-span loads acting at or above the mid-height but un-conservative for loads acting below mid-height.

Mohebkhah (2010) investigated the load height effect on the inelastic lateral torsional buckling of I-beams based a shell FEA model using the ANSYS software. The study focused on simply supported beams. The plastic effects were idealized using an elasto-plastic constitutive model based on the J2 plasticity with bilinear isotropic hardening. Residual stress effects were neglected. The study investigated the effect of moment gradient and load height effects on the inelastic lateral torsional buckling capacity of steel beams. The gradient factors predicted by the FEA were found to agree with the AISC-LRFD (AISC 360-05) only for long-span beams. For shorter beams, the AISC-LRFD moment gradient factors were found to be higher than those based on the FEA model.

Morkhade et al. (2013) developed a nonlinear FEA model based on the shell element SHELL 43 in ANSYS for the inelastic buckling analysis of monosymmetric steel beams subjected to uniformly distributed loads and mid-span point loads. The effects of beam span, cross-section monosymmetry, and load height on buckling resistance were investigated. Results show that the lateral buckling capacity for beams loaded at the bottom flange is always higher than beams with shear center and top flange loading.

Wong et al. (2015) presented a review of previous numerical solutions for estimating lateral torsional buckling capacity of beams with top-flange loading effects. The authors classified previous design solutions into three types: a) The effective length method, b) the overall coefficient method, and c) other methods. Comparisons were made against experimental results from White and Kim (2008). The authors concluded that the methods by Clark and Hill (1961) and Nethercot and Rockey (1971) resulted in better agreement with experimental results but were limited to few loading cases. They proposed conservative length factors for a variety of loading scenarios for simply supported beams.

The above studies showed that the LTB resistance decreases as the point of load application moves upwards. Also, Mohebkhah (2010) observed that load height effect tends to increase as the span decreases.

2.3 Studies on effect of lateral bracing

2.3.1 Effect of Bracing flexibility

Flint (1951) investigated analytically and experimentally the critical moments of simply supported beams with intermediate lateral braces, subjected to mid-span point load and uniform moments. The study formulated the equilibrium conditions based on the stationarity condition of the total potential energy. The study neglected warping effects. Lateral bracing was observed to significantly increase the buckling capacity when applied above the shear center. Satisfactory agreement was reported between the analytical and experimental solutions.

Winter (1960) proposed a threshold stiffness for intermediate braces in simply supported columns by introducing fictitious hinges at brace locations. He extended the solution to beams laterally braced by discrete flexible restraint by idealizing the compression zone of the beam as a column.

Lay et al. (1963) obtained closed form solutions for the non-dimensional buckling capacity of rectangular beams subject to uniform moments with mid-span brace at a height offset from the shear centre. The authors reported that the bracing stiffness increases the buckling capacity up to a point, after which no increase in capacity is observed.

Nethercot et al. (1972) developed an FEA model for the lateral torsional buckling capacity of simply supported beams with a central elastic lateral support subjected to uniform moments. Results showed that as the brace magnitude increases, the LTB capacity increases up to a threshold stiffness, after which the LTB capacity does not increase. As the torsional parameter (defined as the Saint Venant to the warping stiffness) increases, the warping effect becomes negligible and the results were found to approach the solution of Flint (1951).

2.3.2 Combined effect of bracing height and flexibility

Mutton and Trahair (1973) developed the lateral torsional buckling governing equations for simply supported I-beams with mid-span lateral and torsional restraints. Uniform moments and mid-span point loads were investigated. Numerical results showed that the critical load increases with brace stiffness and changes the buckling mode from symmetric to anti-symmetric at a threshold bracing stiffness. The threshold stiffness for fully effective

lateral bracing was found to be smaller when the brace is located at the top flange. In some cases where the brace is located below the shear center, a full bracing condition was found unachievable. The authors suggested that a combination of lateral and twisting brace would be an effective means of achieving a full bracing condition.

Wong-Chung and Kitipornchai (1987) conducted an experimental study to investigate the inelastic lateral torsional buckling of simply supported beams with two concentrated loads acting at quarter points and applied at the shear centre. Intermediate discrete flexible lateral and torsional braces were provided at the sections of load application, as well as at mid-span brace. Three types of braces were considered at mid-span: bottom flange lateral bracing, shear centre lateral bracing, and twisting bracing. Test results showed that lateral bracing at shear center is more effective than bottom flange bracing in increasing the inelastic lateral torsional buckling capacity

Based on beam buckling analysis, Wang et al. (1987) determined the buckling capacity of mono-symmetric cantilevers with eccentric vertical load and discrete lateral brace offset from the shear center. The solution was based on the Rayleigh quotient. Results showed that lateral bracing is comparatively less effective in increasing the critical moment than torsional or combined lateral-torsional bracing. Bracing near the tension flange was found to lead to a higher lateral buckling capacity than shear centre or bottom flange bracing. Also, the LTB capacity for shear centre loading was observed to be larger that top flange loading.

Tong and Chen (1988) developed the differential equations of equilibrium for mono-symmetric beams with mid-span flexible lateral and torsional bracing that were offset from shear center, and subjected to uniform moments. Closed form solutions were provided for the threshold bracing stiffness and critical buckling moments.

Samanta and Kumar (2008) developed an FEA model for mono-symmetric cantilever I-beams based on the S8R5 shell element in ABAQUS with subjected to point loading and uniformly distributed loading and three lateral braces. For long beams, the top flange bracing was found to be more effective than bottom flange bracing and corresponds to a significant increase in buckling capacity. Bracing both flanges was reported to be most effective in increasing the LTB capacity. For short beams, lateral bracing at top or bottom flanges was found to be only moderately effective in increasing the LTB capacity. The

authors attributed this phenomenon to distortional effects which are comparatively low for long span beams but significant in short span beams.

2.4 Combined effect of load and bracing heights

Schmidt (1965) used Timoshenko's method to develop the equilibrium equation for beams with end torsional restraints and a central lateral brace and subjected to mid-span point load, both acting at the same position. The study provided the critical load as a function of the brace/load height, and lateral brace stiffness. The effect of warping was neglected in the study. Two possible buckling modes were identified: symmetric and anti-symmetric. The buckling capacity corresponding to the symmetric mode was observed to increase with the central brace stiffness while that based on the symmetric mode was observed to be independent from the brace/load height and lateral brace stiffness.

Kitipomchai et al. (1984) developed the differential equations of equilibrium for lateral torsional buckling of cantilever I-beams with an intermediate restraint. Using the finite integral method, the study investigated the effect of brace location along the span, load height positions, loading types beam parameter on the buckling capacity. Results have shown that (a) the lateral bracing beneficial effect is greatest for beams with high slenderness parameter and (b) torsional bracing is more effective than lateral bracing in increasing the lateral torsional capacity. Combined lateral and torsional brace are most effective in increasing LTB capacity. Results also showed that the buckling capacity is higher when braces are located at the top face at the section where loading is applied. The numerical results were in very good agreement with experimental results.

In a conceptual study, Yura (2001) extended the concepts of column buckling to beam lateral torsional buckling. Beam buckling resistance was shown to increase with brace stiffness and buckles in a symmetric mode. After reaching a threshold stiffness for the brace, beam buckling capacity was shown to remain constant while buckling in an anti-symmetric full sine wave buckling mode. Centroidal bracing was reported to be ineffective for top flange loading since there is virtually no lateral displacement near the centroid for top flange loading. The study provided sample results for the characteristics of the LTB behaviour of braced beams with eccentric loading.

McCann (2013) developed a closed form solution for determining critical moments and threshold brace stiffness for simply supported doubly symmetric I-beams with an arbitrary number of equally spaced discrete linearly elastic braces. The solution was based on the stationarity of the total potential energy of the system and is restricted to equidistant bracing and uniform moments._Two assumed displacement functions were considered: (a) an approximate single harmonic displacement function, and (b) a Fourier series representation of the displacement functions. The single harmonic representation was shown to overestimate the critical moment compared to the complete Fourier series solution.

2.5 Conclusions:

The large number of studies on load height effect reported in Section 2.2 suggests that the load height effect has been heavily researched. Relatively fewer studies focused on the effect of lateral bracing (Section 2.3) while only a few studies have considered the combined effect of load and bracing heights (Section 2.4). These few studies have various limitations. For example, the solution of Schmidt (1965) assumes the load height to coincide with the bracing height and neglects the warping contribution. The study of Kitipomchai et al. (1984) is limited to cantilevers. The study of Yura (2001) is conceptual and did not attempt to generalize the findings to other loading cases and beam cross-section. The study of McCann (2013) is limited to uniform moments. Within this context, chapters 3 and 4 develop more comprehensive models and provide simplified design equations which capture the effect of warping, load height and mid-span bracing height on the LTB capacity of simply supported wooden beams. The models are based on Fourier decompositions of the buckling displacement fields and pre-buckling moments. The methodology establishes a mathematical basis to understand and quantify the characteristics of symmetric and anti-symmetric buckling modes and their dependence on bracing height and stiffness.

References:

[1] Austin WJ, Yegian S and Tung TP (1955), Lateral buckling of elastically end-restrained I-beams, Transactions of the American Society of Civil Engineers, 122(1), 374-388

[2] Andrade A and Camotim D (2005), Lateral-torsional buckling of singly symmetric tapered beams: theory and applications, Journal of engineering mechanics, 131, 586-597

[3] Andrade A, Camotim D and Dinis PB (2007), Lateral-torsional buckling of singly symmetric web-tapered thin-walled I-beams:1D model vs. shell FEA, Computers and Structures, 85, 1343-1359

[4] Erkmen RE and Mohareb M (2008), Buckling analysis of thin-walled open members-A finite element formulation, Thin-Walled Structures, doi:10.1016/j.tws.2007.12.002

[5] Flint AR (1951), the influence of restraints on the stability of beams, The Structural Engineer, 29(9), 235-246

[6] Helwig T, Frank K and Yura J (1997), Lateral-torsional buckling of singly symmetric I-beams, Journal of Structural Engineering, 123(9), 1172-1179

[7] Ings NL and Trahair NS (1987), Beam and column buckling under directed loading, Journal of Structural Engineering, 113(6), 1251-1263

[8] Jingping L, Zaitian G and Chen S (1988), Buckling of transversely loaded I-Beam columns, Journal of Structural Engineering, 114(9), 2109-2118

[9] Kerensky OA, Flint AR, and Brown WC (1956), The basis for design of beams and plate girders in the revised British Standard 153, In Proceedings of the Institution of Civil Engineers, 5(3), 396–461

[10] Kitipomchai S, Dux PF and Richter NJ. (1984), Buckling and bracing of cantilevers, Journal of Structural Engineering, 110(9), 2250-2262

[11] Lamb AW and Eamon CD (2015), Load height and moment factors for doubly symmetric wide flange beams, Journal of Structural Engineering, 10.1061/(ASCE)ST.1943-541X.0001332, 04015069

[12] Lay MG, Galambos TV and Schmidt LC (1963), Lateral bracing force of steel I beams, Journal of Engineering Mechanics Division, 89(EM3), 217-224

[13] McCann F, Wadee MA and Gardner L (2013), Lateral stability of imperfect discretely braced steel beams, Journal of Engineering Mechanics, 139(10), 1341-1349

[14] Mohebkhah A (2010), Lateral buckling resistance of inelastic I-beams under off-shear center loading, Thin-walled Structure, 49(3), 431-436

[15] Mohri F and Potier-Ferry M (2006), Effects of load height application and pre-buckling deflection on lateral buckling of thin-walled beams, Steel and Composite Structures, 6(5), 1-15

[16] Morkhade SG and Gupta LM (2013), Effect of load height on buckling resistance of steel beams, Procedia Engineering, 51, 151-158

[17] Mutton BR and Trahair NS (1973), Stiffness requirement for lateral bracing, Journal of the structural division, 99(10), 2167-2182

[18] Nethercot DA and Rockey KC (1971), A unified approach to the elastic lateral buckling of beams, The Structural Engineer, 49(7), 321-330

[19] Nethercot DA and Rockey KC (1972), The lateral buckling of beams having discrete intermediate restraints, The Structural Engineer, 50(10), 391-403

[20] Pi YL, Traihair NS and Rajasekaran S (1992), Energy equation for beam lateral buckling, Journal of Structural Engineering, 118(6), 1462-1479

[21] Prescott J and Carrington H (1920), The Buckling of deep beams, Philosophical Magazine Series 6, 39(230), 194-233

[22] Pettersson O (1952), Combined bending and torsion of I-beams of monosymmetrical cross section, Bulletin No.10, Division of Building Statics and Structural Engineering, Royal Institute of Technology, Stockholm, Sweden

[23] Schmidt LC (1965), Restraints against elastic lateral buckling, Journal of Engineering Mechanics Division, 91(EM6), 1-10

[24] Schrader RK (1941), Discussion of paper by G. Winter, Transactions of the American Society of Civil Engineers, 108(1), 260-268

[25] Sahraei A, Wu L and Mohareb M (2015), Finite element formulation for lateral torsional buckling analysis of shear deformable mono-symmetric thin-walled members, Thin-Walled Structures, 89, 212-226

[26] Samanta A and Kumar A (2006), Distortional buckling in monosymmetric I-beams, Thin-Walled Structures, 44(1), 51-56

[27] Samanta, A, Kumar, A. (2008), Distortional buckling in braced-cantilever I-beams, Thin-Walled Structures, 46(6), 637-645

[28] Timoshenko S, Theory of elastic stability, McGraw-Hill Book Company, Inc., New York (1936)

[29] Trahair NS (2013), Bending and buckling of tapered steel beam structures, Engineering Structures, 59, 229-237

[30] Tong GS and Chen SF (1988), Buckling of laterally torsionally braced beams. Journal of Constructional Steel Research, 11(1), 41-55

[31] Winter G (1941), Lateral stability of unsymmetrical I-beams and trusses in bending, Transactions of the American Society of Civil Engineers, 108(1), 247-260

[32] Winter G (1960), Lateral bracing of columns and beams, Transactions of the American Society of Civil Engineers, 125 (1), 807-826

[33] White DW and Kim YD (2008), Unified Flexural Resistance Equations for Stability Design of Steel I-Section Members: Moment Gradient Tests, Journal of Structural Engineering, 134(9), 1450-1470

[34] Wang CM, Kitrporncha S and Thevendran V (1987), Buckling of braced monosymmetric cantilevers. Int. J. Mech. Sci. 29(5), 321-337

[35] Wong-Chung AD and Kitipomchai S (1987), Partially braced inelastic beam buckling experiments, Journal of Constructional Steel Research, 7(3), 189-211

[36] Wong E, Driver RG and Heal TW (2015), Simplified approach to estimating the elastic lateral–torsional buckling capacity of steel beams with top-flange loading, Canadian Journal of Civil Engineering, 42(2), 130-138

[37] Wu L and Mohareb M (2010), Buckling formulation for shear deformable thin-walled members-II. Finite element formulation, Thin-walled structures, doi:10.1016/j.tws.2010.09.026

[38] Yura JA (2001), Fundamental of Beam Bracing, Engineering Journal, Engineering Journal, 38(1), 11-26

[39] Yura J, Helwig TA and Zhou C (2008), Global lateral buckling of I-shaped girder system, Journal of Structural Engineering, 134(9), 1487-1494

3. LATERAL TORSIONAL BUCKLING OF WOODEN BEAMS WITH MID-SPAN RIGID LATERAL BRACING OFFSET FROM SECTION MID-HEIGHT

Abstract:

An energy based solution is developed for the lateral torsional buckling analysis of wooden beams with a mid-span lateral brace subjected to uniformly distributed loads or mid-span point load. The predicted critical moments and mode shapes are shown to agree with results based on three dimensional finite element analysis. The study indicates that beams are prone to two buckling patterns; a symmetric mode and an anti-symmetric mode. Whether the symmetric or the anti-symmetric mode governs the critical moment capacity is shown to depend on the bracing height. A technique is then developed to determine the threshold bracing height required to maximize the critical moment. A parametric study is then conducted to investigate the effect of lateral bracing and load height effects on the critical moments. Simple design equations are developed to predict critical moments for a practical range of cases. The limitations of the simplified procedure are discussed. For cases outside the scope of the simplified procedure, designers are recommended to adopt the more detailed energy based solution. Design examples are provided to illustrate the merits and applicability of the proposed procedure in practical situations.

Keywords:

Lateral torsional buckling, lateral bracing, load height, bracing height, simplified design equations

3.1 Introduction and Literature review

Lateral torsional buckling (LTB) is a failure mode frequently governing the capacity of long span laterally unsupported wood beams. The LTB resistance of such beams is known to be influenced by the load height effect and by the presence of lateral bracing provided by adjoining members. In practical design, such beams may be laterally restrained at mid-span with braces offset from the section mid-height. Wood design recommendations (e.g., AFPA 2003) and structural steel standards (e.g., CAN-CSA S16 2014, AS4100 1998, Eurocode 2005, AISC 2010) account for the effect of load height and presence of lateral bracing systems, either through the effective length approach, the equivalent moment factor approach, or other approximate methods. However, no recommendations are provided to account for the influence of bracing heights. Within this context, the present study investigates the combined effect of load height and bracing height on the lateral torsional buckling capacity of simply supported wood beams.

3.1.1 Load height effect

The load height effect for various support conditions has been investigated in older studies by Prescott and Carrington (1920), Timoshenko (1936), Winter (1941), Schrader (1941), Austin et al. (1955), Pettersson et al. (1952). Kerensky et al. (1956) developed a solution that captures the effect of top flange loading for beams by introducing the effective length approach. Nethercot and Rockey (1971) accounted for the load height effect for simply supported beams by introducing design coefficients in critical moment equations. Based on the Rayleigh-Ritz method, JingPing et al. (1988) evaluated the inelastic LTB capacity of beam-columns subjected to two symmetric transverse loads. Helwig et al. (1997) and Samanta and Kumar (2006) investigated the load height effect by conducting a shell-based FEA for mono-symmetric beams. A few studies investigated cases involving top flange, mid-height and bottom flange loading: Yura et al. (2008) developed an expression for the elastic critical moment for twin girders with doubly symmetric and singly symmetric cross sections. White and Kim (2008) conducted experiments to verify LTB predictions in AASHTO (2004) and AISC (2005). Mohebkhah (2010) developed an FEA model to investigate inelastic LTB capacity of simply supported I-beams. Wong et al. (2015) compared previous design recommendations with experimental results of White and Kim

(2008) and extended the effective length factor concept to a variety of loading scenarios for simply supported beams. While the above studies were primarily aimed at examining the load height effect on LTB resistance, the topic has been partly investigated in various investigations such as Ings and Trahair (1987), Pi et al. (1992), Andrade and Camotim (2005), Mohri and Potier-Ferry (2006), Andrade et al. (2007), Erkmen and Mohareb (2008), Wu and Mohareb (2010), Trahair (2013), Lamb and Eamon (2015), Sahraei et al. (2015), and Sahraei and Mohareb (2016). A common observation in the above studies is that the elastic and inelastic LTB resistances for beams decrease as the point of application of loads induced by gravity moves upwards.

3.1.2 Lateral restraint effect

The effect of continuous rigid lateral top-flange bracing on the LTB analysis of simply supported beams was investigated by Park et al. (2004) by developing a FEA model. A comparison of the results has shown that the moment gradient factor equation of Yura (1993) leads to un-conservative results for uniformly distributed loads. For such cases, Park et al. (2004) proposed supplementary design equations. Samanta and Kumar (2008) developed a FEA model for the LTB analysis of mono-symmetric cantilever I-beams with three types of rigid lateral braces at top flange, bottom flange, and both flanges. For long span beams, top flange bracing was found to be more effective than bottom flange bracing and corresponded to a significant increase in buckling capacity. Bracing both flanges was reported to be most effective in increasing the LTB capacity. For short span beams, lateral bracing at top and bottom flanges was found to be only moderately effective.

Several experimental and analytical studies have investigated the effect of flexible lateral restraint on the LTB capacity (e.g. Flint, 1951). In the above studies, top flange lateral bracing was observed to significantly increase the LTB resistance of beams when compared to shear centre or bottom flange bracing.

Only a few studies investigated the combined effect of load height and lateral bracing height. Schmidt (1965) analytically and numerically investigated the LTB of beams with central lateral bracing subjected to mid-span point loading. The lateral bracing point coincided with the loading point and both were assumed to be offset from the shear centre. Kitipomchai et al. (1984) investigated the LTB of cantilever I-beams with offset intermediate restraint and vertical loads. Wang et al. (1987) numerically determined the

LTB capacity of mono-symmetric cantilevers with eccentric vertical loading and discrete lateral bracing offset from the shear centre. Both studies (Kitipomchai, 1984 and Wang et al., 1987) did not specifically address the benefits of bracing height. McCann et al. (2013) investigated simply supported beams with doubly symmetric I sections subjected to uniform moments with discrete equally spaced eccentric linearly elastic braces. In the study, the lateral bracing point was assumed to coincide with the loading point and the warping effect was omitted. The study did not investigate the load height effect. Within this context, the present study investigates the combined effect of bracing height and load height on the elastic LTB capacity of wooden beams with emphasis on: (a) developing a mathematical model able capture the important characteristics of the solution, (b) investigating the effect of bracing height on the LTB capacity and mode shapes, (c) conducting a parametric study to investigate the effects of key parameters on the LTB resistance, and (d) developing simplified equations for bracing height requirement and corresponding critical moments.

3.2 Statement of the Problem

A wooden beam with a doubly symmetric cross-section is simply supported relative to the vertical and lateral displacements and twist at both ends. The beam is subjected to a reference distributed load $q(z)$ offset from the section mid-height axis by a height a taken as positive when the load is above the section mid-height. A mid-span lateral brace offset from the section mid-height is provided at a height b taken as positive when above the section mid-height (Fig 3.1). The reference loads $q(z)$ are assumed to increase to reach a critical value $\lambda q(z)$ where the system becomes in a neutral state of stability, at which it has a tendency to undergo lateral torsional buckling without further increase in loading. It is required to determine the critical load magnitude $\lambda q(z)$ at the onset of buckling.

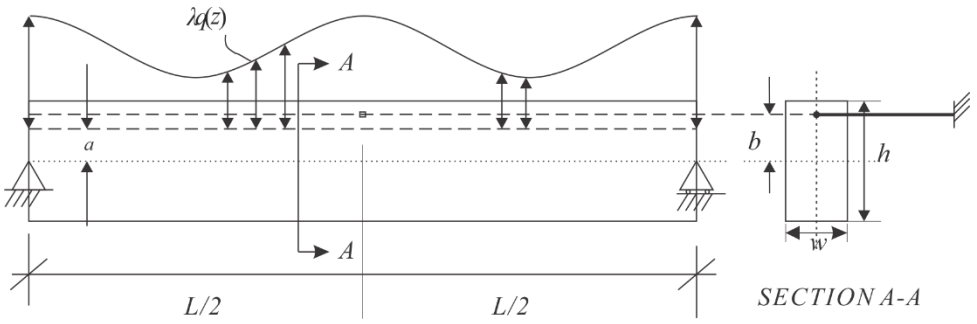

Figure 3.1 Load height and brace effect

3.3 Assumptions

The following assumptions are made

1. The material is linearly elastic and orthotropic. Given that properties of wood in the tangential and radial directions are nearly equal (FPL, 2010), the nine orthotropic constitutive constants are shown to reduce to six (Xiao 2014). Also, based on a 3D finite element buckling analysis, Xiao (2014) has shown that only two constitutive properties are influential on the elastic lateral buckling resistance: the longitudinal Young's modulus E and the shear modulus G for shear stresses on the normal plane acting either in the radial or tangential directions. Thus, the present study characterizes the constitutive behaviour of wood using only constants E and G in a manner similar to isotropic materials.
2. Load distribution is symmetric about the beam mid-span.
3. The direction of applied load is constant (i.e., conservative loading), and

3.4 Formulation

3.4.1 Variational Principle

The total potential energy $\pi = U + V$ is the summation of the internal strain energy U and the load potential energy gained V. The internal strain energy U is given by (e.g., Trahair 1993)

$$U = \frac{1}{2}\int_0^L EI_{yy}u''^2 dz + \frac{1}{2}\int_0^L GJ\theta'^2 dz + \frac{1}{2}\int_0^L EC_w\theta''^2 dz \qquad (5.1)$$

where $u = u(z)$ is lateral displacement, $\theta = \theta(z)$ is the twist angle, both being functions of the longitudinal coordinate z, L is the span, E is Young's modulus, I_{yy} is the weak moment of inertia, G is shear modulus, J is the Saint-Venant torsional constant, and C_w

is the warping constant. The load potential energy gained by the load V consists of two components $V = V_1 + V_2$ and is given by (e. g., Trahair 1993)

$$V_1 = \lambda \int_0^L M(z)\theta u'' dz, \quad V_2 = -\frac{\lambda}{2}\int_0^L q(z) a\theta^2 dz \qquad (5.2)\text{a,b}$$

where V_1 is the load potential energy gained by the strong axis bending moments $M = M(z)$ induced by the transverse loads, undergoing lateral displacements $u(z)$ and angle of twist $\theta(z)$ and V_2 is the load potential gained by the distributed load $q(z)$ acting at a distance a above the section mid-height undergoing an angle of twist $\theta(z)$ and λ is a load multiplier to determined based on a buckling analysis.

3.4.2 Assumed Displacement Functions

The displacement functions are assumed to take the form

$$u(z) = \left(\sum_{i=1}^{2n} A_i \sin \frac{i\pi z}{L} \right) + A_{2n+1} \sin \frac{(2n+1)\pi z}{L} \qquad (5.3)$$

$$\theta(z) = \sum_{j=1}^{2n} B_j \sin \frac{j\pi z}{L} \qquad (5.4)$$

The above displacement functions meet the essential and natural boundary conditions $u(0) = u''(0) = u(L) = u''(L) = 0$ and $\theta(0) = \theta''(0) = \theta(L) = \theta''(L) = 0$. The presence of a mid-span lateral brace at a height b above section mid-height provides a kinematic constraint between the displacement $u(L/2)$ and the angle of twist $\theta(L/2)$ at beam mid-span. From Fig 3.2, one obtains the kinematic constraint $u(L/2) = -\theta(L/2)b$. From Eqs. (5.3) and (5.4) by setting $z = L/2$, and substituting into the kinematic constraint equation, one can express constant A_{2n+1} in terms of the remaining constants A_i, B_i ($i = 1,..n$) as $A_{2n+1} = -\sum_1^{2n} (-1)^n (A_i + bB_i) \sin(i\pi/2)$. Then, from the expression for A_{2n+1} , by substituting into Eq.(5.3), one obtains

$$u(z)=\sum_{i=1}^{2n}A_i\left[\sin\frac{i\pi z}{L}+(-1)^{n+1}\sin\frac{i\pi}{2}\sin\frac{(2n+1)\pi z}{L}\right]+b\sum_{i=1}^{2n}B_i(-1)^{n+1}\sin\frac{i\pi}{2}\sin\frac{(2n+1)\pi z}{L} \tag{5.5}$$

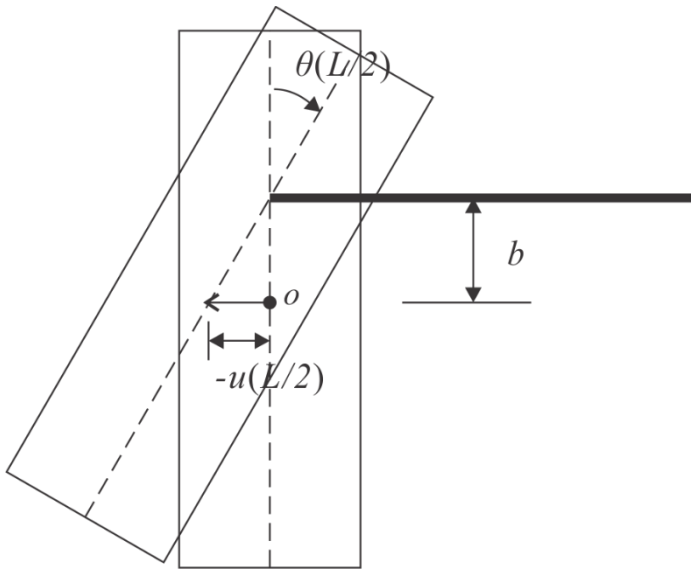

Figure 3.2 Beam cross section at mid-span

3.4.3 Internal Strain Energy

From Eqs. (5.4) and (5.5), by substituting into the internal strain energy expression given in Eq.(5.1), one obtains

$$U=\frac{1}{2}\left\langle \mathbf{A_a}^{\mathbf{T}} \quad \mathbf{A_b}^{\mathbf{T}} \right\rangle \begin{bmatrix} \mathbf{k}_1 & \mathbf{0} \\ \mathbf{0} & \mathbf{k}_2 \end{bmatrix} \begin{Bmatrix} \mathbf{A}_a \\ \mathbf{A}_b \end{Bmatrix} \tag{5.6}$$

where

$$\mathbf{A}_{a\ 1\times 2n}^{\mathbf{T}}=\langle A_2 \quad B_2 \quad A_4 \quad B_4 \quad \cdots \quad A_{2n} \quad B_{2n}\rangle,$$

$$\mathbf{A}_{b\ 1\times 2n}^{\mathbf{T}}=\langle A_1 \quad B_1 \quad A_3 \quad B_3 \quad \cdots \quad A_{2n-1} \quad B_{2n-1}\rangle,$$

$$\mathbf{k}_1=\begin{bmatrix} \mathbf{m}_{1,1} & \mathbf{m}_{1,3} & \cdots & \mathbf{m}_{1,2i-1} & \cdots & \mathbf{m}_{1,2n-1} \\ \mathbf{m}_{3,1} & \mathbf{m}_{3,3} & \cdots & \mathbf{m}_{3,2i-1} & \cdots & \mathbf{m}_{3,2n-1} \\ \vdots & \vdots & \ddots & \vdots & \iddots & \vdots \\ \mathbf{m}_{2j-1,1} & \mathbf{m}_{2j-1,3} & \cdots & \mathbf{m}_{2j-1,2i-1} & \cdots & \mathbf{m}_{2j-1,2n-1} \\ \vdots & \vdots & \iddots & \vdots & \ddots & \vdots \\ \mathbf{m}_{2n-1,1} & \mathbf{m}_{2n-1,3} & \cdots & \mathbf{m}_{2n-1,2i-1} & \cdots & \mathbf{m}_{2n-1,2n-1} \end{bmatrix}, \mathbf{k}_2=\begin{bmatrix} \mathbf{m}_{2,2} & \mathbf{m}_{2,4} & \cdots & \mathbf{m}_{2,2i} & \cdots & \mathbf{m}_{2,2n} \\ \mathbf{m}_{4,2} & \mathbf{m}_{4,4} & \cdots & \mathbf{m}_{4,2i} & \cdots & \mathbf{m}_{4,2n} \\ \vdots & \vdots & \ddots & \vdots & \iddots & \vdots \\ \mathbf{m}_{2j,2} & \mathbf{m}_{2j,4} & \cdots & \mathbf{m}_{2j,2i} & \cdots & \mathbf{m}_{2j,2n} \\ \vdots & \vdots & \iddots & \vdots & \ddots & \vdots \\ \mathbf{m}_{2n,2} & \mathbf{m}_{2n,4} & \cdots & \mathbf{m}_{2n,2i} & \cdots & \mathbf{m}_{2n,2n} \end{bmatrix}$$

$$\mathbf{m_{j,i}} = \begin{bmatrix} m_{1,i,j} & 0 \\ 0 & m_{3,i,j} \end{bmatrix} + b\begin{bmatrix} 0 & m_{2,i,j} \\ m_{2,i,j} & 0 \end{bmatrix} + b^2\begin{bmatrix} 0 & 0 \\ 0 & m_{4,i,j} \end{bmatrix} \tag{5.7}$$

$$\begin{aligned}
m_{1,i,j} &= EI_{yy}\left[\left(\frac{i\pi}{L}\right)^2\left(\frac{j\pi}{L}\right)^2\int_0^L \sin\frac{i\pi z}{L}\sin\frac{j\pi z}{L}dz + \frac{L}{2}\sin\frac{i\pi}{2}\sin\frac{j\pi}{2}\left(\frac{(2n+1)\pi}{L}\right)^4\right] \\
m_{2,i,j} &= \frac{L}{2}EI_{yy}\sin\frac{i\pi}{2}\sin\frac{j\pi}{2}\left(\frac{(2n+1)\pi}{L}\right)^4 \\
m_{3,i,j} &= GJ\left(\frac{i\pi}{L}\right)\left(\frac{j\pi}{L}\right)\int_0^L \cos\frac{i\pi z}{L}\cos\frac{j\pi z}{L}dz + EC_w\left(\frac{i\pi}{L}\right)^2\left(\frac{j\pi}{L}\right)^2\int_0^L \sin\frac{i\pi z}{L}\sin\frac{j\pi z}{L}dz \\
m_{4,i,j} &= \frac{L}{2}EI_{yy}\sin\frac{i\pi}{2}\sin\frac{j\pi}{2}\left(\frac{(2n+1)\pi}{L}\right)^4
\end{aligned} \tag{5.8}$$

3.4.4 Fourier Expansion of bending moments:

A given bending moment $M(z)$ can be expressed in a Fourier series as

$$M(z) = \sum_{k=1,2}^{kmax} m_k \sin\frac{k\pi z}{L} \qquad m_k = \frac{2}{L}\int_0^L M(z)\sin\frac{k\pi z}{L}dz \tag{5.9)a,b}$$

For the case of a mid-span load, the moment distribution is given by $\lambda M(z) = \lambda Qz/2, \quad 0 \le z \le L/2$ and $\lambda M(z) = \lambda Q(L-z)/2, 0 \le z \le L/2$. By substituting into Eq. (5.9)b, one obtains $m_k = 2QL/k^2\pi^2, (k = 1,3,5\ldots)$. For the case of a uniformly distributed load λq , the bending moment expression takes the form $\lambda M(z) = \lambda q(Lz - z^2)/2$. Using the Fourier expansion in Eq.(5.9), one obtains the Fourier coefficients $m_k = 4\lambda qL^2/(k\pi)^3 \qquad (k = 1,3,5\ldots)$

3.4.5 Destabilizing term due to bending moments

From Eqs.(5.4), (5.5) and (5.9)a, by substituting into Eq. (5.2)a, one obtains the load potential energy function

$$V_1 = \frac{\lambda}{2}\left\langle \mathbf{A}_a{}^T \quad \mathbf{A}_b{}^T \right\rangle \begin{bmatrix} \mathbf{k}_{g1} & \mathbf{k}_{g12}^T \\ \mathbf{k}_{g12}^T & \mathbf{k}_{g2} \end{bmatrix} \begin{Bmatrix} \mathbf{A}_a \\ \mathbf{A}_b \end{Bmatrix} \tag{5.10}$$

where

$$\mathbf{k}_{g1}=\begin{bmatrix} \mathbf{n}_{1,1} & \mathbf{n}_{1,3} & \cdots & \mathbf{n}_{1,2i-1} & \cdots & \mathbf{n}_{1,2n-1} \\ \mathbf{n}_{3,1} & \mathbf{n}_{3,3} & \cdots & \mathbf{n}_{3,2i-1} & \cdots & \mathbf{n}_{3,2n-1} \\ \vdots & \vdots & \ddots & \vdots & \iddots & \vdots \\ \mathbf{n}_{2j-1,1} & \mathbf{n}_{2j-1,3} & \cdots & \mathbf{n}_{2j-1,2i-1} & \cdots & \mathbf{n}_{2j-1,2n-1} \\ \vdots & \vdots & \iddots & \vdots & \ddots & \vdots \\ \mathbf{n}_{2n-1,1} & \mathbf{n}_{2n-1,3} & \cdots & \mathbf{n}_{2n-1,2i-1} & \cdots & \mathbf{n}_{2n-1,2n-1} \end{bmatrix}, \mathbf{k}_{g2}=\begin{bmatrix} \mathbf{n}_{2,2} & \mathbf{n}_{2,4} & \cdots & \mathbf{n}_{2,2i} & \cdots & \mathbf{n}_{2,2n} \\ \mathbf{n}_{4,2} & \mathbf{n}_{4,4} & \cdots & \mathbf{n}_{4,2i} & \cdots & \mathbf{n}_{4,2n} \\ \vdots & \vdots & \ddots & \vdots & \iddots & \vdots \\ \mathbf{n}_{2j,2} & \mathbf{n}_{2j,4} & \cdots & \mathbf{n}_{2j,2i} & \cdots & \mathbf{n}_{2j,2n} \\ \vdots & \vdots & \iddots & \vdots & \ddots & \vdots \\ \mathbf{n}_{2n,2} & \mathbf{n}_{2n,4} & \cdots & \mathbf{n}_{2n,2i} & \cdots & \mathbf{n}_{2n,2n} \end{bmatrix}$$

$$\mathbf{K}_{g12}=\begin{bmatrix} \mathbf{n}_{1,2} & \mathbf{n}_{1,4} & \cdots & \mathbf{n}_{1,2i} & \cdots & \mathbf{n}_{1,2n} \\ \mathbf{n}_{3,2} & \mathbf{n}_{3,4} & \cdots & \mathbf{n}_{3,2i} & \cdots & \mathbf{n}_{3,2n} \\ \vdots & \vdots & \ddots & \vdots & \iddots & \vdots \\ \mathbf{n}_{2j-1,2} & \mathbf{n}_{2j-1,4} & \cdots & \mathbf{n}_{2j-1,2i} & \cdots & \mathbf{n}_{2j-1,2n} \\ \vdots & \vdots & \iddots & \vdots & \ddots & \vdots \\ \mathbf{n}_{2n-1,2} & \mathbf{n}_{2n-1.4} & \cdots & \mathbf{n}_{2n-1,2i} & \cdots & \mathbf{n}_{2n-1,2n} \end{bmatrix}, \quad \mathbf{n}_{j,i}=\left[\begin{array}{c|c} 0 & m_{5,i,j} \\ \hline m_{6,i,j} & 0 \end{array}\right]+b\left[\begin{array}{c|c} 0 & 0 \\ \hline 0 & m_{7,i,j} \end{array}\right]$$

(5.11)a-d

$$\begin{aligned} m_{5,i,j} &= -\frac{(j\pi)^2}{L}\beta(j,i,k_{max})+(-1)^n\left(\frac{1}{L}\right)\left[(2n+1)\pi\right]^2\sin\frac{j\pi}{2}\beta(2n+1,i,k_{max}) \\ m_{6,i,j} &= -\frac{(i\pi)^2}{L}\beta(i,j,k_{max})+(-1)^n\left(\frac{1}{L}\right)\left[(2n+1)\pi\right]^2\sin\frac{i\pi}{2}\beta(2n+1,j,k_{max}) \\ m_{7,i,j} &= (-1)^n\left(\frac{1}{L}\right)\left[(2n+1)\pi\right]^2\beta(2n+1,j,k_{max})\sin\frac{i\pi}{2} \\ &\quad +(-1)^n\left(\frac{1}{L}\right)\left[(2n+1)\pi\right]^2\beta(2n+1,i,k_{max})\sin\frac{j\pi}{2} \end{aligned} \tag{5.12}$$

where

$$\beta(i,j,k_{max})=\frac{1}{L}\int_0^L\sum_{k=1,2}^{kmax}m_k\sin\frac{i\pi z}{L}\sin\frac{j\pi z}{L}\sin\frac{k\pi z}{L}dz \tag{5.13}$$

3.4.5.1 Special considerations for symmetric loading

For loading symmetric with respect to $z=L/2$, bending moments are symmetric and Eq. (5.9) yields

$$M(z)=\sum_{k=1,3,5}^{kmax}m_k\sin\frac{k\pi z}{L} \tag{5.14}$$

where k takes only the values 1,3,5… When one of i, j is odd and the other is even, matrix $\mathbf{n}_{j,i}$ as defined in Eq. (5.11) can be shown to vanish. This is the case since function $\sin(i\pi z/L)\sin(j\pi z/L)$ is anti-symmetric with respect to $z = L/2$ and $\sum_{k=1,2}^{k_{max}} m_k \sin(i\pi z/L)\sin(j\pi z/L)\sin(k\pi z/L)$ in Eq. (5.13) is also anti-symmetric and

$$\beta(i, j, k_{max}) = \frac{1}{L}\int_0^L \sum_{k=1,2}^{k_{max}} m_k \sin\frac{i\pi z}{L}\sin\frac{j\pi z}{L}\sin\frac{k\pi z}{L}dz = 0 \tag{5.15}$$

Also, for the case where one of i, j is odd and the other is even, one can show that

$$\sin\frac{j\pi}{2}\beta(2n+1, i, k_{max}) = \sin\frac{i\pi}{2}\beta(2n+1, j, k_{max}) = 0 \tag{5.16}$$

From Eq. (5.15) and (5.16) by substituting into Eq.(5.12), one has $\mathbf{n}_{j,i} = \mathbf{0}$ when one of i, j is odd and the other is even and thus $\mathbf{k}_{g12} = \mathbf{0}$, and Eq. (5.10) takes the form

$$V_1 = \frac{\lambda}{2}\left\langle \mathbf{A}_a{}^T \quad \mathbf{A}_b{}^T \right\rangle \begin{bmatrix} \mathbf{k}_{g1} & \mathbf{0} \\ \mathbf{0} & \mathbf{k}_{g2} \end{bmatrix} \begin{Bmatrix} \mathbf{A}_a \\ \mathbf{A}_b \end{Bmatrix} \tag{5.17}$$

3.4.6 Destabilizing term due to load height effect

3.4.6.1 Case1- Mid-span load offset from section mid-height

A mid-span point load λQ can be mathematically expressed as $\lambda q(z) = \lambda Q\delta(z - L/2)$ where δ is the Dirac Delta function. If the load is acting at a distance a above the section mid-height, the load potential energy gain V_2 as determined from in Eq. (5.2)b takes the form

$$V_2 = -\frac{\lambda}{2}\int_0^L Q\delta\left(z - \frac{L}{2}\right)a\theta(z)^2\,dz = -\frac{\lambda}{2}Qa\theta\left(\frac{L}{2}\right)^2 = -\frac{\lambda}{2}Qa\sum_{i=1,2}^{2n}\sum_{j=1,2}^{2n} B_i B_j \sin\left(\frac{i\pi}{2}\right)\sin\left(\frac{j\pi}{2}\right) \tag{5.18}$$

In a matrix form, V_2 can be expressed as

$$V_2 = \frac{\lambda}{2}\left\langle \mathbf{A}_a{}^T \quad \mathbf{A}_b{}^T \right\rangle \begin{bmatrix} \mathbf{k}_{g3} & \mathbf{k}_{g34} \\ \mathbf{k}_{g34}^T & \mathbf{k}_{g4} \end{bmatrix} \begin{Bmatrix} \mathbf{A}_a \\ \mathbf{A}_b \end{Bmatrix} \tag{5.19}$$

where

$$\mathbf{k}_{g3} = Qa \begin{bmatrix} \mathbf{r}_{1,1} & \mathbf{r}_{1,3} & \cdots & \mathbf{r}_{1,2i-1} & \cdots & \mathbf{r}_{1,2n-1} \\ \mathbf{r}_{3,1} & \mathbf{r}_{3,3} & \cdots & \mathbf{r}_{3,2i-1} & \cdots & \mathbf{r}_{3,2n-1} \\ \vdots & \vdots & \ddots & \vdots & \iddots & \vdots \\ \mathbf{r}_{2j-1,1} & \mathbf{r}_{2j-1,3} & \cdots & \mathbf{r}_{2j-1,2i-1} & \cdots & \mathbf{r}_{2j-1,2n-1} \\ \vdots & \vdots & \iddots & \vdots & \ddots & \vdots \\ \mathbf{r}_{2n-1,1} & \mathbf{r}_{2n-1,3} & \cdots & \mathbf{r}_{2n-1,2i-1} & \cdots & \mathbf{r}_{2n-1,2n-1} \end{bmatrix}, \mathbf{k}_{g4} = Qa \begin{bmatrix} \mathbf{r}_{2,2} & \mathbf{r}_{2,4} & \cdots & \mathbf{r}_{2,2i} & \cdots & \mathbf{r}_{2,2n} \\ \mathbf{r}_{4,2} & \mathbf{r}_{4,4} & \cdots & \mathbf{r}_{4,2i} & \cdots & \mathbf{r}_{4,2n} \\ \vdots & \vdots & \ddots & \vdots & \iddots & \vdots \\ \mathbf{r}_{2j,2} & \mathbf{r}_{2j,4} & \cdots & \mathbf{r}_{2j,2i} & \cdots & \mathbf{r}_{2j,2n} \\ \vdots & \vdots & \iddots & \vdots & \ddots & \vdots \\ \mathbf{r}_{2n,2} & \mathbf{r}_{2n,4} & \cdots & \mathbf{r}_{2n,2i} & \cdots & \mathbf{r}_{2n,2n} \end{bmatrix}$$

$$\mathbf{k}_{g34} = Qa \begin{bmatrix} \mathbf{r}_{1,2} & \mathbf{r}_{1,4} & \cdots & \mathbf{r}_{1,2i} & \cdots & \mathbf{r}_{1,2n} \\ \mathbf{r}_{3,2} & \mathbf{r}_{3,4} & \cdots & \mathbf{r}_{3,2i} & \cdots & \mathbf{r}_{3,2n} \\ \vdots & \vdots & \ddots & \vdots & \iddots & \vdots \\ \mathbf{r}_{2j-1,2} & \mathbf{r}_{2j-1,4} & \cdots & \mathbf{r}_{2j-1,2i} & \cdots & \mathbf{r}_{2j-1,2n} \\ \vdots & \vdots & \iddots & \vdots & \ddots & \vdots \\ \mathbf{r}_{2n-1,2} & \mathbf{r}_{2n-1.4} & \cdots & \mathbf{r}_{2n-1,2i} & \cdots & \mathbf{r}_{2n-1,2n} \end{bmatrix}, \quad \mathbf{r}_{j,i} = \begin{bmatrix} 0 & 0 \\ 0 & \sin\frac{i\pi}{2}\sin\frac{j\pi}{2} \end{bmatrix} \tag{5.20}$$

when either of i, j are even and the other is odd, the expression $\sin(i\pi/2)\sin(j\pi/2)$ vanishes. In this case, matrix $\mathbf{k}_{g34}$ vanishes and

$$V_2 = \frac{\lambda}{2}\left\langle \mathbf{A}_a{}^T \quad \mathbf{A}_b{}^T \right\rangle \begin{bmatrix} \mathbf{k}_{g3} & \mathbf{0} \\ \mathbf{0} & \mathbf{k}_{g4} \end{bmatrix}_{(1)} \begin{Bmatrix} \mathbf{A}_a \\ \mathbf{A}_b \end{Bmatrix} \tag{5.21}$$

3.4.6.2 Case2- Uniformly Distributed load offset from section mid-height

For the case of uniformly distributed load applied at height a above the section mid-height, the load potential gain can be expressed as

$$\begin{aligned} V_2 &= -\frac{\lambda}{2}\int_0^L qa\theta(z)^2\,dz = -\frac{\lambda}{2}qa\int_0^L \sum_{i=1,2}^{2n}\sum_{j=1,2}^{2n} B_i B_j \sin\left(\frac{i\pi z}{L}\right)\sin\left(\frac{j\pi z}{L}\right)dz \\ &= \frac{\lambda}{2}\left\langle \mathbf{A}_a{}^T \quad \mathbf{A}_b{}^T \right\rangle \begin{bmatrix} \mathbf{k}_{g3} & \mathbf{0} \\ \mathbf{0} & \mathbf{k}_{g4} \end{bmatrix}_{(2)} \begin{Bmatrix} \mathbf{A}_a \\ \mathbf{A}_b \end{Bmatrix} \end{aligned} \tag{5.22}$$

where

$$\mathbf{k}_{g3} = \mathbf{k}_{g4} = -\frac{1}{2} qLa\mathbf{Diag}\left(0,1,0,1...0,1\right) \tag{5.23}$$

3.4.7 Stationarity conditions

From Eqs. (5.6), (5.17), and (5.21) or (5.22), by substituting into $\pi = U + V_1 + V_2$, by evoking the stationarity conditions $\partial\pi/\partial\mathbf{A}_a = \partial\pi/\partial\mathbf{A}_b = \mathbf{0}$, one obtains

$$\left\{\begin{bmatrix}\mathbf{k}_1 & \mathbf{0}\\ \mathbf{0} & \mathbf{k}_2\end{bmatrix} + \lambda\left(\begin{bmatrix}\mathbf{k}_{g1} & \mathbf{0}\\ \mathbf{0} & \mathbf{k}_{g2}\end{bmatrix} + \begin{bmatrix}\mathbf{k}_{g3} & \mathbf{0}\\ \mathbf{0} & \mathbf{k}_{g4}\end{bmatrix}\right)\right\}\begin{Bmatrix}\mathbf{A}_a\\ \mathbf{A}_b\end{Bmatrix} = 0 \tag{5.24}$$

The two partitions of Eq. (5.24) can be expanded to yield the separate Eigenvalue problems

$$\left(\mathbf{k}_1 + \lambda_1\left(\mathbf{k}_{g1} + \mathbf{k}_{g3}\right)\right)\mathbf{A}_a = 0 \tag{5.25}$$

$$\left(\mathbf{k}_2 + \lambda_2\left(\mathbf{k}_{g2} + \mathbf{k}_{g4}\right)\right)\mathbf{A}_b = 0 \tag{5.26}$$

By solving Eq. (5.25) and Eq. (5.26), two distinct groups of eigenvalues λ_1 and λ_2 are recovered. The fundamental buckling mode is the one corresponding to the smallest eigenvalue. It is noted that the entries of vector $\mathbf{A}_a$ always correspond to a symmetric buckling mode while the coefficients of vector $\mathbf{A}_b$ correspond to an anti-symmetric mode (Appendix 3.A).

3.4.8 Recovering the threshold bracing height

As shown in the results (e.g., Fig. 6), while the critical load corresponding to Mode 1 (symmetric) depends on the bracing height, that based on Mode 2 (anti-symmetric) is found to be independent of the bracing height, yielding a constant critical moment value for a given beam geometry and load configuration. In contrast, the buckling moment corresponding to Mode 1 decreases as the bracing height is lowered. Conceptually, there is a threshold bracing height b_{cr} at which both modes yield the same critical moments. When the brace is above this threshold height, the member attains its maximal capacity as dictated by the anti-symmetric mode. The present section develops a methodology to recover the critical bracing height: Eq. (5.26) is solved for the eigenvalue λ_2 , and one sets

$\lambda_1 = \lambda_2$. Eq. (5.25) is then solved for the threshold bracing height b_{cr}. From Eqs.(5.7), the elastic stiffness matrix $\mathbf{k}_1$ can be re-written as the sum of three matrices

$$\mathbf{k}_1 = \bar{\mathbf{k}}_1 + b_{cr}\bar{\bar{\mathbf{k}}}_1 + b_{cr}^2\bar{\bar{\bar{\mathbf{k}}}}_1 \tag{5.27}$$

where

$$\bar{\mathbf{k}}_{11} = \begin{bmatrix} \mathbf{m}'_{1,1} & \mathbf{m}'_{1,3} & \cdots & \mathbf{m}'_{1,2i-1} & \cdots & \mathbf{m}'_{1,2n-1} \\ \mathbf{m}'_{3,1} & \mathbf{m}'_{3,3} & \cdots & \mathbf{m}'_{3,2i-1} & \cdots & \mathbf{m}'_{3,2n-1} \\ \vdots & \vdots & \ddots & \vdots & \iddots & \vdots \\ \mathbf{m}'_{2j-1,1} & \mathbf{m}'_{2j-1,3} & \cdots & \mathbf{m}'_{2j-1,2i-1} & \cdots & \mathbf{m}'_{2j-1,2n-1} \\ \vdots & \vdots & \iddots & \vdots & \ddots & \vdots \\ \mathbf{m}'_{2n-1,1} & \mathbf{m}'_{2n-1,3} & \cdots & \mathbf{m}'_{2n-1,2i-1} & \cdots & \mathbf{m}'_{2n-1,2n-1} \end{bmatrix}, \bar{\mathbf{m}}_{j,i} = \begin{bmatrix} m_1 & 0 \\ 0 & m_3 \end{bmatrix}$$

$$\bar{\bar{\mathbf{k}}}_1 = \begin{bmatrix} \mathbf{m}''_{1,1} & \mathbf{m}''_{1,3} & \cdots & \mathbf{m}''_{1,2i-1} & \cdots & \mathbf{m}''_{1,2n-1} \\ \mathbf{m}''_{3,1} & \mathbf{m}''_{3,3} & \cdots & \mathbf{m}''_{3,2i-1} & \cdots & \mathbf{m}''_{3,2n-1} \\ \vdots & \vdots & \ddots & \vdots & \iddots & \vdots \\ \mathbf{m}''_{2j-1,1} & \mathbf{m}''_{2j-1,3} & \cdots & \mathbf{m}''_{2j-1,2i-1} & \cdots & \mathbf{m}''_{2j-1,2n-1} \\ \vdots & \vdots & \iddots & \vdots & \ddots & \vdots \\ \mathbf{m}''_{2n-1,1} & \mathbf{m}''_{2n-1,3} & \cdots & \mathbf{m}''_{2n-1,2i-1} & \cdots & \mathbf{m}''_{2n-1,2n-1} \end{bmatrix}, \bar{\bar{\mathbf{m}}}_{j,i} = \begin{bmatrix} 0 & m_2 \\ m_2 & 0 \end{bmatrix}$$

and

$$\bar{\bar{\bar{\mathbf{k}}}}_1 = \begin{bmatrix} \mathbf{m}'''_{1,1} & \mathbf{m}'''_{1,3} & \cdots & \mathbf{m}'''_{1,2i-1} & \cdots & \mathbf{m}'''_{1,2n-1} \\ \mathbf{m}'''_{3,1} & \mathbf{m}'''_{3,3} & \cdots & \mathbf{m}'''_{3,2i-1} & \cdots & \mathbf{m}'''_{3,2n-1} \\ \vdots & \vdots & \ddots & \vdots & \iddots & \vdots \\ \mathbf{m}'''_{2j-1,1} & \mathbf{m}'''_{2j-1,3} & \cdots & \mathbf{m}'''_{2j-1,2i-1} & \cdots & \mathbf{m}'''_{2j-1,2n-1} \\ \vdots & \vdots & \iddots & \vdots & \ddots & \vdots \\ \mathbf{m}'''_{2n-1,1} & \mathbf{m}'''_{2n-1,3} & \cdots & \mathbf{m}'''_{2n-1,2i-1} & \cdots & \mathbf{m}'''_{2n-1,2n-1} \end{bmatrix}, \bar{\bar{\bar{\mathbf{m}}}}_{j,i} = \begin{bmatrix} 0 & 0 \\ 0 & m_4 \end{bmatrix}$$

Also, from Eq.(5.11), the geometric stiffness matrix $\mathbf{k}_{g1}$ can be expressed as

$$\mathbf{k}_{g1} = \bar{\mathbf{k}}_{g1} + b_{cr}\bar{\bar{\mathbf{k}}}_{g1} \tag{5.28}$$

where

$$\bar{\mathbf{k}}_{g11} = \begin{bmatrix} \mathbf{n}'_{1,1} & \mathbf{n}'_{1,3} & \cdots & \mathbf{n}'_{1,2i-1} & \cdots & \mathbf{n}'_{1,2n-1} \\ \mathbf{n}'_{3,1} & \mathbf{n}'_{3,3} & \cdots & \mathbf{n}'_{3,2i-1} & \cdots & \mathbf{n}'_{3,2n-1} \\ \vdots & \vdots & \ddots & \vdots & \iddots & \vdots \\ \mathbf{n}'_{2j-1,1} & \mathbf{n}'_{2j-1,3} & \cdots & \mathbf{n}'_{2j-1,2i-1} & \cdots & \mathbf{n}'_{2j-1,2n-1} \\ \vdots & \vdots & \iddots & \vdots & \ddots & \vdots \\ \mathbf{n}'_{2n-1,1} & \mathbf{n}'_{2n-1,3} & \cdots & \mathbf{n}'_{2n-1,2i-1} & \cdots & \mathbf{n}'_{2n-1,2n-1} \end{bmatrix}, \bar{\mathbf{n}}_{j,i} = \left[\begin{array}{c|c} 0 & m_5 \\ \hline m_6 & 0 \end{array}\right]$$

$$\bar{\bar{\mathbf{k}}}_{g12} = \begin{bmatrix} \mathbf{n}''_{1,1} & \mathbf{n}''_{1,3} & \cdots & \mathbf{n}''_{1,2i-1} & \cdots & \mathbf{n}''_{1,2n-1} \\ \mathbf{n}''_{3,1} & \mathbf{n}''_{3,3} & \cdots & \mathbf{n}''_{3,2i-1} & \cdots & \mathbf{n}''_{3,2n-1} \\ \vdots & \vdots & \ddots & \vdots & \iddots & \vdots \\ \mathbf{n}''_{2j-1,1} & \mathbf{n}''_{2j-1,3} & \cdots & \mathbf{n}''_{2j-1,2i-1} & \cdots & \mathbf{n}''_{2j-1,2n-1} \\ \vdots & \vdots & \iddots & \vdots & \ddots & \vdots \\ \mathbf{n}''_{2n-1,1} & \mathbf{n}''_{2n-1,3} & \cdots & \mathbf{n}''_{2n-1,2i-1} & \cdots & \mathbf{n}''_{2n-1,2n-1} \end{bmatrix}, \bar{\bar{\mathbf{n}}}_{j,i} = \left[\begin{array}{c|c} 0 & 0 \\ \hline 0 & m_7 \end{array}\right]$$

From Eqs. (5.27) and (5.28), by substituting into Eq. (5.25), one obtains a quadratic eigenvalue problem in the unknown critical bracing height b_{cr}

$$\left[\left(\bar{\mathbf{k}}_1 + \lambda_2 \bar{\mathbf{k}}_{g1} + \lambda_2 \mathbf{k}_{g3}\right) + b_{cr}\left(\bar{\bar{\mathbf{k}}}_1 + \lambda_2 \bar{\bar{\mathbf{k}}}_{g1}\right) + b_{cr}^2 \bar{\bar{\bar{\mathbf{k}}}}_1\right]\mathbf{A}_a = \mathbf{0} \tag{5.29}$$

Given λ_2, one can recover the sought critical bracing height by solving the quadratic eigen value problem defined in Eq. (5.29).

3.5 Verification Example

To verify the validity of the model, the critical moments of a reference beam is investigated using the present model and comparisons are provided to the predictions of a 3D FEA eigen-value buckling analyses based on a 3D eigen value analysis based on the commercial software ABAQUS for various bracing heights. The reference beam has a width $w = 130mm$, a height $h = 950mm$ and a span of $13,000mm$. For a rectangular section of width w and depth h, $I_{yy} = hw^3/12 = 1.74\times10^8 mm^4$, $C_w = w^3h^3/144 = 1.31\times10^{13} mm^6$ and the Saint-Venant torsional constant as given in the detailed method of Pai (2007) is $J = 6.36\times10^8 mm^4$. Material is assumed to be glued-laminated timber, Spruce-Lodgepole Pine with 20f-EX grade. The modulus of elasticity in the longitudinal direction is taken as

$E = E_L = 10{,}300MPa$ (CSA O86 2014) and shear modulus is $G = G_{LT} = G_{LR} = 474MPa$ (FPL 2010).

3.5.1 Convergence study of present solution

To determine the number of Fourier terms *n* needed for convergence, a convergence study was conducted on 20 cases with different load configurations (uniformly distributed, mid-span point loads), brace heights $b/h = -0.5, 0.0, 0.5$ and load heights $a/h = -0.5, 0.0, 0.5$. Detailed descriptions and results from the convergence study can be found in (Appendix 3.B). The ratio of critical moments based on $n = 4$ to those based on $n = 6$ where shown to be less than 0.63% in all 20 cases considered. Given that the computational time involved is nearly instantaneous, the number of modes n was conservatively set to 9 in subsequent runs, (i.e., 18 Fourier terms were taken in Eqs. (5.3) and (5.4)).

3.5.2 The 3D finite element model

The C3D8 brick element in ABAQUS was used to discretize the beam. The C3D8 element is three-dimensional continuum elements in ABAQUS consisting of 8 nodes at the corners and 24 degrees of freedom in total (three translations at each node) (Simulia, 2011). This type of element uses linear interpolation in each direction. An orthotropic material model is adopted to represent the wood properties. The modulus of elasticity in the longitudinal direction is taken as $E_L = 10300MPa$ and the moduli of elasticity in the tangential and radial directions were taken as $E_T = E_R = 700MPa$ (Xiao 2014). The shear moduli are taken as $G_{LR} = G_{LT} = 474MPa$ and $G_{RT} = 51.5MPa$ (Xiao 2014); Poisson's ratio along longitudinal and radial/longitudinal and tangential direction $\nu_{LR} = \nu_{LT} = 0.347$. Poisson's ratio is taken as $\nu_{RT} = 0.469$. To simulate simply supported boundary conditions, two groups of restraints were enforced at both ends of the model: (1) As shown in Fig. 3, a set of constraints related to vertical displacements were imposed along axes AB and $A'B'$ at the end cross sections. For axes CD and $C'D'$, the lateral displacements were restrained by imposing another group of constraints. (2) The centroid of the cross section at one end was longitudinally restrained (Fig 3.3a), while that at the other end was left free to move longitudinally (Fig 3.3b). The mid-span lateral brace was simulated by retraining the lateral

displacement at the node located at the target bracing height on the mid-span vertical line passing through the section centroid. A mesh sensitivity analysis was conducted on 12 cases with different load configurations (uniformly distributed, mid-span point loads), brace heights $b/h = -0.5, 0.0, 0.5$ and load heights $a/h = -0.5, 0.0, 0.5$. The governing modes were symmetric in some of the runs and anti-symmetric in other runs. The results (Hu 2016) showed that critical moment predictions based on 410 elements longitudinally, 50 elements along the height, 10 elements along the width do not change by more than 0.08% when finer meshes are taken. Thus, a 410x50x10 mesh will be taken in subsequent runs.

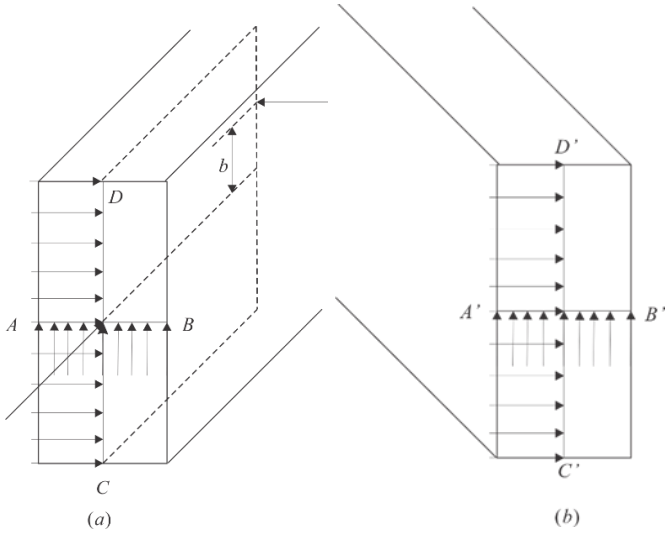

Figure 3.3 Boundary conditions (all arrows denote restrained degree of freedoms) (a) left end (b) right end

3.5.3 Comparison of critical moments

Three sets of comparisons were conducted by varying bracing height with different load height cases (i.e. top face, mid-height, and bottom face) between the results of formulation developed in the present study and those based on the ABAQUS model. The buckling load magnitudes obtained from the two solutions are overlaid in Fig 3.4. Both models predict two types of buckling modes: symmetric and anti-symmetric. The anti-symmetric mode is associated with a critical moment value that is independent of the bracing height while critical moment based on the symmetric mode is found to depend on the bracing height. Fig. 4 shows close agreement between the predictions of the present study and those of the

ABAQUS simulations. Percentage differences were found to be within 1.09%-4.08% (Appendix 3.C). The buckling load values obtained from the present study are slightly higher than those obtained from the ABAQUS simulation. The difference is due to the fact that the present model is based on the simplifying kinematic assumptions that neglect distortional and shear deformation effects and thus provides a slightly higher representation of the beam stiffness than the ABAQUS model which allows distortion and shear deformations effects. The symmetric and anti-symmetric buckling modes are compared to ABAQUS 3D results (Fig 3.5) for the cases of point load and uniformly distributed load for the case . Close agreement is observed between the present model and those based on the ABAQUS simulations. Similar agreement is observed for the mode shapes for other loading and bracing heights (Appendix 3.C).

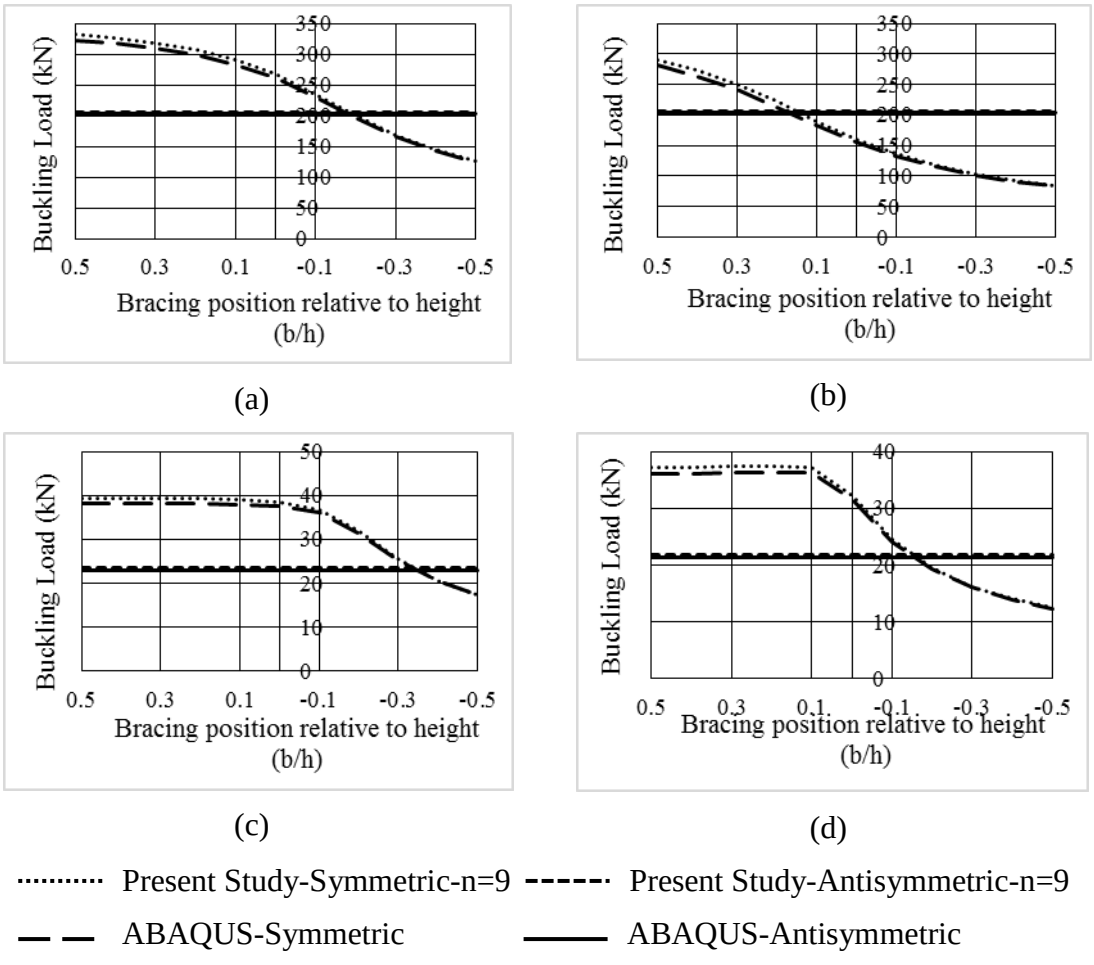

Figure 3.4 buckling load comparison relative to different bracing height when load is (a) point load, mid-height $a = 0$ (b) point load, top face $a = 0.5h$ (c) uniformly distributed load, mid-height $a = 0$ (d) uniformly distributed load, top face $a = 0.5h$

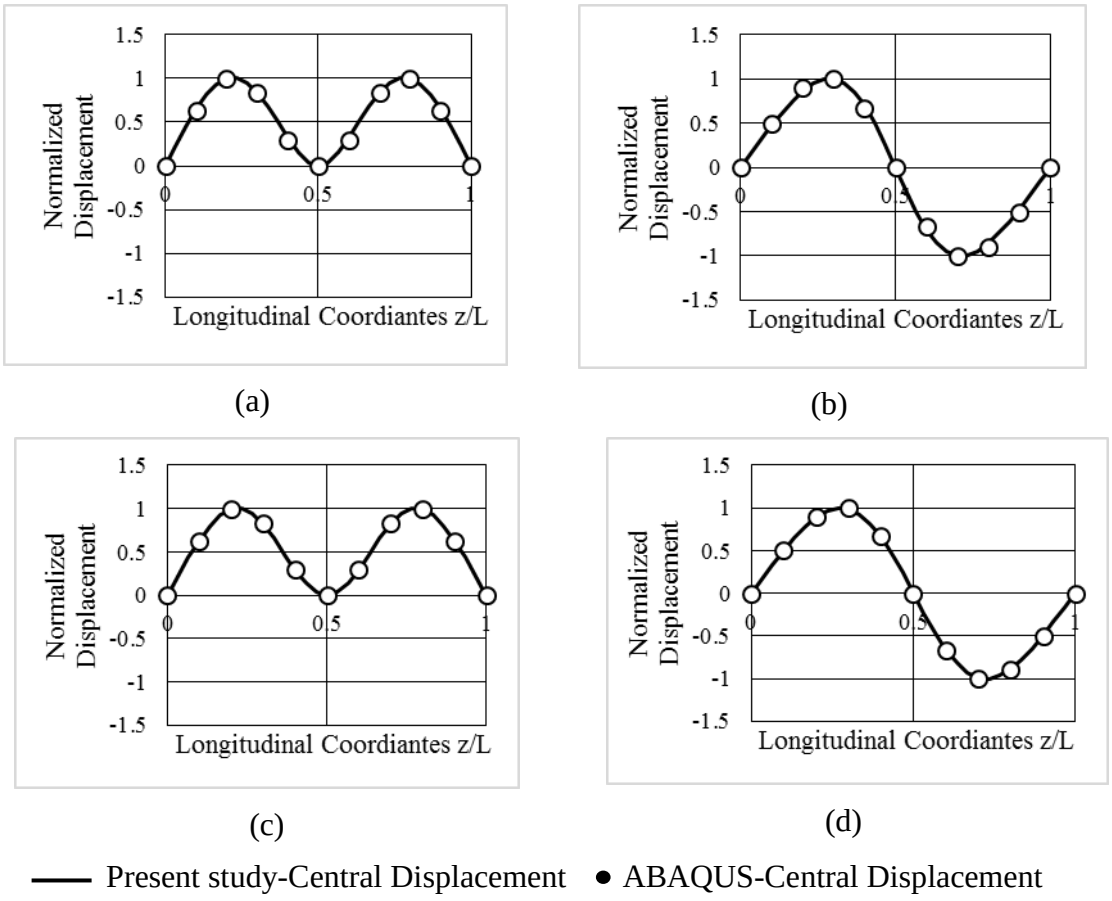

Figure 3.5 Comparison of buckling mode shape for point load and brace with different height Point load, symmetric mode $a=0, b=0$ (b) point load, anti-symmetric mode $a=0, b=0$ (c) uniformly distributed load, symmetric mode $a=0, b=0$ (d) uniformly distributed load, anti-symmetric mode $a=0, b=0$

3.6 Parametric study

A parametric study was conducted by varying the bracing height and load heights (i.e. top face, mid-height and bottom face) for point load and uniformly distributed load cases (Fig 3.6). The buckling load corresponding to the anti-symmetric mode (Mode 2) is observed to be independent of the bracing height. For both loading cases, the buckling load for Mode 1 decreases when the lateral brace is moved downwards. Also, for both loading cases, the buckling load corresponding Mode 1 decreases with load height increase. For Mode 2, the buckling load is observed to be independent of load height for the case of point load but found to decrease with load height increase for the case of uniformly distributed load.

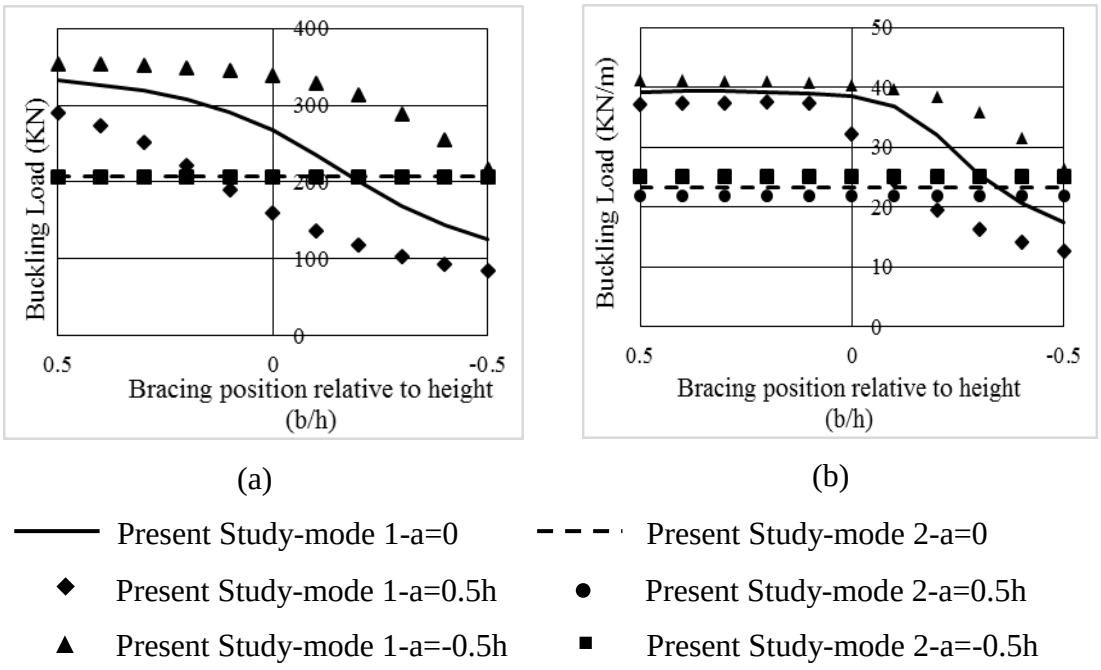

Figure 3.6 Effect of brace position under for different load height (a) point load (b) uniformly distributed load

3.7 Development of Simplified design expressions

A database of 148 runs (Appendix 3.D) was developed to investigate the effect of various geometric and elastic properties on threshold bracing height and the critical moment. Of the 148 cases, 68 runs investigated the case of point load and 80 runs were conducted for the case of uniformly distributed load. Ranges of material properties were chosen to conform to those provided in CSA O86 (2014) and (FPL, 2010). The ranges of parameters investigated are $0.137 \le w/h \le 0.856$, $8.42 \le L/h \le 21.05$, and $1/10 \le G/E \le 1/20$. Subsequently, approximate design expressions were developed based on regressing analysis.

3.7.1 Point load

The relationship between the critical bracing height to section height ratio $\bar{b}_{cr}/h$ and the parameters $w/h, L/h, a/h, G/E$ were found to exhibit a nearly linear dependence (Appendix 3.E). Therefore, the approximate critical height ratio $\bar{b}_{cr}/h$ was postulated to take the form

$$\left(\frac{\bar{b}_{cr}}{h}\right) \approx \alpha_0 + \alpha_1\left(\frac{w}{h}\right) + \alpha_2\left(\frac{L}{h}\right) + \alpha_3\left(\frac{a}{h}\right) + \alpha_4\left(\frac{G}{E}\right) \tag{5.30}$$

where $\alpha_0, \alpha_1, \alpha_2, \alpha_3, \alpha_4$ are coefficients to be determined from the regression analysis. The sum of the squares of the differences between the values of (b_{cr}/h) as obtained by the present solution and that based on the expression in Eq. (5.30) is minimized, i.e.

$$D_1 = \sum_{i=1}^{m}\left[\left(\frac{\bar{b}_{cr}}{h}\right) - \left(\frac{b_{cr}}{h}\right)\right]_i^2 = \min \tag{5.31}$$

where m is the number of runs conducted, by enforcing the minimization conditions $\partial D_1/\partial \alpha_i = 0 \quad (i = 0,1..4)$ yielding the regression constants $\alpha_0 = 0.08089, \alpha_1 = 0.07364$, $\alpha_2 = -0.01529, \alpha_3 = 0.6870, \alpha_4 = -1.5130$. The domain validity of the regression coefficients is that of the database of runs, i.e., $0.137 \le w/h \le 0.856, 8.42 \le L/h \le 21.05$, and $1/10 \le G/E \le 1/20$. Within these domains, the average difference between the predictions of the regression equation to that of the present solution was found to be 0.00 with a standard deviation of 0.0041.

When the bracing height b is greater than the critical bracing height b_{cr} (or $\bar{b}_{cr}$ as estimated by Eq. (5.30)), the critical moment will be maximized and will attain that based on the anti-symmetric mode. Under this mode, the lateral displacement and angle of twist vanish at beam mid-span and the unsupported length is $L_u = L/2$. The corresponding critical moment M_{cr} is then given by

$$\bar{M}_{cr} \approx C_b \frac{\pi}{L_u}\sqrt{EI_{yy}GJ + \left(\frac{\pi E}{L_u}\right)^2 I_{yy}C_w} \tag{5.32}$$

where C_b is a moment gradient factor within the beam half-span. Given the critical moment values M_{cr} based on the present analysis (Appendix 3.D) and knowing E, I_{yy}, G, J, C_w and L_u, the moment gradient factor C_b is determined for each run. The procedure

was repeated for all 68 runs and was found to range from 1.78 to 1.81 with an average value of 1.80 and a standard deviation of 0.008. The value $C_b = 1.80$ obtained is in line with that based on quarter point formulas of the AFPA (2003) of 1.67, CAN-CSA S16 (2014) of 1.74, and, AS4100 (1998) of 1.82.

3.7.2 Uniformly distributed load

The approximate critical height ratio $\bar{\bar{b}}_{cr}/h$ was postulated to take the form

$$\left(\frac{\bar{\bar{b}}_{cr}}{h}\right) \approx \beta_0 + \beta_1\left(\frac{w}{h}\right) + \beta_2\left(\frac{L}{h}\right) + \beta_3\left(\frac{a}{h}\right) + \beta_4\left(\frac{a}{h}\right)^2 + \beta_5\left(\frac{G}{E}\right) \tag{5.33}$$

where *m* is the number of runs conducted (Appendix 3.D) by enforcing the conditions $\partial D_1/\partial\beta_i = 0 \quad i = 0,1,2..5$ yielding the regression constants $\beta_0 = 0.1740$, $\beta_1 = 0.1368$, $\beta_2 = -0.02950$, $\beta_3 = 0.2944$, $\beta_4 = 0.1595$, $\beta_5 = -2.9995$. The domain validity of the regression coefficients is $0.137 \le w/h \le 0.856$, $-0.5 \le a/h \le 0.5$, $8.42 \le L/h \le 15.79$ and $1/10 \le G/E \le 1/20$. Within this domain, the average difference between the predictions of the regression equation to that of the present solution is 0.00 and the standard deviation is 0.0066.

When the bracing height is greater than the critical bracing height b_{cr} or $\bar{\bar{b}}_{cr}$ as estimated by Eq. (5.33), the buckling capacity will be maximized and will attain the critical moment of the anti-symmetric mode. Under this mode, the lateral displacement and angle of twist vanish at mid-span. Under these conditions, the unsupported length is $L_u = L/2$. As the critical moments based on the anti-symmetric mode changes with the load height position (e.g., Fig 3.6), additional terms to capture the load height effect should be added to the approximate function. The results of database of runs have shown that the difference between the critical moments for mid-height loading and those based on loading acting at height a above the centroid are nearly proportional to the term $aEI_{yy}/L_u^{\,2}$. As such, the following equation was proposed to estimate the critical moments including load height effects (Appendix 3.F):

$$\bar{\bar{M}}_{cr} = C_b \frac{\pi}{L_u} \sqrt{EI_{yy} GJ + \left(\frac{\pi E}{L_u} \right)^2 I_{yy} C_w} - C_e \frac{aEI_{yy}}{L_u^{\,2}} \tag{5.34}$$

The sum of the squares of the differences between the values of the buckling capacity obtained by the present solution (Appendix 3.D) and that based on (5.34) minimized, i.e.

$$D_2 = \sum_{i=1}^{m} \left[\bar{\bar{M}}_{cr} - M_{cr} \right]_i^2 = \min \tag{5.35}$$

The minimization process yields the constants $C_b = 1.32$ and the load position modifier $C_e = 1.68$. The average value of C_b is consistent with that based on CAN-CSA S16 (2014) of 1.32, AFPA (2003) of 1.30, and AS4100 (1998) of 1.33.

3.7.3 Example 1- Beam under mid-span point load:

A simply supported glulam beam with a rectangular section of depth $h = 570mm$ and width $w = 130mm$ has a span of $11,500mm$. The beam is subjected to a mid-span point load acting at top face of the cross section. The beam is laterally braced at mid-span. Two bracing heights are considered: (a) $200mm$ and (b) $0mm$. It is required to determine the critical moment capacity based on the present detailed analytical model and compare the results with those based on the simplified procedure. Sectional properties are: Saint-Venant torsional constant $J = 3.57 \times 10^8 mm^4$, weak moment of inertia $I_{yy} = 1.04 \times 10^8 mm^4$, and warping constant $C_w = 2.83 \times 10^{12} mm^6$ and material properties are $E = 10,300MPa$ and $G = 515MPa$.

3.7.3.1 Bracing height check:

For the present problem, one has $w/h = 0.228, L/h = 20.2, a/h = 0.5$ and $G/E = 1/20$. These ratios meet the applicability conditions for Eq. (5.30). The threshold bracing height ratio as computed from Eq. (5.30) is $\bar{b}_{cr}/h = 0.057$. This compares to $b_{cr}/h = 0.073$ as predicted by the detailed procedure in Eq. (5.29), a 0.02 difference. Thus, a bracing height above $0.057 \times 570 = 33mm$ is deemed high enough to fully restrain the angle of twist at mid-span and maximize the critical moments by forcing the beam to buckle in an anti-

symmetric mode. This condition is satisfied for Case a where the bracing height is $200mm > 33mm$ but not in Case b for a bracing height of $0mm < 33mm$.

3.7.3.2 Critical moment for case (a)

Given that w/h, L/h, a/h, G/E lie within the domain of applicability of the regression equation, the simplified moment calculation procedure provided by Eq. (5.32) can be applied. As discussed, when twist and lateral displacements vanish at mid-span, the mid-span point can be considered as a point of full lateral and torsional restraint and the unbraced length of the beam becomes $L_u = L/2 = 5,750mm$. The critical moment $\bar{\bar{M}}_{cr}$ as determined from Eq. (5.32) is found to be $447kNm$. This value compares to $444kNm$ as predicted by the present detailed formulation, corresponding to a 0.69% difference, and $437kNm$ as predicted by the 3D ABAQUS model, corresponding to a 2.23% difference.

3.7.3.3 Critical moment for case (b)

For zero bracing height, the mid-span section will be only partially restrained from twisting, and the beam capacity will be governed by the symmetric buckling mode. Under this scenario, the critical moment can no longer be calculated using the simplified Eq. (5.32) and a detailed analysis based on the present formulation would be needed. The critical moment is found to be $M_{cr} = 411kNm$, which compares to $397kNm$ based on the ABAQUS 3D model. As expected, the critical moment is smaller compared to that of Case (a). A lower bound for the critical moment in case (b) can be obtained by entirely omitting the bracing effect at mid-span. Under this scenario, $L_u = L = 11,500mm$ and moment gradient C_b based on the AFPA (2003) recommendations is 1.33. Comparable values are obtained from CAN-CSA S16 (2014) which yields 1.26, or AS4100 (1998) which yields 1.39 (Appendix 3.G). For a point load applied at the top of the cross-section, the AFPA (2003) load eccentricity factor is given by $C_e = \sqrt{\eta^2 + 1} - \eta$ where $\eta = \left(k^* h/2L_u\right)\sqrt{EI_{yy}/GJ}$ where $k^* = 1.72$ for the case of point loading, yielding $C_e = 0.815$. The sought lower bound of the critical moment is given by $M_{cr} = \left(C_e C_b \pi/L_u\right)\sqrt{EI_{yy}GJ + \left(\pi E/L_u\right)^2 I_{yy}C_w}$ yielding $M_{cr} = 132kNm$. In summary, the critical moment of $411kNm$ based on the

detailed procedure is significantly higher than the critical moment based on no intermediate support restraint but slightly less than the critical moment of $444kNm$ based on the case of full bracing.

3.7.4 Example 2 –Beam under a uniformly distributed load:

A simply supported glulam beam with rectangular section of depth $h = 798mm$, width $w = 215mm$ is spanning $10,000mm$. The beam is subjected to a uniformly distributed load acting at the top face of the beam. The beam is laterally braced at mid-span. Sectional and material properties are: $J = 2.19\times10^{9}\,mm^{4}$, $I_{yy} = 6.61\times10^{8}\,mm^{4}$, $C_w = 3.51\times10^{13}\,mm^{6}$, $E = 10,300MPa$ and $G = 644MPa$. Two bracing heights are considered: (a) $100mm$ and (b) $-300mm$ (the negative sign indicates that the bracing is located below the section mid-height). It is required to determine the critical moment capacity.

The dimensionless ratios $w/h = 0.27, L/h = 12.5, a/h = 0.5$ and $G/E = 1/16$ are within the applicability limits of the threshold bracing height and critical moment equations. The threshold bracing height ratio as determined from Eq. (5.33) is $\bar{\bar{b}}_{cr}/h = -0.158$. This compares to -0.157 based on the detailed procedure, a 0.002 difference. Thus, a bracing height above $-0.158\times 798 = -126.1mm$ is deemed high enough to fully restrain the angle of twist at mid-span. This happens to be the case for a bracing height of $100mm$ (Case a), but is not for a bracing height of $-300mm$ (Case b). The unbraced length is $L_u = L/2 = 5,000mm$ and the critical moment based on Eq. (5.34) is found to be $252kNm$. This value compares to $253kNm$ as predicted by the detailed procedure provided, a 0.050% difference.

When the bracing height is $-300mm$, the mid-span section will only be partially restrained from twisting and the beam critical moment based on the detailed analysis is found to be $M_{cr} = 171kNm$. As expected, the critical moment is found smaller than that based on Case (a). A lower bound for the critical moment in case (b) can be obtained based on an unsupported length $L_u = L = 10,000mm$ and the moment gradient C_b is determined as 1.13 from the AFPA recommendations (2003), and a load eccentricity factor One can also

apply the $C_e = \sqrt{\eta^2 + 1} - \eta$ (AFPA 2003) where $\eta = \left(k^* h / 2L_u\right)\sqrt{EI_{yy}/GJ}$ and $k^* = 1.44$ for uniformly distributed load, yielding a value $C_e = 0.779$. The corresponding critical moment is $M_{cr} = \left(C_e C_b \pi / L_u\right)\sqrt{EI_{yy}GJ + \left(\pi E / L_u\right)^2 I_{yy} C_w} = 101 kNm$. This lower bound is again significantly lower than the critical moment obtained by the present detailed solution.

3.8 Summary and conclusions

Analytical solutions were developed for the lateral torsional buckling analysis of simply supported wooden beams with discrete lateral supports at mid-span subjected to symmetric moment load distributions relative to mid-span. The model accounts for the combined effect of eccentricities of the bracing and the loads. The models were validated against a 3D FEA solutions and parametric study to investigate the influence of mid-span bracing height and load height was conducted. The conclusions can be summarized as follows:

1. The model predicts two possible buckling modes: symmetric and anti-symmetric, which depends on the load height and bracing height. For a given load height, simple expressions were developed for determining the threshold bracing height at which the capacity is governed by the antisymmetric mode.

2. For point load and uniformly distributed load, critical moments based on the symmetric mode are observed to decrease when the load height increases

3. For point load loading, critical moments based on the anti-symmetric modes are found to be independent from the load height. In contrast, for uniformly distributed loads, they are found to decrease as the point of application of the load moves upwards.

4. For mid-span point loading, the threshold bracing height normalized relative to cross section height b_{cr}/h was observed correlate nearly linearly with geometric and elastic parameters a/h, L/h, w/h and G/E.

5. For uniformly distributed loading, the normalized threshold bracing height b_{cr}/h was observed to have a nearly linear correlation with geometric and parameters a/h, w/h and G/E, while having a nearly quadratic correlation with L/h.

6. Simplified design equations were developed to reliably estimate the threshold bracing height required to maximize the critical moments and quantify the critical moments for

cases where the bracing location is above the threshold height as computed by the simplified equation.

Notation:

a = Distance of load offset from cross-section shear centre;

b = Distance of brace offset from cross-section shear centre;

b_{cr} = Threshold bracing height;

$\bar{b}_{cr}$ = Approximate threshold bracing height for point load case;

$\bar{\bar{b}}_{cr}$ = Approximate threshold bracing height for uniformly distributed load case;

C_w = Warping constant;

C_b = Moment gradient;

C_e = Factors regrading load eccentricity effect;

E = Young's modulus of wooden beam along the longitudinal direction;

G = Shear modulus of the beam;

h = Cross section height;

I_{yy} = Weak moment of inertia;

J = Saint-Venant torsional constant;

L = Beam span;

m = Number of runs conducted in threshold bracing height studies;

M_u = Bending capacity without load eccentricity effect;

M_e = Bending capacity terms regarding load eccentricity effect;

M_r = Bending capacity;

n = Number of Fourier terms;

P_{cr} = Buckling load;

Q = Point load magnitude;

u = Lateral displacement of central axis;

U = Internal strain energy;

V = Load potential energy gained;

w = Cross section width;

π = Total potential energy;

θ = Twisting angle;

λ = Load multiplier; and

ω = Coefficient to account for moment gradient and mid-span lateral brace;

References

[1] Austin, W.J., Yegian, S. Tung, T. P. (1955). "Lateral buckling of elastically end-restrained I-beams." *Transactions of the American Society of Civil Engineers*, 122(1), 374-388

[2] Andrade, A., and Camotim, D. (2005). "Lateral-torsional buckling of singly symmetric tapered beams: theory and applications." *Journal of engineering mechanics*, 131(6), 586-597

[3] Andrade, A., Camotim, D. Dinis, P.B. (2007). "Lateral-torsional buckling of singly symmetric web-tapered thin-walled I-beams: 1D model vs. shell FEA." *Computers and Structures*, 85(17-18), 1343-1359

[4] American Forest and Paper Association. (2003). Technical Report 14: Designing for lateral-torsional stability in wood members. Washington, D.C.

[5] American Institution of Steel Construction. (2010). Specification for structure steel buildings. ANSI/AISC 2010a. Chicago, U.S.

[6] American Institution of Steel Construction. (2010). Commentary on the specification for structure steel buildings. ANSI/AISC 2010b. Chicago, U.S.

[7] Canadian Standards Association. (2014). Design of steel structures. CSA standard S16-14. Mississauga, ON.

[8] European Committee for Standardization (2005). Design of steel structures part 1.1: general rules and rules for buildings. EN 1993-1-1:2005. Brussels, Belgium.

[9] Erkmen, R.E. and Mohareb, M. (2008). "Buckling analysis of thin-walled open members-A finite element formulation." *Thin-Walled Structures,* 46(6), 618-636

[10] Flint, A.R. (1951), "The influence of restraints on the stability of beams." *The Structure Engineer,* 29(9), 235-246

[11] Helwig, T., Frank, K., Yura, J. (1997). "Lateral-torsional buckling of singly symmetric I-beams." *Journal of Structural Engineering,* 123(9), 1172-1179

[12] Ings, N.L. and Trahair, N.S. (1987). "Beam and column buckling under directed loading." *Journal of Engineering Mechanics*, 113(6), 1251-1263

[13] Jingping, L., Zaitian, G. Chen, S. (1988). "Buckling of transversely loaded I-Beam columns." *Journal of Structural Engineering,* 114(9), 2109-2118

[14] Kerensky, O.A., Flint, A.R., Brown, W.C. (1956). "The basis for design of beams and plate girders in the revised British Standard 153." *In Proceedings of the Institution of Civil Engineers*, 5(3), 396–461

[15] Kitipomchai, S., Dux, P.F., Richter, N.J. (1984). "Buckling and bracing of cantilevers." *Journal of Structural Engineering,* 110(9), 2250-2262

[16] Lay, M.G., Galambos, T.V., Schmidt, L.C. (1963). "Lateral bracing force of steel I beams." *Journal of Engineering Mechanics Division,* 89(EM3), 217-224

[17] Lamb, A.W., and Eamon, C.D. (2015). "Load height and moment factors for doubly symmetric wide flange beams." *Journal of Structural Engineering*, 10.1061/(ASCE)ST.1943-541X.0001332, 04015069

[18] Mutton, B.R., and Trahair, N.S. (1973). “Stiffness requirement for lateral bracing.” *Journal of the Structural Division*, 99(10), 2167-2182

[19] Mohri, F., and Potier-Ferry, M. (2006). “Effects of load height application and pre-buckling deflection on lateral buckling of thin-walled beams.” *Steel and Composite Structures*, 6(5), 1-15

[20] Mohebkhah, A. (2010). “Lateral buckling resistance of inelastic I-beams under off-shear center loading.” *Thin-Walled Structures*, 49(3), 431-436

[21] McCann, F., Wadee, M.A., Gardner, L. (2013). “Lateral stability of imperfect discretely braced steel beams.” *Journal of Engineering Mechanics*, 139(10), 1341-1349

[22] Morkhade, S.G., and Gupta, L.M. (2013). “Effect of load height on buckling resistance of steel beams.” *Procedia Engineering*, 51, 151-158

[23] Nethercot, D.A., and Rockey, K.C. (1971). “A unified approach to the elastic lateral buckling of beams.” *The Structural Engineer*, 49(7), 321-330

[24] Nethercot, D.A., and Rockey, K.C. (1972). “The lateral buckling of beams having discrete intermediate restraints.” *The Structural Engineer*, 50(10), 391-403

[25] Pi, Y.L., Traihair, N.S., Rajasekaran, S. (1992). “Energy equation for beam lateral buckling.” *Journal of Structural Engineering*, 118(6), 1462-1479

[26] Prescott, J., and Carrington, H. (1920). “The Buckling of deep beams.” *Philosophical Magazine Series 6*, 39(230), 194-233

[27] Pettersson, O. (1952). “Combined bending and torsion of I-beams of monosymmetrical cross section.” Bulletin No.10, *Division of Building Statics and Structural Engineering*, Royal Institute of Technology, Stockholm, Sweden

[28] Park, J.S., Stalling, M.J., Kang, Y.J. (2004). “Lateral-torsional buckling of prismatic beams with continuous top flange bracing.” *Journal of Constructional Steel Research*, 60(2), 147–160

[29] Pai, PF. Highly flexible structures: modeling, computation, and experimentation, AIAA Educational Series; 2007.

[30] Schrader, R.K. (1941). “Discussion of paper by G. Winter.” *T. Am. Soc. Civ. Eng.*, 108(1), 260-268

[31] Standards Australia. (1998). Steel structures. Australian standard AS 4100-1998. Homebush, Australia.

[32] Samanta, A., and Kumar, A. (2006). “Distortional buckling in monosymmetric I-beams.” *Thin-Walled Structures*, 44(1), 51-56

[33] Samanta, A., Kumar, A. (2008). “Distortional buckling in braced-cantilever I-beams.” *Thin-Walled Strcutures*, 46(6), 637-645

[34] Sahraei, A., Wu, L., Mohareb, M. (2015). “Finite element formulation for lateral torsional buckling analysis of shear deformable mono-symmetric thin-walled members.” *Thin-Walled Structures*, doi:10.1016/j.tws.2014.11.023

[35] Schmidt, L.C., (1965). “Restraints against elastic lateral buckling.” *Journal of Engineering Mechanics Division*, 91(EM6), 1-10

[36] Timoshenko, S. (1936). *Theory of elastic stability*, McGraw-Hill Book Company, Inc., New York

[37] Tong, G.S., and Chen, S.F. (1988). “Buckling of laterally torsionally braced beams.” *Journal of Constructional Steel Research*, 11(1), 41-55

[38] Trahair, N.S. (1993). *Flexural-Torsional Buckling of Structures*. E & FN Spon, London.

[39] Trahair, N.S. (2013). “Bending and buckling of tapered steel beam structures.” *Engineering Structures*, 59, 229-237

[40] Yura, J.A. (2001). “Fundamental of Beam Bracing, Engineering Journal.” *Engineering Journal*, 38(1), 11-26

[41] Yura, J., Helwig, T.A., Zhou, C. (2008). “Global lateral buckling of I-shaped girder system.” *Journal of Structural Engineering*, 134(9), 1487-1494

[42] Winter, G. (1941). “Lateral stability of unsymmetrical I-beams and trusses in bending.” *Transactions of the American Society of Civil Engineers*, 108(1), 247-260

[43] Winter, G. (1960). “Lateral bracing of columns and beams.” *Transactions of the American Society of Civil Engineers*, 125 (1), 807-826

[44] Wong-Chung, A.D., and Kitipomchai, S. (1987). “Partially braced inelastic beam buckling experiments.” *Journal of Constructional Steel Research*, 7(3), 189-211

[45] Wang, C.M., Kitrporncha, S. Thevendran, V. (1987). “Buckling of braced monosymmetric cantilevers.” *International Journal of Mechanical Sciences*, 29(5), 321-337

[46] White, D.W., and Kim, Y.D. (2008). “Unified Flexural Resistance Equations for Stability Design of Steel I-Section Members: Moment Gradient Tests.” *Journal of Structural Engineering*, 134(9), 1450-1470

[47] Wong, E., Driver, R.G., Heal, T.W. (2015). “Simplified approach to estimating the elastic lateral–torsional buckling capacity of steel beams with top-flange loading.” *Canadian Journal of Civil Engineering*, 42(2), 130-138

[48] Wu, L., and Mohareb, M. (2010). “Buckling formulation for shear deformable thin-walled members-II. Finite element formulation.” *Thin-Walled Structures*, 49(1), 208-222

Appendix 3.A-Symmetry properties of buckling modes

The purpose of Appendix 3.A is to provide a mathematical proof of the symmetry properties of two groups of buckling mode resulting in Eqs. (5.25) and (5.26). We recall the mode shapes as given by Eq. (5.4) and (5.5)

$$u(z)=\sum_{i=1}^{2n}A_i\left[\sin\frac{i\pi z}{L}+(-1)^{n+1}\sin\frac{i\pi}{2}\sin\frac{(2n+1)\pi z}{L}\right]+b\sum_{i=1}^{2n}B_i(-1)^{n+1}\sin\frac{i\pi}{2}\sin\frac{(2n+1)\pi z}{L}$$

$$\theta(z)=\sum_{j=1}^{2n}B_j\sin\frac{j\pi z}{L}$$

where $i=1,2,3\ldots,\quad j=1,2,3\ldots$. The displacements at $(L-z)$ are

$$\begin{aligned}u(L-z)&=\sum_{i=1}^{2n}A_i\left[\sin\frac{i\pi(L-z)}{L}+(-1)^{n+1}\sin\frac{i\pi}{2}\sin\frac{(2n+1)\pi(L-z)}{L}\right]\\&\quad+b\sum_{i=1}^{2n}B_i(-1)^{n+1}\sin\frac{i\pi}{2}\sin\frac{(2n+1)\pi(L-z)}{L}\\&=\sum_{i=1}^{2n}A_i\left(\sin\left(i\pi-\frac{i\pi z}{L}\right)+(-1)^{n+1}\sin\frac{i\pi}{2}\sin\left[(2n+1)\pi-\frac{(2n+1)\pi z}{L}\right]\right)\\&\quad+b\sum_{i=1}^{2n}B_i(-1)^{n+1}\sin\frac{i\pi}{2}\sin\left[(2n+1)\pi-\frac{(2n+1)\pi z}{L}\right]\end{aligned}$$

$$\theta(L-z)=\sum_{j=1}^{2n}B_j\sin\frac{j\pi(L-z)}{L}=\sum_{j=1}^{2n}B_j\sin\left(j\pi-\frac{j\pi z}{L}\right)$$

Symmetry of Mode 1

For the case (i, j=1, 3, 5), since

$$\sin\left[(2n+1)\pi-\frac{(2n+1)\pi z}{L}\right]=\sin\frac{(2n+1)\pi z}{L}\ ,\sin\left(i\pi-\frac{i\pi z}{L}\right)=\sin\frac{i\pi z}{L}$$

and

$$\sin\left(j\pi-\frac{j\pi z}{L}\right)=\sin\frac{j\pi z}{L}$$

one has

$$u(z)=u(L-z) \tag{3.A.1}$$

$$\theta(L)=\theta(L-z) \tag{3.A.2}$$

Equations (3.A.1) and (3.A.2) indicate that the modes $i=1,3,5..$ and $j=1,3,5..$ correspond to a symmetric mode.

Anti-Symmetry Mode 2

For the case (i, j=2, 4, 6), since

$$\sin\left(i\pi-\frac{i\pi z}{L}\right)=-\sin\frac{i\pi z}{L}\ ,\ \sin\frac{i\pi}{2}\sin\left[(2n+1)\pi-\frac{(2n+1)\pi z}{L}\right]=\sin\frac{i\pi}{2}\sin\frac{(2n+1)\pi z}{L}=0$$

and

$$\sin\left(j\pi-\frac{j\pi z}{L}\right)=-\sin\frac{j\pi z}{L}$$

one has

$$u(z)=-u(L-z) \tag{3.A.3}$$

$$\theta(L)=-\theta(L-z) \tag{3.A.4}$$

Equations (3.A.3) and (3.A.4) indicate that $i=2,4,6..$ and $j=2,4,6..$ correspond to an anti-symmetric mode.

Appendix 3.B-Convergence study of present energy formulation and 3D FEA model

The accuracy of LTB critical moment obtained from (5.25) and (5.26) hinges on the number of terms used in Eqs. (5.3) and (5.4). Table 3.B.1 present the critical moment results based on a maximum number of Fourier terms defined in Eqs. (5.3) and (5.4) for the cases $n = 1, 2, 3, 4,$ and 6. The objective is to determine the number of Fourier terms needed for convergence. Table 3.B.2 provides the critical moments for the reference case defined in section titled "The 3D finite element model" by varying the number of finite elements in the longitudinal direction of the beam.

Table 3.B. 1 Convergence study of energy formulation

number of Fourier terms *n*=					1	2	3	4	6	1	2	3	4	6
run	LT (1)	Mode (2)	a/h	b/h	Buckling load P_{cr} (kN), or w_{cr} (kN/m)					% Difference(3)				
1	P	S	0	0	447	277	268	268	267	67	3.62	0.18	0.03	0.00
2	P	S	0.5	0	199	166	162	161	160	24	3.34	0.75	0.27	0.00
3	P	S	-0.5	0	1007	355	339	338	338	198	4.92	0.13	0.04	0.00
4	P	S	0	0.5	1567	355	333	332	332	372	7.07	0.32	0.02	0.00
5	P	S	0	-0.5	137	127	126	126	126	8.91	1.12	0.25	0.09	0.00
6	P	A	0	0	230	207	207	207	207	11	0.29	0.05	0.00	0.00
7	P	A	0.5	0	230	207	207	207	207	11	0.29	0.05	0.00	0.00
8	P	A	-0.5	0	230	207	207	207	207	11	0.29	0.05	0.00	0.00
9	P	A	0	0.5	230	207	207	207	207	11	0.29	0.05	0.00	0.00
10	P	A	0	-0.5	230	207	207	207	207	11	0.29	0.05	0.00	0.00
11	U	S	0	0	155	39.8	38.5	38.5	38.5	302	3.54	0.01	0.01	0.00
12	U	S	0.5	0	36.0	32.5	32.4	32.3	32.3	11	0.56	0.36	0.08	0.00
13	U	S	-0.5	0	665	42.2	40.3	40.3	40.3	1.6e+05	453	1.19	0.63	0.00
14	U	S	0	0.5	1378	41.3	39.3	39.2	39.2	3.4e+03	5.19	0.04	0.00	0.00
15	U	S	0	-0.5	18.7	17.6	17.5	17.5	17.5	6.99	0.58	0.25	0.10	0.00
16	U	A	0	0	24.6	23.4	23.3	23.3	23.3	5.55	0.04	0.01	0.00	0.00
17	U	A	0.5	0	22.9	21.8	21.8	21.8	21.8	4.87	0.05	0.01	0.00	0.00
18	U	A	-0.5	0	26.6	25.0	25.0	25.0	25.0	6.32	0.03	0.01	0.00	0.00
19	U	A	0	0.5	24.6	23.4	23.3	23.3	23.3	5.55	0.04	0.01	0.00	0.00
20	U	A	0	-0.5	24.6	23.4	23.3	23.3	23.3	5.55	0.04	0.01	0.00	0.00

[1]LT=Loading type: P=mid-span point load, U=uniformly distributed

[2] Mode: S=symmetric (mode1), A=anti-symmetric (anti-symmetric mode)

[3] $Difference = Pcr(n) - Pcr(n=6)/Pcr(n=6)$

Table 3.B. 2 Mesh sensitivity results for 3D FEA model

Number of elements in longitudinal direction					50	170	290	410	470	50	170	290	410	470
Number of elements along the depth					50	50	50	50	50	50	50	50	50	50
Number of elements across the width					10	10	10	10	10	10	10	10	10	10
number of elements (thousands)					25	85	145	205	235	25	85	145	205	235
run	LT	Mode	a/h	b/h	Buckling load P_{cr} (kN), or w_{cr} (kN/m)					% Difference				
1	P	S	0	0	290	264	262	262	262	10.6	0.80	0.17	0.00	0.00
2	P	S	0	0.5	361	325	323	322	322	12.0	0.93	0.20	0.00	0.00
3	P	S	0.5	0	164	156	155	155	155	5.60	0.70	0.22	0.00	0.00
4	P	A	0	0	224	205	204	203	203	10.2	0.79	0.17	0.00	0.00
5	P	A	0	0.5	224	205	204	203	203	10.2	0.79	0.17	0.00	0.00
6	P	A	0.5	0	224	205	204	203	203	10.2	0.80	0.17	0.00	0.00
7	U	S	0	0	42	37.8	37.5	37.5	37.4	11.2	0.89	0.22	0.05	0.00
8	U	S	0	0.5	42.4	38.4	38.2	38.1	38.1	11.3	0.92	0.23	0.05	0.00
9	U	S	0.5	0	33	31.8	31.7	31.7	31.6	4.40	1.00	0.21	0.05	0.00
10	U	A	0	0	25.3	23.2	23.1	23.0	23.0	10.1	0.83	0.21	0.08	0.00
11	U	A	0	0.5	25.3	23.2	23.1	23.0	23.0	10.1	0.83	0.21	0.04	0.00
12	U	A	0.5	0	23.5	21.6	21.5	21.4	21.4	9.50	0.79	0.21	0.04	0.00

Appendix 3.C verification between present detailed formulation and 3D FEA model

To assess the validity of the energy formulation formulated in the section titled "Formulation", the results obtained from present energy formulation are compared against those obtained from ABAQUS model for different load height and brace positions. There are two types of results compared in the Appendix: a) comparing the critical moment obtained from both models, and b) comparing the buckling mode shape obtained from both models. Table 3.C.1-3 are presenting the critical moment data that plotted in Figure 3.C.1 and 3.C.2.

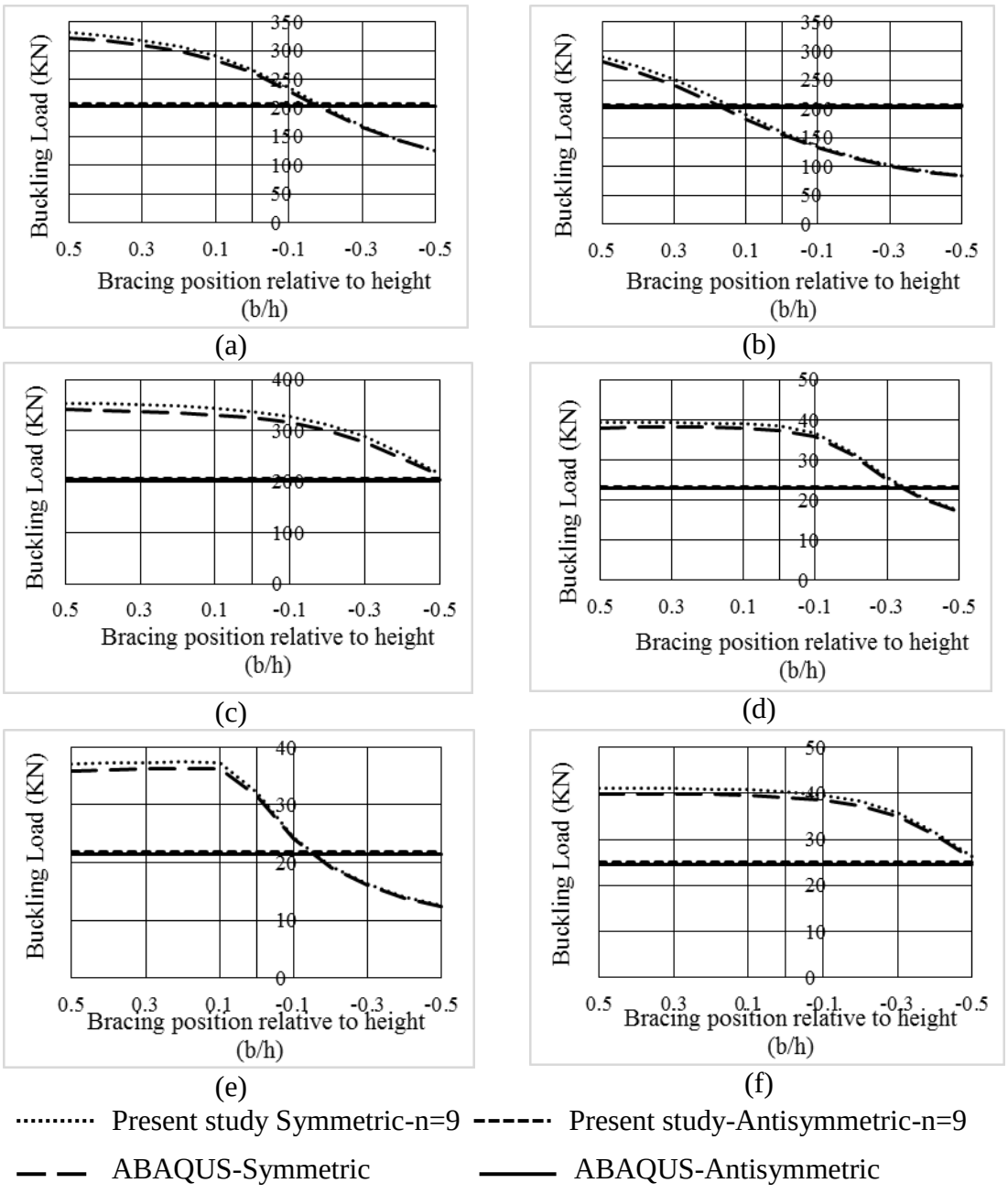

Figure 3.C.1 buckling load comparison relative to different bracing height when load at (a) point load, mid-height $a = 0$ (b) point load, top face $a = 0.5h$ (c) point load, bottom face $a = -0.5h$ (d) uniformly distributed load, mid-height $a = 0$ (b) uniformly distributed load, top face $a = 0.5h$ (c) uniformly distributed load, bottom face $a = -0.5h$

Table 3.C. 1 Comparison of buckling load (present study versus 3D FEA model)

(1) bracing height (b/h)	(2)Present Study-Symmtric-n=9 (kNm)	(3) Abaqus - Symmetric (kNm)	((2)-(3))/(2) (%)	(4) Present Study-Antisymmetric-n=9 (kNm)	(5) Abaqus - Antisymmetric (kNm)	((4)-(5))/(4) (%)
Point load at centroid (a=0)						
0.5	1078	1048	2.83	671	661	1.50
0.4	1061	1031	2.81	671	661	1.50
0.3	1036	1007	2.79	671	661	1.50
0.2	1000	972	2.75	671	661	1.50
0.1	947	922	2.63	671	661	1.50
0	869	851	2.02	671	661	1.50
-0.1	765	749	2.14	671	661	1.50
-0.2	652	640	1.83	671	661	1.50
-0.3	549	541	1.52	671	661	1.50
-0.4	469	463	1.28	671	661	1.50
-0.5	409	404	1.21	671	661	1.50
Point load at top face (a=0.5h)						
0.5	941	913	3.01	671	661	1.50
0.4	888	856	3.66	671	661	1.50
0.3	815	783	3.95	671	661	1.50
0.2	721	692	4.08	671	661	1.50
0.1	618	594	3.81	671	661	1.50
0	521	504	3.30	671	661	1.50
-0.1	442	429	2.75	671	661	1.50
-0.2	381	372	2.31	671	661	1.50
-0.3	335	329	1.98	671	661	1.50
-0.4	301	296	1.74	671	661	1.50
-0.5	275	271	1.61	671	661	1.50
Point load at bottom face (a=-0.5h）						
0.5	1151	1110	3.51	671	661	1.49
0.4	1147	1106	3.53	671	661	1.49
0.3	1141	1100	3.57	671	661	1.49
0.2	1132	1091	3.65	671	661	1.49
0.1	1119	1077	3.72	671	661	1.49
0	1099	1057	3.80	671	661	1.49
-0.1	1067	1026	3.88	671	661	1.49
-0.2	1017	978	3.90	671	661	1.49
-0.3	938	903	3.73	671	661	1.49
-0.4	827	801	3.13	671	661	1.49
-0.5	704	692	1.59	671	661	1.49

Table 3.C. 1 (cont) Comparison of buckling load (present study versus 3D FEA model)

(1) bracing height (b/h)	(2)Present Study-Symmtric-n=9 (kNm)	(3) Abaqus - Symmetric (kNm)	((2)-(3))/(2) (%)	(4) Present Study-Antisymmetric-n=9 (kNm)	(5) Abaqus - Antisymmetric (kNm)	((4)-(5))/(4) (%)
Uniformly distributed load at central axis (a=0）						
0.5	828	803	3.07	493	486	1.34
0.4	829	806	2.80	493	486	1.34
0.3	829	806	2.76	493	486	1.34
0.2	828	805	2.73	493	486	1.34
0.1	823	801	2.68	493	486	1.34
0	812	791	2.58	493	486	1.34
-0.1	778	760	2.29	493	486	1.34
-0.2	676	664	1.68	493	486	1.34
-0.3	538	532	1.27	493	486	1.34
-0.4	437	432	1.09	493	486	1.34
-0.5	369	364	1.13	493	486	1.34
Uniformly distributed load at top face (a=0.5h）						
0.5	785	760	3.19	460	453	1.57
0.4	787	763	3.12	460	453	1.57
0.3	789	765	3.07	460	453	1.57
0.2	791	767	3.01	460	453	1.57
0.1	787	765	2.83	460	453	1.57
0	681	669	1.90	460	453	1.57
-0.1	516	508	1.53	460	453	1.57
-0.2	411	405	1.32	460	453	1.57
-0.3	343	339	1.19	460	453	1.57
-0.4	297	293	1.12	460	453	1.57
-0.5	264	261	1.13	460	453	1.57

Table 3.C. 1 (cont) Comparison of buckling load (present study versus 3D FEA model)

(1) bracing height (b/h)	(2)Present Study-Symmtric-n=9 (kNm)	(3) Abaqus - Symmetric (kNm)	((2)-(3))/(2) (%)	(4) Present Study-Antisymmetric-n=9 (kNm)	(5) Abaqus - Antisymmetric (kNm)	((4)-(5))/(4) (%)
Uniformly distributed load at bottom face (a=-0.5h）						
0.5	870	843	3.07	528	519	1.59
0.4	869	843	3.04	528	519	1.59
0.3	868	841	3.02	528	519	1.59
0.2	865	839	3.00	528	519	1.59
0.1	860	835	2.97	528	519	1.59
0	852	827	2.93	528	519	1.59
-0.1	837	813	2.84	528	519	1.59
-0.2	810	789	2.65	528	519	1.59
-0.3	757	740	2.27	528	519	1.59
-0.4	665	653	1.78	528	519	1.59
-0.5	555	545	1.72	528	519	1.59

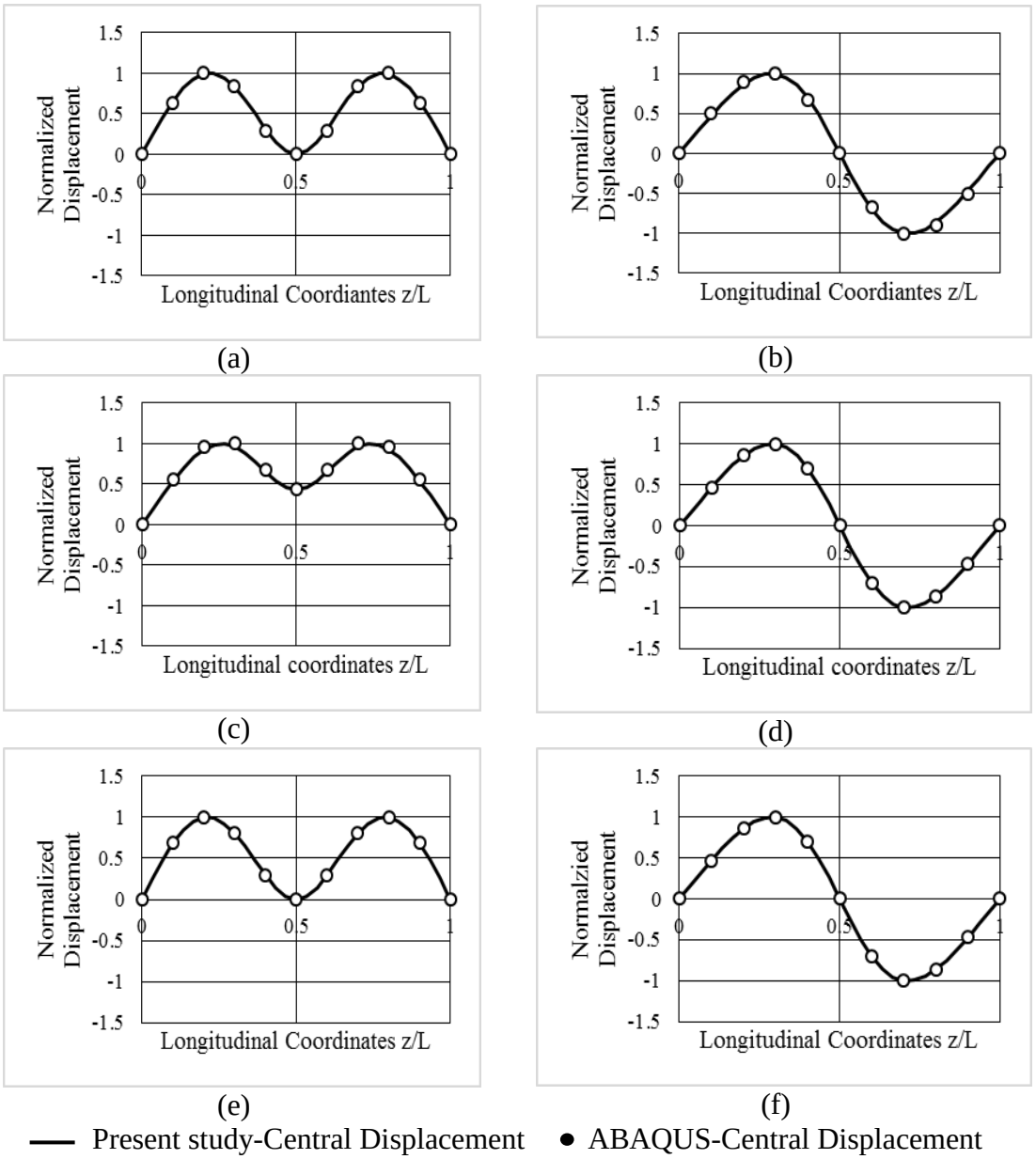

Figure 3.C. 2 Comparison of buckling mode shape for different load and brace height(a) point load, symmetric mode, $a=0, b=0$ **(b) point load, anti-symmetric mode** $a=0, b=0$ **(c) point load, symmetric mode,** $a=0$, $b=0.5h$ **(d) point load, anti-symmetric mode,** $a=0$, $b=0.5h$ **(e) point load, symmetric mode,** $a=0.5h$, $b=0$ **(f) uniformly distributed load, anti-symmetric mode,** $a=0.5h$, $b=0$

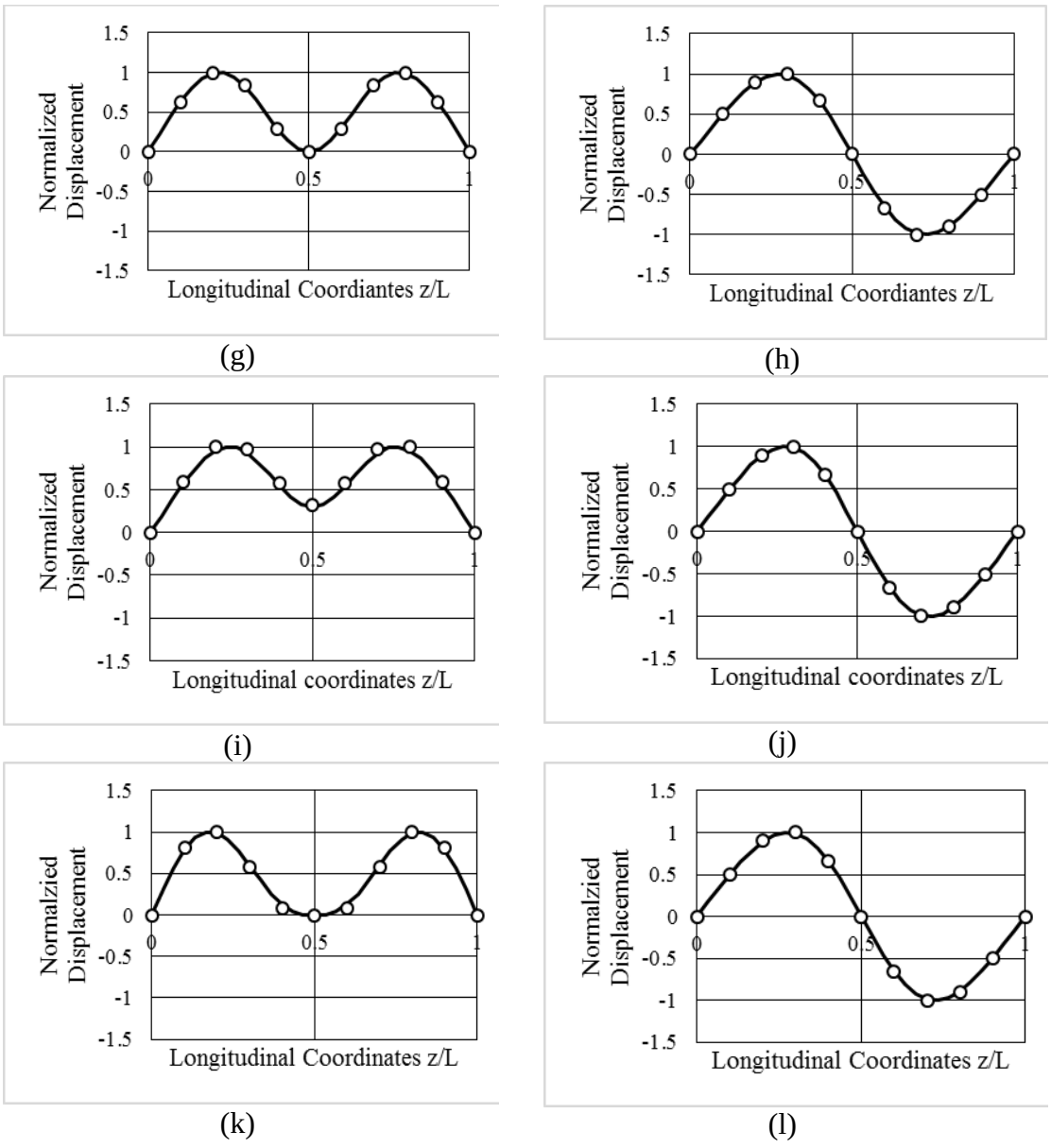

Figure 3.C. 2 (cont) Comparison of buckling mode shape for different load and brace height(g) uniformly distributed load, symmetric mode $a=0, b=0$ **(h) uniformly distributed load, anti-symmetric mode** $a=0, b=0$ **(i) uniformly distributed load, symmetric mode,** $a=0$, $b=0.5h$ **(j) uniformly distributed load, anti-symmetric mode,** $a=0$, $b=0.5h$ **(k) uniformly distributed load, symmetric mode,** $a=0.5h$, $b=0$ **(l) uniformly distributed load, anti-symmetric mode,** $a=0.5h$, $b=0$

Appendix 3.D-Results for threshold bracing height and maximum critical moment

Based on the present energy formulation, the critical moments based on the symmetric mode and threshold bracing height can be obtained for simply supported beams with different geometric and elastic properties. Table 3.D.1-9 presents the results of 148 runs obtained based on the present formulation by varying the values dimensionless parameters of w/h , L/h , a/h and G/E to assist the regression analysis of design expressions described in section titled “Development of Simplified design expressions” for point load and uniformly distributed load cases, respectively.

Table 3.D. 1 mid-span point loading

Run	Geometric parameters				Elastic parameters		Dimensionless parameters				results				
	w(m)	h(m)	L (m)	a(m)	E (10^4MPa)	G (10^2MPa)	w/h	L/h	a/h	G/E	M_{cr} (present solution) (10^3kNm)	M_{cr} (based on regression) (10^3kNm)	Diff[1] (%)	b_{cr} (m) based on present solution	Normalized bracing height bcr/h
1	0.13	0.95	10.0	0	1.03	6.44	0.137	10.5	0	0.0625	1.03	1.03	-0.23	-0.16	-0.16
2	0.13	0.87	9.2	0	1.03	6.44	0.149	10.5	0	0.0625	1.03	1.02	-0.24	-0.14	-0.16
3	0.13	0.80	8.4	0	1.03	6.44	0.163	10.5	0	0.0625	1.02	1.02	-0.25	-0.13	-0.16
4	0.13	0.72	7.6	0	1.03	6.44	0.180	10.5	0	0.0625	1.02	1.01	-0.26	-0.12	-0.16
5	0.13	0.65	6.8	0	1.03	6.44	0.201	10.5	0	0.0625	1.01	1.01	-0.28	-0.10	-0.16
6	0.13	0.57	6.0	0	1.03	6.44	0.228	10.5	0	0.0625	1.00	0.999	-0.30	-0.09	-0.16
7	0.13	0.53	5.6	0	1.03	6.44	0.244	10.5	0	0.0625	9.97	0.994	-0.31	-0.08	-0.16
8	0.13	0.46	4.8	0	1.03	6.44	0.285	10.5	0	0.0625	0.984	0.981	-0.35	-0.07	-0.15

[1] $Difference = \left(M_{cr}appx - M_{cr}\right)/M_{cr}appx$

Table 3.D. 1 (cont) mid-span point loading

Run	Geometric parameters				Elastic parameters		Dimensionless parameters				Results				
	w(m)	h(m)	L (m)	a(m)	E (10^4MPa)	G (10^2MPa)	w/h	L/h	a/h	G/E	M_{cr} (present solution) (10^3kNm)	M_{cr} (based on regression) (10^3kNm)	Diff[1] (%)	b_{cr} (m) based on present solution	Normalized bracing height bcr/h
9	0.13	0.38	4.0	0	1.03	6.44	0.342	10.5	0	0.0625	0.966	0.962	-0.40	-0.06	-0.15
10	0.13	0.30	3.2	0	1.03	6.44	0.428	10.5	0	0.0625	0.937	0.933	-0.48	-0.04	-0.15
11	0.13	0.23	2.4	0	1.03	6.44	0.570	10.5	0	0.0625	0.889	0.884	-0.63	-0.03	-0.14
12	0.13	0.95	10.0	-0.475	1.03	6.44	0.137	10.5	-0.5	0.0625	1.03	1.03	-0.23	-0.48	-0.51
13	0.13	0.95	10.0	-0.380	1.03	6.44	0.137	10.5	-0.4	0.0625	1.03	1.03	-0.23	-0.42	-0.44
14	0.13	0.95	10.0	-0.285	1.03	6.44	0.137	10.5	-0.3	0.0625	1.03	1.03	-0.23	-0.35	-0.37
15	0.13	0.95	10.0	-0.190	1.03	6.44	0.137	10.5	-0.2	0.0625	1.03	1.03	-0.23	-0.28	-0.30
16	0.13	0.95	10.0	-0.095	1.03	6.44	0.137	10.5	-0.1	0.0625	1.03	1.03	-0.23	-0.22	-0.23
17	0.13	0.95	10.0	0.095	1.03	6.44	0.137	10.5	0.1	0.0625	1.03	1.03	-0.23	-0.09	-0.10
18	0.13	0.95	10.0	0.190	1.03	6.44	0.137	10.5	0.2	0.0625	1.03	1.03	-0.23	-0.03	-0.03
19	0.13	0.95	10.0	0.285	1.03	6.44	0.137	10.5	0.3	0.0625	1.03	1.03	-0.23	0.03	0.04
20	0.13	0.95	10.0	0.380	1.03	6.44	0.137	10.5	0.4	0.0625	1.03	1.03	-0.23	0.10	0.10
21	0.13	0.95	10.0	0.475	1.03	6.44	0.137	10.5	0.5	0.0625	1.03	1.03	-0.23	0.16	0.17
22	0.13	0.95	15.0	0	1.03	6.44	0.137	15.8	0	0.0625	0.660	0.663	0.54	-0.23	-0.25
23	0.13	0.95	14.0	0	1.03	6.44	0.137	15.0	0	0.0625	0.710	0.714	0.43	-0.22	-0.23
24	0.13	0.95	13.0	0	1.03	6.44	0.137	13.7	0	0.0625	0.770	0.772	0.30	-0.20	-0.21
25	0.13	0.95	12.0	0	1.03	6.44	0.137	12.6	0	0.0625	0.841	0.842	0.15	-0.19	-0.20

[1] $Difference = \left(M_{cr}appx - M_{cr}\right)/M_{cr}appx$

Table 3.D. 1 (cont) mid-span point loading

Run	Geometric parameters				Elastic parameters		Dimensionless parameters				Results				
	w(m)	h(m)	L (m)	a(m)	E (10^4MPa)	G (10^2MPa)	w/h	L/h	a/h	G/E	M_{cr} (present solution) (10^3kNm)	M_{cr} (based on regression) (10^3kNm)	Diff[1] (%)	b_{cr} (m) based on present solution	Normalized bracing height bcr/h
26	0.13	0.95	11.0	0	1.03	6.44	0.137	11.6	0	0.0625	0.926	0.926	-0.03	-0.17	-0.18
27	0.13	0.95	9.0	0	1.03	6.44	0.137	9.5	0	0.0625	1.16	1.16	-0.47	-0.14	-0.15
28	0.13	0.95	8.0	0	1.03	6.44	0.137	8.4	0	0.0625	1.34	1.33	-0.74	-0.12	-0.13
29	0.13	0.95	10.0	0	1.03	10.30	0.137	10.5	0	0.1000	1.27	1.27	0.25	-0.20	-0.21
30	0.13	0.95	10.0	0	1.03	8.58	0.137	10.5	0	0.0833	1.17	1.17	0.07	-0.18	-0.19
31	0.13	0.95	10.0	0	1.03	7.36	0.137	10.5	0	0.0714	1.09	1.09	-0.09	-0.17	-0.17
32	0.13	0.95	10.0	0	1.03	5.72	0.137	10.5	0	0.0556	0.980	0.977	-0.36	-0.15	-0.15
33	0.13	0.95	10.0	0	1.03	5.15	0.137	10.5	0	0.0500	0.937	0.933	-0.48	-0.14	-0.15
34	0.13	0.87	13.8	0	1.03	6.44	0.149	15.79	0	0.0625	60.657	60.661	0.54	-0.214	-0.245
35	0.13	0.80	12.6	0	1.03	6.44	0.163	15.79	0	0.0625	0.654	0.658	0.53	-0.194	-0.243
36	0.13	0.72	11.4	0	1.03	6.44	0.180	15.79	0	0.0625	0.651	0.654	0.52	-0.175	-0.242
37	0.13	0.65	10.2	0	1.03	6.44	0.201	15.79	0	0.0625	0.646	0.649	0.51	-0.155	-0.24
38	0.13	0.57	9.0	0	1.03	6.44	0.228	15.79	0	0.0625	0.640	0.643	0.49	-0.135	-0.238
39	0.13	0.53	8.4	0	1.03	6.44	0.244	15.79	0	0.0625	0.637	0.640	0.48	-0.126	-0.236
40	0.13	0.46	7.2	0	1.03	6.44	0.285	15.79	0	0.0625	0.628	0.630	0.46	-0.106	-0.233
41	0.13	0.38	6.0	0	1.03	6.44	0.342	15.79	0	0.0625	0.615	0.617	0.42	-0.086	-0.228
42	0.13	0.30	4.8	0	1.03	6.44	0.428	15.79	0	0.0625	0.595	0.597	0.36	-0.067	-0.22
43	0.13	0.23	3.6	0	1.03	6.44	0.570	15.79	0	0.0625	0.562	0.563	0.24	-0.047	-0.206

[1] $Difference = \left(M_{cr}appx - M_{cr}\right)/M_{cr}appx$

Table 3.D. 1 (cont) mid-span point loading

Run	Geometric parameters				Elastic parameters		Dimensionless parameters				Results				
	w(m)	h(m)	L (m)	a(m)	E (10^4MPa)	G (10^2MPa)	w/h	L/h	a/h	G/E	M_{cr} (present solution) (10^3kNm)	M_{cr} (based on regression) (10^3kNm)	Diff[1] (%)	b_{cr} (m) based on present solution	Normalized bracing height bcr/h
44	0.13	0.95	15.0	-0.475	1.03	6.44	0.137	15.79	-0.5	0.0625	0.660	0.663	0.54	-0.566	-0.595
45	0.13	0.95	15.0	-0.38	1.03	6.44	0.137	15.79	-0.4	0.0625	0.660	0.663	0.54	-0.499	-0.525
46	0.13	0.95	15.0	-0.285	1.03	6.44	0.137	15.79	-0.3	0.0625	0.660	0.663	0.54	-0.432	-0.455
47	0.13	0.95	15.0	-0.19	1.03	6.44	0.137	15.79	-0.2	0.0625	0.660	0.663	0.54	-0.365	-0.385
48	0.13	0.95	15.0	-0.095	1.03	6.44	0.137	15.79	-0.1	0.0625	0.660	0.663	0.54	-0.299	-0.315
49	0.13	0.95	15.0	0.095	1.03	6.44	0.137	15.79	0.1	0.0625	0.660	0.663	0.54	-0.168	-0.176
50	0.13	0.95	15.0	0.19	1.03	6.44	0.137	15.79	0.2	0.0625	0.660	0.663	0.54	-0.102	-0.108
51	0.13	0.95	15.0	0.285	1.03	6.44	0.137	15.79	0.3	0.0625	0.660	0.663	0.54	-0.037	-0.039
52	0.13	0.95	15.0	0.38	1.03	6.44	0.137	15.79	0.4	0.0625	0.660	0.663	0.54	0.027	0.0289
53	0.13	0.95	15.0	0.475	1.03	6.44	0.137	15.79	0.5	0.0625	0.660	0.663	0.54	0.092	0.0967
54	0.13	0.95	20.0	0	1.03	6.44	0.137	21.05	0	0.0625	0.487	0.492	0.92	-0.31	-0.326
55	0.13	0.95	19.0	0	1.03	6.44	0.137	20	0	0.0625	0.514	0.518	0.86	-0.295	-0.31
56	0.13	0.95	18.0	0	1.03	6.44	0.137	18.95	0	0.0625	0.544	0.548	0.80	-0.279	-0.294
57	0.13	0.95	17.0	0	1.03	6.44	0.137	17.89	0	0.0625	0.578	0.582	0.72	-0.264	-0.278
58	0.13	0.95	16.0	0	1.03	6.44	0.137	16.84	0	0.0625	0.616	0.620	0.64	-0.249	-0.262
59	0.13	0.95	14.0	0	1.03	6.44	0.137	14.74	0	0.0625	0.710	0.714	0.43	-0.218	-0.229
60	0.13	0.95	13.0	0	1.03	6.44	0.137	13.68	0	0.0625	0.770	0.772	0.30	-0.202	-0.213
61	0.13	0.95	12.0	0	1.03	6.44	0.137	12.63	0	0.0625	0.841	0.842	0.15	-0.187	-0.196
62	0.13	0.95	11.0	0	1.03	6.44	0.137	11.58	0	0.0625	0.926	0.926	-0.03	-0.171	-0.18
63	0.13	0.95	10.0	0	1.03	6.44	0.137	10.53	0	0.0625	1.03	1.03	-0.23	-0.155	-0.163

[1] $Difference = \left(M_{cr}appx - M_{cr}\right)/M_{cr}appx$

Table 3.D. 1 (cont) mid-span point loading

Run	Geometric parameters				Elastic parameters		Dimensionless parameters				Results				
	w(m)	h(m)	L (m)	a(m)	E (10^4MPa)	G (10^2MPa)	w/h	L/h	a/h	G/E	M_{cr} (present solution) (10^3kNm)	M_{cr} (based on regression) (10^3kNm)	Diff[1] (%)	b_{cr} (m) based on present solution	Normalized bracing height bcr/h
64	0.13	0.95	15.0	0	1.03	10.30	0.137	15.79	0	0.1000	0.823	0.830	0.86	-0.294	-0.31
65	0.13	0.95	15.0	0	1.03	8.58	0.137	10.53	0	0.0833	0.755	0.761	0.75	-0.269	-0.283
66	0.13	0.95	15.0	0	1.03	7.36	0.137	10.53	0	0.0714	0.702	0.707	0.64	-0.249	-0.262
67	0.13	0.95	15.0	0	1.03	5.72	0.137	10.53	0	0.0556	0.625	0.628	0.45	-0.22	-0.232
68	0.13	0.95	15.0	0	1.03	5.15	0.137	10.53	0	0.0500	0.595	0.597	0.36	-0.209	-0.22

[1] $Difference = \left(M_{cr}appx - M_{cr}\right)/M_{cr}appx$

Table 3.D. 2 uniformly distributed load

run	Geometric parameters				Elastic parameters		Dimensionless parameters				Results				
	w (m)	h (m)	L (m)	a (m)	E (10^4MPa)	G (10^2MPa)	w/h	L/h	a/h	G/E	M_{cr} (present solution) (10^3kNm)	M_{cr} (based on regression) (10^3kNm)	Diff[1] (%)	b_{cr} (m) based on present solution	Normalized bracing height bcr/h
1	0.13	0.95	10.0	0	1.03	6.44	0.137	10.5	0	0.063	7.56	7.56	-0.03	-0.288	-0.30
2	0.13	0.874	9.2	0	1.03	6.44	0.149	10.5	0	0.063	7.53	7.54	-0.03	-0.264	-0.30
3	0.13	0.798	8.4	0	1.03	6.44	0.163	10.5	0	0.063	7.50	7.50	-0.02	-0.240	-0.30
4	0.13	0.722	7.6	0	1.03	6.44	0.180	10.5	0	0.063	7.46	7.46	-0.01	-0.216	-0.30
5	0.13	0.646	6.8	0	1.03	6.44	0.201	10.5	0	0.063	7.41	7.41	-0.01	-0.191	-0.30
6	0.13	0.57	6.0	0	1.03	6.44	0.228	10.5	0	0.063	7.35	7.35	0.00	-0.167	-0.29
7	0.13	0.532	5.6	0	1.03	6.44	0.244	10.5	0	0.063	7.31	7.31	0.01	-0.155	-0.29
8	0.13	0.456	4.8	0	1.03	6.44	0.285	10.5	0	0.063	7.22	7.21	0.03	-0.131	-0.29
9	0.13	0.38	4.0	0	1.03	6.44	0.342	10.5	0	0.063	7.08	7.07	0.05	-0.106	-0.28
10	0.13	0.304	3.2	0	1.03	6.44	0.428	10.5	0	0.063	6.87	6.86	0.09	-0.082	-0.27
11	0.13	0.228	2.4	0	1.03	6.44	0.570	10.5	0	0.063	6.51	6.50	0.16	-0.058	-0.25
12	0.13	0.152	1.6	0	1.03	6.44	0.855	10.5	0	0.063	5.81	5.80	0.32	-0.033	-0.22
13	0.13	0.95	10.0	-0.475	1.03	6.44	0.137	10.5	-0.5	0.063	8.15	8.13	0.21	-0.392	-0.41
14	0.13	0.95	10.0	-0.380	1.03	6.44	0.137	10.5	-0.4	0.063	8.03	8.02	0.13	-0.377	-0.40
15	0.13	0.95	10.0	-0.285	1.03	6.44	0.137	10.5	-0.3	0.063	7.91	7.91	0.07	-0.359	-0.38
16	0.13	0.95	10.0	-0.190	1.03	6.44	0.137	10.5	-0.2	0.063	7.79	7.79	0.02	-0.339	-0.36
17	0.13	0.95	10.0	-0.095	1.03	6.44	0.137	10.5	-0.1	0.063	7.68	7.68	-0.02	-0.315	-0.33
18	0.13	0.95	10.0	0.095	1.03	6.44	0.137	10.5	0.1	0.063	7.45	7.45	-0.03	-0.258	-0.27
19	0.13	0.95	10.0	0.190	1.03	6.44	0.137	10.5	0.2	0.063	7.34	7.34	0.00	-0.224	-0.24
20	0.13	0.95	10.0	0.285	1.03	6.44	0.137	10.5	0.3	0.063	7.22	7.22	0.05	-0.187	-0.20
21	0.13	0.95	10.0	0.380	1.03	6.44	0.137	10.5	0.4	0.063	7.12	7.11	0.12	-0.146	-0.15

Table 3.D. 2 (cont) uniformly distributed load

run	Geometric parameters				Elastic parameters		Dimensionless parameters				Results				
	w (m)	h (m)	L (m)	a (m)	E (10^4MPa)	G (10^2MPa)	w/h	L/h	a/h	G/E	M_{cr} (present solution) (10^3kNm)	M_{cr} (based on regression) (10^3kNm)	Diff[1] (%)	b_{cr}(m) based on present solution	Normalized bracing height bcr/h
22	0.13	0.95	10.0	0.475	1.03	6.44	0.137	10.5	0.5	0.063	7.01	6.99	0.21	-0.101	-0.11
23	0.13	0.95	15.0	0	1.03	6.44	0.137	15.8	0	0.063	4.86	4.88	-0.40	-0.438	-0.46
24	0.13	0.95	14.0	0	1.03	6.44	0.137	15.0	0	0.063	5.23	5.25	-0.35	-0.408	-0.43
25	0.13	0.95	13.0	0	1.03	6.44	0.137	13.7	0	0.063	5.66	5.68	-0.29	-0.378	-0.40
26	0.13	0.95	12.0	0	1.03	6.44	0.137	12.6	0	0.063	6.18	6.19	-0.21	-0.348	-0.37
27	0.13	0.95	11.0	0	1.03	6.44	0.137	11.6	0	0.063	6.80	6.81	-0.13	-0.318	-0.34
28	0.13	0.95	9.0	0	1.03	6.44	0.137	9.5	0	0.063	8.52	8.52	0.08	-0.258	-0.27
29	0.13	0.95	8.0	0	1.03	6.44	0.137	8.4	0	0.063	9.78	9.76	0.22	-0.228	-0.24
30	0.13	0.95	7.0	0	1.03	6.44	0.137	7.4	0	0.063	11.5	11.4	0.37	-0.197	-0.21
31	0.13	0.95	6.0	0	1.03	6.44	0.137	6.3	0	0.063	13.9	13.8	0.54	-0.167	-0.18
32	0.13	0.95	5.0	0	1.03	6.44	0.137	5.3	0	0.063	17.7	17.5	0.73	-0.136	-0.14
33	0.13	0.95	10.0	0	1.03	10.30	0.137	10.5	0	0.100	9.33	9.36	-0.26	-0.368	-0.39
34	0.13	0.95	10.0	0	1.03	8.58	0.137	10.5	0	0.083	8.59	8.61	-0.18	-0.335	-0.35
35	0.13	0.95	10.0	0	1.03	7.36	0.137	10.5	0	0.071	8.02	8.03	-0.10	-0.309	-0.33
36	0.13	0.95	10.0	0	1.03	5.72	0.137	10.5	0	0.056	7.18	7.18	0.03	-0.271	-0.29
37	0.13	0.95	10.0	0	1.03	5.15	0.137	10.5	0	0.050	6.87	6.86	0.09	-0.256	-0.27
38	0.13	0.95	10.0	0	1.03	4.68	0.137	10.5	0	0.045	6.60	6.59	0.15	-0.244	-0.26
39	0.13	0.95	10.0	0	1.03	4.29	0.137	10.5	0	0.042	6.36	6.35	0.20	-0.233	-0.25
40	0.13	0.95	15	0	1.03	6.44	0.14	15.789	0	0.063	4.86	4.88	0.40	-0.438	-0.46
41	0.13	0.874	13.8	0	1.03	6.44	0.15	15.789	0	0.063	4.84	4.86	0.40	-0.401	-0.46
42	0.13	0.798	12.6	0	1.03	6.44	0.16	15.789	0	0.063	4.82	4.84	0.40	-0.364	-0.46
43	0.13	0.722	11.4	0	1.03	6.44	0.18	15.789	0	0.063	4.79	4.81	0.39	-0.327	-0.45

Table 3.D. 2 (cont) uniformly distributed load

run	Geometric parameters				Elastic parameters		Dimensionless parameters				Results				
	w (m)	h (m)	L (m)	a (m)	E (10^4MPa)	G (10^3MPa)	w/h	L/h	a/h	G/E	M_{cr} (present solution) (10^3kNm)	M_{cr} (based on regression) (10^3kNm)	Diff[1] (%)	b_{cr}(m) based on present solution	Normalized bracing height bcr/h
44	0.13	0.646	10.2	0	1.03	6.44	0.20	15.789	0	0.063	4.76	4.78	0.39	-0.291	-0.45
45	0.13	0.57	9.0	0	1.03	6.44	0.23	15.789	0	0.063	4.71	4.73	0.38	-0.254	-0.45
46	0.13	0.532	8.4	0	1.03	6.44	0.24	15.789	0	0.063	4.69	4.70	0.37	-0.236	-0.44
47	0.13	0.456	7.2	0	1.03	6.44	0.29	15.789	0	0.063	4.62	4.64	0.36	-0.199	-0.44
48	0.13	0.38	6.0	0	1.03	6.44	0.34	15.789	0	0.063	4.53	4.54	0.34	-0.162	-0.43
49	0.13	0.304	4.8	0	1.03	6.44	0.43	15.789	0	0.063	4.38	4.39	0.31	-0.125	-0.41
50	0.13	0.228	3.6	0	1.03	6.44	0.57	15.789	0	0.063	4.13	4.14	0.26	-0.088	-0.39
51	0.13	0.95	15.0	-0.475	1.03	6.44	0.14	15.789	-0.5	0.063	5.12	5.13	0.34	-0.542	-0.57
52	0.13	0.95	15.0	-0.38	1.03	6.44	0.14	15.789	-0.4	0.063	5.06	5.08	0.36	-0.525	-0.55
53	0.13	0.95	15.0	-0.285	1.03	6.44	0.14	15.789	-0.3	0.063	5.01	5.03	0.39	-0.507	-0.53
54	0.13	0.95	15.0	-0.19	1.03	6.44	0.14	15.789	-0.2	0.063	4.96	4.98	0.40	-0.486	-0.51
55	0.13	0.95	15.0	-0.095	1.03	6.44	0.14	15.789	-0.1	0.063	4.91	4.93	0.41	-0.463	-0.49
56	0.13	0.95	15.0	0.095	1.03	6.44	0.14	15.789	0.1	0.063	4.81	4.83	0.39	-0.410	-0.43
57	0.13	0.95	15.0	0.19	1.03	6.44	0.14	15.789	0.2	0.063	4.76	4.78	0.37	-0.379	-0.40
58	0.13	0.95	15.0	0.285	1.03	6.44	0.14	15.789	0.3	0.063	4.71	4.73	0.34	-0.346	-0.36
59	0.13	0.95	15.0	0.38	1.03	6.44	0.14	15.789	0.4	0.063	4.66	4.68	0.30	-0.310	-0.33
60	0.13	0.95	15.0	0.475	1.03	6.44	0.14	15.789	0.5	0.063	4.61	4.63	0.25	-0.270	-0.28
61	0.13	0.95	20.0	0	1.03	6.44	0.14	21.053	0	0.063	3.59	3.62	0.58	-0.585	-0.62
62	0.13	0.95	19.0	0	1.03	6.44	0.14	20	0	0.063	3.79	3.81	0.56	-0.556	-0.59
63	0.13	0.95	18.0	0	1.03	6.44	0.14	18.947	0	0.063	4.01	4.03	0.53	-0.526	-0.55
64	0.13	0.95	17.0	0	1.03	6.44	0.14	17.895	0	0.063	4.26	4.28	0.49	-0.497	-0.52
65	0.13	0.95	16.0	0	1.03	6.44	0.14	16.842	0	0.063	4.54	4.56	0.45	-0.467	-0.49

Table 3.D. 2 (cont) uniformly distributed load

run	Geometric parameters				Elastic parameters		Dimensionless parameters				Results				
	w (m)	h (m)	L (m)	a (m)	E (10^4MPa)	G (10^2MPa)	w/h	L/h	a/h	G/E	M_{cr} (present solution) (10^3kNm)	M_{cr} (based on regression) (10^3kNm)	Diff[1] (%)	b_{cr}(m) based on present solution	Normalized bracing height bcr/h
66	0.13	0.95	14.0	0	1.03	6.44	0.14	14.737	0	0.063	5.23E+05	5.25	0.35	-0.408	-0.43
67	0.13	0.95	13.0	0	1.03	6.44	0.14	13.684	0	0.063	5.66E+05	5.68	0.29	-0.378	-0.40
68	0.13	0.95	12.0	0	1.03	6.44	0.14	12.632	0	0.063	6.18E+05	6.19	0.21	-0.348	-0.37
69	0.13	0.95	11.0	0	1.03	6.44	0.14	11.579	0	0.063	6.80E+05	6.81	0.13	-0.318	-0.34
70	0.13	0.95	10.0	0	1.03	6.44	0.14	10.526	0	0.063	7.56E+05	7.56	0.03	-0.288	-0.30
71	0.13	0.95	15.0	0	1.03	10.30	0.14	15.789	0	0.100	6.07E+05	6.11	0.56	-0.555	-0.58
72	0.13	0.95	15.0	0	1.03	9.36	0.14	15.789	0	0.091	5.80E+05	5.83	0.53	-0.529	-0.56
73	0.13	0.95	15.0	0	1.03	8.58	0.14	15.789	0	0.083	5.57E+05	5.59	0.50	-0.506	-0.53
74	0.13	0.95	15.0	0	1.03	7.92	0.14	15.789	0	0.077	5.36E+05	5.38	0.48	-0.486	-0.51
75	0.13	0.95	15.0	0	1.03	7.36	0.14	15.789	0	0.071	5.17E+05	5.20	0.45	-0.468	-0.49
76	0.13	0.95	15.0	0	1.03	6.87	0.14	15.789	0	0.067	5.01E+05	5.03	0.43	-0.452	-0.48
77	0.13	0.95	15.0	0	1.03	6.06	0.14	15.789	0	0.059	4.72E+05	4.74	0.38	-0.424	-0.45
78	0.13	0.95	15.0	0	1.03	5.72	0.14	15.789	0	0.056	4.60E+05	4.62	0.36	-0.412	-0.43
79	0.13	0.95	15.0	0	1.03	5.42	0.14	15.789	0	0.053	4.48E+05	4.50	0.34	-0.401	-0.42
80	0.13	0.95	15.0	0	1.03	5.15	0.14	15.789	0	0.050	4.38E+05	4.39	0.31	-0.390	-0.41

Appendix 3.E Trends of threshold bracing height with key geometric and material properties

The present appendix provides the trends of threshold bracing height ratio with the section aspect ratio w/h, span to height ratio L/h, load height to section height ratio a/h and shear modulus ratio G/E as determined from the runs presented in Appendix 3.D. The shown trends provided the basis to assume the form of the proposed regression equations (Eq. (5.30) and (5.33)).

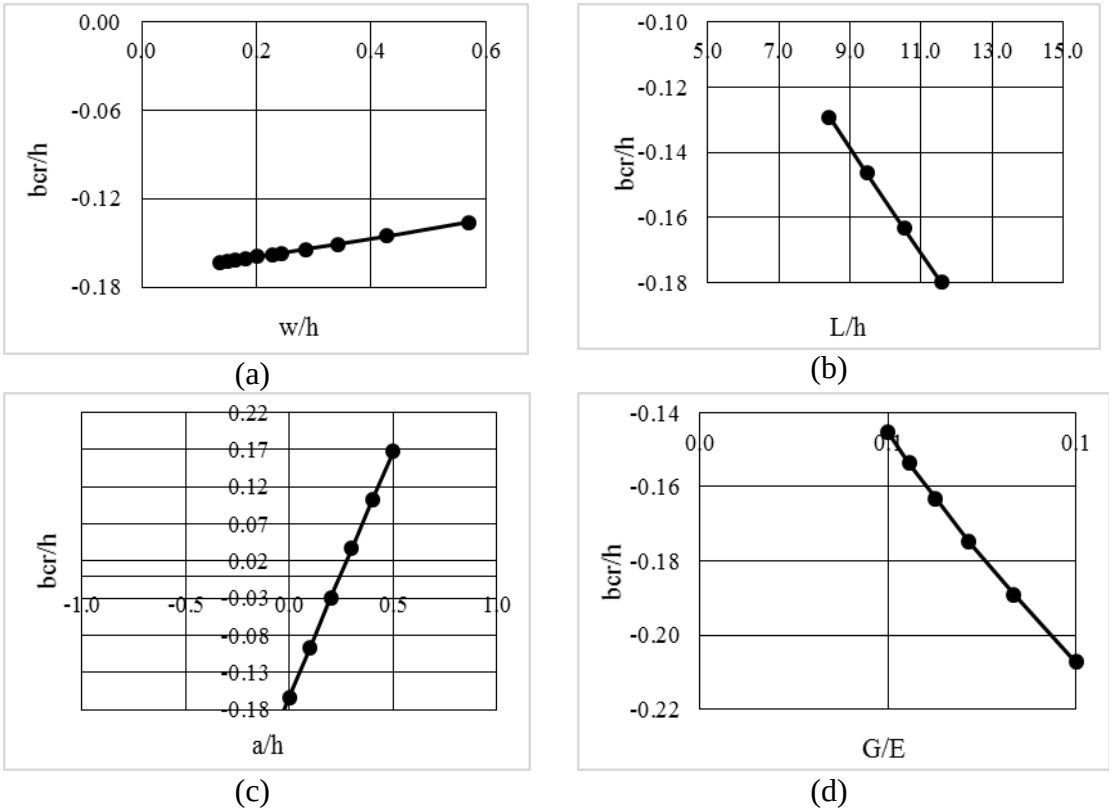

Figure 3.E Normalized threshold bracing height relative to cross-sectional height (bcr/h) as a function of (a) section width to height w/h, point load, (b) span to height (L/h), point load (c) load height to section height (a/h), point load(d) shear modulus to Young modulus ratio (G/E), point load

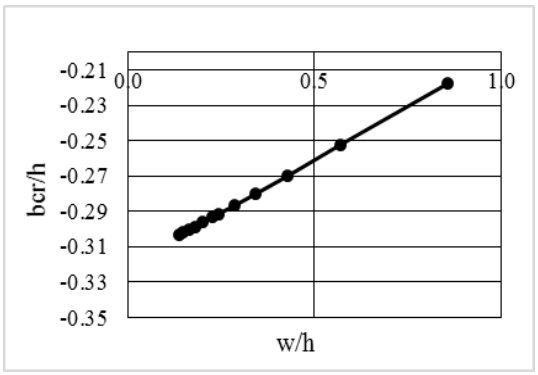

(e)

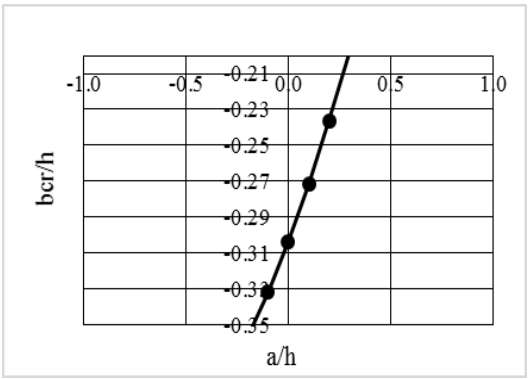

(f)

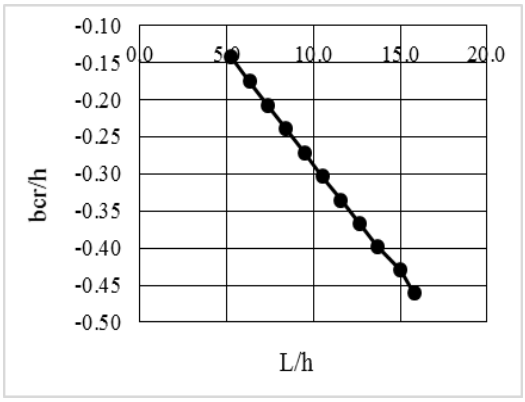

(g)

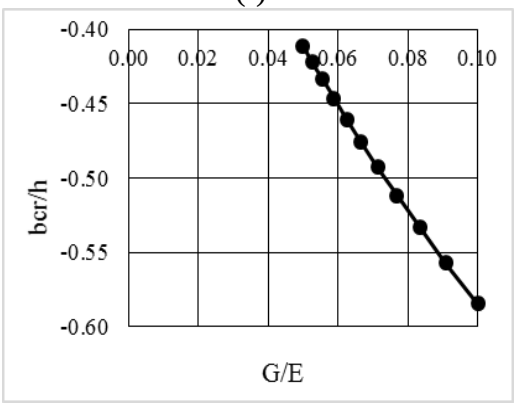

(h)

Figure 3.E (cont) Normalized threshold bracing height relative to cross-sectional height (bcr/h) as a function of (e) section width to height w/h, uniformly distributed load (f) span to height (L/h), uniformly distributed load (g) load height to section height (a/h), uniformly distributed load and (h) shear modulus to Young modulus ratio (G/E), uniformly distributed load.

Appendix 3.F Characteristics of slope relative to different parameters for uniformly distributed load

The present appendix provides the trends of maximum critical moment ratio with the reciprocal of span square $1/L^2$, Elastic modulus E, cubic of cross section width w^3 and square of cross section width h^2. The shown trends provided the basis to assume the form of the proposed regression equations (Eq. (5.34)).

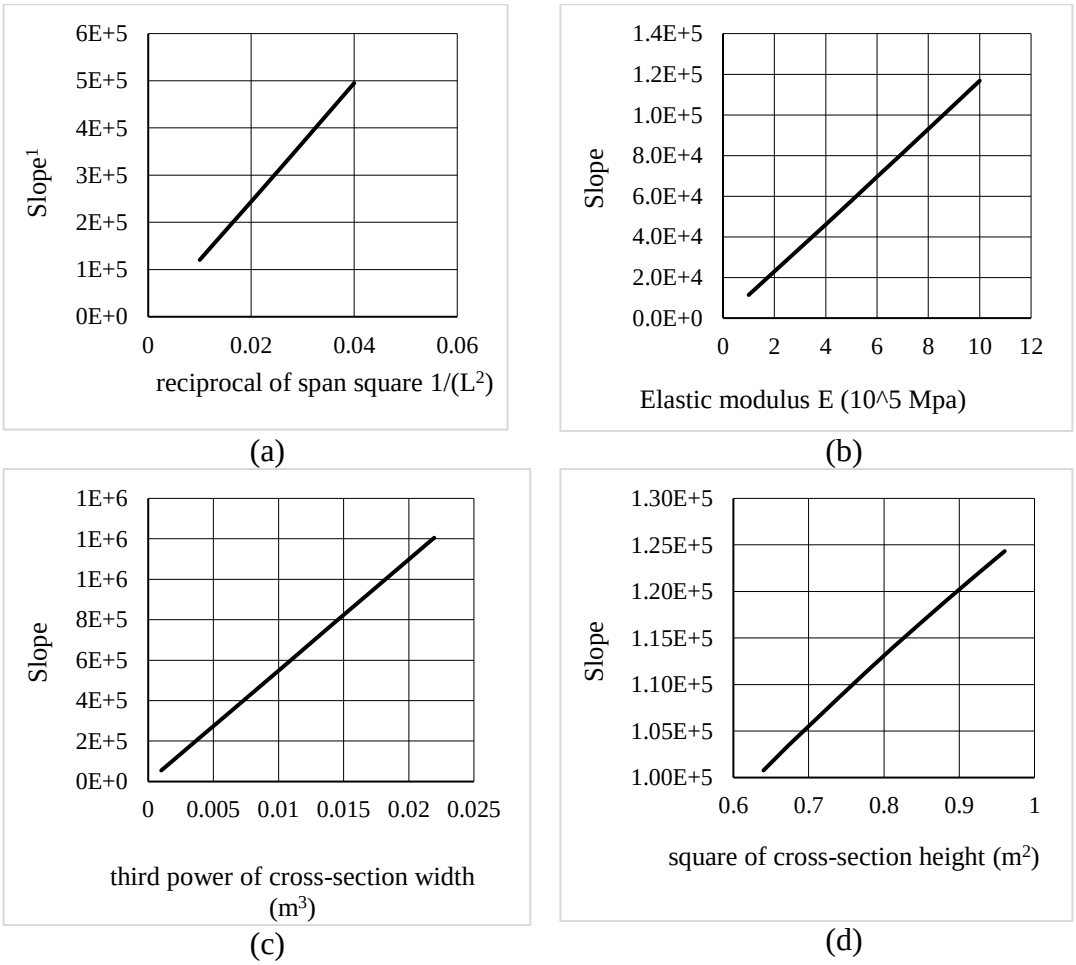

[1] $Slope = \left[M_{cr}(bottom) - M_{cr}(top)\right]/h$

Figure 3.F Moment variation slope relative to different parameters

Appendix 3.G Moment gradient calculation

Moment gradient factor which are referred in section titled "Application of design expressions" can be determined from various design standards as Eqs. (3.G.1), (3.G.2) and (3.G.3)

1) CAN-CSA S16 (2014)

$$C_b = \frac{4M_{\max}}{\sqrt{M_{\max}^2 + 4M_A^2 + 7M_B^2 + 4M_C^2}} \le 2.5 \quad (3.G.1)$$

2) AFPA (2003)

$$C_b = \frac{12.5M_{\max}}{2.5M_{\max} + 3M_A + 4M_B + 3M_C} \quad (3.G.2)$$

3) AS4100 (1998)

$$C_b = \frac{1.7M_{\max}}{\sqrt{M_A^2 + M_B^2 + M_C^2}} \quad (3.G.3)$$

where $M_{\max}$ is the maximum moment within the unsupported segment, and M_A and M_C is the moment at the quarter points of the unsupported segment, M_B is the mid-span moment of the unsupported segment.

Moment gradient factor for point load with mid-span brace

For a simply supported beam subjected to lateral mid-span, one has $L_u = L/2$ and

$M_{\max} = M\left(z = L/2\right), M_A = M\left(z = L/8\right), M_B = M\left(z = L/4\right), M_C = M\left(z = 3L/8\right).$

Knowing $M_{\max}$, M_A , M_B and M_C , one determines the moment gradient from AFPA (2003) as1.67, from CAN-CSA S16 (2014) as 1.74, and from AS4100 (1998) as 1.82.

Moment gradient factor for uniformly distributed load with mid-span brace

For uniformly distributed loading, the moment distribution is given by $\lambda M\left(z\right) = \lambda q\left(Lz - z^2\right)/2$. When a simply supported beam has a lateral brace at mid-span,

one has $L_u = L/2$, $M_{\max} = M\left(z = L/2\right), M_A = M\left(z = L/8\right),$ $M_B = M\left(z = L/4\right),$ and $M_C = M\left(z = 3L/8\right)$. Knowing $M_{\max}$, M_A , M_B and M_C , one can determine the moment gradient factor from CAN-CSA S16 (2014) as 1.32, from AFPA (2003) as1.30, and from AS4100 (1998) as 1.33.

Moment gradient factor for point load without mid-span brace

For a simply supported beam subjected to lateral mid-span, one has $L_u = L$ and

$$M_{\max} = M\left(z = L/2\right), M_A = M\left(z = L/4\right), M_B = M\left(z = L/2\right), M_C = M\left(z = 3L/4\right).$$

Knowing $M_{\max}$, M_A , M_B and M_C , one determines the moment gradient from AFPA (2003) as 1.33, from CAN-CSA S16 (2014) as 1.26, and from AS4100 (1998) as 1.39.

Moment gradient factor for uniformly distributed load without mid-span brace

For uniformly distributed loading, the moment distribution is given by $\lambda M\left(z\right) = \lambda q\left(Lz - z^2\right)/2$. When a simply supported beam has a lateral brace at mid-span, one has $L_u = L$, $M_{\max} = M\left(z = L/2\right), M_A = M\left(z = L/4\right), M_B = M\left(z = L/2\right),$ and $M_C = M\left(z = 3L/4\right)$. Knowing $M_{\max}$, M_A , M_B and M_C , one can determine the moment gradient factor from CAN-CSA S16 (2014) as 1.13, AFPA (2003) as 1.14, and AS4100 (1998) as 1.17 by Eqs. (3.G.1), (3.G.2) and (3.G.3).

4. EFFECT OF ECCENTRIC LATERAL BRACING STIFFNESS ON LATERAL TORSIONAL BUCKLING RESISTANCE OF WOODEN BEAMS

Abstract

An energy based solution is developed for the lateral torsional buckling analysis of wooden beams with flexible mid-span lateral bracing subjected to uniformly distributed or mid-span point load. The study indicates that beams are prone to two potential buckling patterns; a symmetric mode and an anti-symmetric mode. Whether the symmetric or the anti-symmetric mode govern the critical moment is shown to depend on the lateral brace stiffness. The symmetric mode governs the capacity of the beam for low bracing stiffness while the anti-symmetric mode governs the capacity when the bracing stiffness exceed a threshold value. A formulation is then developed to directly determine the threshold bracing stiffness and the technique is used to develop a parametric study to investigate the effect of lateral bracing height, load height effect, and bracing stiffness on the critical moments of the beam. A large database of runs is generated and used to develop simple expressions for determining the bracing stiffness required to maximize the elastic lateral torsional buckling resistance.

Keywords:

Lateral torsional buckling, lateral bracing, bracing stiffness, load height, bracing height, simplified design equations

4.1 Introduction and Literature review

Lateral torsional buckling is a mode of failure known to govern the resistance of long span laterally unsupported beams. Design standards for wood members (e.g., CAN-CSA-O86 2014, NDS 2015) recognize lateral torsional buckling (LTB) as a potential mode of failure and provide design recommendations for simply supported beams subjected to various loading conditions. More complex loading scenarios and other lateral support configurations, either rigid or flexible, may arise in practical design of wooden beams. For such cases, no design guidelines are available in standards. Within this context, the present study aims at determining the critical moments for simply supported beams with loads offset from the section centroid and with a flexible lateral eccentric brace at mid-span. Emphasis is on determining the bracing stiffness required to maximize the critical moment capacity. An overview of the effect of load height and bracing height effects on lateral torsional buckling is provided in Yura (2001). A review of key studies on the subject is provided in the following.

4.1.1 Effect of bracing height

Flint (1951) analytically and experimentally investigated the critical moments of simply supported beams with intermediate lateral braces, subjected to mid-span point load and uniformly moments. Winter (1960) extended the concept of threshold stiffness of discrete flexible restraint for columns to laterally braced beams. Lay et al. (1963) developed a model for predicting the critical moments of rectangular beams with eccentric mid-span bracing. Nethercot et al. (1972) developed an FEA model for predicting the LTB resistance of simply supported beams with a central elastic lateral support subjected to uniformly moments. Mutton and Trahair (1973) analytically and numerically investigated simply supported I-beams with mid-span lateral and torsional restraints subjected to mid-span point load and uniform moments. Wong-Chung and Kitipornchai (1987) experimentally investigated the inelastic LTB capacity of simply supported beams subjected to quarter point loads with three intermediate flexible lateral and torsional braces located at quarter points. Tong and Chen (1988) investigated the LTB capacity of mono-symmetric beams with offset mid-span flexible lateral and torsional braces subjected to uniform moments.

They observed that top flange lateral bracing can significantly increase the LTB resistance when compared to shear centre or bottom flange bracing.

4.1.2 Effect of load height

Design guidelines in AFPA 2003 provide means to estimate the load height effect on the critical moments. Kerensky et al. (1956) incorporated load height effects through the effective length method. Nethercot and Rockey (1971) developed design coefficients to be applied to the critical moment expressions. JingPing et al. (1988) developed a Rayleigh-Ritz solution to determine the LTB capacity of beam-columns. Using shell FEA modelling, Helwig et al. (1997) and Samanta and Kumar (2006) investigated the load height effect on the buckling moments of mono-symmetric beams. Yura et al. (2008) developed an expression for the load height effect and a solution for the elastic LTB capacity for twin girders. White and Kim (2008) conducted tests to verify the LTB capacity predictions in the AASHTO (2004) and AISC (2005) design standards. Mohebkhah (2010) investigated the inelastic LTB capacity of simply supported I-beams. Wong et al. (2015) compared the results from the experimental study of White and Kim (2008) with previous design solutions and proposed effective length factors for the design of simply supported beams. While the above studies were primarily aimed to investigate the effect of load height, the topic has been investigated as part of other numerical models including the work of Ings and Trahair (1987), Pi et al. (1992), Andrade and Camotim (2005), Mohri and Potier-Ferry (2006), Andrade et al. (2007), Erkmen and Mohareb (2008), Wu and Mohareb (2010), Trahair (2013), Lamb and Eamon (2015), Sahraei et al. (2015), and Sahraei and Mohareb (2016).

4.1.3 Combined effects of load and bracing height

The LTB of beams subjected to a concentrated load at mid-span and with central lateral bracing was investigated by Schmidt (1965). Kitipomchai et al. (1984) investigated the effect of offset intermediate restraint and transverse loads on the LTB of cantilever I-beams. Through a numerical study, Wang et al. (1987) investigated the LTB capacity of mono-symmetric cantilevers with eccentric vertical loading and discrete lateral bracing offset from the shear centre. McCann et al. (2013) investigated equally spaced eccentric discrete elastic braces on simply supported doubly symmetric I-beams subjected to uniform

moments. The aforementioned studies have various limitations. For example, the study of Schmidt (1965) omitted warping effects and assumed the bracing height to coincide with the loading height. The studies of Kitipomchai et al. (1984) and Wang et al. (1987) are limited to cantilever I-beams. The study of McCann et al. (2013) investigated only the case for uniform moments. Within this context, the present study accounts for warping effects, assumes different bracing and loading heights, and tackles the cases of uniform moments, mid-span point and uniformly distributed loading. The study focuses on determining the critical moments and threshold bracing stiffness requirements.

4.2 Statement of the problem

A wooden beam with a doubly symmetric cross-section is simply supported at both ends relative to vertical and lateral displacements and twist. The beam is subjected to a distributed load with a reference value $q(z)$ that is offset from the section mid-height by a height a taken as positive when the load is above the section mid-height. A mid-span lateral brace with stiffness k_0 is offset from the section mid-height and located at a height b taken as positive when above the section mid-height (Fig 4.1). The reference load $q(z)$ is assumed to increase until the system attains the state of onset of buckling at a critical value $\lambda q(z)$ at which the system has a tendency to undergo lateral torsional buckling without further increase in loading. The present studies aims at determining to the critical load level $\lambda q(z)$ at the onset of buckling.

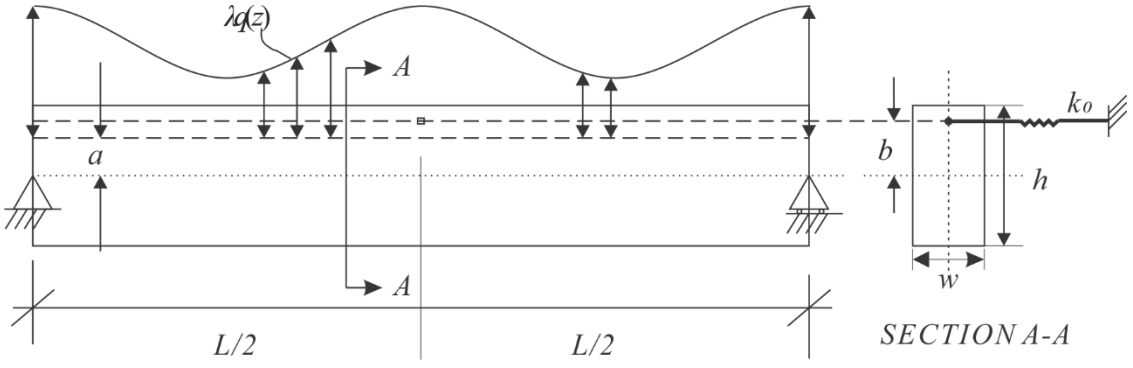

Figure 4.1 General overview of wood beam under flexible lateral restraint

4.3 Assumptions

The following assumptions are made

1. The material is assumed to be linearly elastic and orthotropic. Given that material properties for wood in the tangential and radial directions are nearly equal (FPL 2010), the nine othotropic constitutive constants reduce to six independent parameters. Based on 3D finite element buckling analyses, Xiao et al. (2014) has shown that only two of the six constitutive properties are influential on the elastic lateral buckling capacity: the longitudinal Young modulus E and the shear modulus G for shear stresses acting on the normal plane either in the radial or tangential directions. The present formulation thus characterizes the constitutive behaviour of wood only by two constants E and G in a manner identical to isotropic materials.
2. Load distribution is symmetric about the beam mid-span.
3. The direction of applied load is constant (i.e., conservative loading), and
4. Cross-sectional distortions and shear deformation effects are assumed to be negligible.

4.4 Formulation

4.4.1 Total potential Energy

The total potential energy $\pi = U + V$ is the summation of the internal strain energy U and the load potential energy V gained by the loads. The internal strain energy U is given by (e.g., Trahair 1993)

$$U = U_1 + U_2 \tag{6.1}$$

where

$$U_1 = \frac{1}{2}\int_0^L EI_{yy}u''^2 dz + \frac{1}{2}\int_0^L GJ\theta'^2 dz + \frac{1}{2}\int_0^L EC_w\theta''^2 dz, \qquad U_2 = \frac{1}{2}k_0 u_{sp}\left(L/2\right)^2 \tag{6.2}a,b$$

where $u = u(z)$ is lateral displacement, $\theta = \theta(z)$ is the twist angle, both being functions of the longitudinal coordinate z, L is the span, I_{yy} is the weak moment of inertia, J is the Saint-Venant torsional constant, and C_w is the warping constant. The load potential energy

gained by the load V consists of two components $V = V_1 + V_2$ and is given by (e.g., Trahair 1993)

$$V_1 = \lambda \int_0^L M(z)\theta u'' dz, \quad V_2 = -\frac{1}{2}\lambda \int_0^L q(z) a \theta^2 dz \qquad (6.3)\text{a,b}$$

where V_1 is the load potential energy gained by strong axis bending moment $M = M(z)$ induced by the transverse loads, undergoing twist $\theta(z)$ and lateral displacement $u(z)$ and V_2 is the load potential gained by the distributed load $q(z)$ acting at a height a above section mid-height undergoing an angle of twist $\theta(z)$ and λ is a load scaling factor to determined based on a buckling analysis.

4.4.2 Assumed Displacement Functions

The displacement fields are assumed to take the form.

$$u(z) = \sum_{i=1}^{2n} A_i \sin\frac{i\pi z}{L}, \qquad \theta(z) = \sum_{j=1}^{2n} B_j \sin\frac{j\pi z}{L} \qquad (6.4)\text{a,b}$$

The assumed displacement fields meet the essential and natural boundary conditions for simply supported conditions, i.e., $u(0) = u''(0) = u(L) = u''(L) = 0$ and $\theta(0) = \theta''(0) = \theta(L) = \theta''(L) = 0$. Displacement $u_{sp}(L/2)$ at the bracing height (Fig. 4.2) can be related to the angle of twist $\theta(L/2)$ and lateral displacement $u(L/2)$ though

$$u_{sp}(L/2) = u(L/2) + b\theta(L/2) \qquad (6.5)$$

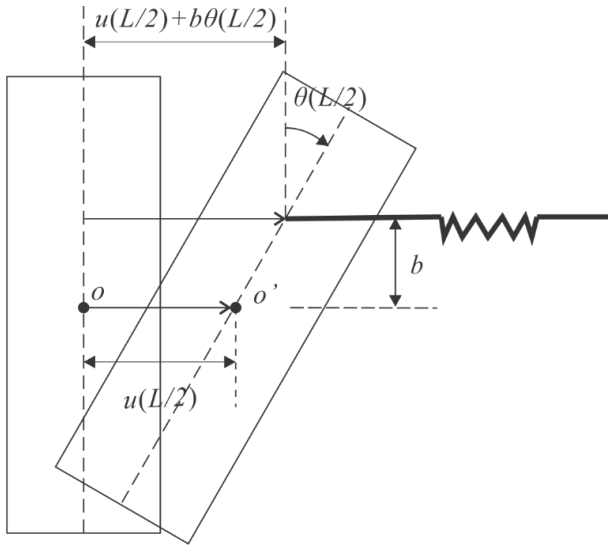

Figure 4.2 Beam mid-span cross-section

4.4.3 Internal Strain Energy

From Eqs. (4.4-4.5), by substituting into the internal strain energy in Eqs. ((6.2) a-b), one obtains

$$U = \frac{1}{2}\left\langle \mathbf{A_a}^{\mathbf{T}} \quad \mathbf{A_b}^{\mathbf{T}} \right\rangle \begin{bmatrix} \mathbf{k}_1 & \mathbf{0} \\ \mathbf{0} & \mathbf{k}_2 \end{bmatrix} \begin{Bmatrix} \mathbf{A}_a \\ \mathbf{A}_b \end{Bmatrix} \tag{6.6}$$

where

$$\mathbf{A}_{a\ 1\times 2n}^{\mathbf{T}} = \left\langle A_1 \quad B_1 \quad A_3 \quad B_3 \quad \cdots \quad A_{2n-1} \quad B_{2n-1} \right\rangle,$$

$$\mathbf{A}_{b\ 1\times 2n}^{\mathbf{T}} = \left\langle A_2 \quad B_2 \quad A_4 \quad B_4 \quad \cdots \quad A_{2n} \quad B_{2n} \right\rangle,$$

$$\mathbf{k}_1 = \begin{bmatrix} \mathbf{m}_{1,1} & \mathbf{m}_{1,3} & \cdots & \mathbf{m}_{1,2i-1} & \cdots & \mathbf{m}_{1,2n-1} \\ \mathbf{m}_{3,1} & \mathbf{m}_{3,3} & \cdots & \mathbf{m}_{3,2i-1} & \cdots & \mathbf{m}_{3,2n-1} \\ \vdots & \vdots & \ddots & \vdots & \iddots & \vdots \\ \mathbf{m}_{2j-1,1} & \mathbf{m}_{2j-1,3} & \cdots & \mathbf{m}_{2j-1,2i-1} & \cdots & \mathbf{m}_{2j-1,2n-1} \\ \vdots & \vdots & \iddots & \vdots & \ddots & \vdots \\ \mathbf{m}_{2n-1,1} & \mathbf{m}_{2n-1,3} & \cdots & \mathbf{m}_{2n-1,2i-1} & \cdots & \mathbf{m}_{2n-1,2n-1} \end{bmatrix}, \mathbf{k}_2 = \begin{bmatrix} \mathbf{m}_{2,2} & \mathbf{m}_{2,4} & \cdots & \mathbf{m}_{2,2i} & \cdots & \mathbf{m}_{2,2n} \\ \mathbf{m}_{4,2} & \mathbf{m}_{4,4} & \cdots & \mathbf{m}_{4,2i} & \cdots & \mathbf{m}_{4,2n} \\ \vdots & \vdots & \ddots & \vdots & \iddots & \vdots \\ \mathbf{m}_{2j,2} & \mathbf{m}_{2j,4} & \cdots & \mathbf{m}_{2j,2i} & \cdots & \mathbf{m}_{2j,2n} \\ \vdots & \vdots & \iddots & \vdots & \ddots & \vdots \\ \mathbf{m}_{2n,2} & \mathbf{m}_{2n,4} & \cdots & \mathbf{m}_{2n,2i} & \cdots & \mathbf{m}_{2n,2n} \end{bmatrix}$$

and

$$\mathbf{m}_{j,i} = \begin{bmatrix} m_{1,i,j} & 0 \\ 0 & m_{2,i,j} \end{bmatrix} + k_0 \begin{bmatrix} m_{3,i,j} & m_{4,i,j} \\ m_{4,i,j} & m_{5,i,j} \end{bmatrix} \tag{6.7}$$

where

$$m_{1,i,j} = EI_{yy}\left[\left(\frac{i\pi}{L}\right)^2\left(\frac{j\pi}{L}\right)^2\int_0^L \sin\frac{i\pi z}{L}\sin\frac{j\pi z}{L}\,dz\right]$$

$$m_{2,i,j} = GJ\,\frac{i\pi}{L}\frac{j\pi}{L}\int_0^L \cos\frac{i\pi z}{L}\cos\frac{j\pi z}{L}\,dz + EC_w\left(\frac{i\pi}{L}\right)^2\left(\frac{j\pi}{L}\right)^2\int_0^L \sin\frac{i\pi z}{L}\sin\frac{j\pi z}{L}\,dz$$

$$m_{3,i,j} = \sin\frac{i\pi}{2}\sin\frac{j\pi}{2}, \qquad m_{4,i,j} = b\sin\frac{i\pi}{2}\sin\frac{j\pi}{2}, \qquad m_{5,i,j} = b^2\sin\frac{i\pi}{2}\sin\frac{j\pi}{2}$$

4.4.4 Fourier Expansion of bending moments

A bending moment field $M(z)$ can be expressed using a Fourier series as

$$M(z) = \sum_{k=1,2}^{kmax} m_k \sin\frac{k\pi z}{L} \qquad m_k = \frac{2}{L}\int_0^L M(z)\sin\frac{k\pi z}{L}dz \tag{6.8)a,b}$$

where coefficients m_k are given for the loading cases of interest in the present study. For uniform moments, the moment distribution is $\lambda M(z) = \lambda M_0$ and the corresponding Fourier terms are $m_k = (2\lambda M_0/k\pi)\left[1-\cos(k\pi z/L)\right]$. For mid-span point load, the moment distribution is $\lambda M(z) = \lambda Q z/2, \quad 0 \le z \le L/2$, $\lambda M(z) = \lambda Q(L-z)/2,$ $0 \le z \le L/2$, and the corresponding Fourier terms are $m_k = \left(2QL/k^2\pi^2\right), k = 1,3,5\ldots$. Also for uniformly distributed loads, one has $\lambda M(z) = \lambda q\left(Lz - z^2\right)/2$ and corresponding Fourrier terms are $m_k = 4\lambda qL^2/(k\pi)^3, \quad k = 1,3,5\ldots$

4.4.5 Destabilizing term due to bending moments

From Eqs.(6.4), (6.5) and (6.8)a by substituting into Eq. (6.3)a and performing integrals, the load potential energy gain can be expressed as

$$V_1 = \frac{\lambda}{2}\left\langle \mathbf{A}_a{}^T \quad \mathbf{A}_b{}^T \right\rangle \begin{bmatrix} \mathbf{k}_{g1} & \mathbf{k}_{g12}^T \\ \mathbf{k}_{g12}^T & \mathbf{k}_{g2} \end{bmatrix} \begin{Bmatrix} \mathbf{A}_a \\ \mathbf{A}_b \end{Bmatrix} \tag{6.9}$$

where

$$\mathbf{k_{g1}} = \begin{bmatrix} \mathbf{n}_{1,1} & \mathbf{n}_{1,3} & \cdots & \mathbf{n}_{1,2i-1} & \cdots & \mathbf{n}_{1,2n-1} \\ \mathbf{n}_{3,1} & \mathbf{n}_{3,3} & \cdots & \mathbf{n}_{3,2i-1} & \cdots & \mathbf{n}_{3,2n-1} \\ \vdots & \vdots & \ddots & \vdots & \iddots & \vdots \\ \mathbf{n}_{2j-1,1} & \mathbf{n}_{2j-1,3} & \cdots & \mathbf{n}_{2j-1,2i-1} & \cdots & \mathbf{n}_{2j-1,2n-1} \\ \vdots & \vdots & \iddots & \vdots & \ddots & \vdots \\ \mathbf{n}_{2n-1,1} & \mathbf{n}_{2n-1,3} & \cdots & \mathbf{n}_{2n-1,2i-1} & \cdots & \mathbf{n}_{2n-1,2n-1} \end{bmatrix}, \mathbf{k_{g2}} = \begin{bmatrix} \mathbf{n}_{2,2} & \mathbf{n}_{2,4} & \cdots & \mathbf{n}_{2,2i} & \cdots & \mathbf{n}_{2,2n} \\ \mathbf{n}_{4,2} & \mathbf{n}_{4,4} & \cdots & \mathbf{n}_{4,2i} & \cdots & \mathbf{n}_{4,2n} \\ \vdots & \vdots & \ddots & \vdots & \iddots & \vdots \\ \mathbf{n}_{2j,2} & \mathbf{n}_{2j,4} & \cdots & \mathbf{n}_{2j,2i} & \cdots & \mathbf{n}_{2j,2n} \\ \vdots & \vdots & \iddots & \vdots & \ddots & \vdots \\ \mathbf{n}_{2n,2} & \mathbf{n}_{2n,4} & \cdots & \mathbf{n}_{2n,2i} & \cdots & \mathbf{n}_{2n,2n} \end{bmatrix}$$

$$\mathbf{K_{g12}} = \begin{bmatrix} \mathbf{n}_{1,2} & \mathbf{n}_{1,4} & \cdots & \mathbf{n}_{1,2i} & \cdots & \mathbf{n}_{1,2n} \\ \mathbf{n}_{3,2} & \mathbf{n}_{3,4} & \cdots & \mathbf{n}_{3,2i} & \cdots & \mathbf{n}_{3,2n} \\ \vdots & \vdots & \ddots & \vdots & \iddots & \vdots \\ \mathbf{n}_{2j-1,2} & \mathbf{n}_{2j-1,4} & \cdots & \mathbf{n}_{2j-1,2i} & \cdots & \mathbf{n}_{2j-1,2n} \\ \vdots & \vdots & \iddots & \vdots & \ddots & \vdots \\ \mathbf{n}_{2n-1,2} & \mathbf{n}_{2n-1.4} & \cdots & \mathbf{n}_{2n-1,2i} & \cdots & \mathbf{n}_{2n-1,2n} \end{bmatrix}, \quad \mathbf{n_{j,i}} = \left[\begin{array}{c|c} 0 & m_{6,i,j} \\ \hline m_{7,i,j} & 0 \end{array}\right]$$

(6.10)a-d

in which, one has

$$m_{6,i,j} = -\left(\frac{j\pi}{L}\right)^2 L\beta(j,i,k_{max}), \qquad m_{7,i,j} = -\left(\frac{i\pi}{L}\right)^2 L\beta(i,j,k_{max}) \tag{6.11}$$

$$\beta(i,j,k_{max}) = \frac{1}{L}\int_0^L \sum_{k=1,2}^{kmax} m_k \sin\frac{i\pi z}{L}\sin\frac{j\pi z}{L}\sin\frac{k\pi z}{L}dz \tag{6.12}$$

4.4.5.1 Special considerations for symmetric loading

For symmetric loading with respect to $z = L/2$ and symmetric boundary conditions, the moments are symmetric and Eq. (6.8)a can be shown to take the form

$$M(z) = \sum_{k=1,3,5}^{kmax} m_k \sin\frac{k\pi z}{L} \tag{6.13}$$

where the summation in Eq.(6.13) is only on the odd terms $k = 1,3,5..$ Thus, when either one of i, j is odd and the other is even, matrix $\mathbf{n}_{j,i}$ in Eq. (6.10)d can be shown to vanish. This is the case since function $\sin(i\pi z/L)\sin(j\pi z/L)$ is anti-symmetric with respect to

$z = L/2$ and the summation $\sum_{k=1,2}^{k_{max}} m_k \sin(i\pi z/L)\sin(j\pi z/L)\sin(k\pi z/L)$ arising in Eq. (6.12) is also anti-symmetric. Hence $\beta(i,j,k_{max})=(1/L)\int_0^L \sum_{k=1,2}^{k_{max}} m_k \sin(i\pi z/L)\sin(j\pi z/L)\sin(k\pi z/L)dz = 0$. By substituting into Eq. (6.11), one has $\mathbf{n}_{j,i} = \mathbf{0}$, $\mathbf{k}_{g12} = \mathbf{0}$, and Eq. (6.9)simplifies to

$$V_1 = \frac{\lambda}{2}\begin{Bmatrix}\mathbf{A}_a{}^T & \mathbf{A}_b{}^T\end{Bmatrix}\begin{bmatrix}\mathbf{k}_{g1} & \mathbf{0}\\ \mathbf{0} & \mathbf{k}_{g2}\end{bmatrix}\begin{Bmatrix}\mathbf{A}_a\\ \mathbf{A}_b\end{Bmatrix} \tag{6.14}$$

4.4.6 Destabilizing terms due to load height effect

4.4.6.1 Case1-Mid-span load offset from section centroid

The loading function corresponding to a mid-span point load λQ is $\lambda q(z) = \lambda Q\delta(z - L/2)$ in which δ the Dirac Delta function. By substitution into Eq. (6.3) b, and expressing the result in a matrix form, one obtains

$$V_2 = -\frac{\lambda}{2}\int_0^L Q\delta\left(z-\frac{L}{2}\right)a\theta(z)^2\,dz = \frac{\lambda}{2}\begin{Bmatrix}\mathbf{A}_a{}^T & \mathbf{A}_b{}^T\end{Bmatrix}\begin{bmatrix}\mathbf{k}_{g3} & \mathbf{k}_{g34}\\ \mathbf{k}_{g34}^T & \mathbf{k}_{g4}\end{bmatrix}\begin{Bmatrix}\mathbf{A}_a\\ \mathbf{A}_b\end{Bmatrix} \tag{6.15}$$

where

$$\mathbf{k}_{g3} = Qa\begin{bmatrix}\mathbf{r}_{1,1} & \mathbf{r}_{1,3} & \cdots & \mathbf{r}_{1,2i-1} & \cdots & \mathbf{r}_{1,2n-1}\\ \mathbf{r}_{3,1} & \mathbf{r}_{3,3} & \cdots & \mathbf{r}_{3,2i-1} & \cdots & \mathbf{r}_{3,2n-1}\\ \vdots & \vdots & \ddots & \vdots & \iddots & \vdots\\ \mathbf{r}_{2j-1,1} & \mathbf{r}_{2j-1,3} & \cdots & \mathbf{r}_{2j-1,2i-1} & \cdots & \mathbf{r}_{2j-1,2n-1}\\ \vdots & \vdots & \iddots & \vdots & \ddots & \vdots\\ \mathbf{r}_{2n-1,1} & \mathbf{r}_{2n-1,3} & \cdots & \mathbf{r}_{2n-1,2i-1} & \cdots & \mathbf{r}_{2n-1,2n-1}\end{bmatrix}, \mathbf{k}_{g4} = Qa\begin{bmatrix}\mathbf{r}_{2,2} & \mathbf{r}_{2,4} & \cdots & \mathbf{r}_{2,2i} & \cdots & \mathbf{r}_{2,2n}\\ \mathbf{r}_{4,2} & \mathbf{r}_{4,4} & \cdots & \mathbf{r}_{4,2i} & \cdots & \mathbf{r}_{4,2n}\\ \vdots & \vdots & \ddots & \vdots & \iddots & \vdots\\ \mathbf{r}_{2j,2} & \mathbf{r}_{2j,4} & \cdots & \mathbf{r}_{2j,2i} & \cdots & \mathbf{r}_{2j,2n}\\ \vdots & \vdots & \iddots & \vdots & \ddots & \vdots\\ \mathbf{r}_{2n,2} & \mathbf{r}_{2n,4} & \cdots & \mathbf{r}_{2n,2i} & \cdots & \mathbf{r}_{2n,2n}\end{bmatrix}$$

$$\mathbf{k}_{g34} = Qa\begin{bmatrix}\mathbf{r}_{1,2} & \mathbf{r}_{1,4} & \cdots & \mathbf{r}_{1,2i} & \cdots & \mathbf{r}_{1,2n}\\ \mathbf{r}_{3,2} & \mathbf{r}_{3,4} & \cdots & \mathbf{r}_{3,2i} & \cdots & \mathbf{r}_{3,2n}\\ \vdots & \vdots & \ddots & \vdots & \iddots & \vdots\\ \mathbf{r}_{2j-1,2} & \mathbf{r}_{2j-1,4} & \cdots & \mathbf{r}_{2j-1,2i} & \cdots & \mathbf{r}_{2j-1,2n}\\ \vdots & \vdots & \iddots & \vdots & \ddots & \vdots\\ \mathbf{r}_{2n-1,2} & \mathbf{r}_{2n-1.4} & \cdots & \mathbf{r}_{2n-1,2i} & \cdots & \mathbf{r}_{2n-1,2n}\end{bmatrix}, \quad \mathbf{r}_{j,i} = \left[\begin{array}{c|c} 0 & 0\\ \hline 0 & \sin\dfrac{i\pi}{2}\sin\dfrac{j\pi}{2}\end{array}\right] \tag{6.16}$$

when either of i , j are even and the other is odd, the expression $\sin(i\pi/2)\sin(j\pi/2)$ vanishes and hence matrix $\mathbf{k}_{g34}$ vanishes and the load potential energy V_2 takes the form

$$V_2 = \frac{\lambda}{2}\left\langle \mathbf{A}_a^{\mathrm{T}} \quad \mathbf{A}_b^{\mathrm{T}} \right\rangle \begin{bmatrix} \mathbf{k}_{g3} & \mathbf{0} \\ \mathbf{0} & \mathbf{k}_{g4} \end{bmatrix}_{(1)} \begin{Bmatrix} \mathbf{A}_a \\ \mathbf{A}_b \end{Bmatrix} \tag{6.17}$$

and subscript (1) denotes case 1.

4.4.6.2 Case2- Distributed load offset from section centroid

The load potential gain induced by the load height can be expressed as

$$\begin{aligned} V_2 &= -\frac{\lambda}{2}\int_0^L qa\theta(z)^2\,dz = -\frac{\lambda}{2}qa\int_0^L \sum_{i=1,2}^{2n}\sum_{j=1,2}^{2n} B_i B_j \sin\left(\frac{i\pi z}{L}\right)\sin\left(\frac{j\pi z}{L}\right)dz \\ &= \frac{\lambda}{2}\left\langle \mathbf{A}_a^{\mathrm{T}} \quad \mathbf{A}_b^{\mathrm{T}} \right\rangle \begin{bmatrix} \mathbf{k}_{g3} & \mathbf{0} \\ \mathbf{0} & \mathbf{k}_{g4} \end{bmatrix}_{(2)} \begin{Bmatrix} \mathbf{A}_a \\ \mathbf{A}_b \end{Bmatrix} \end{aligned} \tag{6.18}$$

where subscript (2) denotes case 2 and

$$\mathbf{k}_{g3} = \mathbf{k}_{g4} = -\frac{1}{2}qLa\mathbf{Diag}(0,1,0,1...0,1) \tag{6.19}$$

4.4.7 Stationarity conditions

From Eqs. (6.6), (6.9), (6.17) and (6.18), by substituting into the total potential energy $\pi = U + V$, and evoking the stationarity conditions $\partial\pi/\partial\mathbf{A}_a = \partial\pi/\partial\mathbf{A}_b = \mathbf{0}$, one obtains

$$\left\{ \begin{bmatrix} \mathbf{k}_1 & \mathbf{0} \\ \mathbf{0} & \mathbf{k}_2 \end{bmatrix} + \lambda\left(\begin{bmatrix} \mathbf{k}_{g1} & \mathbf{0} \\ \mathbf{0} & \mathbf{k}_{g2} \end{bmatrix} + \begin{bmatrix} \mathbf{k}_{g3} & \mathbf{0} \\ \mathbf{0} & \mathbf{k}_{g4} \end{bmatrix} \right) \right\} \begin{Bmatrix} \mathbf{A}_a \\ \mathbf{A}_b \end{Bmatrix} = 0 \tag{6.20}$$

The two partitions of Eq. (5.24) can be expanded to yield the separate Eigenvalue problems

$$\left(\mathbf{k}_1 + \lambda_1\left(\mathbf{k}_{g1} + \mathbf{k}_{g3}\right)\right)\mathbf{A}_a = 0 \tag{6.21}$$

$$\left(\mathbf{k}_2 + \lambda_2\left(\mathbf{k}_{g2} + \mathbf{k}_{g4}\right)\right)\mathbf{A}_b = 0 \tag{6.22}$$

Eqs. (6.23) and Eq. (6.24) are solved yielding two groups of eigenvalues λ_1 and λ_2. The buckling mode of interest is the one corresponding to the smallest eigenvalue. The entries

of vector $\mathbf{A}_a$ always correspond to a symmetric buckling mode while those of vector $\mathbf{A}_b$ correspond to an anti-symmetric mode (Appendix 4.A).

4.4.8 Recovering the threshold bracing stiffness

As shown in the results (e.g., Fig 4.8), while the critical load corresponding to Mode 1 (symmetric) depends on the lateral bracing stiffness, that based on Mode 2 (anti-symmetric) is found to be independent of the bracing stiffness, yielding a constant critical moment value for a given beam geometry and load configuration. In contrast, the buckling moment corresponding to Mode 1 decreases as the bracing stiffness decreases. Conceptually, there is a threshold bracing stiffness k_{cr} at which both modes yield the same critical moments. The concept of threshold bracing stiffness has also been discussed in Mutton and Trahair (1973), Tong and Cheng (1988) and Yura (2001). When the lateral bracing stiffness is above this threshold value, the member attains its maximal capacity as dictated by the anti-symmetric mode. The present section develops a methodology to directly recover the critical bracing stiffness. Eq. (6.22) is first solved for the eigenvalue λ_2, and one sets $\lambda_1 = \lambda_2$. Equation (6.21) is then solved for the threshold bracing stiffness. From Eqs. (6.7), the elastic stiffness matrix $\mathbf{k}_1$ can be expressed as the sum of two matrices

$$\mathbf{k}_1 = \bar{\mathbf{k}}_1 + k_{cr}\bar{\bar{\mathbf{k}}}_1 \tag{6.25}$$

where

$$\bar{\mathbf{k}}_1 = \begin{bmatrix} \mathbf{m}'_{1,1} & \mathbf{m}'_{1,3} & \cdots & \mathbf{m}'_{1,2i-1} & \cdots & \mathbf{m}'_{1,2n-1} \\ \mathbf{m}'_{3,1} & \mathbf{m}'_{3,3} & \cdots & \mathbf{m}'_{3,2i-1} & \cdots & \mathbf{m}'_{3,2n-1} \\ \vdots & \vdots & \ddots & \vdots & \iddots & \vdots \\ \mathbf{m}'_{2j-1,1} & \mathbf{m}'_{2j-1,3} & \cdots & \mathbf{m}'_{2j-1,2i-1} & \cdots & \mathbf{m}'_{2j-1,2n-1} \\ \vdots & \vdots & \iddots & \vdots & \ddots & \vdots \\ \mathbf{m}'_{2n-1,1} & \mathbf{m}'_{2n-1,3} & \cdots & \mathbf{m}'_{2n-1,2i-1} & \cdots & \mathbf{m}'_{2n-1,2n-1} \end{bmatrix}, \bar{\mathbf{m}}_{j,i} = \left[\begin{array}{c:c} m_{1,i,j} & 0 \\ \hdashline 0 & m_{2,i,j} \end{array}\right]$$

$$\bar{\bar{\mathbf{k}}}_1 = \begin{bmatrix} \mathbf{m}''_{1,1} & \mathbf{m}''_{1,3} & \cdots & \mathbf{m}''_{1,2i-1} & \cdots & \mathbf{m}''_{1,2n-1} \\ \mathbf{m}''_{3,1} & \mathbf{m}''_{3,3} & \cdots & \mathbf{m}''_{3,2i-1} & \cdots & \mathbf{m}''_{3,2n-1} \\ \vdots & \vdots & \ddots & \vdots & \iddots & \vdots \\ \mathbf{m}''_{2j-1,1} & \mathbf{m}''_{2j-1,3} & \cdots & \mathbf{m}''_{2j-1,2i-1} & \cdots & \mathbf{m}''_{2j-1,2n-1} \\ \vdots & \vdots & \iddots & \vdots & \ddots & \vdots \\ \mathbf{m}''_{2n-1,1} & \mathbf{m}''_{2n-1,3} & \cdots & \mathbf{m}''_{2n-1,2i-1} & \cdots & \mathbf{m}''_{2n-1,2n-1} \end{bmatrix}, \bar{\bar{\mathbf{m}}}_{j,i} = \left[\begin{array}{c:c} m_{3,i,j} & m_{4,i,j} \\ \hdashline m_{4,i,j} & m_{5,i,j} \end{array}\right] \tag{6.26}$$

From Eq.(6.25), (6.26), by substituting into Eq.(6.21), one obtains a linear eigenvalue problem in the eigen-pairs (k_{cr} , $\mathbf{A}_{\mathrm{a}}$) of the form

$$\left(\left(\bar{\mathbf{k}}_1 + \lambda_2 \mathbf{k}_{\mathrm{g1}} + \lambda_2 \mathbf{k}_{\mathrm{g3}}\right) + k_{cr} \bar{\bar{\mathbf{k}}}_1\right) \mathbf{A}_{\mathrm{a}} = \mathbf{0} \tag{6.27}$$

Given matrices $\left(\bar{\mathbf{k}}_1 + \lambda_2 \mathbf{k}_{\mathrm{g1}} + \lambda_2 \mathbf{k}_{\mathrm{g3}}\right)$ and $\bar{\bar{\mathbf{k}}}_1$, Eq. (6.27) can be solved for k_{cr} and $\mathbf{A}_{\mathrm{a}}$ to yield the critical load.

4.5 Convergence study

To determine the number of Fourier terms *n* needed for convergence, a convergence study was conducted on 32 cases with different load configurations (uniformly distributed, mid-span point loads), brace heights, load heights and elastic restraint stiffness (Appendix 4.B). The ratio of critical moments based on $n = 4$ were compared to those based on $n = 6$ with a difference of 0.2% or less in all 32 cases considered. It is concluded that $n = 4$ is enough to achieve convergence. Given that the computational run time involved is nearly instantaneous, the number of modes n was conservatively set to 9, (i.e., 18 Fourier terms were taken in Eqs. (6.4)) in all subsequent analyses.

4.6 Verification

To assess the validity of the present solution, a series of problems were solved and results were compared to those based on 3D FEA eigen-value buckling analyses based on the commercial software ABAQUS. The reference problem chosen for comparison consisted a wood beam with a width $w = 130mm$, a height $h = 950mm$, and a span $L = 13,000mm$. The weak axis moment of inertia is $I_{yy} = hw^3 / 12 = 1.74 \times 10^8 mm^4$, the Saint-Venant torsional constant as determined in (Pai 2007) is $J = 6.36 \times 10^8 mm^4$ and the warping constant

is $C_w = w^3h^3/144 = 1.31\times10^{13} mm^6$. Beam material is assumed to be glued-laminated timber, Spruce-Lodgepole Pine with 20f-EX grade. The modulus of elasticity in the longitudinal direction is $E = E_L = 10,300MPa$ (CSA O86 2014) and shear modulus is taken as $G = G_{LT} = G_{LR} = 474MPa$ (FPL, 2010). The beam was modeled using ABAQUS using the C3D8 brick element in ABAQUS to discretize the beam. The C3D8 element is three-dimensional continuum element with 8 nodes at the corners and three translational degrees of freedom per node, totalling and 24 degrees of freedom (Simulia, 2011). The element uses linear interpolation of the displacement fields. The input beam material properties conformed to those listed in for the reference case. Additional material properties needed for ABAQUS input were taken from (FPL 2011): the tangential direction and radial direction $E_T = E_R = 700MPa$, shear modulus $G_{RT} = 51.5MPa$, Poisson's ratios $\nu_{LR} = \nu_{LT} = 0.347$; and $\nu_{RT} = 0.469$. Two groups of restraints were enforced at both ends of the model to simulate the simply supported boundary conditions (Fig. 4.3): 1) A set of constraints related to vertical displacements were imposed along axes AB and $A'B'$ at the end cross sections. For axes CD and $C'D'$, the lateral displacements were restrained by imposing another group of constraints. 2) The centre of the cross section at one end was longitudinally restrained (Fig 4.3a), while the other end was free to move longitudinally (Fig 4.3b). A mid-span lateral brace was simulated by adding a SPRING1 element located at the central vertical axis of the mid-span section. The SPRING1 element is used to model springs between a given node and ground, along a specified direction (horizontal in the present problem). The above FEA model was used to conduct a mesh sensitivity analysis was conducted on 8 cases with different load configurations (uniformly distributed load, mid-span point load) with various values of lateral bracing stiffness. The governing buckling modes were found symmetric in some cases and anti-symmetric in others. The results (Appendix 4.B) showed that critical moment predictions based on 410 elements longitudinally, 50 elements along the height, and 10 elements are along width do not change by more than 0.04% when finer meshes are taken. Thus, a 410x50x10 mesh was taken in subsequent verification runs.

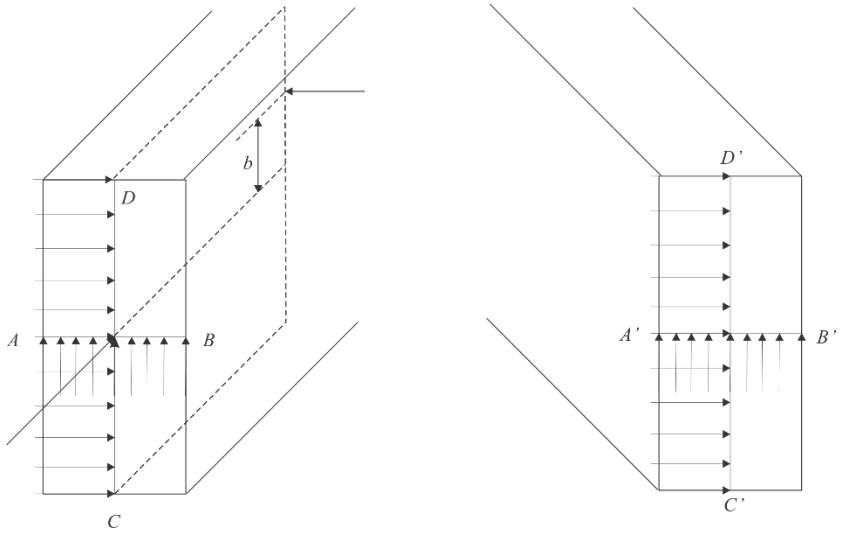

Figure 4.3a,b Boundary conditions (all arrows denote restrained degrees of freedoms)

A comparison of predicted buckling load versus the normalized bracing height (b/h) for reference case is provided in Fig. 4.4. Four groups of runs were conducted in which the loading type (concentrated, uniformly distributed), the load height a (top face, mid-height) and brace stiffness ($10^3\ kN/m$ and $10^4\ kN/m$) were varied. In all cases, the buckling loads based on the symmetric and antisymmetric modes were provided. The buckling loads based on the present solution are found to agree within 0.57%-4.27% with the ABAQUS solution (Appendix 4.C). Critical loads based on the present study are slightly higher than those based on the ABAQUS simulations since the underlying formulation of the present model is based on the simplifying beam kinematic assumptions neglecting distortional and shear deformation effects and thus provide a slightly stiffer representation of the beam than the ABAQUS model which captures distortion and shear deformations effects. Figure 4.5 provides a comparison between the buckling mode shape based on the present solution and that based on the ABAQUS simulation for point load and uniformly distributed loads, both for the symmetric and anti-symmetric modes, and for a variety of bracing heights. Close agreement is observed between the results based present model and those based on the ABAQUS simulations. Similar agreement between mode shapes is observed for other loading and bracing height combinations.

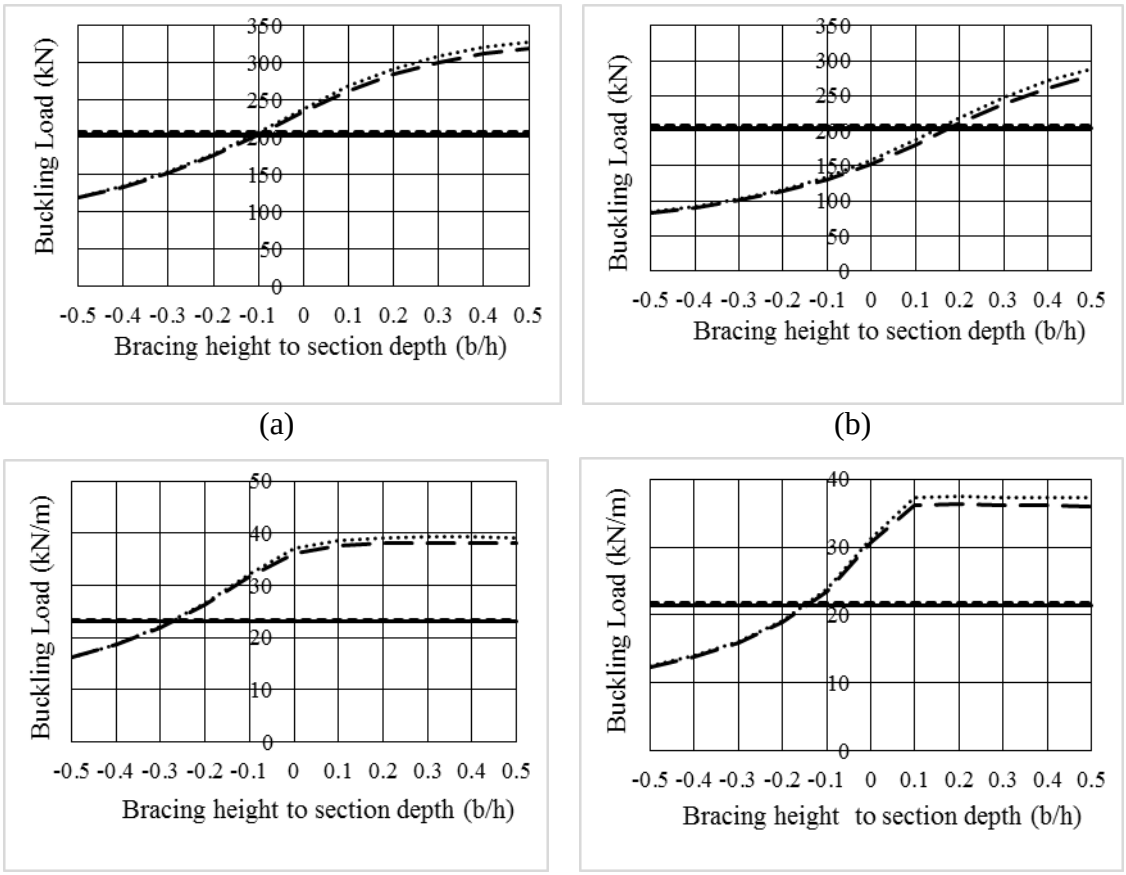

Figure 4.4 Buckling load of reference case for (a) Point load, $a = 0$, $k_0 = 10^3 kN/m$ **, (b) point load,** $a = 0.5h$, $k_0 = 10^4 kN/m$, **(c) uniformly distributed load,** $a = 0$, $k_0 = 10^3 kN/m$, **and (d) uniformly distributed load,** $a = 0.5h$, $k_0 = 10^4 kN/m$

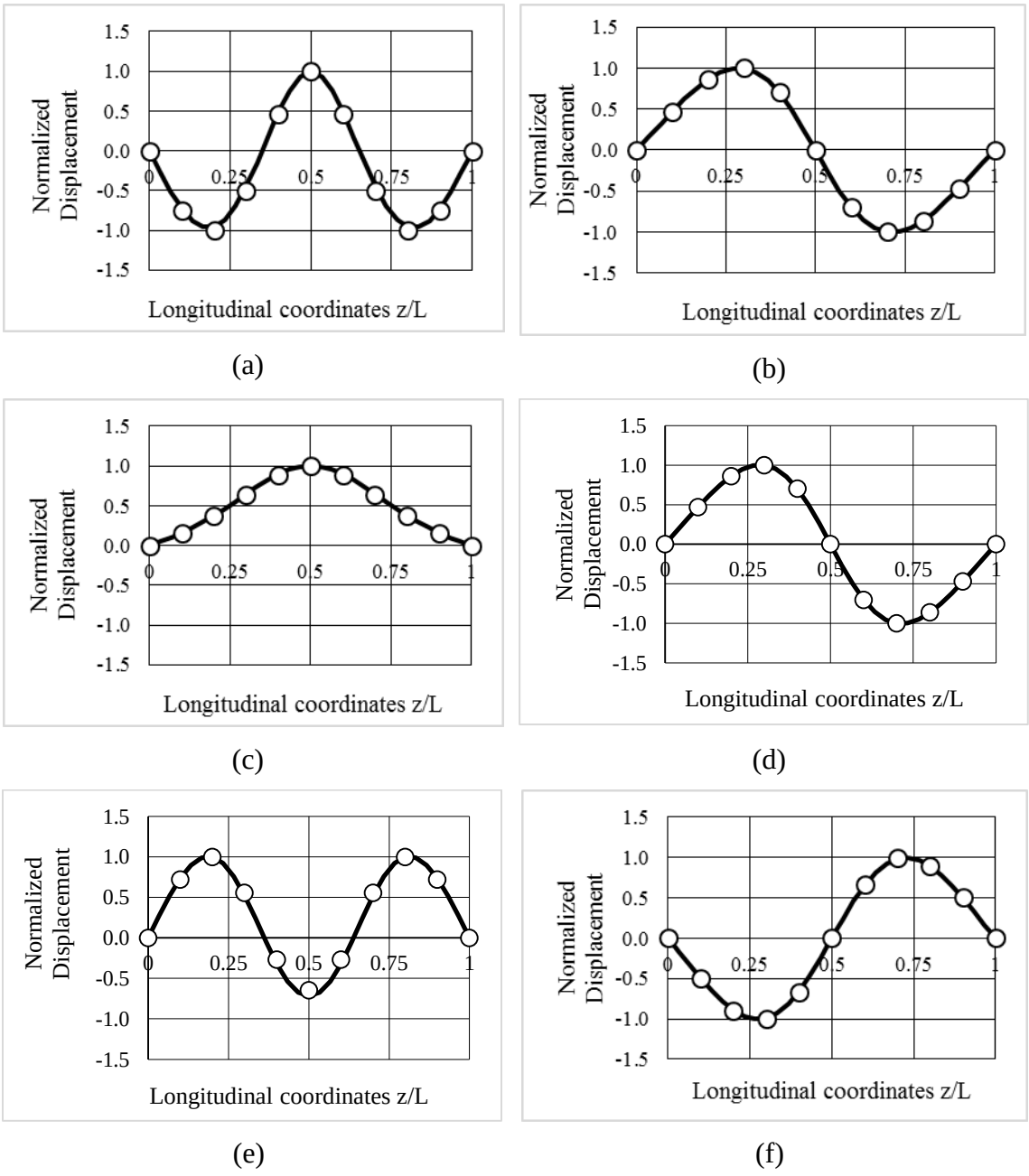

Figure 4.5 Lateral displacement diagrams for buckling mode shape for beams subject to mid-span point load (a-d) and uniformly distributed loads (e-h) (a) Symmetric mode, $k_0 = 10^3 kN/m$ $a = 0$, $b = 0$ **(b) Anti-symmetric mode,** $k_0 = 10^3 kN/m$ $a = 0$, $b = 0$ **(c) Symmetric mode,** $k_0 = 10^2 kN/m$ $a = 0$, $b = 0.5h$ **(d) Anti-symmetric mode,** $k_0 = 10^2 kN/m$ $a = 0$, $b = 0.5h$ **(e) Uniformly distributed load, symmetric mode,** $k_0 = 10^3 kN/m$ $a = 0$, $b = 0$ **(f) Uniformly distributed load, anti-symmetric mode,** $k_0 = 10^3 kN/m$ $a = 0$, $b = 0$

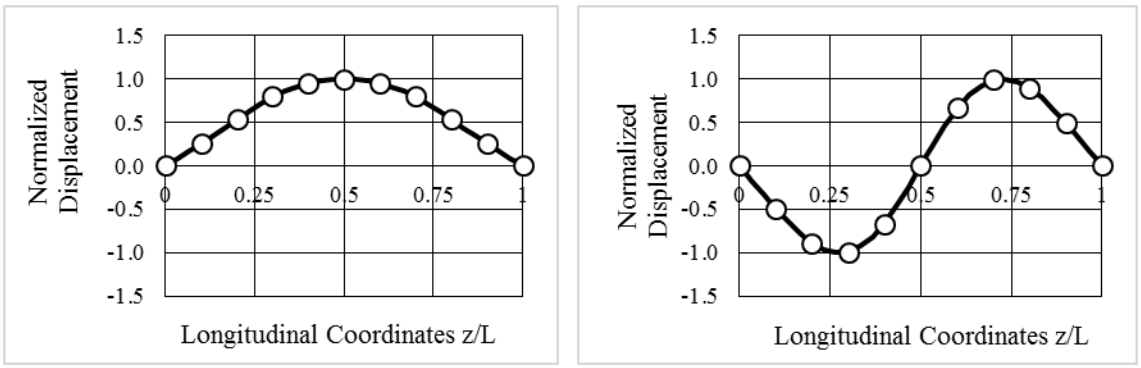

(g) (h)

Figure 4.5 (cont) Lateral displacement diagrams for buckling mode shape for beams subject to mid-span point load (a-d) and uniformly distributed loads (e-h) (g) Uniformly distributed load, symmetric mode, $k_0 = 10^2\, kN/m \;\; a = 0$, $b = 0.5h$ **(h) Uniformly distributed load, anti-symmetric mode,** $k_0 = 10^2\, kN/m \;\; a = 0$, $b = 0.5h$

4.7 Comparison with previous research

Schmidt (1965) developed a lateral torsional buckling solution for beams with rectangular sections subjected to a point load at mid-span. The model involved two elastic torsional restraints at both ends and an elastic lateral restraint at mid-span. Unlike the present study, the solution in Schmidt (1965) neglects warping and assumes that the bracing height coincides with the load height. A comparison between the predictions of the present model and those based on the Schmidt solution is provided in Fig 4.6 for $kL^3/48EI_{yy} = 5, 10, 40$. In the solution by Schmidt (1965), the stiffness of the end torsional restraints was set to infinity to emulate the end conditions of interest in the present study i.e., $\theta(0) = \theta(L) = 0$. The lateral torsional buckling capacity based present study is observed to be slightly higher than Schmidt results. The difference is attributed to the warping effect which is captured only in the present study. Excellent agreement is obtained between both solutions when omitting the warping contribution in present study, as evidenced by the nearly overlapping results in Fig. 4.6.

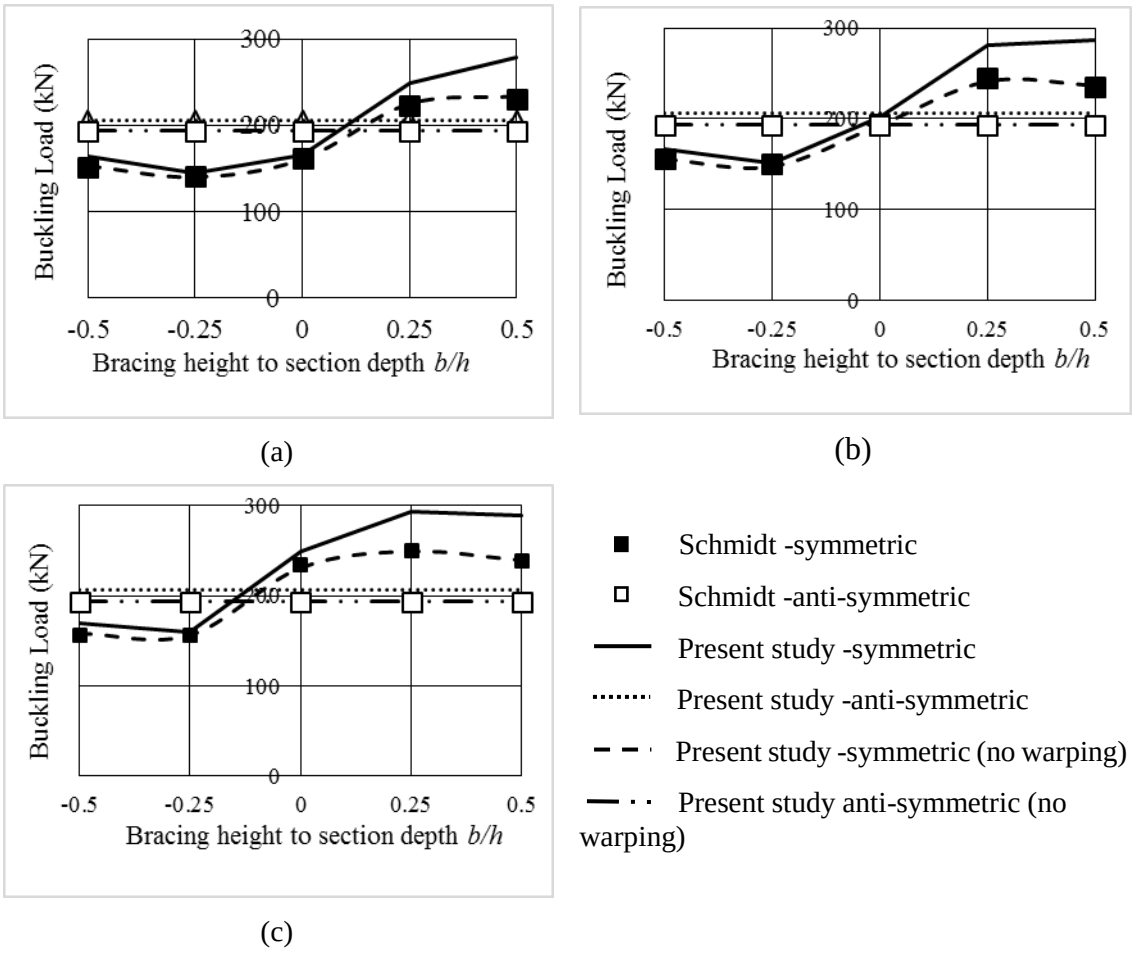

Figure 4.6 Critical loads predictions of present study versus Schmidt for (a) $kL^3/48EI_{yy} = 5$ **(b)** $kL^3/48EI_{yy} = 10$ **(c)** $kL^3/48EI_{yy} = 40$

McCann (2013) developed a solution for the buckling moment and threshold stiffness k_{cr} for simply supported beams subjected to uniform moments, with a number of equidistant intermediate eccentric lateral braces. The validity of the model can be assessed by setting the number of lateral restraints to one. Results are shown in Fig 4.7, where β is the brace height normalized relative to cross-section shear center $\beta = b\sqrt{I_{yy}/C_w}$, β_{cr} is the normalized brace height required to achieve full bracing condition, and $M_{cr,a}$ is the critical moment based on the anti-symmetric mode. The buckling load predictions based on the present study are in very good agreement with those based on McCann (2013), both for the symmetric and anti-symmetric modes, for various bracing heights, and for various elastic stiffness.

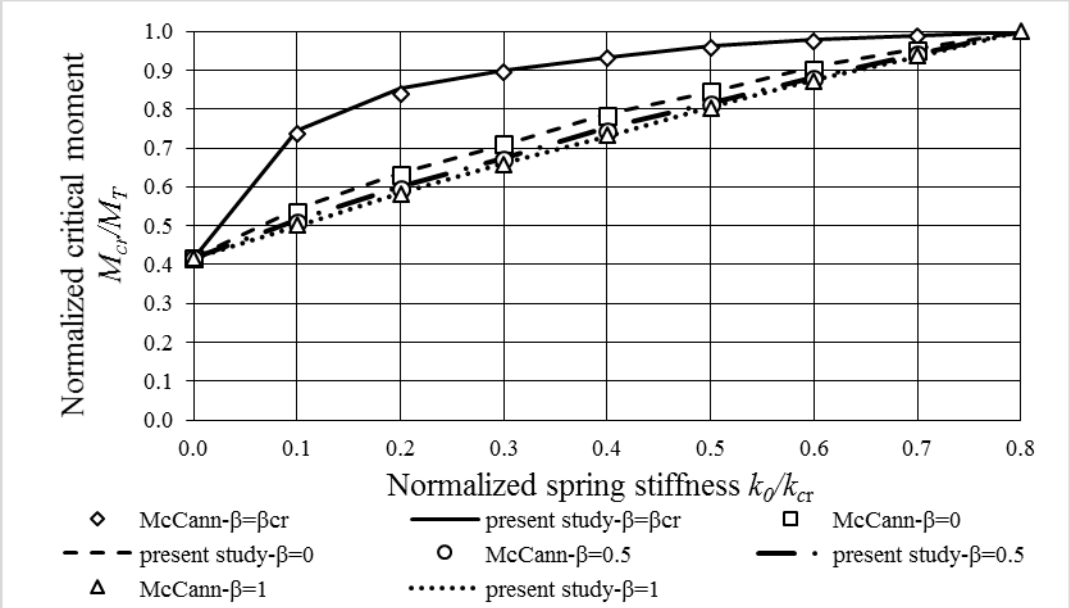

Figure 4.7 Comparison between present study and McCann for single mid-span lateral brace

4.8 Parametric study

The effect of brace stiffness is investigated by varying the bracing stiffness from $10\,kN/m$ to $10^6\ kN/m$ for the reference case described in section titled "Description of the Model. The results (Fig 4.8) reveal that the buckling load magnitude corresponding to the anti-symmetric mode are independent of the lateral bracing stiffness. In contrast, for symmetric mode, the critical load decreases with the lateral bracing stiffness. For bracing located at the centroid or the top face, the critical moments based on the symmetric mode can attain those based on the anti-symmetric mode when the bracing stiffness attains a threshold value. In contrast, for bracing at bottom face, the critical moments based on the symmetric mode are found to be always smaller those based on the anti-symmetric mode irrespective of the bracing stiffness magnitude.

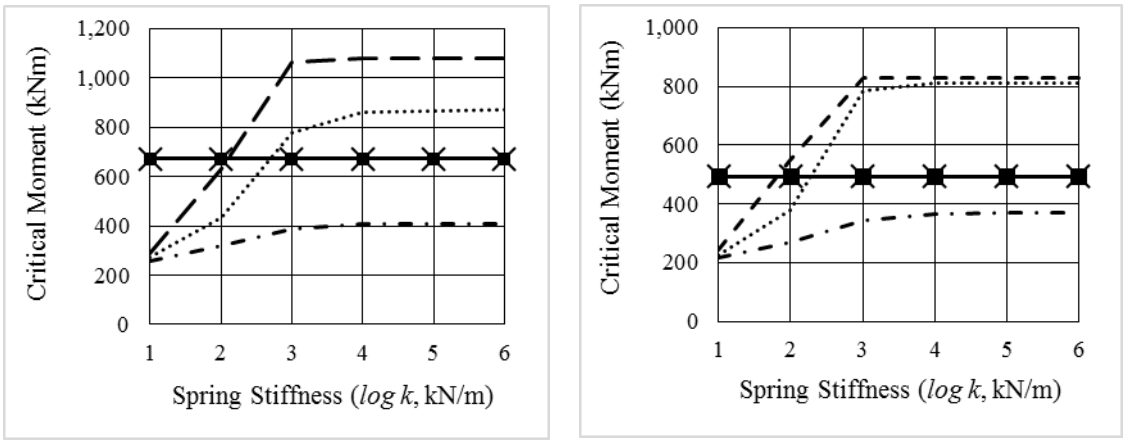

(a) (b)

brace at centroid (b = 0) Symmetric
brace at centroid (b =0) Anti-symmetric
brace at top (b = 0.5h) Symmetric
brace at top (b = 0.5h) Anti-symmetric
brace at bottom (b = -0.5h) Symmetric
brace at bottom (b = -0.5h) Anti-symmetric

Figure 4.8 Parametric study by varying bracing stiffness when load at central axis (a) point load (b) uniformly distributed load

4.9 Simplified expressions for threshold bracing stiffness

For design purposes, it is desirable to determine the lateral brace stiffness required to maximize the critical moment. The objective of this section is to develop a simplified expression for estimating such a critical brace stiffness $\bar{k}_{cr}$. In a dimensionless form, critical brace stiffness depends on five parameters, i.e. $\left(\bar{k}_{cr}L^3/EI_{yy}\right) = f_0\left(w/h, a/h, b/h, L/h, G/E\right)$. To reduce the number of parameters involved to a manageable size, the simplified solution sought will focus on the common case where the point of load application also provides a lateral restraint, i.e., $a = b$. In such a case, one has $\left(\bar{k}_{cr}L^3/EI_{yy}\right) = f_1\left(w/h, b/h, L/h, G/E\right)$.

4.9.1 Reference Cases

Two reference cases have been defined in the present analysis. For both cases, the section width is taken as $w = 130mm$, the height is $h = 950mm$, the modulus of elasticity is $E_L = 10300MPa$ and the shear modulus is $G = 644MPa$. The spans of the two reference cases are 10m and 15m, both of which yield an elastic lateral torsional buckling mode of failure according to CAN-CSA-O86-2014.

4.9.2 Sensitivity analysis

The four parameters $w/h, b/h, L/h, G/E$ were varied in the practical range of values, i.e., $0.137 \le w/h \le 0.570, -0.5 \le b/h \le 0.5, 5.263 \le L/h \le 21.053$ and $0.0500 \le G/E \le 0.100$ which cover the elastic lateral torsional buckling and inelastic lateral torsional buckling modes of failure according to CSA O86 (2014). A database of 434 runs (Appendices C and D) was developed within the ranges specified. For each run, the threshold stiffness k_{cr} was determined from the eigenvalue problem defined in Eq. (6.27).

Of the 434 runs conducted, 44 runs (Appendix 4.D) were conducted by varying G/E from 0.05 to 0.1. By varying G/E from 0.05 to 0.1 (Fig 4.9a) the normalized threshold bracing is observed to decrease only by 7.15%, suggesting that the G/E ratio has a negligible effect on the normalized threshold bracing stiffness $k_{cr}/\left(EI/L^3\right)$. Also, another 44 runs were conducted by varying the cross-section aspect ratio w/h from 0.137 to 0.57. The normalized threshold bracing stiffness $k_{cr}/\left(EI/L^3\right)$ was observed to vary only within 4.47% (Fig 4.9b), suggesting that the section aspect ratio w/h has a negligible effect the normalized threshold bracing stiffness. The span to depth ratio L/h was varied from 5.26 to 21.1. Fig 4.9c shows a pronounced effect of L/h on the normalized threshold bracing stiffness $k_{cr}/\left(EI/L^3\right)$. The percentage difference between the smallest and largest value was 32.7%. The ratio b/h the of load height to section depth was varied from -0.5 to 0.5. The results in Fig 4.9d indicate that b/h has a very pronounced effect on the normalized threshold bracing stiffness. In summary, the above sensitivity analysis suggests that the normalized threshold bracing can be reasonably approximated as a function of two key parameters, i.e.

$$\bar{k}_{cr}/\left(EI_{yy}/L^3\right) \approx f_3\left(L/h, b/h\right) \tag{6.28}$$

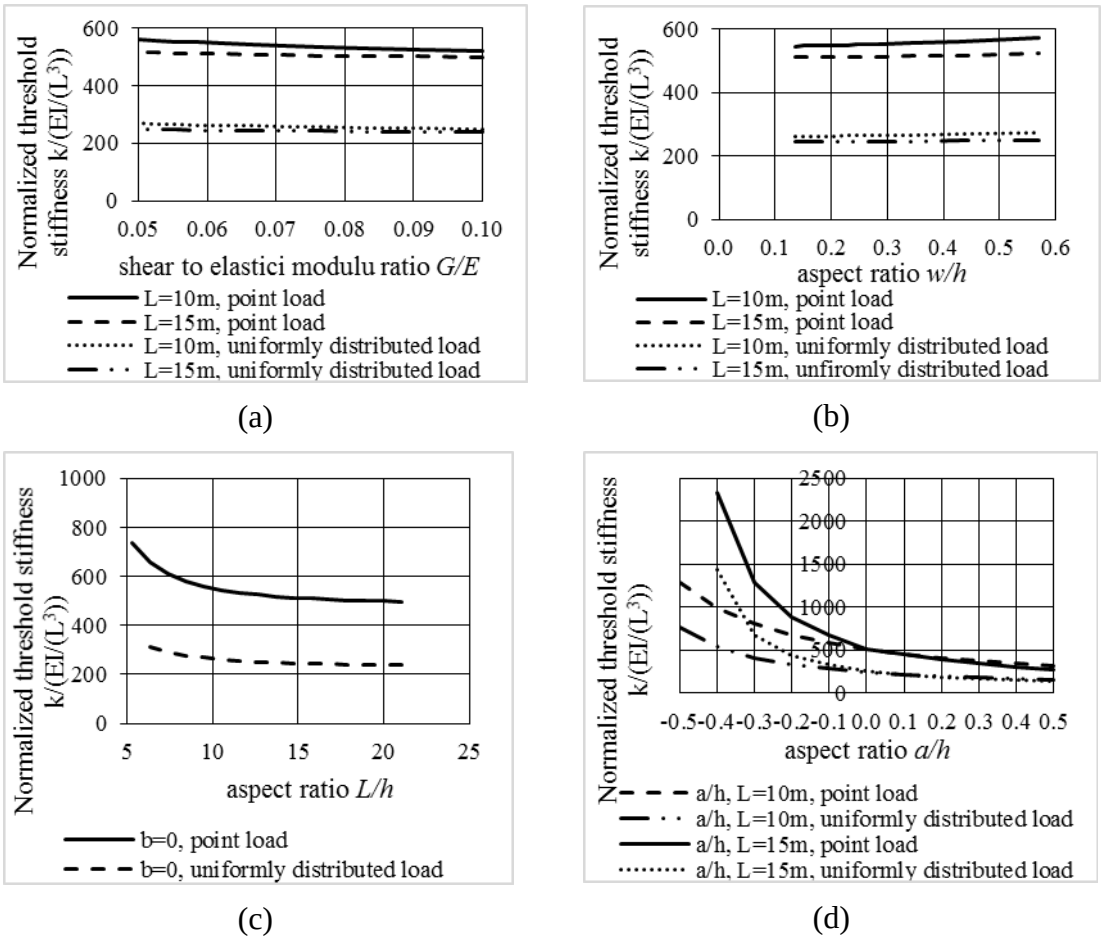

Figure 4.9 Sensitivity analysis for normalized threshold stiffness for point load and uniformly distributed load (a) effect of shear to elastic moduli G/E, (b) effect of aspect ratio w/h, (c) span to depth ratio L/h, and (d) load height to section depth ratio b/h

4.9.3 Regression analysis

A single regression equation of the form $Z \approx f\left(X,Y\right)$ where $Z = \log\left(\bar{k}_{cr}L^3/EI_{yy}\right)$, $X = L/h$ and $Y = b/h$ was originally sought and was found unattainable. Thus, 11 separate regression equations of the form $Z_{Y_i}\left(X\right)$ for the cases $Y_i = -0.5....0,....0.5$, were developed, i.e.,

$$Z_{Y_i} \approx a_{0i} + a_{1i}X + ... + a_{j_{\max}i}X^{j_{\max}} = \sum_{j=0}^{j_{\max}} a_{ji}X^{j} \tag{6.29}$$

where $j_{\max}$ is the number of terms needed to fit the results obtained from the parametric runs (Appendix 4.E) and a_{ji} is coefficients determined from the regression analysis. The

sum of the squares of the differences between the values of $\overline{Z}_{Yi}$ based on the present solution and that based on the approximation sought in Eq. (6.29) is minimized, i.e.,

$$D_i = \sum_{k=1}^{k\,\max} \left[\overline{Z}_{Yi} - \sum_{j=0}^{j_{\max}} a_{ji} X^j \right]^2 = \min \tag{6.30}$$

in which $k_{\max}$ is the number of runs conducted. By enforcing the conditions $\partial D_i / \partial a_{ji} = 0$ the regression constants were determined. The results are depicted in Fig 4.10 and the corresponding regression constants are provided in Table 4.1 both for uniformly distributed and point loading. For load height ratios $a/h = 0.1, 0.2, \ldots 0.5$, excellent fits were obtained by setting the order of regression polynomial to $j_{\max} = 2$. For beams with $a/h = -0.1, -0.2, \ldots -0.5$, more terms were found necessary and $j_{\max}$ was set equal to 5 for point loading and 4 for uniformly distributed loading. For a/h values lying between Y_i and Y_{i+1}, linear interpolation can be used to determine $Z = \log\left(k_{cr} L^3 / EI_{yy}\right)$. For the cases of short span to height ratios *L/h* and cross-section aspect ratios b/h = -0.3, -0.4, and-0.5 a small reduction in *L/h* is associated with a large increase in threshold stiffness as shown in Figs 4.10(b, d).

Table 4.1 Regression coefficients of simplified design equations

Point load							
i / a/h	0	1	2	3	4	5	R^*
-0.5	123.8	-36.40	4.39	-2.64E-01	7.89E-03	-9.37E-05	1.000
-0.4	74.17	-23.45	3.08	-2.00E-01	6.41E-03	-8.12E-05	0.998
-0.3	35.00	-11.26	1.57	-1.08E-01	3.65E-03	-4.84E-05	0.996
-0.2	17.05	-5.30	7.90E-01	-5.72E-02	2.03E-03	-2.81E-05	0.996
-0.1	5.09	-7.20E-01	9.50E-02	-6.38E-03	2.14E-04	-2.80E-06	1.000
0.0	3.00	-3.48E-02	9.95E-04	-	-	-	0.980
0.1	2.74	-1.07E-02	3.43E-04	-	-	-	0.944
0.2	2.55	4.29E-03	-4.22E-05	-	-	-	0.997
0.3	2.42	0.46E-02	-2.93E-04	-	-	-	1.000
0.4	2.30	2.20E-02	-4.67E-04	-	-	-	1.000
0.5	2.21	2.76E-02	-5.93E-04	-	-	-	0.999
Uniformly distributed load							
-0.5	40.22	-8.33	7.00E-01	-2.64E-02	3.73E-04	-	1.000
-0.4	18.38	-3.64	3.20E-01	-1.27E-02	1.89E-04	-	0.999
-0.3	10.02	-1.81	1.69E-01	-7.07E-03	1.10E-04	-	0.999
-0.2	6.37	-1.00	1.01E-01	-4.49E-03	7.40E-05	-	0.997
-0.1	3.68	-2.80E-01	2.57E-02	-1.08E-03	1.71E-05	-	1.000
0.0	2.65	-3.10E-02	8.72E-04	-	-	-	0.984
0.1	2.42	-1.16E-02	3.67E-04	-	-	-	0.954
0.2	2.26	9.06E-04	5.72E-05	-	-	-	0.989
0.3	2.13	9.78E-03	-1.55E-04	-	-	-	1.000
0.4	2.02	1.65E-02	-3.12E-04	-	-	-	1.000
0.5	1.93	2.19E-02	-4.35E-04	-	-	-	1.000

* R = correlation coefficient.

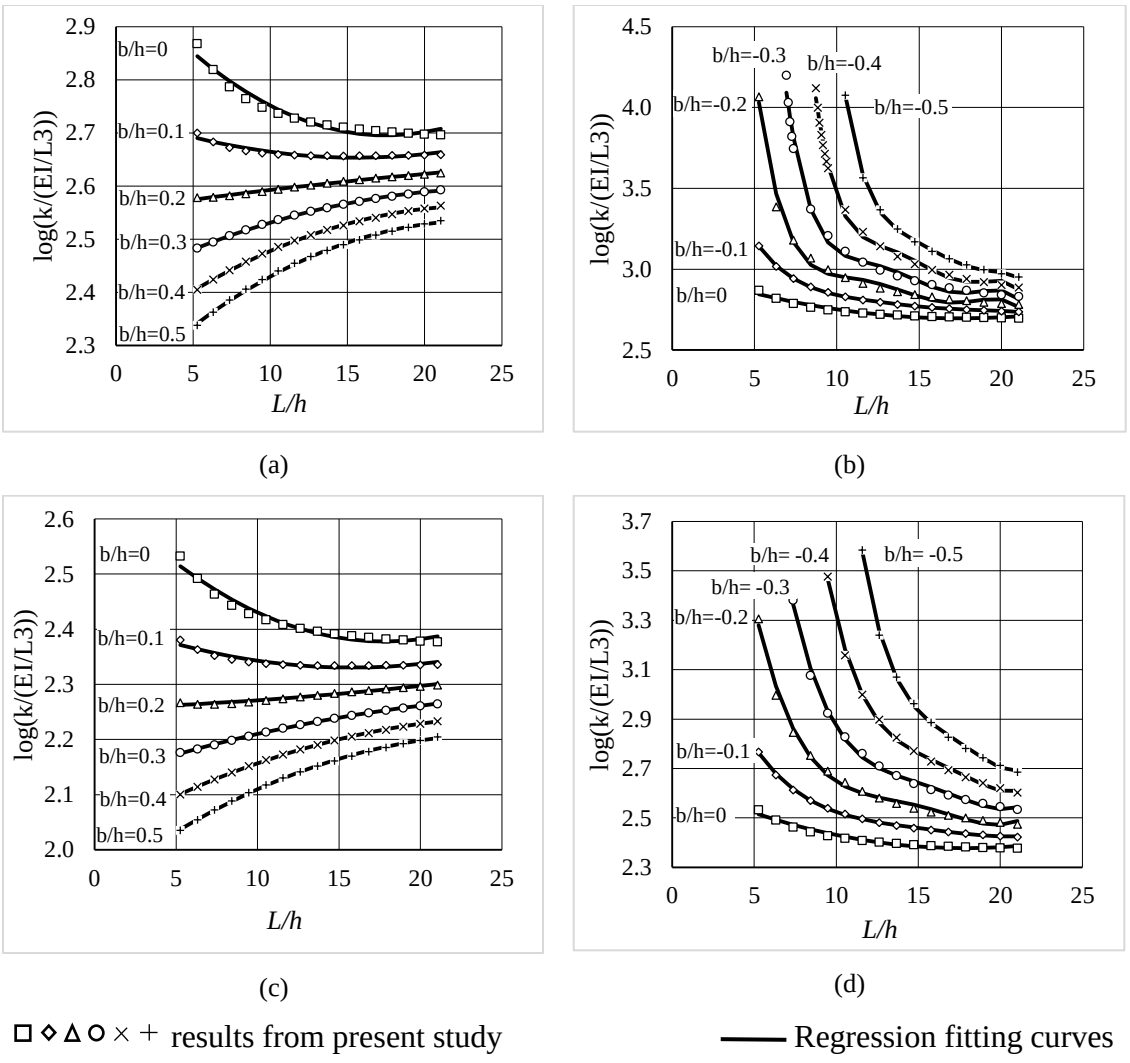

Figure 4.6 Threshold bracing stiffness versus span to height ratio for (a) point load above mid-height (b) point load below mid-height (c) uniformly distributed load above mid-height (d) uniformly distributed load below mid-height

4.9.4 Assessing errors in critical moment predictions induced by interpolation

To check the accuracy of adopting linear interpolation in dealing with cases where a/h values lies between Y_i and Y_{i+1}, the effect of approximation introduced by linear interpolation on the critical moments is assessed by comparing the critical moments as predicted by the present eigenvalue solution to that based on interpolation for four cases involving point load and uniformly distributed load and various ratios L/h and a/h ratios (Table 4.2). In all four cases, the difference between both methods is found to be less than 0.5% suggesting the validity of the interpolation solution.

Table 4.2 Comparison of critical moments as determined based on the present model and the simplified regression method with interpolation

Load type	a/h (b/h)	L/h	Critical moment based on present model (kNm)	Critical moment based on interpolation (kNm)	difference
point load	-0.25	10	1092.9	1087.4	0.50%
	0.35	11	980.6	980.3	0.03%
uniformly distributed load	-0.15	12	666.8	666.8	0.00%
	0.25	13	580.4	580.4	0.00%

4.9.5 Threshold stiffness outside the investigated range

As shown in Fig 4.9 (b,d), for cases of bottom loading a/h = -0.3,-0.4,-0.5, when L/h is smaller than the range investigated i.e. the threshold bracing stiffness can reach very large magnitudes. In the absence of information within this range, the designer may opt to adopt the largest value $\bar{k}_{cr}$ shown on Fig 4.9. It is of practical interest to assess the error induced by such an approximation on the critical moments computed. Six cases with different loading, and various a/h and L/h were investigated. The results in Table 4.3 show a large difference between the peak critical bracing stiffness depicted in Fig 4.10 and that based on the eigenvalue solution. For example, for run 6, the critical bracing stiffness based on the eigenvalue solution is $1.83\times10^{4} kN/m$. This value is significantly higher compared to the peak stiffness of $5.18\times10^{3} kN/m$ based on Fig 4.10. Nevertheless, the corresponding difference in critical moments based on both values is 3.17%. For all six cases considered, adopting the highest critical stiffness on Fig 4.10 are found to introduce an error of no more than 5.87%.

Table 4.3 Comparison of threshold bracing as determined based on the present solution and the approximate regression equations

		Threshold bracing stiffness (kN/m)		Critical Moment (kNm) based on detailed solution		
(1) b/h	(2) L/h	(3) Based on eigenvalue solution (k_{cr})	(4) Maximum $\bar{k}_{cr}$ based on Figs. 10b,d	(5) Based on k_{cr}	(6) Based on $\bar{k}_{cr}$	Difference ((5)-(6))/(5) (%)
Point load						
-0.3	6.84	2.01E+05	9.86E+04	1.72E+03	1.71E+03	0.64
-0.4	8.53	1.32E+05	4.13E+04	1.32E+03	1.30E+03	0.96
-0.5	10.32	4.53E+04	2.14E+04	1.05E+03	1.05E+03	0.75
Uniformly distributed load						
-0.3	6.84	3.80E+04	1.26E+04	1.34E+03	1.26E+03	5.87
-0.4	8.95	2.25E+04	7.38E+03	9.76E+02	9.36E+02	4.14
-0.5	11.05	1.83E+04	5.18E+03	7.69E+02	7.45E+02	3.17

4.10 Summary and Conclusions

1. An analytical solution was developed for the prediction of lateral torsional buckling capacity of simply supported wooden beams with discrete elastic lateral restraints at mid-span subjected to symmetric loads relative to mid-span.

2. The validity of model was established through comparisons with ABAQUS results and through comparisons with published studies by Schmidt (1965) and McCann (2013).

3. Depending on the load and bracing heights and elastic restrain magnitude, two possible lateral torsional buckling modes were observed; symmetric and antisymmetric

4. Critical moments based on the symmetric mode were observed to decrease with a decrease in mid-span bracing height, while those based on anti-symmetric modes remain independent of the mid-span bracing height.

5. For relatively weak bracing stiffness, the symmetric mode tends to govern the buckling capacity of the beam while for relatively stiff bracing, the anti-symmetric mode tends to govern the buckling capacity of the beam.

6. Critical moments based on the symmetric modes decrease when the load height increases. In contrast, critical moments based on the anti-symmetric mode are observed to be independent of the load height and bracing stiffness for the case of mid-span loading, but are observed to decrease for the case of uniformly distributed load as the point of application of the load moves upwards.

8. In most cases, for a given load height and a given bracing height, a threshold bracing stiffness was found to exist. Above this threshold value, the critical moment is dictated by the anti-symmetric critical moment while below this threshold value, the critical moment is dictated by the symmetric mode, which corresponds to a smaller critical moment.

9. For the common case where the point of load application coincides with the bracing height, simplified equations have been developed to determine the threshold bracing stiffness required to achieve the critical moment based on the anti-symmetric mode.

Notation

The following symbols are used in this paper:

a = load height from cross-section centroid;

b = bracing height from cross-section centroid;

C_w = warping constant;

E = Young's modulus of wooden beam along the longitudinal direction;

G = shear modulus of the beam;

h = cross section height;

I_{yy} = weak moment of inertia;

J = Saint-Venant torsional constant;

k_{cr} = threshold stiffness from as obtained from eigenvalue analysis;

$\bar{k}_{cr}$ = approximate threshold bracing stiffness;

k_0 = spring constant reflecting the lateral bracing stiffness;

L = beam span;

$M_{cr,a}$ = critical moment based on the anti-symmetric mode.

m_k = Fourier coefficient;

n = number of Fourier terms;

P_{cr} = critical load;

Q = reference point load;

q = reference uniformly distributed load;

u = lateral displacement at section centroidal axis:

u_{sp} = lateral deformation at the lateral bracing location;

U = internal strain energy of the beam-spring system;

V = load potential energy gain of the system;

w = cross section width;

w_{cr} = critical load;

β = normalized brace height relative to cross-section shear centre;

β_{cr} = normalized threshold bracing height relative to cross-section centre;

θ = twisting angle;

λ = load multiplier;

μ_{LT} = Poisson's ratio for deformation along the tangential direction cause by stress along the longitudinal direction;

π = total potential energy of the system;

References

[1] Andrade, A., and Camotim, D. (2005). “Lateral-torsional buckling of singly symmetric tapered beams: theory and applications.” *J. Eng. Mech.*, 131(6), 586-597

[2] Andrade, A., Camotim, D. Dinis, P.B. (2007). “Lateral-torsional buckling of singly symmetric web-tapered thin-walled I-beams: 1D model vs. shell FEA.” *Comput. Struct.*, 85(17-18), 1343-1359

[3] American Forest and Paper Association (AFPA). (2003). “Technical Report 14: Designing for lateral torsional stability in wood members.” Washington, D.C., U.S.

[4] American Wood Council (AWC). (2015). “National design specification for wood construction.” ANSI/AWC NDS-2015, Virginia, U.S.

[5] Canadian Standard Association (CSA). (2014). “Engineering design in wood.” *O86-14*, Mississauga, Ontario, Canada.

[6] Erkmen, R.E. and Mohareb, M. (2008). “Buckling analysis of thin-walled open members-A finite element formulation.” *Thin. Wall. Struct.*, 46(6), 618-636

[7] Flint, A.R. (1951), “The influence of restraints on the stability of beams.” *Struct. Eng.*, 29(9), 235-246

[8] Forest Products Laboratory (FPL). (2010). *Wood handbook-Wood as an engineering material*. Wisconsin, U.S.

[9] Helwig, T., Frank, K., Yura, J. (1997). “Lateral-torsional buckling of singly symmetric I-beams.” *J. Struct. Eng.*, 123(9), 1172-1179

[10] Ings, N.L. and Trahair, N.S. (1987). “Beam and column buckling under directed loading.” *J. Eng. Mech.*, 113(6), 1251-1263

[11] Jingping, L., Zaitian, G. Chen, S. (1988). “Buckling of transversely loaded I-Beam columns.” *J. Struct. Eng.*, 114(9), 2109-2118

[12] Kerensky, O.A., Flint, A.R., Brown, W.C. (1956). “The basis for design of beams and plate girders in the revised British Standard 153.” *P. I. Civil. Eng.*, 5(3), 396–461

[13] Kitipomchai, S., Dux, P.F., Richter, N.J. (1984). “Buckling and bracing of cantilevers.” *J. Struct. Eng.*, 110(9), 2250-2262

[14] White, D.W. and Kim, Y.D. (2008), “Unified Flexural Resistance Equations for Stability Design of Steel I-Section Members: Moment Gradient Tests.” *J. Struct. Eng.,* 134(9), 1450-1470
[15] Lay, M.G., Galambos, T.V., Schmidt, L.C. (1963). “Lateral bracing force of steel I beams.” *J. Eng. Mech. Div.,* 89(EM3), 217-224
[16] Lamb, A.W., and Eamon, C.D. (2015). “Load height and moment factors for doubly symmetric wide flange beams.” *J. Struct. Eng.,* 10.1061/(ASCE)ST.1943-541X.0001332, 04015069
[17] Mutton, B.R., and Trahair, N.S. (1973). “Stiffness requirement for lateral bracing.” *J. Struct. Eng. Div.,* 99(10), 2167-2182
[18] Mohri, F., and Potier-Ferry, M. (2006). “Effects of load height application and pre-buckling deflection on lateral buckling of thin-walled beams.” *Steel. Compos. Struct;,* 6(5), 1-15
[19] Mohebkhah A (2010), “Lateral buckling resistance of inelastic I-beams under off-shear center loading.” *Thin. Wall. Struct.,* 49(3), 431-436
[20] McCann, F., Wadee, M.A., Gardner, L. (2013). “Lateral stability of imperfect discretely braced steel beams.” *J. Eng. Mech.,* 139(10), 1341-1349
[21] Nethercot, D.A., and Rockey, K.C. (1971). “A unified approach to the elastic lateral buckling of beams.” *Struct. Eng.,* 49(7), 321-330
[22] Nethercot, D.A., and Rockey, K.C. (1972). “The lateral buckling of beams having discrete intermediate restraints.” *Struct. Eng.,* 50(10), 391-403
[23] Pi, Y.L., Traihair, N.S., Rajasekaran, S. (1992). “Energy equation for beam lateral buckling.” *J. Struct. Eng.,* 118(6), 1462-1479
[24] Samanta, A., and Kumar, A. (2006). “Distortional buckling in monosymmetric I-beams.” *Thin. Wall. Struct.,* 44(1), 51-56
[25] Arash, S., and Mohareb, M. (2016). “Upper and lower bound solutions for lateral-torsional buckling of doubly symmetric members.” *Thin. Wall. Struct.,* doi:10.1016/j.tws.2016.01.015 0263-8231
[26] Sahraei, A., Wu, L., Mohareb, M. (2015). “Finite element formulation for lateral torsional buckling analysis of shear deformable mono-symmetric thin-walled members.” *Thin. Wall. Struct.,* doi:10.1016/j.tws.2014.11.023

[27] Schmidt, L.C., (1965). “Restraints against elastic lateral buckling.” *J. Eng. Mech. Div.*, 91(EM6), 1-10

[28] Timoshenko, S. (1936). *Theory of elastic stability*, McGraw-Hill Book Company, Inc., New York

[29] Tong, G.S., and Chen, S.F. (1988). “Buckling of laterally torsionally braced beams.” *J. Constr. Steel. Res.*, 11(1), 41-55

[30] Trahair, N.S. (2013). “Bending and buckling of tapered steel beam structures.” *Eng. Struct.*, 59, 229-237

[31] Xiao, Q. (2014). “Lateral Torsional Buckling of Wood Beams”, M.A.Sc. thesis, Dept. of Civil Engineering, Uni. of Ottawa, Ontario, Canada.

[32] Yura, J.A. (2001). “Fundamental of Beam Bracing, Engineering Journal.” *Eng. J.*, 38(1), 11-26

[33] Yura, J., Helwig, T.A., Zhou, C. (2008). “Global lateral buckling of I-shaped girder system.” *J. Struct. Eng.*, 134(9), 1487-1494

[34] Winter, G. (1960). “Lateral bracing of columns and beams.” *T. Am. Soc. Civ. Eng.*, 125 (1), 807-826

[35] Wong-Chung, A.D., and Kitipomchai, S. (1987). “Partially braced inelastic beam buckling experiments.” *J. Constr. Steel. Res.*, 7(3), 189-211

[36] Wang, C.M., Kitrporncha, S. Thevendran, V. (1987). “Buckling of braced monosymmetric cantilevers.” *Int. J. Mech. Sci.*, 29(5), 321-337

[37] White, D.W., and Kim, Y.D. (2008). “Unified Flexural Resistance Equations for Stability Design of Steel I-Section Members: Moment Gradient Tests.” *J. Struct. Eng.*, 134(9), 1450-1470

[38] Wu, L., and Mohareb, M. (2010). “Buckling formulation for shear deformable thin-walled members-II. Finite element formulation.” *Thin. Wall. Struct.*, 49(1), 208-222

[39] Wong, E., Driver, R.G. and Heal, T.W. (2015). “Simplified approach to estimating the elastic lateral–torsional buckling capacity of steel beams with top-flange loading.” *Can. J. Civ. Eng.*, 42(2), 130-138

Appendix 4.A-Symmetry properties of the buckling modes

The purpose of Appendix 3.A is to provide a mathematical proof of the symmetry properties of two groups of buckling mode resulting in Eqs. (6.21) and (6.22). We recall the mode shapes as given by Eq. (6.4) are

$$u(z)=\sum_{i=1}^{2n} A_i \sin\frac{i\pi z}{L},\quad \theta(z)=\sum_{j=1}^{2n} B_j \sin\frac{j\pi z}{L}$$

where $i=1,2,3\ldots, j=1,2,3\ldots$. The displacements at $(L-z)$ are

$$u(L-z)=\sum_{i=1}^{2n} A_i \sin\left(i\pi-\frac{i\pi z}{L}\right),\qquad \theta(L-z)=\sum_{j=1}^{2n} B_j \sin\left(j\pi-\frac{j\pi z}{L}\right) \tag{4.A.1}$$

Symmetry of Mode 1

For the case (**i, j=1, 3, 5)**, one has

$$u(z)=u(L-z),\theta(z)=\theta(L-z) \tag{4.A.2)a-b}$$

Equations (4.A.2)a-b indicate that $i=1,3,5..$ and $j=1,3,5..$ correspond to a symmetric mode.

Anti-symmetry of Mode 2

For the case (**i, j=2, 4, 6)**, one has

$$u(z)=-u(L-z),\qquad \theta(z)=-\theta(L-z) \tag{4.A.3)a-b}$$

Equations (4.A.3)a,b indicate that $i=2,4,6..$ and $j=2,4,6..$ correspond to an anti-symmetric mode.

Appendix 4.B Convergence study of present energy formulation and 3D FEA model

The accuracy of LTB critical moment obtained from (6.21) and (6.22) hinges on the number of terms used in Eqs. (6.4). Table 4.B.1 present the critical moment results based on various values of the maximum number n of Fourier terms as defined in Eqs. (6.4). The purpose is determine the number of Fourier terms needed for convergence.

Table 4.B.2 present the critical moments for the reference case described in section titled "The ABAQUS model" by varying the number of finite elements in the longitudinal direction of the beam.

Table 4.B. 1 Convergence study of energy formulation

number of Fourier terms n =						1	2	3	4	6	1	2	3	4	6
Run #	LT (1)	Mode (2)	*k* (3)	*a/h*	*b/h*	Buckling load P_{cr} (kN), or w_{cr} (kN/m)					% Difference (4)				
1	P	S	10	0.0	0.0	88.2	83.5	83.5	83.4	83.4	5.7	0.2	0.1	0.0	0.0
2	P	S	1000	0.0	0.0	403.1	246.0	239.6	239.1	239.0	68.6	2.9	0.2	0.0	0.0
3	P	S	10	0.5	0.0	73.8	69.7	69.5	69.4	69.4	6.4	0.5	0.2	0.0	0.0
4	P	S	1000	0.5	0.0	191.4	149.1	146.2	145.6	145.3	31.8	2.6	0.7	0.2	0.0
5	P	S	10	0.0	0.5	94.5	89.7	89.6	89.5	89.5	5.5	0.1	0.1	0.0	0.0
6	P	S	1000	0.0	0.5	1236.9	368.7	329.9	328.4	328.2	276.9	12.4	0.5	0.1	0.0
7	P	S	10	0.5	0.5	79.2	74.9	74.7	74.6	74.6	6.1	0.4	0.1	0.0	0.0
8	P	S	1000	0.5	0.5	691.1	297.3	276.4	274.9	274.6	151.7	8.3	0.7	0.1	0.0
9	P	A	10	0.0	0.0	229.8	207.2	206.7	206.6	206.6	11.2	0.3	0.1	0.0	0.0
10	P	A	1000	0.0	0.0	229.8	207.2	206.7	206.6	206.6	11.2	0.3	0.1	0.0	0.0

[1] LT=Loading type: P=mid-span point load, U=uniformly distributed

[2] Mode: S=symmetric mode (1), A=anti-symmetric mode (2)

[2] k=spring stiffness (kN/m)

[4] Difference=$[P_{cr}(n) - P_{cr}(n=6)]/P_{cr}(n=6)$

Table 4.B. 1 (cont) Convergence study of present solution

number of Fourier terms n =						1	2	3	4	6	1	2	3	4	6
Run #	LT (1)	Mode (2)	*k* (3)	*a/h*	*b/h*	Buckling load P_{cr} (kN), or w_{cr} (kN/m)					% Difference (4)				
11	P	A	10	0.5	0.0	229.8	207.2	206.7	206.6	206.6	11.2	0.3	0.1	0.0	0.0
12	P	A	1000	0.5	0.0	229.8	207.2	206.7	206.6	206.6	11.2	0.3	0.1	0.0	0.0
13	P	A	10	0.0	0.5	229.8	207.2	206.7	206.6	206.6	11.2	0.3	0.1	0.0	0.0
14	P	A	1000	0.0	0.5	229.8	207.2	206.7	206.6	206.6	11.2	0.3	0.1	0.0	0.0
15	P	A	10	0.5	0.5	229.8	207.2	206.7	206.6	206.6	11.2	0.3	0.1	0.0	0.0
16	P	A	1000	0.5	0.5	229.8	207.2	206.7	206.6	206.6	11.2	0.3	0.1	0.0	0.0
17	U	S	10	0.00	0.00	11.0	10.8	10.7	10.7	10.7	2.0	0.1	0.0	0.0	0.0
18	U	S	1000	0	0	50.1	37.7	37.1	37.1	37.1	35.2	1.7	0.1	0.0	0.0
19	U	S	10	0.5	0.0	9.5	9.3	9.3	9.3	9.3	1.6	0.1	0.0	0.0	0.0
20	U	S	1000	0.50	0.00	27.0	25.8	25.3	25.3	25.2	6.9	2.0	0.2	0.1	0.0
21	U	S	10	0.0	0.5	11.7	11.5	11.5	11.5	11.5	1.9	0.1	0.0	0.0	0.0
22	U	S	1000	0.00	0.50	153.8	43.0	39.2	39.2	39.2	292.1	9.7	0.0	0.0	0.0
23	U	S	10	0.5	0.5	10.2	10.0	10.0	10.0	10.0	1.5	0.1	0.0	0.0	0.0
24	U	S	1000	0.50	0.50	97.8	40.8	37.1	37.1	37.1	163.9	10.0	0.1	0.0	0.0
25	U	A	10	0.0	0.0	24.6	23.4	23.3	23.3	23.3	5.6	0.0	0.0	0.0	0.0
26	U	A	1000	0.00	0.00	24.6	23.4	23.3	23.3	23.3	5.6	0.0	0.0	0.0	0.0
27	U	A	10	0.5	0.0	22.9	21.8	21.8	21.8	21.8	4.9	0.0	0.0	0.0	0.0
28	U	A	1000	0.50	0.00	22.9	21.8	21.8	21.8	21.8	4.9	0.0	0.0	0.0	0.0
29	U	A	10	0.0	0.5	24.6	23.4	23.3	23.3	23.3	5.6	0.0	0.0	0.0	0.0
30	U	A	1000	0.00	0.50	24.6	23.4	23.3	23.3	23.3	5.6	0.0	0.0	0.0	0.0
31	U	A	10	0.5	0.5	22.9	21.8	21.8	21.8	21.8	4.9	0.0	0.0	0.0	0.0
32	U	A	1000	0.50	0.50	22.9	21.8	21.8	21.8	21.8	4.9	0.0	0.0	0.0	0.0

[1] LT=Loading type: P=mid-span point load, U=uniformly distributed

[2] Mode: S=symmetric mode (1), A=anti-symmetric mode (2)

[2] k=spring stiffness (kN/m)

[4] Difference=$[P_{cr}(n) - P_{cr}(n=6)]/P_{cr}(n=6)$

Table 4.B. 2 Mesh sensitivity results for ABAQUS model

Number of elements in longitudinal direction						50	170	290	410	470	50	170	290	410	470
Number of elements along the depth						50	50	50	50	50	50	50	50	50	50
Number of elements across the width						10	10	10	10	10	10	10	10	10	10
number of elements (thousands)						25	85	145	205	235	25	85	145	205	235
run	LT	Mode	k_0	a/h	b/h	Buckling load P_{cr} (KN), or w_{cr} (KN/m)					%Difference				
1	P	S	10	0.0	0.0	138.3	133.5	133.2	133.1	133.0	3.9	0.4	0.1	0.0	0.0
2	P	S	1000	0.0	0.0	253.7	237.0	235.8	235.5	235.4	7.8	0.6	0.2	0.0	0.0
3	P	A	10	0.0	0.0	224.1	205.0	203.7	203.4	203.3	10.2	0.8	0.2	0.0	0.0
4	P	A	1000	0.0	0.0	224.1	205.0	203.7	203.4	203.3	10.2	0.8	0.2	0.0	0.0
5	U	S	10	0.0	0.0	18.3	17.8	17.7	17.7	17.7	3.4	0.3	0.1	0.0	0.0
6	U	S	1000	0.0	0.0	39.5	36.6	36.3	36.3	36.3	8.9	0.8	0.2	0.0	0.0
7	U	A	10	0.0	0.0	25.3	23.2	23.1	23.0	23.0	10.1	0.8	0.2	0.0	0.0
8	U	A	1000	0.0	0.0	25.3	23.2	23.1	23.0	23.0	10.1	0.8	0.2	0.0	0.0

Appendix 4.C Verification of present study results against 3D FEA model solution

To assess the validity of the energy formulation formulated in the section titled "Formulation", the results obtained from present energy formulation are compared against those obtained from ABAQUS model for different load height and brace positions. There are two types of results compared in the Appendix: a) comparing the critical moment obtained from both models, and b) comparing the buckling mode shape obtained from both models. Table 4.C are presenting the critical moment data that plotted in Figure 4.C.

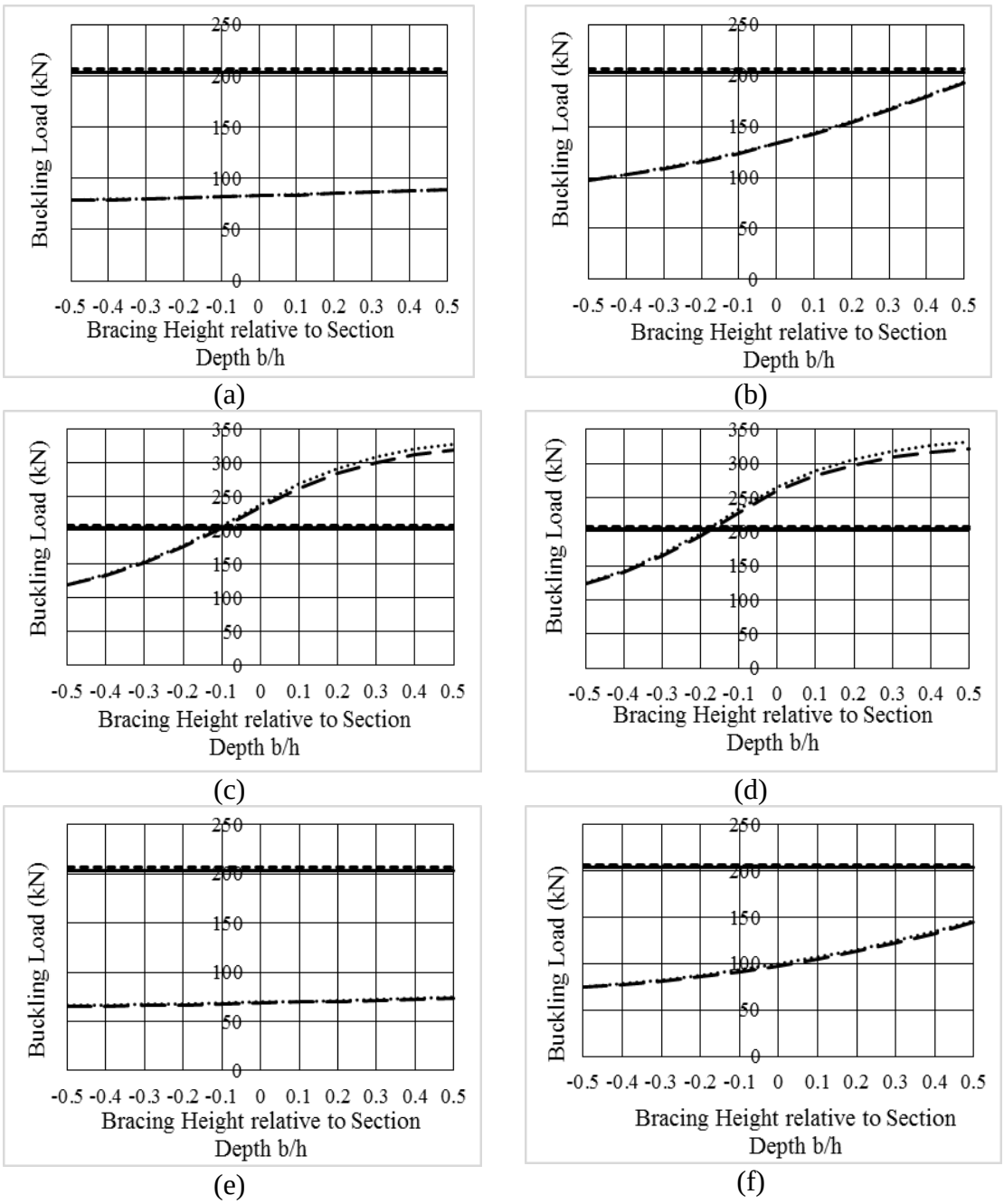

Figure 4.C.1 Buckling load for different load height and elastic restraint stiffness (a) Point load, $a = 0$, $10kN/m$ **(b) point load,** $a = 0$ **(c) point load,** $a = 0$, $10^3 kN/m$ **(d) point load,** $a = 0$, $10^4 kN/m$ **(e) point load,** $a = 0.5h$, $10kN/m$ **(f) point load,** $a = 0.5h$, $10^2 kN/m$

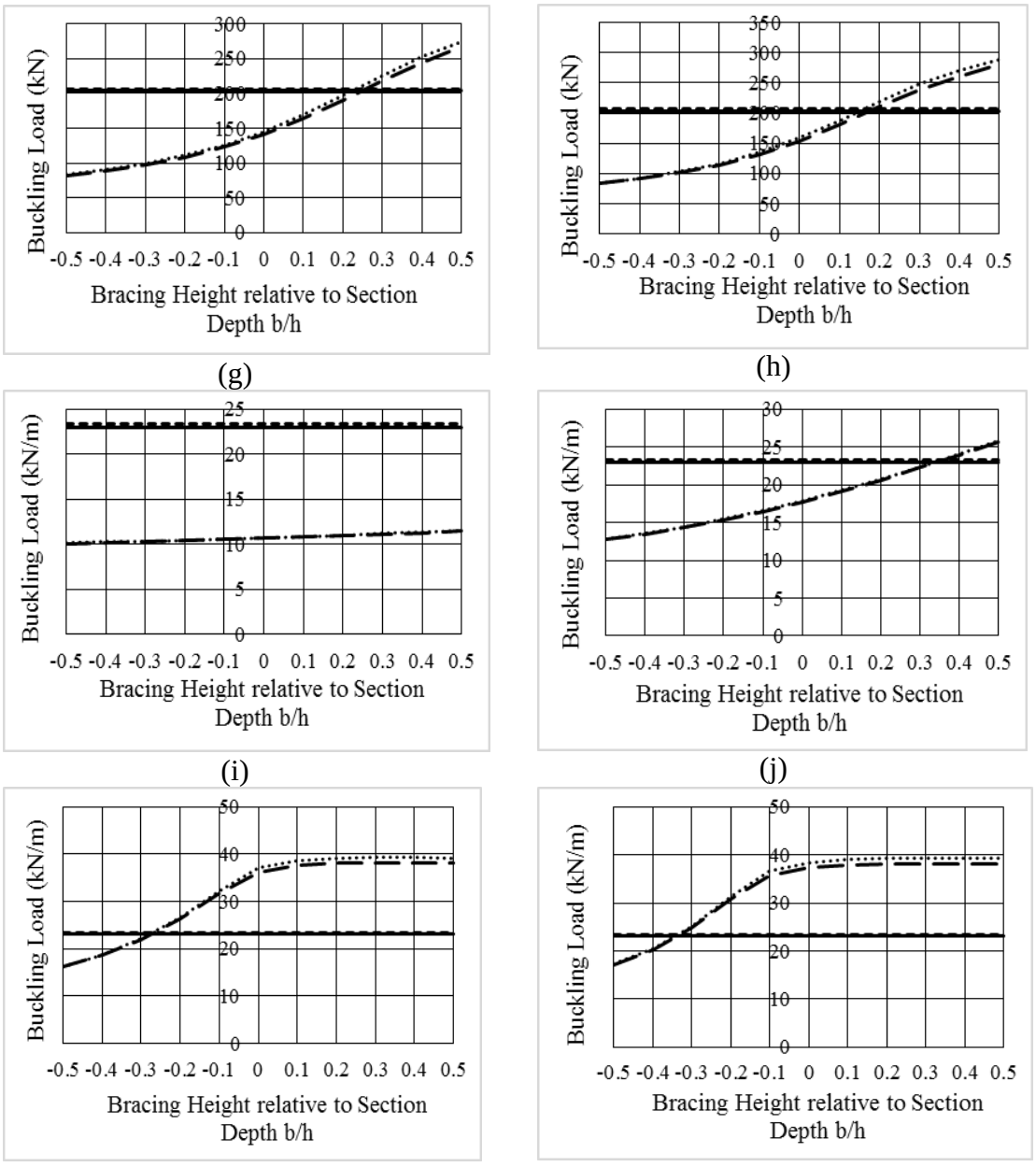

Figure 4.C.1 (cont) Buckling load for different load height and elastic restraint stiffness (g) point load, $a = 0.5h, 10^3 kN/m$ **(h) point load,** $a = 0.5h$, $10^4 kN/m$ **(i) uniformly distributed load,** $a = 0, 10kN/m$ **(j) uniformly distributed load,** $a = 0$, $10^2 kN/m$ **(k) uniformly distributed load,** $a = 0, 10^3 kN/m$ **(l) uniformly distributed load,** $a = 0$, $10^4 kN/m$

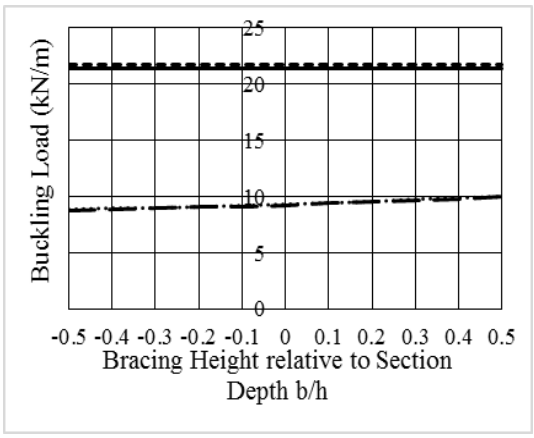

(m)

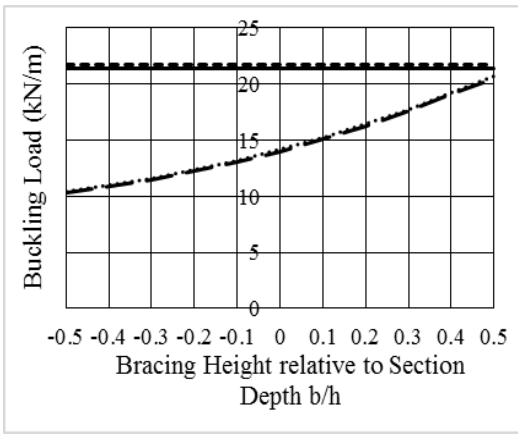

(n)

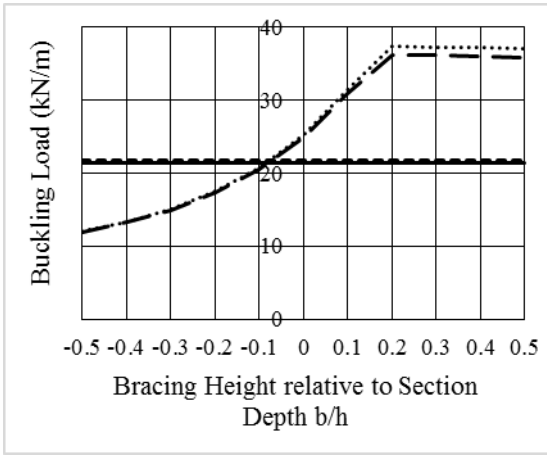

(o)

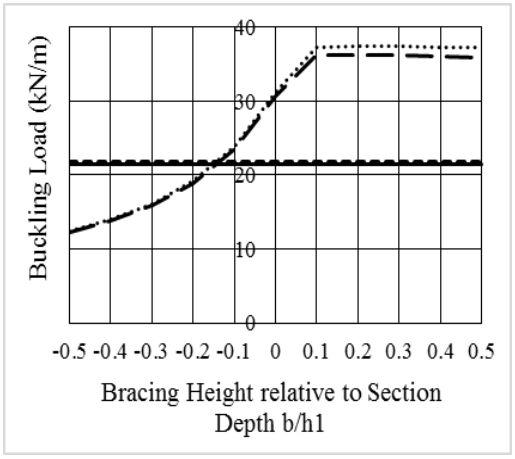

(p)

····· Present Study-Symmetric-n=9 ------ Present Study-Antisymmetric-n=9

— — ABAQUS-Symmetric ——— ABAQUS-Antisymmetric

Figure 4.C.1 (cont) Buckling load for different load height and elastic restraint stiffness (m) uniformly distributed load, $a = 0.5h$, $10kN/m$ **(n) uniformly distributed load,** $a = 0.5h$, $10^2 kN/m$ **(o) uniformly distributed load,** $a = 0.5h$, $10^3 kN/m$ **(p) uniformly distributed load,** $a = 0.5h$, $10^4 kN/m$

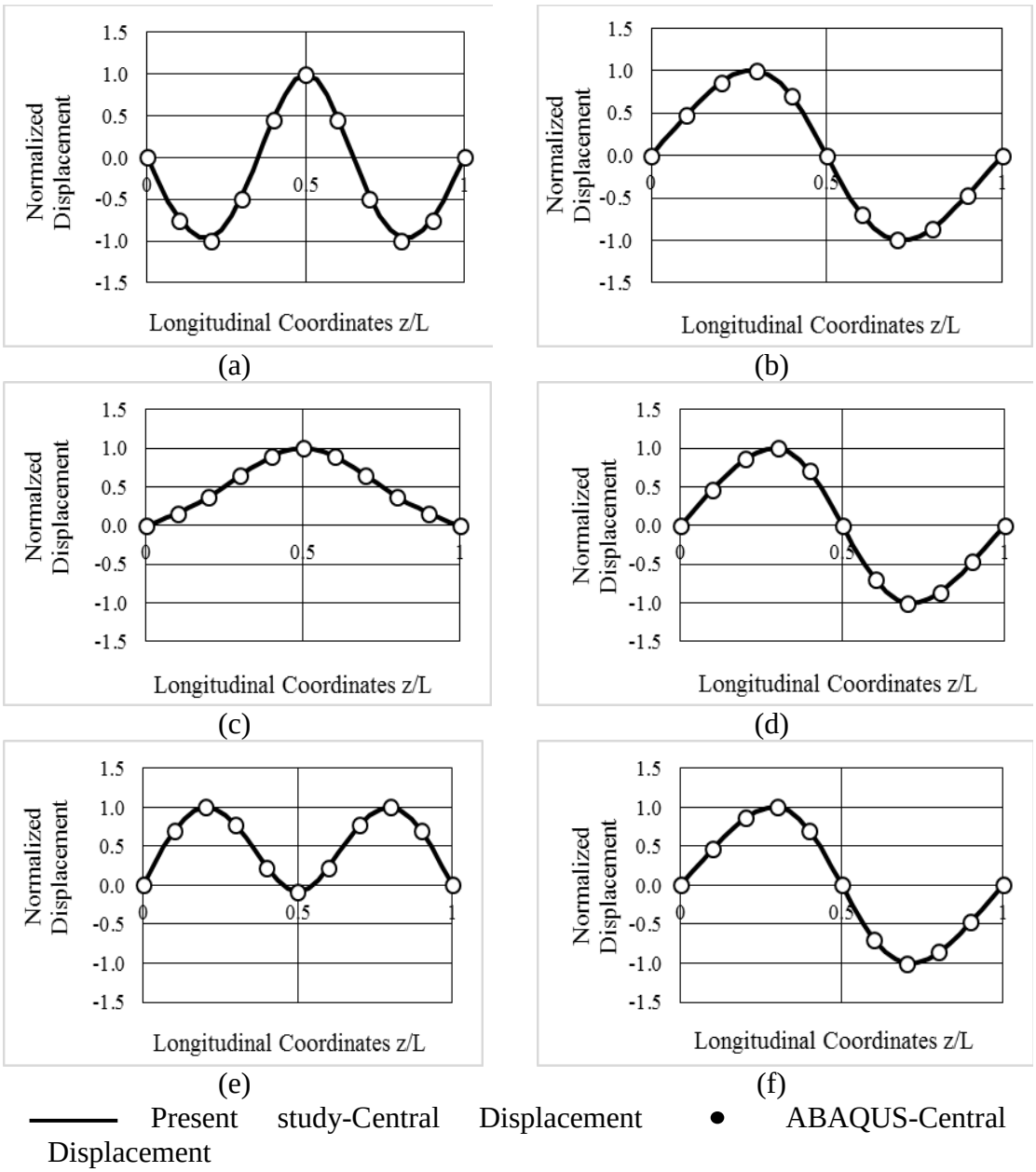

Figure 4.C. 2 Comparison of buckling mode shape when load and brace at different height. (a) point load, symmetric mode, $k = 1000kN/m$ $a = 0, b = 0$ **(b) point load, anti-symmetric mode,** $k = 1000kN/m$ $a = 0$ $, b = 0$ **(c) point load, symmetric mode,** $k = 100kN/m$ $a = 0$, $b = 0.5h$ **(d) point load, anti-symmetric mode,** $k = 100kN/m$ $a = 0$, $b = 0.5h$ **(e) point load, symmetric mode,** $k = 10000kN/m$ $a = 0.5h$, $b = 0$ **(f) point load, anti-symmetric mode,** $k = 10000kN/m$ $a = 0.5h$, $b = 0$

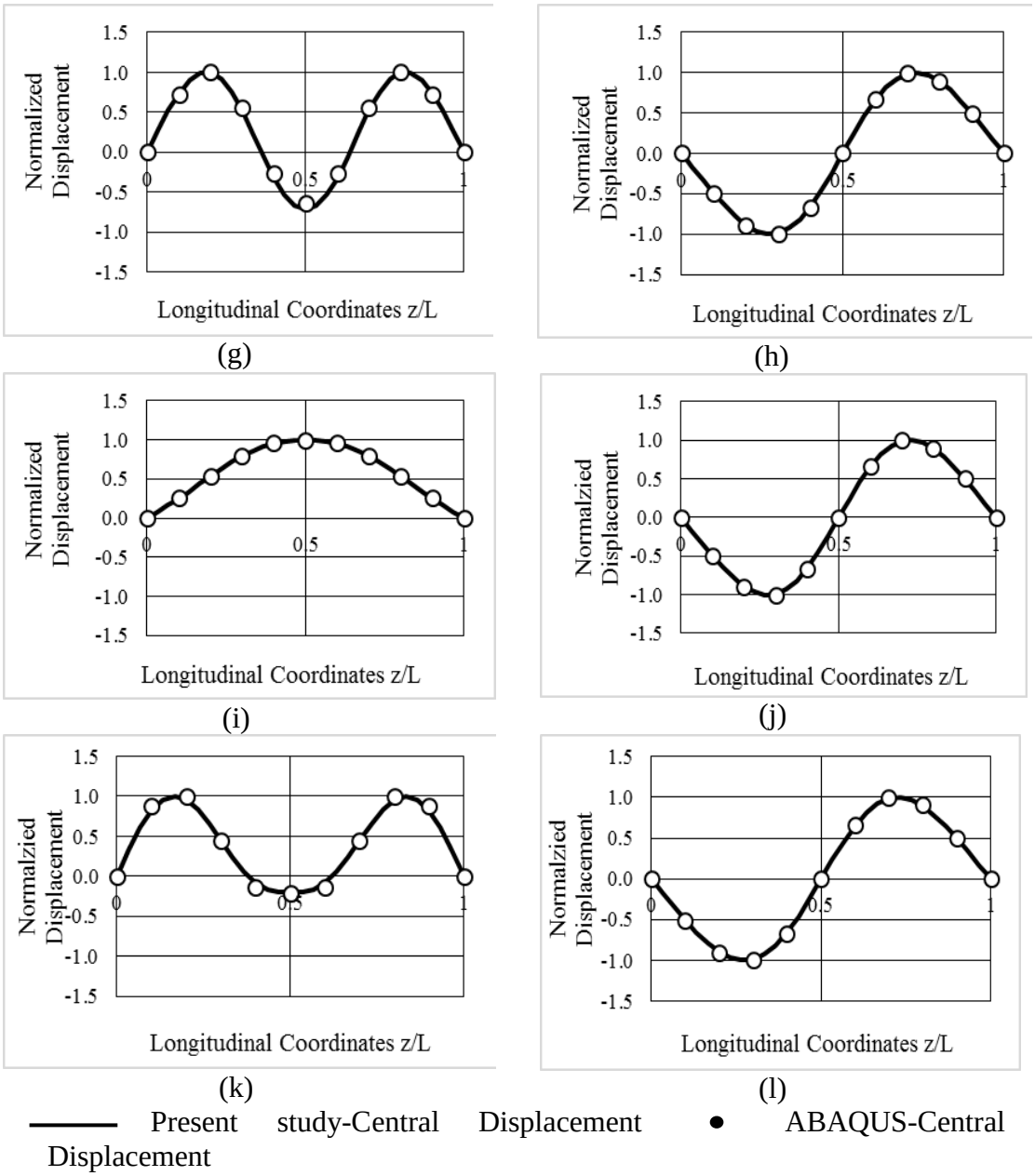

Figure 4.C. 2 (cont) Comparison of buckling mode shape when load and brace at different height (g) uniformly distributed load, symmetric mode, $k = 1000kN/m$ $a = 0, b = 0$ **(h) uniformly distributed load, anti-symmetric mode,** $k = 1000kN/m$ $a = 0$, $b = 0$ **i) uniformlye distributed load, symmetric mode,** $k = 100kN/m$ $a = 0$, $b = 0.5h$ **(j) uniformly distributed load, anti-symmetric mode,** $k = 100kN/m$ $a = 0$, $b = 0.5h$ **(k) uniformly distributed load, symmetric mode,** $k = 10000kN/m$ $a = 0.5h$, $b = 0$ **(l) uniformly distributed load, anti-symmetric mode,** $k = 10000kN/m$ $a = 0.5h$, $b = 0$

Table 4.C Comparison of critical moment

(1) bracing height (b/h)	(2) Present Study symmetric mode (kNm)	(3) Abaqus symmetric mode (kNm)	((2)-(3))/(2) (%)	(4) Present Study anti-symmetric mode (kNm)	(5) Abaqus anti-symmetric mode (kNm)	((4)-(5))/(4) (%)
point load, $a = 0$, $10 kN/m$						
-0.5	257	255	0.650	671	661	1.54
-0.4	259	257	0.657	671	661	1.54
-0.3	262	260	0.664	671	661	1.54
-0.2	265	263	0.669	671	661	1.54
-0.1	268	266	0.668	671	661	1.54
0	271	269	0.650	671	661	1.54
0.1	275	273	0.659	671	661	1.54
0.2	278	277	0.648	671	661	1.54
0.3	282	281	0.629	671	661	1.54
0.4	287	285	0.602	671	661	1.54
0.5	291	289	0.569	671	661	1.54
point load, $a = 0$, $10^2 kN/m$						
-0.5	318	315	0.740	671	661	1.54
-0.4	335	333	0.752	671	661	1.54
-0.3	356	353	0.791	671	661	1.54
-0.2	379	376	0.811	671	661	1.54
-0.1	406	402	0.813	671	661	1.54
0	435	432	0.657	671	661	1.54
0.1	468	465	0.793	671	661	1.54
0.2	505	501	0.781	671	661	1.54
0.3	544	540	0.730	671	661	1.54
0.4	586	582	0.668	671	661	1.54
0.5	630	626	0.703	671	661	1.54
point load, $a = 0$, $10^3 kN/m$						
-0.5	390	386	1.08	671	661	1.54
-0.4	438	433	1.13	671	661	1.54
-0.3	500	494	1.28	671	661	1.54
-0.2	579	571	1.48	671	661	1.54
-0.1	674	663	1.67	671	661	1.54
0	777	765	1.47	671	661	1.54

Table 4.C (cont) Comparison of critical moment

(1) bracing height (b/h)	(2) Present Study symmetric mode (kNm)	(3) Abaqus symmetric mode (kNm)	((2)-(3))/(2) (%)	(4) Present Study anti-symmetric mode (kNm)	(5) Abaqus anti-symmetric mode (kNm)	((4)-(5))/(4) (%)
0.1	873	854	2.21	671	661	1.54
0.2	949	926	2.45	671	661	1.54
0.3	1004	978	2.60	671	661	1.54
0.4	1041	1013	2.67	671	661	1.54
0.5	1066	1037	2.75	671	661	1.54
point load, $a = 0$, $10^4 kN/m$						
-0.5	407	402	1.21	671	661	1.54
-0.4	466	460	1.28	671	661	1.54
-0.3	544	536	1.51	671	661	1.54
-0.2	643	632	1.81	671	661	1.54
-0.1	756	740	2.12	671	661	1.54
0	860	843	2.00	671	661	1.54
0.1	941	916	2.63	671	661	1.54
0.2	996	969	2.77	671	661	1.54
0.3	1034	1005	2.82	671	661	1.54
0.4	1060	1030	2.84	671	661	1.54
0.5	1078	1047	2.87	671	661	1.54
point load, $a = 0.5h$, $10kN/m$						
-0.5	244	241	1.27	671	661	1.54
-0.4	255	252	1.31	671	661	1.54
-0.3	268	265	1.37	671	661	1.54
-0.2	284	280	1.43	671	661	1.54
-0.1	302	298	1.48	671	661	1.54
0	323	318	1.53	671	661	1.54
0.1	347	341	1.54	671	661	1.54
0.2	374	368	1.52	671	661	1.54
0.3	404	398	1.44	671	661	1.54
0.4	438	432	1.29	671	661	1.54
0.5	474	470	0.80	671	661	1.54

Table 4.C (cont) Comparison of critical moment

(1) bracing height (b/h)	(2) Present Study symmetric mode (kNm)	(3) Abaqus symmetric mode (kNm)	((2)-(3))/(2) (%)	(4) Present Study anti-symmetric mode (kNm)	(5) Abaqus anti-symmetric mode (kNm)	((4)-(5))/(4) (%)
point load, $a = 0.5h$,$10^2 kN/m$						
-0.5	244	241	1.27	671	661	1.54
-0.4	255	252	1.31	671	661	1.54
-0.3	268	265	1.37	671	661	1.54
-0.2	284	280	1.43	671	661	1.54
-0.1	302	298	1.48	671	661	1.54
0	323	318	1.53	671	661	1.54
0.1	347	341	1.54	671	661	1.54
0.2	374	368	1.52	671	661	1.54
0.3	404	398	1.44	671	661	1.54
0.4	438	432	1.29	671	661	1.54
0.5	474	470	0.80	671	661	1.54
point load, $a = 0.5h$,$10^3 kN/m$						
-0.5	270	266	1.52	671	661	1.54
-0.4	292	288	1.62	671	661	1.54
-0.3	322	316	1.81	671	661	1.54
-0.2	360	353	2.04	671	661	1.54
-0.1	409	399	2.35	671	661	1.54
0	472	459	2.71	671	661	1.54
0.1	549	532	3.08	671	661	1.54
0.2	639	618	3.36	671	661	1.54
0.3	734	708	3.45	671	661	1.54
0.4	821	794	3.33	671	661	1.54
0.5	892	869	2.63	671	661	1.54
point load, $a = 0.5h$, $10^4 kN/m$						
-0.5	275	270	1.58	671	661	1.54
-0.4	300	295	1.71	671	661	1.54
-0.3	334	327	1.93	671	661	1.54
-0.2	378	370	2.25	671	661	1.54
-0.1	438	426	2.67	671	661	1.54
0	515	498	3.19	671	661	1.54

Table 4.C (cont) Comparison of critical moment

(1) bracing height (b/h)	(2) Present Study symmetric mode (kNm)	(3) Abaqus symmetric mode (kNm)	((2)-(3))/(2) (%)	(4) Present Study anti-symmetric mode (kNm)	(5) Abaqus anti-symmetric mode (kNm)	((4)-(5))/(4) (%)
0.1	610	587	3.71	671	661	1.54
0.2	713	684	4.00	671	661	1.54
0.3	807	775	3.95	671	661	1.54
0.4	883	850	3.69	671	661	1.54
0.5	938	909	3.02	671	661	1.54
uniformly distributed load, $a = 0$,$10kN/m$						
-0.5	215	213	0.62	493	486	1.39
-0.4	217	216	0.63	493	486	1.39
-0.3	219	218	0.64	493	486	1.39
-0.2	222	220	0.64	493	486	1.39
-0.1	224	223	0.64	493	486	1.39
0	227	226	0.64	493	486	1.39
0.1	230	229	0.63	493	486	1.39
0.2	233	232	0.62	493	486	1.39
0.3	236	235	0.60	493	486	1.39
0.4	240	239	0.58	493	486	1.39
0.5	244	242	0.55	493	486	1.39
uniformly distributed load, $a = 0$, $10^2 kN/m$						
-0.5	271	269	0.67	493	486	1.39
-0.4	287	285	0.66	493	486	1.39
-0.3	305	303	0.67	493	486	1.39
-0.2	326	324	0.68	493	486	1.39
-0.1	350	347	0.69	493	486	1.39
0	377	374	0.68	493	486	1.39
0.1	406	403	0.66	493	486	1.39
0.2	438	436	0.63	493	486	1.39
0.3	473	470	0.59	493	486	1.39
0.4	509	506	0.59	493	486	1.39
0.5	547	543	0.76	493	486	1.39

Table 4.C (cont) Comparison of critical moment

(1) bracing height (b/h)	(2) Present Study symmetric mode (kNm)	(3) Abaqus symmetric mode (kNm)	((2)-(3))/(2) (%)	(4) Present Study anti-symmetric mode (kNm)	(5) Abaqus anti-symmetric mode (kNm)	((4)-(5))/(4) (%)
uniformly distributed load, $a=0, 10^3 kN/m$						
-0.5	345	342	0.99	493	486	1.39
-0.4	396	392	0.93	493	486	1.39
-0.3	466	461	1.01	493	486	1.39
-0.2	561	554	1.15	493	486	1.39
-0.1	680	670	1.44	493	486	1.39
0	783	766	2.14	493	486	1.39
0.1	819	797	2.62	493	486	1.39
0.2	827	805	2.75	493	486	1.39
0.3	830	806	2.81	493	486	1.39
0.4	830	806	2.86	493	486	1.39
0.5	829	804	2.91	493	486	1.39
uniformly distributed load, $a=0, 10^4 kN/m$						
-0.5	366	362	1.12	493	486	1.39
-0.4	432	427	1.07	493	486	1.39
-0.3	529	523	1.24	493	486	1.39
-0.2	663	652	1.62	493	486	1.39
-0.1	772	755	2.27	493	486	1.39
0	811	790	2.61	493	486	1.39
0.1	824	801	2.73	493	486	1.39
0.2	828	805	2.78	493	486	1.39
0.3	830	806	2.82	493	486	1.39
0.4	830	806	2.85	493	486	1.39
0.5	829	805	2.89	493	486	1.39

Table 4.C (cont) Comparison of critical moment

(1) bracing height (b/h)	(2) Present Study symmetric mode (kNm)	(3) Abaqus symmetric mode (kNm)	((2)-(3))/(2) (%)	(4) Present Study anti-symmetric mode (kNm)	(5) Abaqus anti-symmetric mode (kNm)	((4)-(5))/(4) (%)
uniformly distributed load, $a = 0.5h$, $10kN/m$						
-0.5	187	186	0.867	460	453	1.62
-0.4	189	187	0.872	460	453	1.62
-0.3	191	189	0.877	460	453	1.62
-0.2	193	191	0.880	460	453	1.62
-0.1	195	193	0.880	460	453	1.62
0	197	196	0.878	460	453	1.62
0.1	200	198	0.871	460	453	1.62
0.2	203	201	0.859	460	453	1.62
0.3	206	204	0.842	460	453	1.62
0.4	209	207	0.818	460	453	1.62
0.5	212	210	0.793	460	453	1.62
uniformly distributed load, $a = 0.5h$, $10^2 kN/m$						
-0.5	221	219	0.909	460	453	1.62
-0.4	232	230	0.909	460	453	1.62
-0.3	246	243	0.924	460	453	1.62
-0.2	261	259	0.933	460	453	1.62
-0.1	279	276	0.940	460	453	1.62
0	299	296	0.932	460	453	1.62
0.1	322	319	0.916	460	453	1.62
0.2	348	345	0.886	460	453	1.62
0.3	376	373	0.854	460	453	1.62
0.4	406	403	0.847	460	453	1.62
0.5	438	434	0.985	460	453	1.62

Table 4.C (cont) Comparison of critical moment

(1) bracing height (b/h)	(2) Present Study symmetric mode (kNm)	(3) Abaqus symmetric mode (kNm)	((2)-(3))/(2) (%)	(4) Present Study anti-symmetric mode (kNm)	(5) Abaqus anti-symmetric mode (kNm)	((4)-(5))/(4) (%)
uniformly distributed load, $a = 0.5h$, $10^3 kN/m$						
-0.5	256	253	1.09	460	453	1.62
-0.4	283	280	1.08	460	453	1.62
-0.3	320	316	1.13	460	453	1.62
-0.2	369	365	1.19	460	453	1.62
-0.1	438	432	1.28	460	453	1.62
0	533	526	1.39	460	453	1.62
0.1	663	652	1.56	460	453	1.62
0.2	791	766	3.15	460	453	1.62
0.3	788	763	3.19	460	453	1.62
0.4	786	760	3.24	460	453	1.62
0.5	783	757	3.31	460	453	1.62
uniformly distributed load, $a = 0.5h$, $10^4 kN/m$						
-0.5	270	261	3.16	466	453	2.71
-0.4	303	293	3.19	466	453	2.71
-0.3	350	339	3.29	466	453	2.71
-0.2	420	405	3.41	466	453	2.71
-0.1	526	508	3.55	466	453	2.71
0	693	668	3.63	466	453	2.71
0.1	795	765	3.81	466	453	2.71
0.2	799	767	4.00	466	453	2.71
0.3	798	765	4.07	466	453	2.71
0.4	795	763	4.13	466	453	2.71
0.5	793	760	4.20	466	453	2.71

Appendix 4.D Effect of width to height ratio and shear elastic modulus on threshold bracing stiffness

The present appendix provides the results of 88 runs based on the model developed in the present study to illustrate that the section aspect ratio w/h and shear to elastic moduli ratios have a negligible effect on the normalized stiffness kl^3/EI_{yy} . This finding has been used in proposing the simplified form for the critical threshold bracing stiffness equation in Eq. (6.28)

Table 4.D Sensitivity of aspect ratio to normalized threshold bracing stiffness

run	Geometric parameters					Elastic parameters		Dimensionless parameters		Threshold stiffness	
	Point load case										
	w (m)	h (m)	L (m)	a (m)	b (m)	E (10^4MPa)	G (10^2MPa)	w/h	G/E	k (10^2kN/m)	Normalized k/(EIyy/L^3)
1	0.13	0.95	10.0	0.000	0.000	1.03	6.438	0.137	0.0625	9.77	545.19
2	0.13	0.874	9.2	0.000	0.000	1.03	6.438	0.149	0.0625	11.55	545.72
3	0.13	0.798	8.4	0.000	0.000	1.03	6.438	0.163	0.0625	13.87	546.37
4	0.13	0.722	7.6	0.000	0.000	1.03	6.438	0.180	0.0625	16.97	547.16
5	0.13	0.646	6.8	0.000	0.000	1.03	6.438	0.201	0.0625	21.24	548.17
6	0.13	0.57	6.0	0.000	0.000	1.03	6.438	0.228	0.0625	27.34	549.50
7	0.13	0.532	5.6	0.000	0.000	1.03	6.438	0.244	0.0625	31.44	550.33
8	0.13	0.456	4.8	0.000	0.000	1.03	6.438	0.285	0.0625	42.96	552.49
9	0.13	0.38	4.0	0.000	0.000	1.03	6.438	0.342	0.0625	62.23	555.76
10	0.13	0.304	3.2	0.000	0.000	1.03	6.438	0.428	0.0625	98.19	561.23
11	0.13	0.228	2.4	0.000	0.000	1.03	6.438	0.570	0.0625	177.93	572.08
12	0.13	0.95	15	0.000	0.000	1.03	6.438	0.137	0.0625	2.70	509.37
13	0.13	0.874	13.8	0.000	0.000	1.03	6.438	0.149	0.0625	3.20	509.61
14	0.13	0.798	12.6	0.000	0.000	1.03	6.438	0.163	0.0625	3.84	509.90
15	0.13	0.722	11.4	0.000	0.000	1.03	6.438	0.180	0.0625	4.69	510.26
16	0.13	0.646	10.2	0.000	0.000	1.03	6.438	0.201	0.0625	5.86	510.72
17	0.13	0.57	9.0	0.000	0.000	1.03	6.438	0.228	0.0625	7.54	511.31

Table 4.D (cont) sensitivity of aspect ratio to normalized threshold bracing stiffness

run	Geometric parameters					Elastic parameters		Dimensionless parameters		results	
	Point load case										
	w (m)	h (m)	L (m)	a (m)	b (m)	E (10^4MPa)	G (10^2MPa)	w/h	G/E	k (10^2kN/m)	k/(EI/L^3)
14	0.13	0.798	12.6	0.000	0.000	1.03	6.438	0.163	0.0625	3.84	509.90
15	0.13	0.722	11.4	0.000	0.000	1.03	6.438	0.180	0.0625	4.69	510.26
16	0.13	0.646	10.2	0.000	0.000	1.03	6.438	0.201	0.0625	5.86	510.72
17	0.13	0.57	9.0	0.000	0.000	1.03	6.438	0.228	0.0625	7.54	511.31
18	0.13	0.532	8.4	0.000	0.000	1.03	6.438	0.244	0.0625	8.66	511.69
19	0.13	0.456	7.2	0.000	0.000	1.03	6.438	0.285	0.0625	11.81	512.66
20	0.13	0.38	6.0	0.000	0.000	1.03	6.438	0.342	0.0625	17.06	514.13
21	0.13	0.304	4.8	0.000	0.000	1.03	6.438	0.428	0.0625	26.78	516.59
22	0.13	0.228	3.6	0.000	0.000	1.03	6.438	0.570	0.0625	48.05	521.47
23	0.13	0.95	10.0	0.000	0.000	1.03	10.300	0.137	0.1000	9.33	521.07
24	0.13	0.95	10.0	0.000	0.000	1.03	9.364	0.137	0.0909	9.41	525.11
25	0.13	0.95	10.0	0.000	0.000	1.03	8.583	0.137	0.0833	9.48	529.13
26	0.13	0.95	10.0	0.000	0.000	1.03	7.923	0.137	0.0769	9.55	533.15
27	0.13	0.95	10.0	0.000	0.000	1.03	7.357	0.137	0.0714	9.62	537.17
28	0.13	0.95	10.0	0.000	0.000	1.03	6.867	0.137	0.0667	9.70	541.18
29	0.13	0.95	10.0	0.000	0.000	1.03	6.438	0.137	0.0625	9.77	545.19
30	0.13	0.95	10.0	0.000	0.000	1.03	6.059	0.137	0.0588	9.84	549.20

Table 4.D (cont) sensitivity of aspect ratio to normalized threshold bracing stiffness

run	Geometric parameters					Elastic parameters		Dimensionless parameters		results	
	Point load case										
	w (m)	h (m)	L (m)	a (m)	b (m)	E (10^4MPa)	G (10^2MPa)	w/h	G/E	k (10^2kN/m)	k/(EI/L^3)
31	0.13	0.95	10.0	0.000	0.000	1.03	5.722	0.137	0.0556	9.91	553.20
32	0.13	0.95	10.0	0.000	0.000	1.03	5.421	0.137	0.0526	9.98	557.21
33	0.13	0.95	10.0	0.000	0.000	1.03	5.150	0.137	0.0500	10.05	561.21
34	0.13	0.95	15.0	0.000	0.000	1.03	10.300	0.137	0.1000	2.65	498.50
35	0.13	0.95	15.0	0.000	0.000	1.03	9.364	0.137	0.0909	2.66	500.32
36	0.13	0.95	15.0	0.000	0.000	1.03	8.583	0.137	0.0833	2.67	502.13
37	0.13	0.95	15.0	0.000	0.000	1.03	7.923	0.137	0.0769	2.67	503.95
38	0.13	0.95	15.0	0.000	0.000	1.03	7.357	0.137	0.0714	2.68	505.76
39	0.13	0.95	15.0	0.000	0.000	1.03	6.867	0.137	0.0667	2.69	507.57
40	0.13	0.95	15.0	0.000	0.000	1.03	6.438	0.137	0.0625	2.70	509.37
41	0.13	0.95	15.0	0.000	0.000	1.03	6.059	0.137	0.0588	2.71	511.18
42	0.13	0.95	15.0	0.000	0.000	1.03	5.722	0.137	0.0556	2.72	512.98
43	0.13	0.95	15.0	0.000	0.000	1.03	5.421	0.137	0.0526	2.73	514.78
44	0.13	0.95	15.0	0.000	0.000	1.03	5.150	0.137	0.0500	2.74	516.58
Uniformly distributed load											
45	0.13	0.95	10.0	0.000	0.000	1.03	6.438	0.137	0.0625	4.682	261.37
46	0.13	0.874	9.2	0.000	0.000	1.03	6.438	0.149	0.0625	5.537	261.62
47	0.13	0.798	8.4	0.000	0.000	1.03	6.438	0.163	0.0625	6.650	261.91

Table 4.D (cont) sensitivity of aspect ratio to normalized threshold bracing stiffness

run	Geometric parameters					Elastic parameters		Dimensionless parameters		results	
	Point load case										
	w (m)	h (m)	L (m)	a (m)	b (m)	E (10^4MPa)	G (10^2MPa)	w/h	G/E	k (10^2kN/m)	k/(EI/L^3)
48	0.13	0.722	7.6	0.000	0.000	1.03	6.438	0.180	0.0625	8.135	262.28
49	0.13	0.646	6.8	0.000	0.000	1.03	6.438	0.201	0.0625	10.179	262.74
50	0.13	0.57	6.0	0.000	0.000	1.03	6.438	0.228	0.0625	13.105	263.35
51	0.13	0.532	5.6	0.000	0.000	1.03	6.438	0.244	0.0625	15.066	263.73
52	0.13	0.456	4.8	0.000	0.000	1.03	6.438	0.285	0.0625	20.583	264.72
53	0.13	0.38	4.0	0.000	0.000	1.03	6.438	0.342	0.0625	29.806	266.20
54	0.13	0.304	3.2	0.000	0.000	1.03	6.438	0.428	0.0625	47.005	268.68
55	0.13	0.228	2.4	0.000	0.000	1.03	6.438	0.570	0.0625	85.076	273.54
56	0.13	0.95	15.0	0.000	0.000	1.03	6.438	0.137	0.0625	1.298	244.46
57	0.13	0.874	13.8	0.000	0.000	1.03	6.438	0.149	0.0625	1.534	244.58
58	0.13	0.798	12.6	0.000	0.000	1.03	6.438	0.163	0.0625	1.841	244.72
59	0.13	0.722	11.4	0.000	0.000	1.03	6.438	0.180	0.0625	2.251	244.89
60	0.13	0.646	10.2	0.000	0.000	1.03	6.438	0.201	0.0625	2.814	245.11
61	0.13	0.57	9.0	0.000	0.000	1.03	6.438	0.228	0.0625	3.618	245.40
62	0.13	0.532	8.4	0.000	0.000	1.03	6.438	0.244	0.0625	4.157	245.58
63	0.13	0.456	7.2	0.000	0.000	1.03	6.438	0.285	0.0625	5.669	246.05
64	0.13	0.38	6.0	0.000	0.000	1.03	6.438	0.342	0.0625	8.186	246.76
65	0.13	0.304	4.8	0.000	0.000	1.03	6.438	0.428	0.0625	12.852	247.94
66	0.13	0.228	3.6	0.000	0.000	1.03	6.438	0.570	0.0625	23.063	250.27
67	0.13	0.95	10.0	0.000	0.000	1.03	10.300	0.137	0.1000	4.480	250.08

Table 4.D (cont) sensitivity of aspect ratio to normalized threshold bracing stiffness

run	Geometric parameters					Elastic parameters		Dimensionless parameters		results	
	Point load case										
	w (m)	h (m)	L (m)	a (m)	b (m)	E (10^4MPa)	G (10^2MPa)	w/h	G/E	k (10^2kN/m)	k/(EI/L^3)
68	0.13	0.95	10.0	0.000	0.000	1.03	9.364	0.137	0.0909	4.514	252.00
69	0.13	0.95	10.0	0.000	0.000	1.03	8.583	0.137	0.0833	4.549	253.90
70	0.13	0.95	10.0	0.000	0.000	1.03	7.923	0.137	0.0769	4.582	255.79
71	0.13	0.95	10.0	0.000	0.000	1.03	7.357	0.137	0.0714	4.616	257.66
72	0.13	0.95	10.0	0.000	0.000	1.03	6.867	0.137	0.0667	4.649	259.52
73	0.13	0.95	10.0	0.000	0.000	1.03	6.438	0.137	0.0625	4.682	261.37
74	0.13	0.95	10.0	0.000	0.000	1.03	6.059	0.137	0.0588	4.715	263.21
75	0.13	0.95	10.0	0.000	0.000	1.03	5.722	0.137	0.0556	4.748	265.04
76	0.13	0.95	10.0	0.000	0.000	1.03	5.421	0.137	0.0526	4.781	266.86
77	0.13	0.95	10.0	0.000	0.000	1.03	5.150	0.137	0.0500	4.813	268.67
78	0.13	0.95	15.0	0.000	0.000	1.03	10.300	0.137	0.1000	1.269	239.15
79	0.13	0.95	15.0	0.000	0.000	1.03	9.364	0.137	0.0909	1.274	240.04
80	0.13	0.95	15.0	0.000	0.000	1.03	8.583	0.137	0.0833	1.279	240.94
81	0.13	0.95	15.0	0.000	0.000	1.03	7.923	0.137	0.0769	1.284	241.82
82	0.13	0.95	15.0	0.000	0.000	1.03	7.357	0.137	0.0714	1.288	242.71
83	0.13	0.95	15.0	0.000	0.000	1.03	6.867	0.137	0.0667	1.293	243.59
84	0.13	0.95	15.0	0.000	0.000	1.03	6.438	0.137	0.0625	1.298	244.46
85	0.13	0.95	15.0	0.000	0.000	1.03	6.059	0.137	0.0588	1.302	245.34
86	0.13	0.95	15.0	0.000	0.000	1.03	5.722	0.137	0.0556	1.307	246.21
87	0.13	0.95	15.0	0.000	0.000	1.03	5.421	0.137	0.0526	1.311	247.07
88	0.13	0.95	15.0	0.000	0.000	1.03	5.150	0.137	0.0500	1.316	247.94

Appendix 4.E Results for threshold bracing stiffness

Based on the present energy formulation, the threshold bracing stiffness can be obtained for simply supported beams with different geometric and elastic properties.

Table 4.E.1-17 presents 346 results obtained from present energy formulation through varying the dimensionless parameters of L/h and a/h to assist the regression analysis of design expressions described in section titled "Simplified expressions for threshold bracing stiffness" for point load and uniformly distributed load, respectively.

Table 4.E.1 mid-span point loading

run	Geometric parameters						Elastic parameters		Dimensionless parameters				results	
	Point load case													
	w (m)	h (m)	M_{cr} (kNm)	L (m)	a (m)	b (m)	E (10^4MPa)	G (10^2MPa)	L/h	a/h	G/E	b/h	k (10^2kN/m)	log(k/(EI/L^3))
1	0.13	0.95	486.99	20.0	0.000	0.000	1.03	6.438	21.053	0.0	0.0625	0.0	1.112	2.696
2	0.13	0.95	513.78	19.0	0.000	0.000	1.03	6.438	20.000	0.0	0.0625	0.0	1.302	2.698
3	0.13	0.95	543.76	18.0	0.000	0.000	1.03	6.438	18.947	0.0	0.0625	0.0	1.537	2.699
4	0.13	0.95	577.52	17.0	0.000	0.000	1.03	6.438	17.895	0.0	0.0625	0.0	1.834	2.702
5	0.13	0.95	615.84	16.0	0.000	0.000	1.03	6.438	16.842	0.0	0.0625	0.0	2.213	2.704
6	0.13	0.95	659.72	15.0	0.000	0.000	1.03	6.438	15.789	0.0	0.0625	0.0	2.704	2.707
7	0.13	0.95	710.49	14.0	0.000	0.000	1.03	6.438	14.737	0.0	0.0625	0.0	3.353	2.711
8	0.13	0.95	769.94	13.0	0.000	0.000	1.03	6.438	13.684	0.0	0.0625	0.0	4.231	2.715
9	0.13	0.95	840.53	12.0	0.000	0.000	1.03	6.438	12.632	0.0	0.0625	0.0	5.449	2.721
10	0.13	0.95	925.74	11.0	0.000	0.000	1.03	6.438	11.579	0.0	0.0625	0.0	7.188	2.728
11	0.13	0.95	1030.73	10.0	0.000	0.000	1.03	6.438	10.526	0.0	0.0625	0.0	9.767	2.737
12	0.13	0.95	1163.35	9.0	0.000	0.000	1.03	6.438	9.474	0.0	0.063	0.0	13.767	2.748
13	0.13	0.95	1336.23	8.0	0.000	0.000	1.03	6.438	8.421	0.0	0.063	0.0	20.336	2.764
14	0.13	0.95	1570.95	7.0	0.000	0.000	1.03	6.438	7.368	0.0	0.063	0.0	31.954	2.787
15	0.13	0.95	1907.53	6.0	0.000	0.000	1.03	6.438	6.316	0.0	0.063	0.0	54.663	2.819
16	0.13	0.95	2428.12	5.0	0.000	0.000	1.03	6.438	5.263	0.0	0.063	0.0	105.763	2.868
17	0.13	0.95	486.99	20.0	0.095	0.095	1.03	6.438	21.053	0.1	0.0625	0.1	1.021	2.659
18	0.13	0.95	513.78	19.0	0.095	0.095	1.03	6.438	20.000	0.1	0.0625	0.1	1.190	2.658
19	0.13	0.95	543.76	18.0	0.095	0.095	1.03	6.438	18.947	0.1	0.0625	0.1	1.398	2.658
20	0.13	0.95	577.52	17.0	0.095	0.095	1.03	6.438	17.895	0.1	0.0625	0.1	1.657	2.658

Table 4.E.1 (cont) mid-span point loading

run	Geometric parameters						Elastic parameters		Dimensionless parameters				results	
	Point load case													
	w (m)	h (m)	M_{cr} (kNm)	L (m)	a (m)	b (m)	E (10^4MPa)	G (10^2MPa)	L/h	a/h	G/E	b/h	k (10^2kN/m)	log(k/(EI/L^3))
21	0.13	0.95	615.84	16.0	0.095	0.095	1.03	6.438	16.842	0.1	0.0625	0.1	1.986	2.657
22	0.13	0.95	659.72	15.0	0.095	0.095	1.03	6.438	15.789	0.1	0.0625	0.1	2.409	2.657
23	0.13	0.95	710.49	14.0	0.095	0.095	1.03	6.438	14.737	0.1	0.0625	0.1	2.963	2.657
24	0.13	0.95	769.94	13.0	0.095	0.095	1.03	6.438	13.684	0.1	0.0625	0.1	3.701	2.657
25	0.13	0.95	840.53	12.0	0.095	0.095	1.03	6.438	12.632	0.1	0.0625	0.1	4.709	2.657
26	0.13	0.95	925.74	11.0	0.095	0.095	1.03	6.438	11.579	0.1	0.0625	0.1	6.125	2.658
27	0.13	0.95	1030.73	10.0	0.095	0.095	1.03	6.438	10.526	0.1	0.0625	0.1	8.180	2.660
28	0.13	0.95	1163.35	9.0	0.095	0.095	1.03	6.438	9.474	0.1	0.063	0.1	11.284	2.662
29	0.13	0.95	1336.23	8.0	0.095	0.095	1.03	6.438	8.421	0.1	0.063	0.1	16.215	2.666
30	0.13	0.95	1570.95	7.0	0.095	0.095	1.03	6.438	7.368	0.1	0.063	0.1	24.567	2.672
31	0.13	0.95	1907.53	6.0	0.095	0.095	1.03	6.438	6.316	0.1	0.063	0.1	39.960	2.683
32	0.13	0.95	2428.12	5.0	0.095	0.095	1.03	6.438	5.263	0.1	0.063	0.1	71.801	2.700
33	0.13	0.95	486.99	20.0	0.190	0.190	1.03	6.438	21.053	0.2	0.0625	0.2	0.943	2.625
34	0.13	0.95	513.78	19.0	0.190	0.190	1.03	6.438	20.000	0.2	0.0625	0.2	1.095	2.622
35	0.13	0.95	543.76	18.0	0.190	0.190	1.03	6.438	18.947	0.2	0.0625	0.2	1.281	2.620
36	0.13	0.95	577.52	17.0	0.190	0.190	1.03	6.438	17.895	0.2	0.0625	0.2	1.512	2.618
37	0.13	0.95	615.84	16.0	0.190	0.190	1.03	6.438	16.842	0.2	0.0625	0.2	1.802	2.615
38	0.13	0.95	659.72	15.0	0.190	0.190	1.03	6.438	15.789	0.2	0.0625	0.2	2.172	2.612
39	0.13	0.95	710.49	14.0	0.190	0.190	1.03	6.438	14.737	0.2	0.0625	0.2	2.652	2.609
40	0.13	0.95	769.94	13.0	0.190	0.190	1.03	6.438	13.684	0.2	0.0625	0.2	3.287	2.605

Table 4.E.1 (cont) mid-span point loading

run	Geometric parameters						Elastic parameters		Dimensionless parameters				results	
	Point load case													
	w (m)	h (m)	M_{cr} (kNm)	L (m)	a (m)	b (m)	E (10^4MPa)	G (10^2MPa)	L/h	a/h	G/E	b/h	k (10^2kN/m)	log(k/(EI/L^3))
41	0.13	0.95	840.53	12.0	0.190	0.190	1.03	6.438	12.632	0.2	0.0625	0.2	4.144	2.602
42	0.13	0.95	925.74	11.0	0.190	0.190	1.03	6.438	11.579	0.2	0.0625	0.2	5.333	2.598
43	0.13	0.95	1030.73	10.0	0.190	0.190	1.03	6.438	10.526	0.2	0.0625	0.2	7.031	2.594
44	0.13	0.95	1163.35	9.0	0.190	0.190	1.03	6.438	9.474	0.2	0.063	0.2	9.552	2.590
45	0.13	0.95	1336.23	8.0	0.190	0.190	1.03	6.438	8.421	0.2	0.063	0.2	13.471	2.585
46	0.13	0.95	1570.95	7.0	0.190	0.190	1.03	6.438	7.368	0.2	0.063	0.2	19.933	2.582
47	0.13	0.95	1907.53	6.0	0.190	0.190	1.03	6.438	6.316	0.2	0.063	0.2	31.451	2.579
48	0.13	0.95	2428.12	5.0	0.190	0.190	1.03	6.438	5.263	0.2	0.063	0.2	54.271	2.578
49	0.13	0.95	486.99	20.0	0.285	0.285	1.03	6.438	21.053	0.3	0.0625	0.3	0.877	2.593
50	0.13	0.95	513.78	19.0	0.285	0.285	1.03	6.438	20.000	0.3	0.0625	0.3	1.014	2.589
51	0.13	0.95	543.76	18.0	0.285	0.285	1.03	6.438	18.947	0.3	0.0625	0.3	1.182	2.585
52	0.13	0.95	577.52	17.0	0.285	0.285	1.03	6.438	17.895	0.3	0.0625	0.3	1.389	2.581

Table 4.E.1 (cont) mid-span point loading

run	Geometric parameters						Elastic parameters		Dimensionless parameters				results	
	Point load case													
	w (m)	h (m)	M_{cr} (kNm)	L (m)	a (m)	b (m)	E (10^4MPa)	G (10^2MPa)	L/h	a/h	G/E	b/h	k (10^2kN/m)	log(k/(EI/L^3))
52	0.13	0.95	577.52	17.0	0.285	0.285	1.03	6.438	17.895	0.3	0.0625	0.3	1.389	2.581
53	0.13	0.95	615.84	16.0	0.285	0.285	1.03	6.438	16.842	0.3	0.0625	0.3	1.648	2.576
54	0.13	0.95	659.72	15.0	0.285	0.285	1.03	6.438	15.789	0.3	0.0625	0.3	1.977	2.571
55	0.13	0.95	710.49	14.0	0.285	0.285	1.03	6.438	14.737	0.3	0.0625	0.3	2.400	2.565
56	0.13	0.95	769.94	13.0	0.285	0.285	1.03	6.438	13.684	0.3	0.0625	0.3	2.955	2.559
57	0.13	0.95	840.53	12.0	0.285	0.285	1.03	6.438	12.632	0.3	0.0625	0.3	3.699	2.552
58	0.13	0.95	925.74	11.0	0.285	0.285	1.03	6.438	11.579	0.3	0.0625	0.3	4.720	2.545
59	0.13	0.95	1030.73	10.0	0.285	0.285	1.03	6.438	10.526	0.3	0.0625	0.3	6.162	2.537
60	0.13	0.95	1163.35	9.0	0.285	0.285	1.03	6.438	9.474	0.3	0.063	0.3	8.276	2.527
61	0.13	0.95	1336.23	8.0	0.285	0.285	1.03	6.438	8.421	0.3	0.063	0.3	11.512	2.517
62	0.13	0.95	1570.95	7.0	0.285	0.285	1.03	6.438	7.368	0.3	0.063	0.3	16.755	2.506
63	0.13	0.95	1907.53	6.0	0.285	0.285	1.03	6.438	6.316	0.3	0.063	0.3	25.905	2.495
64	0.13	0.95	2428.12	5.0	0.285	0.285	1.03	6.438	5.263	0.3	0.063	0.3	43.576	2.483
65	0.13	0.95	486.99	20.0	0.380	0.380	1.03	6.438	21.053	0.4	0.0625	0.4	0.819	2.563
66	0.13	0.95	513.78	19.0	0.380	0.380	1.03	6.438	20.000	0.4	0.0625	0.4	0.944	2.558
67	0.13	0.95	543.76	18.0	0.380	0.380	1.03	6.438	18.947	0.4	0.0625	0.4	1.097	2.553
68	0.13	0.95	577.52	17.0	0.380	0.380	1.03	6.438	17.895	0.4	0.0625	0.4	1.284	2.547
69	0.13	0.95	615.84	16.0	0.380	0.380	1.03	6.438	16.842	0.4	0.0625	0.4	1.518	2.540
70	0.13	0.95	659.72	15.0	0.380	0.380	1.03	6.438	15.789	0.4	0.0625	0.4	1.813	2.534
71	0.13	0.95	710.49	14.0	0.380	0.380	1.03	6.438	14.737	0.4	0.0625	0.4	2.191	2.526
72	0.13	0.95	769.94	13.0	0.380	0.380	1.03	6.438	13.684	0.4	0.0625	0.4	2.684	2.517
73	0.13	0.95	840.53	12.0	0.380	0.380	1.03	6.438	12.632	0.4	0.0625	0.4	3.339	2.508

Table 4.E.1 (cont) mid-span point loading

run	Geometric parameters						Elastic parameters		Dimensionless parameters				results	
	Point load case													
	w (m)	h (m)	M_{cr} (kNm)	L (m)	a (m)	b (m)	E (10^4MPa)	G (10^2MPa)	L/h	a/h	G/E	b/h	k (10^2kN/m)	log(k/(EI/L^3))
74	0.13	0.95	925.74	11.0	0.380	0.380	1.03	6.438	11.579	0.4	0.0625	0.4	4.231	2.497
75	0.13	0.95	1030.73	10.0	0.380	0.380	1.03	6.438	10.526	0.4	0.0625	0.4	5.482	2.486
76	0.13	0.95	1163.35	9.0	0.380	0.380	1.03	6.438	9.474	0.4	0.063	0.4	7.296	2.473
77	0.13	0.95	1336.23	8.0	0.380	0.380	1.03	6.438	8.421	0.4	0.063	0.4	10.045	2.458
78	0.13	0.95	1570.95	7.0	0.380	0.380	1.03	6.438	7.368	0.4	0.063	0.4	14.442	2.442
79	0.13	0.95	1907.53	6.0	0.380	0.380	1.03	6.438	6.316	0.4	0.063	0.4	22.005	2.424
80	0.13	0.95	2428.12	5.0	0.380	0.380	1.03	6.438	5.263	0.4	0.063	0.4	36.374	2.404
81	0.13	0.95	486.99	20.0	0.475	0.475	1.03	6.438	21.053	0.5	0.0625	0.5	0.768	2.535
82	0.13	0.95	513.78	19.0	0.475	0.475	1.03	6.438	20.000	0.5	0.0625	0.5	0.883	2.529
83	0.13	0.95	543.76	18.0	0.475	0.475	1.03	6.438	18.947	0.5	0.0625	0.5	1.023	2.522
84	0.13	0.95	577.52	17.0	0.475	0.475	1.03	6.438	17.895	0.5	0.0625	0.5	1.194	2.515
85	0.13	0.95	615.84	16.0	0.475	0.475	1.03	6.438	16.842	0.5	0.0625	0.5	1.407	2.507
86	0.13	0.95	659.72	15.0	0.475	0.475	1.03	6.438	15.789	0.5	0.0625	0.5	1.674	2.499
87	0.13	0.95	710.49	14.0	0.475	0.475	1.03	6.438	14.737	0.5	0.0625	0.5	2.015	2.489
88	0.13	0.95	769.94	13.0	0.475	0.475	1.03	6.438	13.684	0.5	0.0625	0.5	2.457	2.479
89	0.13	0.95	840.53	12.0	0.475	0.475	1.03	6.438	12.632	0.5	0.0625	0.5	3.041	2.467
90	0.13	0.95	925.74	11.0	0.475	0.475	1.03	6.438	11.579	0.5	0.0625	0.5	3.833	2.454
91	0.13	0.95	1030.73	10.0	0.475	0.475	1.03	6.438	10.526	0.5	0.0625	0.5	4.935	2.440
92	0.13	0.95	1163.35	9.0	0.475	0.475	1.03	6.438	9.474	0.5	0.063	0.5	6.521	2.424
93	0.13	0.95	1336.23	8.0	0.475	0.475	1.03	6.438	8.421	0.5	0.063	0.5	8.904	2.406

Table 4.E.1 (cont) mid-span point loading

run	Geometric parameters						Elastic parameters		Dimensionless parameters				results	
	Point load case													
	w (m)	h (m)	M_{cr} (kNm)	L (m)	a (m)	b (m)	E (10^4MPa)	G (10^2MPa)	L/h	a/h	G/E	b/h	k (10^2kN/m)	log(k/(EI/L^3))
94	0.13	0.95	1570.95	7.0	0.475	0.475	1.03	6.438	7.368	0.5	0.063	0.5	12.682	2.385
95	0.13	0.95	1907.53	6.0	0.475	0.475	1.03	6.438	6.316	0.5	0.063	0.5	19.115	2.363
96	0.13	0.95	2428.12	5.0	0.475	0.475	1.03	6.438	5.263	0.5	0.063	0.5	31.195	2.338
97	0.13	0.95	486.99	20.0	-0.095	-0.095	1.03	6.438	21.053	-0.1	0.0625	-0.1	1.221	2.737
98	0.13	0.95	513.78	19.0	-0.095	-0.095	1.03	6.438	20.000	-0.1	0.0625	-0.1	1.437	2.741
99	0.13	0.95	543.76	18.0	-0.095	-0.095	1.03	6.438	18.947	-0.1	0.0625	-0.1	1.708	2.745
100	0.13	0.95	577.52	17.0	-0.095	-0.095	1.03	6.438	17.895	-0.1	0.0625	-0.1	2.052	2.750
101	0.13	0.95	615.84	16.0	-0.095	-0.095	1.03	6.438	16.842	-0.1	0.0625	-0.1	2.496	2.756
102	0.13	0.95	659.72	15.0	-0.095	-0.095	1.03	6.438	15.789	-0.1	0.0625	-0.1	3.079	2.763
103	0.13	0.95	710.49	14.0	-0.095	-0.095	1.03	6.438	14.737	-0.1	0.0625	-0.1	3.861	2.772
104	0.13	0.95	769.94	13.0	-0.095	-0.095	1.03	6.438	13.684	-0.1	0.0625	-0.1	4.936	2.782
105	0.13	0.95	840.53	12.0	-0.095	-0.095	1.03	6.438	12.632	-0.1	0.0625	-0.1	6.458	2.794
106	0.13	0.95	925.74	11.0	-0.095	-0.095	1.03	6.438	11.579	-0.1	0.0625	-0.1	8.689	2.810
107	0.13	0.95	1030.73	10.0	-0.095	-0.095	1.03	6.438	10.526	-0.1	0.0625	-0.1	12.104	2.830
108	0.13	0.95	1163.35	9.0	-0.095	-0.095	1.03	6.438	9.474	-0.1	0.063	-0.1	17.624	2.856
109	0.13	0.95	1336.23	8.0	-0.095	-0.095	1.03	6.438	8.421	-0.1	0.063	-0.1	27.210	2.891
110	0.13	0.95	1570.95	7.0	-0.095	-0.095	1.03	6.438	7.368	-0.1	0.063	-0.1	45.571	2.941
111	0.13	0.95	1907.53	6.0	-0.095	-0.095	1.03	6.438	6.316	-0.1	0.063	-0.1	86.161	3.017
112	0.13	0.95	2428.12	5.0	-0.095	-0.095	1.03	6.438	5.263	-0.1	0.063	-0.1	199.536	3.144
113	0.13	0.95	486.99	20.0	-0.190	-0.190	1.03	6.438	21.053	-0.2	0.0625	-0.2	1.353	2.781
114	0.13	0.95	513.78	19.0	-0.190	-0.190	1.03	6.438	20.000	-0.2	0.0625	-0.2	1.604	2.788

Table 4.E.1 (cont) mid-span point loading

run	Geometric parameters						Elastic parameters		Dimensionless parameters				results	
	Point load case													
	w (m)	h (m)	M_{cr} (kNm)	L (m)	a (m)	b (m)	E (10^4MPa)	G (10^2MPa)	L/h	a/h	G/E	b/h	k (10^2kN/m)	log(k/(EI/L^3))
115	0.13	0.95	543.76	18.0	-0.190	-0.190	1.03	6.438	18.947	-0.2	0.0625	-0.2	1.920	2.796
116	0.13	0.95	577.52	17.0	-0.190	-0.190	1.03	6.438	17.895	-0.2	0.0625	-0.2	2.328	2.805
117	0.13	0.95	615.84	16.0	-0.190	-0.190	1.03	6.438	16.842	-0.2	0.0625	-0.2	2.860	2.816
118	0.13	0.95	659.72	15.0	-0.190	-0.190	1.03	6.438	15.789	-0.2	0.0625	-0.2	3.572	2.828
119	0.13	0.95	710.49	14.0	-0.190	-0.190	1.03	6.438	14.737	-0.2	0.0625	-0.2	4.546	2.843
120	0.13	0.95	769.94	13.0	-0.190	-0.190	1.03	6.438	13.684	-0.2	0.0625	-0.2	5.918	2.861
121	0.13	0.95	840.53	12.0	-0.190	-0.190	1.03	6.438	12.632	-0.2	0.0625	-0.2	7.919	2.883
122	0.13	0.95	925.74	11.0	-0.190	-0.190	1.03	6.438	11.579	-0.2	0.0625	-0.2	10.968	2.911
123	0.13	0.95	1030.73	10.0	-0.190	-0.190	1.03	6.438	10.526	-0.2	0.0625	-0.2	15.883	2.948
124	0.13	0.95	1163.35	9.0	-0.190	-0.190	1.03	6.438	9.474	-0.2	0.063	-0.2	24.426	2.997
125	0.13	0.95	1336.23	8.0	-0.190	-0.190	1.03	6.438	8.421	-0.2	0.063	-0.2	40.971	3.069
126	0.13	0.95	1570.95	7.0	-0.190	-0.190	1.03	6.438	7.368	-0.2	0.063	-0.2	79.017	3.180
127	0.13	0.95	1907.53	6.0	-0.190	-0.190	1.03	6.438	6.316	-0.2	0.063	-0.2	201.386	3.385
128	0.13	0.95	2428.12	5.0	-0.190	-0.190	1.03	6.438	5.263	-0.2	0.063	-0.2	1666.239	4.065
129	0.13	0.95	486.99	20.0	-0.285	-0.285	1.03	6.438	21.053	-0.3	0.0625	-0.3	1.517	2.831
130	0.13	0.95	513.78	19.0	-0.285	-0.285	1.03	6.438	20.000	-0.3	0.0625	-0.3	1.813	2.841
131	0.13	0.95	543.76	18.0	-0.285	-0.285	1.03	6.438	18.947	-0.3	0.0625	-0.3	2.192	2.853
132	0.13	0.95	577.52	17.0	-0.285	-0.285	1.03	6.438	17.895	-0.3	0.0625	-0.3	2.687	2.867
133	0.13	0.95	615.84	16.0	-0.285	-0.285	1.03	6.438	16.842	-0.3	0.0625	-0.3	3.348	2.884
134	0.13	0.95	659.72	15.0	-0.285	-0.285	1.03	6.438	15.789	-0.3	0.0625	-0.3	4.251	2.904
135	0.13	0.95	710.49	14.0	-0.285	-0.285	1.03	6.438	14.737	-0.3	0.0625	-0.3	5.522	2.927

Table 4.E.1 (cont) mid-span point loading

run	Geometric parameters						Elastic parameters		Dimensionless parameters				results	
	Point load case													
	w (m)	h (m)	M_{cr} (kNm)	L (m)	a (m)	b (m)	E (10^4MPa)	G (10^2MPa)	L/h	a/h	G/E	b/h	k (10^2kN/m)	log(k/(EI/L^3))
136	0.13	0.95	769.94	13.0	-0.285	-0.285	1.03	6.438	13.684	-0.3	0.0625	-0.3	7.379	2.957
137	0.13	0.95	840.53	12.0	-0.285	-0.285	1.03	6.438	12.632	-0.3	0.0625	-0.3	10.219	2.994
138	0.13	0.95	925.74	11.0	-0.285	-0.285	1.03	6.438	11.579	-0.3	0.0625	-0.3	14.839	3.042
139	0.13	0.95	1030.73	10.0	-0.285	-0.285	1.03	6.438	10.526	-0.3	0.0625	-0.3	23.034	3.109
140	0.13	0.95	1163.35	9.0	-0.285	-0.285	1.03	6.438	9.474	-0.3	0.063	-0.3	39.626	3.207
141	0.13	0.95	1336.23	8.0	-0.285	-0.285	1.03	6.438	8.421	-0.3	0.063	-0.3	82.327	3.372
142	0.13	0.95	1570.95	7.0	-0.285	-0.285	1.03	6.438	7.368	-0.3	0.063	-0.3	291.125	3.746
143	0.13	0.95	1599.12	6.9	-0.285	-0.285	1.03	6.438	7.263	-0.3	0.063	-0.3	360.126	3.820
144	0.13	0.95	1628.33	6.8	-0.285	-0.285	1.03	6.438	7.158	-0.3	0.063	-0.3	464.149	3.911
145	0.13	0.95	1658.64	6.7	-0.285	-0.285	1.03	6.438	7.053	-0.3	0.063	-0.3	638.067	4.030
146	0.13	0.95	1690.12	6.6	-0.285	-0.285	1.03	6.438	6.947	-0.3	0.063	-0.3	985.872	4.199
147	0.13	0.95	486.99	20.0	-0.380	-0.380	1.03	6.438	21.053	-0.4	0.0625	-0.4	1.725	2.887
148	0.13	0.95	513.78	19.0	-0.380	-0.380	1.03	6.438	20.000	-0.4	0.0625	-0.4	2.084	2.902
149	0.13	0.95	543.76	18.0	-0.380	-0.380	1.03	6.438	18.947	-0.4	0.0625	-0.4	2.552	2.920
150	0.13	0.95	577.52	17.0	-0.380	-0.380	1.03	6.438	17.895	-0.4	0.0625	-0.4	3.177	2.940
151	0.13	0.95	615.84	16.0	-0.380	-0.380	1.03	6.438	16.842	-0.4	0.0625	-0.4	4.033	2.965
152	0.13	0.95	659.72	15.0	-0.380	-0.380	1.03	6.438	15.789	-0.4	0.0625	-0.4	5.244	2.995
153	0.13	0.95	710.49	14.0	-0.380	-0.380	1.03	6.438	14.737	-0.4	0.0625	-0.4	7.024	3.032
154	0.13	0.95	769.94	13.0	-0.380	-0.380	1.03	6.438	13.684	-0.4	0.0625	-0.4	9.782	3.079
155	0.13	0.95	840.53	12.0	-0.380	-0.380	1.03	6.438	12.632	-0.4	0.0625	-0.4	14.372	3.142
156	0.13	0.95	925.74	11.0	-0.380	-0.380	1.03	6.438	11.579	-0.4	0.0625	-0.4	22.866	3.230

Table 4.E.1 (cont) mid-span point loading

run	Geometric parameters						Elastic parameters		Dimensionless parameters				results	
	Point load case													
	w (m)	h (m)	M_{cr} (kNm)	L (m)	a (m)	b (m)	E (10^4MPa)	G (10^2MPa)	L/h	a/h	G/E	b/h	k (10^2kN/m)	log(k/(EI/L^3))
157	0.13	0.95	1030.73	10.0	-0.380	-0.380	1.03	6.438	10.526	-0.4	0.0625	-0.4	41.691	3.367
158	0.13	0.95	1163.35	9.0	-0.380	-0.380	1.03	6.438	9.474	-0.4	0.063	-0.4	103.776	3.626
159	0.13	0.95	1178.56	8.9	-0.380	-0.380	1.03	6.438	9.368	-0.4	0.063	-0.4	118.053	3.667
160	0.13	0.95	1194.18	8.8	-0.380	-0.380	1.03	6.438	9.263	-0.4	0.063	-0.4	136.026	3.714
161	0.13	0.95	1210.23	8.7	-0.380	-0.380	1.03	6.438	9.158	-0.4	0.063	-0.4	159.291	3.768
162	0.13	0.95	1226.73	8.6	-0.380	-0.380	1.03	6.438	9.053	-0.4	0.063	-0.4	190.518	3.830
163	0.13	0.95	1243.69	8.5	-0.380	-0.380	1.03	6.438	8.947	-0.4	0.063	-0.4	234.525	3.905
164	0.13	0.95	1261.14	8.4	-0.380	-0.380	1.03	6.438	8.842	-0.4	0.063	-0.4	300.992	3.998
165	0.13	0.95	1279.09	8.3	-0.380	-0.380	1.03	6.438	8.737	-0.4	0.063	-0.4	412.646	4.120
166	0.13	0.95	486.99	20.0	-0.475	-0.475	1.03	6.438	21.053	-0.5	0.0625	-0.5	1.999	2.951
167	0.13	0.95	513.78	19.0	-0.475	-0.475	1.03	6.438	20.000	-0.5	0.0625	-0.5	2.449	2.972
168	0.13	0.95	543.76	18.0	-0.475	-0.475	1.03	6.438	18.947	-0.5	0.0625	-0.5	3.052	2.997
169	0.13	0.95	577.52	17.0	-0.475	-0.475	1.03	6.438	17.895	-0.5	0.0625	-0.5	3.882	3.027
170	0.13	0.95	615.84	16.0	-0.475	-0.475	1.03	6.438	16.842	-0.5	0.0625	-0.5	5.067	3.064
171	0.13	0.95	659.72	15.0	-0.475	-0.475	1.03	6.438	15.789	-0.5	0.0625	-0.5	6.833	3.110
172	0.13	0.95	710.49	14.0	-0.475	-0.475	1.03	6.438	14.737	-0.5	0.0625	-0.5	9.633	3.169
173	0.13	0.95	769.94	13.0	-0.475	-0.475	1.03	6.438	13.684	-0.5	0.0625	-0.5	14.476	3.249
174	0.13	0.95	840.53	12.0	-0.475	-0.475	1.03	6.438	12.632	-0.5	0.0625	-0.5	24.128	3.367
175	0.13	0.95	925.74	11.0	-0.475	-0.475	1.03	6.438	11.579	-0.5	0.0625	-0.5	49.473	3.565
176	0.13	0.95	1030.73	10.0	-0.475	-0.475	1.03	6.438	10.526	-0.5	0.0625	-0.5	213.605	4.076

Table 4.E. 2 uniformly distributed load

run	Geometric parameters						Elastic parameters		Dimensionless parameters				results	
	Uniformly distributed load													
	w (m)	h (m)	M_{cr} (kNm)	L (m)	a (m)	b (m)	E (10^4MPa)	G (10^2MPa)	L/h	a/h	G/E	b/h	k (10^2kN/m)	log(k/(EI/L^3))
177	0.13	0.95	359.39	20.0	0.000	0.000	1.03	6.438	21.053	0.0	0.0625	0.0	0.534	2.377
178	0.13	0.95	379.06	19.0	0.000	0.000	1.03	6.438	20.000	0.0	0.0625	0.0	0.625	2.379
179	0.13	0.95	401.03	18.0	0.000	0.000	1.03	6.438	18.947	0.0	0.0625	0.0	0.738	2.380
180	0.13	0.95	425.76	17.0	0.000	0.000	1.03	6.438	17.895	0.0	0.0625	0.0	0.880	2.383
181	0.13	0.95	453.81	16.0	0.000	0.000	1.03	6.438	16.842	0.0	0.0625	0.0	1.062	2.385
182	0.13	0.95	485.90	15.0	0.000	0.000	1.03	6.438	15.789	0.0	0.0625	0.0	1.298	2.388
183	0.13	0.95	522.99	14.0	0.000	0.000	1.03	6.438	14.737	0.0	0.0625	0.0	1.609	2.392
184	0.13	0.95	566.37	13.0	0.000	0.000	1.03	6.438	13.684	0.0	0.0625	0.0	2.031	2.396
185	0.13	0.95	617.81	12.0	0.000	0.000	1.03	6.438	12.632	0.0	0.0625	0.0	2.615	2.402
186	0.13	0.95	679.83	11.0	0.000	0.000	1.03	6.438	11.579	0.0	0.0625	0.0	3.448	2.409
187	0.13	0.95	756.14	10.0	0.000	0.000	1.03	6.438	10.526	0.0	0.0625	0.0	4.682	2.417
188	0.13	0.95	852.40	9.0	0.000	0.000	1.03	6.438	9.474	0.0	0.063	0.0	6.591	2.428
189	0.13	0.95	977.70	8.0	0.000	0.000	1.03	6.438	8.421	0.0	0.063	0.0	9.712	2.443
190	0.13	0.95	1147.63	7.0	0.000	0.000	1.03	6.438	7.368	0.0	0.063	0.0	15.188	2.464
191	0.13	0.95	1391.03	6.0	0.000	0.000	1.03	6.438	6.316	0.0	0.063	0.0	25.742	2.492
192	0.13	0.95	1767.25	5.0	0.000	0.000	1.03	6.438	5.263	0.0	0.063	0.0	48.876	2.533
193	0.13	0.95	356.60	20.0	0.095	0.095	1.03	6.438	21.053	0.1	0.0625	0.1	0.485	2.336
194	0.13	0.95	375.96	19.0	0.095	0.095	1.03	6.438	20.000	0.1	0.0625	0.1	0.565	2.335
195	0.13	0.95	397.58	18.0	0.095	0.095	1.03	6.438	18.947	0.1	0.0625	0.1	0.664	2.335
196	0.13	0.95	421.89	17.0	0.095	0.095	1.03	6.438	17.895	0.1	0.0625	0.1	0.788	2.335

Table 4.E. 2 (cont) uniformly distributed load

run	Geometric parameters						Elastic parameters		Dimensionless parameters				results	
	Uniformly distributed load													
	w (m)	h (m)	M_{cr} (kNm)	L (m)	a (m)	b (m)	E (10^4MPa)	G (10^2MPa)	L/h	a/h	G/E	b/h	k (10^2kN/m)	log(k/(EI/L^3))
197	0.13	0.95	449.43	16.0	0.095	0.095	1.03	6.438	16.842	0.1	0.0625	0.1	0.944	2.334
198	0.13	0.95	480.91	15.0	0.095	0.095	1.03	6.438	15.789	0.1	0.0625	0.1	1.146	2.334
199	0.13	0.95	517.25	14.0	0.095	0.095	1.03	6.438	14.737	0.1	0.0625	0.1	1.409	2.334
200	0.13	0.95	559.69	13.0	0.095	0.095	1.03	6.438	13.684	0.1	0.0625	0.1	1.761	2.334
201	0.13	0.95	609.96	12.0	0.095	0.095	1.03	6.438	12.632	0.1	0.0625	0.1	2.241	2.335
202	0.13	0.95	670.46	11.0	0.095	0.095	1.03	6.438	11.579	0.1	0.0625	0.1	2.917	2.336
203	0.13	0.95	744.77	10.0	0.095	0.095	1.03	6.438	10.526	0.1	0.0625	0.1	3.899	2.338
204	0.13	0.95	838.31	9.0	0.095	0.095	1.03	6.438	9.474	0.1	0.063	0.1	5.384	2.341
205	0.13	0.95	959.80	8.0	0.095	0.095	1.03	6.438	8.421	0.1	0.063	0.1	7.747	2.345
206	0.13	0.95	1124.13	7.0	0.095	0.095	1.03	6.438	7.368	0.1	0.063	0.1	11.755	2.352
207	0.13	0.95	1358.88	6.0	0.095	0.095	1.03	6.438	6.316	0.1	0.063	0.1	19.147	2.363
208	0.13	0.95	1720.70	5.0	0.095	0.095	1.03	6.438	5.263	0.1	0.063	0.1	34.418	2.380
209	0.13	0.95	353.82	20.0	0.190	0.190	1.03	6.438	21.053	0.2	0.0625	0.2	0.446	2.299
210	0.13	0.95	372.88	19.0	0.190	0.190	1.03	6.438	20.000	0.2	0.0625	0.2	0.517	2.297
211	0.13	0.95	394.15	18.0	0.190	0.190	1.03	6.438	18.947	0.2	0.0625	0.2	0.605	2.294
212	0.13	0.95	418.04	17.0	0.190	0.190	1.03	6.438	17.895	0.2	0.0625	0.2	0.714	2.292
213	0.13	0.95	445.08	16.0	0.190	0.190	1.03	6.438	16.842	0.2	0.0625	0.2	0.851	2.289
214	0.13	0.95	475.96	15.0	0.190	0.190	1.03	6.438	15.789	0.2	0.0625	0.2	1.026	2.286
215	0.13	0.95	511.56	14.0	0.190	0.190	1.03	6.438	14.737	0.2	0.0625	0.2	1.254	2.283
216	0.13	0.95	553.09	13.0	0.190	0.190	1.03	6.438	13.684	0.2	0.0625	0.2	1.555	2.280
217	0.13	0.95	602.19	12.0	0.190	0.190	1.03	6.438	12.632	0.2	0.0625	0.2	1.963	2.277

Table 4.E. 2 (cont) uniformly distributed load

run	Geometric parameters						Elastic parameters		Dimensionless parameters				results	
	Uniformly distributed load													
	w (m)	h (m)	M_{cr} (kNm)	L (m)	a (m)	b (m)	E (10^4MPa)	G (10^2MPa)	L/h	a/h	G/E	b/h	k (10^2kN/m)	log(k/(EI/L^3))
218	0.13	0.95	661.21	11.0	0.190	0.190	1.03	6.438	11.579	0.2	0.0625	0.2	2.530	2.274
219	0.13	0.95	733.55	10.0	0.190	0.190	1.03	6.438	10.526	0.2	0.0625	0.2	3.343	2.271
220	0.13	0.95	824.43	9.0	0.190	0.190	1.03	6.438	9.474	0.2	0.063	0.2	4.554	2.268
221	0.13	0.95	942.18	8.0	0.190	0.190	1.03	6.438	8.421	0.2	0.063	0.2	6.447	2.265
222	0.13	0.95	1101.07	7.0	0.190	0.190	1.03	6.438	7.368	0.2	0.063	0.2	9.589	2.264
223	0.13	0.95	1327.42	6.0	0.190	0.190	1.03	6.438	6.316	0.2	0.063	0.2	15.231	2.264
224	0.13	0.95	1675.30	5.0	0.190	0.190	1.03	6.438	5.263	0.2	0.063	0.2	26.507	2.267
225	0.13	0.95	351.07	20.0	0.285	0.285	1.03	6.438	21.053	0.3	0.0625	0.3	0.412	2.265
226	0.13	0.95	369.82	19.0	0.285	0.285	1.03	6.438	20.000	0.3	0.0625	0.3	0.476	2.261
227	0.13	0.95	390.74	18.0	0.285	0.285	1.03	6.438	18.947	0.3	0.0625	0.3	0.555	2.257
228	0.13	0.95	414.22	17.0	0.285	0.285	1.03	6.438	17.895	0.3	0.0625	0.3	0.653	2.253
229	0.13	0.95	440.77	16.0	0.285	0.285	1.03	6.438	16.842	0.3	0.0625	0.3	0.775	2.249
230	0.13	0.95	471.05	15.0	0.285	0.285	1.03	6.438	15.789	0.3	0.0625	0.3	0.930	2.244
231	0.13	0.95	505.92	14.0	0.285	0.285	1.03	6.438	14.737	0.3	0.0625	0.3	1.131	2.239
232	0.13	0.95	546.55	13.0	0.285	0.285	1.03	6.438	13.684	0.3	0.0625	0.3	1.394	2.233
233	0.13	0.95	594.51	12.0	0.285	0.285	1.03	6.438	12.632	0.3	0.0625	0.3	1.748	2.227
234	0.13	0.95	652.06	11.0	0.285	0.285	1.03	6.438	11.579	0.3	0.0625	0.3	2.235	2.220
235	0.13	0.95	722.48	10.0	0.285	0.285	1.03	6.438	10.526	0.3	0.0625	0.3	2.928	2.213
236	0.13	0.95	810.75	9.0	0.285	0.285	1.03	6.438	9.474	0.3	0.063	0.3	3.949	2.206
237	0.13	0.95	924.87	8.0	0.285	0.285	1.03	6.438	8.421	0.3	0.063	0.3	5.523	2.198
238	0.13	0.95	1078.45	7.0	0.285	0.285	1.03	6.438	7.368	0.3	0.063	0.3	8.096	2.190

Table 4.E. 2 (cont) uniformly distributed load

run	Geometric parameters						Elastic parameters		Dimensionless parameters				results	
	Uniformly distributed load													
	w (m)	h (m)	M_{cr} (kNm)	L (m)	a (m)	b (m)	E (10^4MPa)	G (10^2MPa)	L/h	a/h	G/E	b/h	k (10^2kN/m)	log(k/(EI/L^3))
239	0.13	0.95	1296.65	6.0	0.285	0.285	1.03	6.438	6.316	0.3	0.063	0.3	12.636	2.183
240	0.13	0.95	1631.06	5.0	0.285	0.285	1.03	6.438	5.263	0.3	0.063	0.3	21.512	2.176
241	0.13	0.95	348.33	20.0	0.380	0.380	1.03	6.438	21.053	0.4	0.0625	0.4	0.383	2.233
242	0.13	0.95	366.79	19.0	0.380	0.380	1.03	6.438	20.000	0.4	0.0625	0.4	0.442	2.229
243	0.13	0.95	387.36	18.0	0.380	0.380	1.03	6.438	18.947	0.4	0.0625	0.4	0.514	2.223
244	0.13	0.95	410.43	17.0	0.380	0.380	1.03	6.438	17.895	0.4	0.0625	0.4	0.602	2.218
245	0.13	0.95	436.49	16.0	0.380	0.380	1.03	6.438	16.842	0.4	0.0625	0.4	0.712	2.212
246	0.13	0.95	466.18	15.0	0.380	0.380	1.03	6.438	15.789	0.4	0.0625	0.4	0.851	2.205
247	0.13	0.95	500.34	14.0	0.380	0.380	1.03	6.438	14.737	0.4	0.0625	0.4	1.030	2.198
248	0.13	0.95	540.08	13.0	0.380	0.380	1.03	6.438	13.684	0.4	0.0625	0.4	1.264	2.190
249	0.13	0.95	586.92	12.0	0.380	0.380	1.03	6.438	12.632	0.4	0.0625	0.4	1.576	2.182
250	0.13	0.95	643.04	11.0	0.380	0.380	1.03	6.438	11.579	0.4	0.0625	0.4	2.004	2.173
251	0.13	0.95	711.56	10.0	0.380	0.380	1.03	6.438	10.526	0.4	0.0625	0.4	2.606	2.163
252	0.13	0.95	797.29	9.0	0.380	0.380	1.03	6.438	9.474	0.4	0.063	0.4	3.487	2.152
253	0.13	0.95	907.85	8.0	0.380	0.380	1.03	6.438	8.421	0.4	0.063	0.4	4.831	2.140
254	0.13	0.95	1056.28	7.0	0.380	0.380	1.03	6.438	7.368	0.4	0.063	0.4	7.005	2.127
255	0.13	0.95	1266.57	6.0	0.380	0.380	1.03	6.438	6.316	0.4	0.063	0.4	10.787	2.114
256	0.13	0.95	1587.99	5.0	0.380	0.380	1.03	6.438	5.263	0.4	0.063	0.4	18.066	2.101
257	0.13	0.95	345.61	20.0	0.475	0.475	1.03	6.438	21.053	0.5	0.0625	0.5	0.359	2.205
258	0.13	0.95	363.78	19.0	0.475	0.475	1.03	6.438	20.000	0.5	0.0625	0.5	0.413	2.199
259	0.13	0.95	384.01	18.0	0.475	0.475	1.03	6.438	18.947	0.5	0.0625	0.5	0.478	2.192

Table 4.E. 2 (cont) uniformly distributed load

run	Geometric parameters						Elastic parameters		Dimensionless parameters				results	
	Uniformly distributed load													
	w (m)	h (m)	M_{cr} (kNm)	L (m)	a (m)	b (m)	E (10^4MPa)	G (10^2MPa)	L/h	a/h	G/E	b/h	k (10^2kN/m)	log(k/(EI/L^3))
260	0.13	0.95	406.67	17.0	0.475	0.475	1.03	6.438	17.895	0.5	0.0625	0.5	0.559	2.186
261	0.13	0.95	432.25	16.0	0.475	0.475	1.03	6.438	16.842	0.5	0.0625	0.5	0.659	2.178
262	0.13	0.95	461.37	15.0	0.475	0.475	1.03	6.438	15.789	0.5	0.0625	0.5	0.785	2.170
263	0.13	0.95	494.81	14.0	0.475	0.475	1.03	6.438	14.737	0.5	0.0625	0.5	0.947	2.161
264	0.13	0.95	533.67	13.0	0.475	0.475	1.03	6.438	13.684	0.5	0.0625	0.5	1.157	2.152
265	0.13	0.95	579.42	12.0	0.475	0.475	1.03	6.438	12.632	0.5	0.0625	0.5	1.436	2.142
266	0.13	0.95	634.12	11.0	0.475	0.475	1.03	6.438	11.579	0.5	0.0625	0.5	1.817	2.130
267	0.13	0.95	700.80	10.0	0.475	0.475	1.03	6.438	10.526	0.5	0.0625	0.5	2.350	2.118
268	0.13	0.95	784.03	9.0	0.475	0.475	1.03	6.438	9.474	0.5	0.063	0.5	3.123	2.104
269	0.13	0.95	891.14	8.0	0.475	0.475	1.03	6.438	8.421	0.5	0.063	0.5	4.294	2.089
270	0.13	0.95	1034.55	7.0	0.475	0.475	1.03	6.438	7.368	0.5	0.063	0.5	6.171	2.072
271	0.13	0.95	1237.20	6.0	0.475	0.475	1.03	6.438	6.316	0.5	0.063	0.5	9.401	2.054
272	0.13	0.95	1546.10	5.0	0.475	0.475	1.03	6.438	5.263	0.5	0.063	0.5	15.543	2.035
273	0.13	0.95	362.21	20.0	-0.095	-0.095	1.03	6.438	21.053	-0.1	0.0625	-0.1	0.593	2.423
274	0.13	0.95	382.18	19.0	-0.095	-0.095	1.03	6.438	20.000	-0.1	0.0625	-0.1	0.698	2.427
275	0.13	0.95	404.51	18.0	-0.095	-0.095	1.03	6.438	18.947	-0.1	0.0625	-0.1	0.830	2.432
276	0.13	0.95	429.67	17.0	-0.095	-0.095	1.03	6.438	17.895	-0.1	0.0625	-0.1	0.998	2.437
277	0.13	0.95	458.23	16.0	-0.095	-0.095	1.03	6.438	16.842	-0.1	0.0625	-0.1	1.214	2.443
278	0.13	0.95	490.94	15.0	-0.095	-0.095	1.03	6.438	15.789	-0.1	0.0625	-0.1	1.498	2.451
279	0.13	0.95	528.79	14.0	-0.095	-0.095	1.03	6.438	14.737	-0.1	0.0625	-0.1	1.880	2.459
280	0.13	0.95	573.11	13.0	-0.095	-0.095	1.03	6.438	13.684	-0.1	0.0625	-0.1	2.403	2.469

Table 4.E. 2 (cont) uniformly distributed load

run	Geometric parameters						Elastic parameters		Dimensionless parameters				results	
	Uniformly distributed load													
	w (m)	h (m)	M_{cr} (kNm)	L (m)	a (m)	b (m)	E (10^4MPa)	G (10^2MPa)	L/h	a/h	G/E	b/h	k (10^2kN/m)	log(k/(EI/L^3))
281	0.13	0.95	625.74	12.0	-0.095	-0.095	1.03	6.438	12.632	-0.1	0.0625	-0.1	3.143	2.482
282	0.13	0.95	689.31	11.0	-0.095	-0.095	1.03	6.438	11.579	-0.1	0.0625	-0.1	4.224	2.497
283	0.13	0.95	767.66	10.0	-0.095	-0.095	1.03	6.438	10.526	-0.1	0.0625	-0.1	5.871	2.515
284	0.13	0.95	866.69	9.0	-0.095	-0.095	1.03	6.438	9.474	-0.1	0.063	-0.1	8.511	2.539
285	0.13	0.95	995.90	8.0	-0.095	-0.095	1.03	6.438	8.421	-0.1	0.063	-0.1	13.029	2.571
286	0.13	0.95	1171.56	7.0	-0.095	-0.095	1.03	6.438	7.368	-0.1	0.063	-0.1	21.465	2.614
287	0.13	0.95	1423.85	6.0	-0.095	-0.095	1.03	6.438	6.316	-0.1	0.063	-0.1	39.219	2.675
288	0.13	0.95	1814.93	5.0	-0.095	-0.095	1.03	6.438	5.263	-0.1	0.063	-0.1	83.841	2.767
289	0.13	0.95	365.04	20.0	-0.190	-0.190	1.03	6.438	21.053	-0.2	0.0625	-0.2	0.668	2.475
290	0.13	0.95	385.32	19.0	-0.190	-0.190	1.03	6.438	20.000	-0.2	0.0625	-0.2	0.792	2.482
291	0.13	0.95	408.02	18.0	-0.190	-0.190	1.03	6.438	18.947	-0.2	0.0625	-0.2	0.950	2.490
292	0.13	0.95	433.61	17.0	-0.190	-0.190	1.03	6.438	17.895	-0.2	0.0625	-0.2	1.153	2.500
293	0.13	0.95	462.69	16.0	-0.190	-0.190	1.03	6.438	16.842	-0.2	0.0625	-0.2	1.420	2.511
294	0.13	0.95	496.02	15.0	-0.190	-0.190	1.03	6.438	15.789	-0.2	0.0625	-0.2	1.775	2.524
295	0.13	0.95	534.64	14.0	-0.190	-0.190	1.03	6.438	14.737	-0.2	0.0625	-0.2	2.263	2.540
296	0.13	0.95	579.92	13.0	-0.190	-0.190	1.03	6.438	13.684	-0.2	0.0625	-0.2	2.948	2.558
297	0.13	0.95	633.76	12.0	-0.190	-0.190	1.03	6.438	12.632	-0.2	0.0625	-0.2	3.947	2.581
298	0.13	0.95	698.90	11.0	-0.190	-0.190	1.03	6.438	11.579	-0.2	0.0625	-0.2	5.463	2.608
299	0.13	0.95	779.32	10.0	-0.190	-0.190	1.03	6.438	10.526	-0.2	0.0625	-0.2	7.887	2.644
300	0.13	0.95	881.18	9.0	-0.190	-0.190	1.03	6.438	9.474	-0.2	0.063	-0.2	12.037	2.690
301	0.13	0.95	1014.38	8.0	-0.190	-0.190	1.03	6.438	8.421	-0.2	0.063	-0.2	19.834	2.753

Table 4.E. 2 (cont) uniformly distributed load

run	Geometric parameters						Elastic parameters		Dimensionless parameters				results	
	Uniformly distributed load													
	w (m)	h (m)	M_{cr} (kNm)	L (m)	a (m)	b (m)	E (10^4MPa)	G (10^2MPa)	L/h	a/h	G/E	b/h	k (10^2kN/m)	log(k/(EI/L^3))
302	0.13	0.95	1195.90	7.0	-0.190	-0.190	1.03	6.438	7.368	-0.2	0.063	-0.2	36.636	2.846
303	0.13	0.95	1457.34	6.0	-0.190	-0.190	1.03	6.438	6.316	-0.2	0.063	-0.2	82.211	2.996
304	0.13	0.95	1863.71	5.0	-0.190	-0.190	1.03	6.438	5.263	-0.2	0.063	-0.2	290.353	3.307
305	0.13	0.95	367.88	20.0	-0.285	-0.285	1.03	6.438	21.053	-0.3	0.0625	-0.3	0.765	2.534
306	0.13	0.95	388.48	19.0	-0.285	-0.285	1.03	6.438	20.000	-0.3	0.0625	-0.3	0.917	2.546
307	0.13	0.95	411.55	18.0	-0.285	-0.285	1.03	6.438	18.947	-0.3	0.0625	-0.3	1.113	2.559
308	0.13	0.95	437.57	17.0	-0.285	-0.285	1.03	6.438	17.895	-0.3	0.0625	-0.3	1.369	2.575
309	0.13	0.95	467.17	16.0	-0.285	-0.285	1.03	6.438	16.842	-0.3	0.0625	-0.3	1.712	2.593
310	0.13	0.95	501.14	15.0	-0.285	-0.285	1.03	6.438	15.789	-0.3	0.0625	-0.3	2.183	2.614
311	0.13	0.95	540.54	14.0	-0.285	-0.285	1.03	6.438	14.737	-0.3	0.0625	-0.3	2.848	2.640
312	0.13	0.95	586.79	13.0	-0.285	-0.285	1.03	6.438	13.684	-0.3	0.0625	-0.3	3.824	2.671
313	0.13	0.95	641.86	12.0	-0.285	-0.285	1.03	6.438	12.632	-0.3	0.0625	-0.3	5.320	2.710
314	0.13	0.95	708.59	11.0	-0.285	-0.285	1.03	6.438	11.579	-0.3	0.0625	-0.3	7.756	2.761
315	0.13	0.95	791.13	10.0	-0.285	-0.285	1.03	6.438	10.526	-0.3	0.0625	-0.3	12.060	2.828
316	0.13	0.95	895.87	9.0	-0.285	-0.285	1.03	6.438	9.474	-0.3	0.063	-0.3	20.646	2.924
317	0.13	0.95	1033.13	8.0	-0.285	-0.285	1.03	6.438	8.421	-0.3	0.063	-0.3	41.741	3.077
318	0.13	0.95	1220.67	7.0	-0.285	-0.285	1.03	6.438	7.368	-0.3	0.063	-0.3	125.818	3.382
321	0.13	0.95	370.75	20.0	-0.380	-0.380	1.03	6.438	21.053	-0.4	0.0625	-0.4	0.898	2.603
322	0.13	0.95	391.66	19.0	-0.380	-0.380	1.03	6.438	20.000	-0.4	0.0625	-0.4	1.091	2.621
323	0.13	0.95	415.10	18.0	-0.380	-0.380	1.03	6.438	18.947	-0.4	0.0625	-0.4	1.345	2.641
324	0.13	0.95	441.57	17.0	-0.380	-0.380	1.03	6.438	17.895	-0.4	0.0625	-0.4	1.687	2.665

Table 4.E. 2 (cont) uniformly distributed load

run	Geometric parameters						Elastic parameters		Dimensionless parameters				results	
	Uniformly distributed load													
	w (m)	h (m)	M_{cr} (kNm)	L (m)	a (m)	b (m)	E (10^4MPa)	G (10^2MPa)	L/h	a/h	G/E	b/h	k (10^2kN/m)	log(k/(EI/L^3))
325	0.13	0.95	471.70	16.0	-0.380	-0.380	1.03	6.438	16.842	-0.4	0.0625	-0.4	2.161	2.694
326	0.13	0.95	506.31	15.0	-0.380	-0.380	1.03	6.438	15.789	-0.4	0.0625	-0.4	2.841	2.728
327	0.13	0.95	546.49	14.0	-0.380	-0.380	1.03	6.438	14.737	-0.4	0.0625	-0.4	3.856	2.771
328	0.13	0.95	593.72	13.0	-0.380	-0.380	1.03	6.438	13.684	-0.4	0.0625	-0.4	5.459	2.826
329	0.13	0.95	650.05	12.0	-0.380	-0.380	1.03	6.438	12.632	-0.4	0.0625	-0.4	8.196	2.898
330	0.13	0.95	718.39	11.0	-0.380	-0.380	1.03	6.438	11.579	-0.4	0.0625	-0.4	13.449	3.000
331	0.13	0.95	803.08	10.0	-0.380	-0.380	1.03	6.438	10.526	-0.4	0.0625	-0.4	25.835	3.159
332	0.13	0.95	910.75	9.0	-0.380	-0.380	1.03	6.438	9.474	-0.4	0.063	-0.4	73.787	3.477
337	0.13	0.95	373.63	20.0	-0.475	-0.475	1.03	6.438	21.053	-0.5	0.0625	-0.5	1.087	2.686
338	0.13	0.95	394.86	19.0	-0.475	-0.475	1.03	6.438	20.000	-0.5	0.0625	-0.5	1.348	2.713
339	0.13	0.95	418.68	18.0	-0.475	-0.475	1.03	6.438	18.947	-0.5	0.0625	-0.5	1.703	2.744
340	0.13	0.95	445.59	17.0	-0.475	-0.475	1.03	6.438	17.895	-0.5	0.0625	-0.5	2.204	2.781
341	0.13	0.95	476.25	16.0	-0.475	-0.475	1.03	6.438	16.842	-0.5	0.0625	-0.5	2.941	2.828
342	0.13	0.95	511.51	15.0	-0.475	-0.475	1.03	6.438	15.789	-0.5	0.0625	-0.5	4.083	2.886
343	0.13	0.95	552.49	14.0	-0.475	-0.475	1.03	6.438	14.737	-0.5	0.0625	-0.5	5.996	2.963
344	0.13	0.95	600.72	13.0	-0.475	-0.475	1.03	6.438	13.684	-0.5	0.0625	-0.5	9.604	3.071
345	0.13	0.95	658.31	12.0	-0.475	-0.475	1.03	6.438	12.632	-0.5	0.0625	-0.5	18.030	3.240
346	0.13	0.95	728.30	11.0	-0.475	-0.475	1.03	6.438	11.579	-0.5	0.0625	-0.5	51.792	3.585

Appendix 4.F Application of simplified design expressions

Appendix 4.F illustrates how to obtain the results in Tables 4.3 and 4.4 by applying the simplified design expression presented in section titled "Simplified expressions for critical bracing stiffness" in conjunction with interpolation.

Statement of the problem:

A simply supported glulam beam with a rectangular section of depth $h = 950mm$ and width $w = 130mm$. The beam is subjected to a point load and lateral brace at mid-span with same height. It is required to determine the threshold bracing stiffness based on the present detailed analytical model and compare the results with those based on the simplified procedure. Sectional properties are: Saint-Venant torsional constant $J = 6.36 \times 10^8 mm^4$, weak moment of inertia $I_{yy} = 1.74 \times 10^8 mm^4$, and warping constant $C_w = 1.31 \times 10^{13} mm^6$ and material properties are $E = 10,300MPa$ and $G = 644MPa$. Two cases are considered: a) span $L = 9500mm, a = b = -238mm$ b) span $L = 6498mm, a = b = -285mm$.

Solution:

For the case (a), one has $a/h(b/h) = -0.25$ and $L/h = 10$. For mid-span point loading, one can determine the required critical stiffness of the brace from Eqs. (6.29) by interpolation, i.e.,

$$\begin{aligned} Z &= \log\left(\bar{k}_{cr} L^3 / EI_{yy}\right)_{b/h=-0.25, L/h=10} \\ &= 0.5 Z_{b/h=-0.20, L/h=10} + 0.5 Z_{b/h=-0.30, L/h=10} \\ &= 0.5 \times 3.310 + 0.5 \times 3.060 = 3.185 \end{aligned}$$

From which one has $\bar{k}_{cr} = 3.20 \times 10^6 \, kN/m$. This compares to $k_{cr} = 2.36 \times 10^6$ Based on the present energy solution, a 26.17% difference. For Case (b), one has $a/h(b/h) = -0.3$ and $L/h = 6.84$. Thus, one can determine $Z_{b/h=-0.3, L/h=6.84} \approx Z_{b/h=-0.3, L/h=6.947}$ since $Z_{b/h=-0.3, L/h=6.84}$ lies outside the scope of Fig.4.10. For the point load, one can determine that

$Z_{b/h=-0.3,L/h=6.947} = 4.199$ from Eq.(6.29). Hence, one has $Z_{b/h=-0.3,L/h=6.84} = 4.199$ and $\bar{k}_{cr} = 9.86 \times 10^4\ kN/m$.

Verification:

Verification is conducted by comparing the critical moment among the cases based on approximate threshold stiffness $\bar{k}_{cr}$, obtained from present energy formulation, that based on ABAQUS and that based on the simplified maximum critical moment Chapter 3. Results shown in Table 4.F.1 show excellent agreement between all solutions.

Table 4.F Comparison of critical moments

	Present energy solution		FEA Results (kNm)	Simplified maximum critical moment (kNm)
	Symmetric mode (kNm)	Anti-symmetric mode (kNm)		
Case (a)				
$k_0 = \bar{k}_{cr}$	1130	1090	1070	1090
$k_0 = k_{cr}$	1090	1090	1070	
Case (b)				
$k_0 = \bar{k}_{cr}$	1710	1720	1650	1700
$k_0 = k_{cr}$	1720	1720	1650	

5. Summary, Conclusions and Recommendations

5.1 Summary and Conclusions

1. Two models were developed to determine the elastic lateral buckling resistance of simply supported wooden beams with eccentric mid-span lateral braces. The first model provides the solution for the case of rigid lateral braces while the second model provides the solution for the case of flexible braces and provides a basis to assess the bracing stiffness requirements to maximize the elastic lateral torsional buckling resistance for beams.
2. Both formulations are based on beam buckling theory in conjunction with energy formulations and are based on Fourier decomposition of the bending moment, lateral displacement, and angle of twist fields. Twelve Fourier terms were observed to guarantee convergence of results for all cases considered.
3. The validity of both models was assessed through verifications against 3D FEA results. The predictions of critical loads and buckling modes were found to agree within a few percent with those based on 3D analysis.
4. Comparison between the results of the present formulation and previous investigations (i.e. Schmidt 1965 and McCann 2013) have also shown the validity of the present energy formulation for both models.
5. For symmetric loading relative to the beam mid-span, the orthogonality properties of the Fourier terms show that the models predict an anti-symmetric and a symmetric mode of buckling. Either modes can govern the resistance of the beam, depending on the height of the brace. When the brace is located above a threshold height, the critical moments were observed to be governed by the anti-symmetric mode of buckling.
6. For both rigid bracing and flexible bracing models, increasing load height was shown to cause a decrease of critical moment based on the symmetric mode. However, critical moments based on the anti-symmetric mode were observed to decrease with the load height for uniformly distributed load, but remains constant for point load.
7. For both rigid and flexible bracing models, increasing bracing height was shown to lead to an increasing critical moment based on symmetric mode with no influence on the critical moment based on the anti-symmetric mode.

8. For flexible bracing, increasing the bracing stiffness was found to lead to an increasing critical moment based on the symmetric mode, with no influence on the critical moment based on the anti-symmetric mode. After the threshold bracing stiffness is attained, the LTB capacity of the system is observed to remain constant.
9. Simplified analytical expressions were developed through regression analysis to determine their elastic LTB capacity, threshold bracing height and threshold bracing stiffness for common design cases.
10. Design examples were presented to illustrate the applicability of simplified expression in practical design situations.

5.2 Limitations of present research and Recommendations for future research

1. The present research is limited to simply supported beams subjected to symmetric loading. It is recommended to extend the research to other boundary conditions and loading distributions.
2. The present research is limited to beams with of a single intermediate brace at mid-span. It is recommended to extend the work to cases of multiple intermediate lateral braces.
3. The present model neglects the effect of shear deformation and cross-sectional distortion. For the type of problems investigated in the present study, such assumptions didn't affect predictions in agreement with 3D FEA modelling. For cases of multiple braces, similar assumptions may not lead to similar predictions. In such cases, the effects of shear deformation and cross-section distortion may need to be included.
4. The present research has investigated bracing requirements for perfectly straight beams. It is of practical interest to address cases involving initial out-of-straightness.
5. The present research has developed simplified critical moments base on the anti-symmetric mode and the associated threshold bracing height. When practical considerations are such that bracing height is below the threshold value, there is a need to develop a simplified expression of critical moments based on the symmetric mode.
6. It is of practical interest to conduct full scale lateral torsional buckling tests to assess the validity of the model developed.